DAMAGE DEVELOPMENT AND FAILURE OF FIBER-REINFORCED CERAMIC MATRIX COMPOSITES

by

KATHRYN ANN DANNEMANN

B.S., Materials Engineering
Rensselaer Polytechnic Institute
(1980)

M.S., Materials Engineering
Rensselaer Polytechnic Institute
(1982)

Submitted to the Department of
Materials Science and Engineering
in Partial Fulfillment of the Requirements
for the Degree of

DOCTOR OF PHILOSOPHY

at the

MASSACHUSETTS INSTITUTE OF TECHNOLOGY

June 1989

Signature of Author _____
Department of Materials Science and Engineering
May 5, 1989

Certified by _____
Dr. John F. Mandell
Thesis Supervisor

_____
Prof. Frederick J. McGarry
Thesis Supervisor

Accepted by _____
Prof. Samuel M. Allen, Chairman
Departmental Committee on Graduate Students

DAMAGE DEVELOPMENT AND FAILURE OF FIBER-REINFORCED, CERAMIC MATRIX COMPOSITES

by

Kathryn Ann Dannemann

Submitted to the Department of Materials Science and Engineering
on May 5, 1989 in Partial Fulfillment of the Requirements
for the Degree of Doctor of Philosophy

ABSTRACT

The mechanisms which control damage development and tensile failure of fiber-reinforced, glass and glass-ceramic matrix composites were investigated. This encompassed the study of damage modes (including longitudinal and transverse ply cracking, as well as delamination and fiber fracture), the role of fiber/matrix bonding and residual stresses, and the effects of laminate configuration and constituent fiber and matrix properties. The microstructural aspects of fracture were emphasized in an effort to achieve a firm understanding of structure/property relationships.

Four Nicalon fiber-reinforced composite systems with differing interfacial strengths and residual stress fields were studied. Nicalon/CAS and Nicalon/1723 glass had relatively high fiber/matrix bond strengths. Axial residual matrix tensile stresses and radial residual interface compressive stresses developed following elevated temperature processing due to thermal expansion mismatch. Nicalon/LAS and Nicalon/BMAS composites were less strongly bonded, and the residual stress pattern was reversed due to significantly lower matrix expansion coefficients. Both unidirectional and crossply laminates were studied at ambient and elevated temperatures (>500°C).

Fractographic investigations were performed to correlate fracture resistance with fracture surface features (e.g. pullout lengths, matrix crack spacing). The less strongly bonded systems were more resistant to matrix microcracking; fractures were characterized by extensive fiber pullout since minimal frictional resistance was encountered. Several methods were developed to monitor damage accumulation during loading. Longitudinal and transverse ply cracking, and delamination were detected using an edge replication technique and/or SEM study of loaded flexural specimens. Ply residual stresses strongly influenced the damage development process in 0/90 laminates. At room temperature, transverse ply cracks initiated at very low strains (0.02-0.05 %) in Nicalon/1723 and Nicalon/CAS due to residual tensile stresses in the 90° plies. Transverse ply cracking was delayed to higher strains (> 0.1 %) in Nicalon/LAS owing to residual compressive stresses. Ultimate failure was often associated with delamination.

A theoretical model of the damage behavior was developed based on experimentally determined structure-property relationships. Measured crack spacings were compared with relevant brittle cracking theories to determine the factors controlling tensile failure of undirectional composites. For crossply laminates, existing models of transverse ply cracking in polymer-matrix composites were adapted. Transverse ply cracking of fiber-reinforced ceramics can be theoretically predicted by a statistical fracture mechanics model which accounts for residual thermal stresses, statistics of progressive cracking and longitudinal ply cracking. Reasonable agreement was found between theory and experiment for transverse crack density as a function of applied stress level.

The tensile behavior of the four composite systems was unaffected by temperatures up to a limiting temperature. For Nicalon/1723, 500°C was the bounding temperature. The limiting temperature for the glass-ceramic matrix composites was approximately 700°C; embrittlement occurred at higher temperatures. Interface oxidation was found to dominate the elevated temperature embrittlement process. The kinetics of interface oxidation tunnelling from exposed fiber ends was examined for Nicalon/CAS by following the variation in bond strength. Comparison of transverse and axial penetration depths showed the oxidation process was dominated by oxygen tunnelling via a "pipeline mechanism".

Thesis Supervisor: Dr. John F. Mandell

Title: Principal Research Associate

and

Thesis Supervisor: Prof. Frederick J. McGarry

Title: Professor of Materials Science and Engineering

ACKNOWLEDGEMENTS

I am grateful to Dr. John Mandell for providing unending guidance and insight toward understanding these complex materials. Although he maintained the difficult task of thesis advising from Montana during the last year of my graduate tenure, he never tired of my frequent phone calls, Federal Express packets and FAX copies. The encouragement and support of Prof. Frederick McGarry, and the contributions of Prof. Yet-Ming Chiang and Prof. David Roylance as thesis committee members are also greatly appreciated.

Many persons have been of invaluable assistance during this study. It is difficult to cite everyone in such limited space, and risk possible oversight. However, I am especially grateful to my labmates and various support personnel (i.e. machinists, laboratory specialists, etc.). These two groups seldom receive the recognition they deserve. Yet, their technical expertise, as well as their ungiving support, concern, encouragement and friendship, helped me to overcome the many obstacles I encountered.

Several individuals deserve special acknowledgement. The meticulous efforts of Arthur Rudolph in machining, as well as designing and constructing novel devices (particularly the semi-automatic polisher), saved me endless hours at the bench. His positive attitude and willingness to try new methods were instrumental in accomplishing difficult tasks. The guidance of Len Sudenfield in scanning electron microscopy and replication techniques are also greatly appreciated. Without his help, I might still be devising methods to prevent melting of cellulose acetate replicas due to beam damage. The patient guidance and assistance of Jim Schutz with high temperature testing, specimen design and CLPT contributed to the ultimate fulfillment of this thesis. Eric Jao will not be forgotten for his assistance in devising computer programs to solve formidable theoretical modelling problems.

The financial support of Corning Glass Works and NASA Lewis Research Center during the course of this investigation is gratefully acknowledged. I am also thankful to ZONTA International for providing an Amelia Earhart Fellowship during the final year of my studies.

Finally, the sacrifices of my parents during this second sojourn in graduate school are greatly appreciated. Their unceasing moral and financial support were the guiding factors in completion of this final degree.

TABLE OF CONTENTS

LIST OF TABLES

LIST OF FIGURES

1. INTRODUCTION

Ceramic matrix composites (CMC's) have received widespread attention as replacement materials for superalloys in high temperature structural applications, such as gas turbines and heat engines. The popularity of this class of materials is related to their high strength at temperatures exceeding the melting points of superalloys, as well as superior oxidation, wear and corrosion resistance. They have the potential to improve engine efficiency by 30 to 50 % [1] over present technology since higher operating temperatures are possible; weight and frictional losses are reduced. Development has progressed such that CMC's are now available for potential demonstration applications.

Although ceramics are ideally suited for elevated temperature applications, low flaw tolerance has limited their use. Fiber reinforcement of brittle ceramics surmounts this problem and significantly enhances strength and toughness. Although fiber-reinforced, ceramic matrix composites were originally explored in the sixties [2-5], their viability as high performance materials was uncertain until the introduction of oxidation resistant, advanced ceramic fibers [6] in the mid seventies. Nicalon fiber-reinforced glasses and glass-ceramics [7,8] were developed at that time and have pioneered a growing effort in the field of high performance, fiber-reinforced ceramics.

The mechanical behavior of fiber-reinforced glasses and glass-ceramics is the focus of the present work. Extensive characterization of mechanical behavior is required if these materials are to be properly exploited. The results of mechanical property investigations have been reported for a few developmental systems [9-17]. The majority of results were obtained from simple flexure tests. This data is inadequate beyond the early stages of cracking due to stress gradients and a shifting neutral axis of the flexure specimen. Mechanical behavior is more accurately described by tensile stress-strain behavior. The tensile behavior of fiber-reinforced ceramics at ambient and elevated temperatures is characterized in this thesis.

Failure of CMC's is more complex than the single crack advance noted in monolithic ceramics and is complicated by anisotropy and residual stress effects. Some progress has been made in identifying the failure mechanisms of fiber-reinforced glasses and glass-ceramics [12,18], but additional studies are needed. A variety of mechanisms are possible, depending on the stress state and ply configuration. Improved toughness and an increased strain to failure is generally associated with a weak fiber/matrix bond which allows fiber

debonding and matrix crack deflection. However, toughness may be achieved at the expense of poor transverse and off-axis properties due to weak interfacial bonding.

Less attention has been directed towards elevated temperature mechanical behavior which tends to be excellent for most systems studied [8,11,13-15]. Above a certain limiting temperature, embrittlement occurs and is accompanied by significant strength and modulus reductions. The degradation in properties is not yet fully understood, but has been related to changes in the interfacial bond characteristics due to oxidation.[17,19,20]

An improved understanding of the failure process at both ambient and elevated temperatures is necessary for further advances in composite processing and optimum design of composite microstructures. The present program was undertaken to determine the mechanisms which control damage development and failure in several experimental Nicalon fiber-reinforced glass and glass-ceramic composite systems. Four different matrices were investigated including: lithium aluminosilicate (LAS), calcium aluminosilicate (CAS) and barium magnesium aluminosilicate (BMAS) glass-ceramics, and Corning Code 1723 glass (an aluminosilicate glass). Nicalon/1723 and Nicalon/CAS are strongly bonded and have high matrix expansion coefficients. LAS and BMAS matrices have low expansion coefficients, and the composites are less strongly bonded. Thus, a direct comparison of the effects of bond strength and residual stresses on tensile behavior was possible.

The microstructural aspects of fracture are emphasized since a firm understanding of the relationship between structure and properties is essential to understanding the failure process. The effects of ply configuration, thermal residual stress, and fiber/matrix bond strength are considered for a more thorough investigation of the damage process. The experimental findings are combined with analytical studies in an effort to develop a predictive model of fracture based on microstructural parameters.

2. BACKGROUND

2.1 Ceramic-Matrix Composite Development

Ceramics are an important class of materials owing to a range of useful physical and mechanical properties. These include: high stiffness and hardness, low density and thermal expansion, refractoriness, chemical inertness, and wear resistance. High strength and stability at elevated temperatures are probably the most attractive characteristics of ceramics. However, the effectiveness of these materials in high temperature structural applications has not been realized owing to low flaw tolerance. Improving the toughness of brittle ceramics has been the impetus behind recent ceramic-matrix composite developments.

Morphology

Several composite development approaches to toughening have been investigated. Whisker [21-24] and short-fiber [25,26] reinforcements were added to ceramics to increase toughness while retaining the useful properties of the matrix to high temperatures. Substantial toughness increases (in terms of K_{Ic} values) were reported for SiC whisker-reinforced Al_2O_3 [21,22] and Si_3N_4 [23], as well as several glass and glass-ceramic matrices [24]. The toughening mechanism is believed to be similar to that of conventional ceramics: crack pinning and deflection [27]. Discontinuous fiber additions were also found to increase the toughness of ceramics.[25,26] Toughening with short fibers appears to be dominated by fiber pullout and debonding. However, composite strength will be less than that of the unreinforced matrix unless at least partial fiber alignment is attained.[28] Only a limited number of practical whisker or short fiber-reinforced composite systems are possible due to an extreme sensitivity to fiber/matrix thermal expansion mismatch.

At ambient temperatures, short-fiber and whisker-reinforced composites must compete with zirconia-toughened ceramics. Comparable K_{Ic} values have been measured for whisker-toughened and zirconia-toughened ceramics.[29] Transformation toughening was achieved in several stiff ceramic matrices [30] (e.g. Al_2O_3, mullite, stabilized cubic ZrO_2, fine-grained fully tetragonal ZrO_2 materials) by incorporation of ZrO_2 particles. The ZrO_2 particles transform spontaneously from a high temperature tetragonal structure to a room temperature monoclinic structure by a stress-induced martensitic transformation. Phase transformation in the vicinity of a crack tip causes toughening by crack tip shielding and reduction of crack tip stresses. The strength and toughness of zirconia-toughened ceramics decreases as temperature increases owing to a reduced driving force for the phase

transformation. Whisker-reinforced ceramics will be more advantageous at elevated temperatures since the toughness of these materials is unlikely to decrease with temperature.

Continuous fiber reinforcement of brittle ceramics yields the most dramatic toughness improvements. Although long recognized, this approach was not demonstrated with a high temperature matrix until the early seventies. Carbon-fiber reinforced glasses [2-5] exhibiting improved strength and toughness were developed at that time, but are of limited interest due to the oxidative instability of the carbon fiber. These early fiber-reinforced ceramics are discussed in more detail in Ref. 28. Higher temperature fibrous composites became possible in the mid to late seventies with the advent of a melt spun, polycarbosilane-derived, ceramic fiber with improved oxidation resistance.[6] The commercial availability of this continuous, small diameter Nicalon™ fiber facilitated significant fibrous composite developments.

Most development efforts to date have emphasized Nicalon fiber-reinforced systems. Several investigators reported on the processing, microstructure and mechanical behavior of Nicalon-reinforced glasses and glass-ceramics.[7,8,31-33] Since these composites are of primary interest in the present work, they are the focus of the ensuing background discussion. Factors related to damage development and failure are included. The scope of the review is limited, and more complete treatments are provided in Refs. 34 and 35.

Application of fiber-reinforced, ceramic-matrix composites is aimed at high temperature structural markets. Nicalon-reinforced glasses will be most effective in the 400-600°C range; use temperatures exceeding 1000°C are possible for Nicalon-reinforced glass-ceramics. However, Nicalon fibers are unlikely to provide long term reinforcement at temperatures above 1200°C. Fiber susceptibility to decomposition, oxidation, creep and accelerated grain growth is greatly enhanced in this temperature range.[36-42] More refractory ceramic fibers are needed to raise the working temperature limits of ceramic composites. Work on improved reinforcements is underway and some new fibers are currently available. These are listed in Table 2-1 [43], along with other fibers still under development.

™ trademark - Nippon Carbon Company

Processing

One of the most significant attributes of Nicalon fiber-reinforced glasses and glass-ceramics is a relative ease of fabrication. The low viscosity of glass at elevated temperatures makes it possible to adapt many processing techniques commonly used for net shape resin matrix composites. Glass-ceramics provide the unique capability to densify a composite in the glassy state and subsequently crystallize the matrix to ensure high temperature stability. Although a variety of processing methods have been investigated, hot pressing of slurry-infiltrated tapes has proven most effective. It yields a lower porosity matrix than other fabrication techniques and has been applied most commonly to glass and glass-ceramic matrix composites. The Nicalon fiber-reinforced systems under investigation in this work were fabricated by hot pressing.

The hot pressing/slurry infiltration procedure is illustrated in Fig. 2-1 for a glass-matrix composite. First, a tow of fibers is drawn through a slurry consisting of water, an organic binder and glass or glass-ceramic powder. The slurry-impregnated yarn is wound on a mandrel to form a unidirectional tape. The pre-preg tape, which is easily handled, is cut to the desired size to make the plies. To form the composite, the plies are stacked in the desired configuration and densified in a hot pressing operation. The ply stacking sequence is dictated by the structural requirements of the part being fabricated. Burnout of the organic binder is accomplished prior to hot pressing. For proper densification, hot pressing must be conducted at temperatures and pressures whereby a fully dense matrix is obtained with little damage to the fibers. These can approach 1200°C and 6 MPa. Glass-matrix composites are hot-pressed at temperatures near or above the softening point of the glass; densification readily occurs with viscous flow of the matrix. For crystalline matrix composites, a further heat treatment is required following hot pressing to crystallize the matrix.

The hot pressing technique is not without disadvantages. The high temperatures and pressures required for densification can cause fiber degradation, oxidation and other fiber/matrix chemical reactions, as well as grain growth within the fiber. High temperature glasses must be processed at very high temperatures, causing the fibers to degrade. Glass-ceramics are preferred since lower temperature glasses can be employed and subsequently crystallized to increase temperature resistance. The geometric restrictions of hot pressing make this process ill-suited to the fabrication of complex components with near-final shapes and dimensions. Alternative fabrication techniques are available and have been reviewed by Cornie, et al.[44]. These include: chemical synthesis routes (pyrolysis of

liquid organometallic precursors and sol-gel methods), melt infiltration, and gas phase processing (chemical vapor deposition/infiltration).

Chemical synthesis routes have the advantage of greatly reduced processing temperatures if problems of low yield and excessive matrix shrinkage can be overcome. However, formation of dense matrices is not possible without additional processing steps. Melt infiltration is derived from similar resin and metal-matrix composite processing techniques. High matrix densities are theoretically possible, but the method is limited to low-melting ceramic matrices. Consequently, little work has been performed to date on this method.

A gaseous precursor is used to deposit the ceramic onto a heated ceramic fiber preform substrate in gas phase processing. Large complex structures are possible by in-situ chemical reaction. Matrices of various fiber-reinforced ceramic composites (e.g. SiC, Si_3N_4, B_4C, BN, and TiB_2) have been formed by chemical vapor deposition (CVD) , but processing times are excessive (i.e. several weeks). Researchers at Oak Ridge National Laboratory greatly reduced processing times using an alternative chemical vapor infiltration (CVI) technique.[45-47] They achieved 70 to 90% dense SiC and Si_3N_4 matrices on SiC and Si_3N_4 fiber preforms within 2 to 12 hours. The commercial availability of a CVI-formed SiC matrix carbon fiber-reinforced composite [48] is evidence of the extent of CVI process development.

A new reaction-based procedure has introduced the possibility of relatively inexpensive, high toughness ceramic-matrix composites. In the Lanxide™ process, a metal-ceramic composite is formed in-situ during the formation of an oxide from a molten metal solution in a refractory container.[49] Formation of near net-shape products are possible with minimal densification shrinkage. Recent developments in reaction-based processing methods for CMC's have been summarized by Chiang, et al..[50]

2.2 Theory - Mechanical Behavior

Although the primary motivation behind ceramic-matrix composite developments is toughness improvement of brittle ceramics, some composites also benefit from enhanced strength and stiffness. Continuous fiber reinforcement of ceramics can provide both high strength and high toughness if properly engineered. Mechanisms of effective strengthening and toughening are discussed below for unidirectional fiber-reinforced ceramics.

™ Lanxide, Inc., Newark, DE

Strengthening

Failure of CMC's differs from resin and metal-matrix composites since the matrix failure strains are generally less than the fiber breaking strains (~0.05 % vs. 1 %). The low matrix failure strain dictates matrix failure prior to fiber failure. The possible failure modes for unidirectional CMC's are depicted in Fig. 2-2.

For strongly bonded systems (Case B), cracks formed in the matrix propagate through the fibers. The interphase region is unable to withstand the imposed shear stresses upon matrix cracking. Composite failure occurs at the matrix failure strain, ε_{mu}, by propagation of a single matrix crack through the fibers. A linear stress-strain curve (Fig. 2-3a) results due to the brittle nature of the fracture. Composite strength and modulus are expressed by the rule of mixtures:

$$E_c = E_f V_f + E_m (1-V_f)$$
$$\sigma_c = E_c \varepsilon_{mu} = E_m \varepsilon_{mu} [V_f (E_f / E_m) + (1-V_f)]$$

Some strength enhancement is possible with high modulus fibers, but the strength increase via matrix-to-fiber load transfer is small. The composite failure strain remains unchanged from that of the unreinforced matrix. In addition, toughness is not greatly enhanced over that of the matrix. Therefore, a strongly bonded system is not recommended for structural ceramics.

If residual stresses due to thermal expansion mismatch are considered, a negative mismatch ($\alpha_f > \alpha_m$) is generally advantageous for strongly bonded systems.[52,53] The fibers tend to precompress the matrix in the axial direction, thus increasing the overall strain required for failure initiation. The compressive strength of the matrix usually greatly exceeds its tensile strength. However, a strength decrease due to interfacial decohesion (radially) is possible if the mismatch is too large.

The above analysis does not account for the relatively high strengths which have been reported for fiber-reinforced glasses and glass-ceramics.[2-5,7,8,31-35] Fiber reinforcement theory suggests that substantial strengthening can only occur if the fiber modulus exceeds the matrix modulus.[51] Stronger ceramic-matrix composites are possible in weakly bonded systems above a critical fiber volume fraction, V_{cr}. The dependence of composite strength on fiber volume fraction, V_f, is illustrated in Fig. 2-4. If the fiber content is too low, the reinforcing fibers may be unable to support the total load carried by the composite

when the matrix fails. Below V_{cr}, even in weakly bonded systems, composite strength is governed by the strength of the matrix. Failure occurs by single fracture, as described above.

Above V_{cr}, weakly bonded composites (Case C, Fig. 2-2) do not fail by propagation of a single matrix crack.[35,51,54,55] In Nicalon fiber-reinforced composites, a weak bond results due to formation of an interfacial carbon layer upon processing.[9,20] The weak bond (or interphase) prevents spontaneous propagation of matrix cracks through adjacent fibers. After initial cracking of the matrix, the load is transferred to the fibers. The high fiber content allows support of the applied load, and multiple matrix cracking occurs with further stressing. The fiber volume fraction at the transition from single to multiple fracture is: [51]

$$V_{cr} = \frac{\sigma_{mu}}{\sigma_{mu} + \sigma_{fu} - \sigma_f'}$$

where σ_f' is the stress in the fiber at matrix fracture.

Matrix cracking, accompanied by load transfer to the fibers, can continue until a saturation level is achieved. After matrix crack saturation, the fibers bear the load. Failure of the composite occurs when the fracture strength of the fibers is reached. The multiple matrix cracking process has been extensively characterized by Aveston, Cooper and Kelly (ACK) [55] and is described in further detail later in this chapter.

The stress-strain curve for weakly bonded composites (Case C) is non-linear, consisting of three distinct regions as shown in Fig. 2-3b. In the initial linear portion of the curve, the composite stress and modulus are described by the rule of mixtures. A deviation from linearity occurs at the matrix microcracking strain. Further load increases beyond the onset of microcracking cause additional matrix cracking and a permanent decrease in composite stiffness due to a decreased matrix contribution. The final linear regime of the stress-strain curve is governed solely by fiber properties. Failure of optimized composite materials occurs at an ultimate tensile strength approximated by the product of fiber strength and fiber volume fraction. The ultimate composite failure strain is increased over that of the unreinforced matrix and is equivalent to that of the reinforcing fibers.

The addition of high modulus fibers may also enhance the matrix cracking strain of low modulus, brittle matrices. Romauldi and Batson [56] were first to propose that the cracking

strain of concrete should increase upon incorporation of fine fibers. The suppression of matrix cracking by fiber reinforcements, and the corresponding increase in the ultimate matrix fracture strain, has been observed experimentally.[4,57,58] For example, Phillips, et al.[4] reported an increase in ε_{mu} of 2.5 times for glass containing 30 volume percent carbon fibers. The fibers tend to absorb energy as the crack grows, and their presence limits the supply of energy to the crack tip region. The energy available for crack growth is less than in unreinforced ceramics, and matrix cracking is suppressed. The occurrence, implication and suppression of matrix microcracking is an important area for further research.

Aveston, Cooper and Kelly [55] suggested that the friction of sliding the crack-bridging fibers relative to the matrix opposes the displacements of crack surfaces, causing an increased matrix cracking strain. They derived an expression for the enhanced matrix cracking strain, ε_{muc}, using an energy-balance method. The critical matrix strain is given by:

$$\varepsilon_{muc} = \left(\frac{12\tau \, \gamma_m \, E_f \, V_f^2}{E_c \, E_m^2 \, r \, V_m} \right)^{1/3}$$

where τ is the frictional bond strength, r is the fiber radius and γ_m is the fracture surface work in forming a matrix crack. It implies matrix microcracking can be suppressed at high fiber volume fractions, high interfacial shear strengths and/or small fiber radii.

Toughening

The toughness of CMC's cannot be expressed in terms of conventional fracture mechanics parameters (i.e. critical stress intensity factor) since failure does not occur by the growth of a single crack. Although the improved toughness of fiber-reinforced ceramics relative to monolithic ceramics is marked by an increased failure strain, it is difficult to quantify this improvement. Several possibilities have been suggested, including [59,60]: (i) a stress intensity based on the first matrix microcracking stress, (ii) a work of fracture measured as the area under a tensile stress-strain curve, and (iii) a toughness parameter based on failure strain. Rice [61,62] and Shetty [53] have reviewed the possible toughening mechanisms in CMC's. Several energy dissipative processes which contribute to the work of fracture were identified. These are summarized below for fiber-reinforced ceramics.

Fiber debonding occurs when the fiber/matrix interface is weak and the interfacial shear resistance is low. It is also promoted by a negative thermal expansion mismatch ($\alpha_f > \alpha_m$)

which puts the interface in radial tension upon cooling from fabrication temperatures. Debonding occurs prior to fiber pullout and work must be done to rupture the fiber/matrix interfacial bond. The debonding event is accompanied by an energy release as the stress in the fiber relaxes over a characteristic distance. In the stress field of a crack, debonding causes crack deflection parallel to the fibers. Progressive delamination of the specimen may follow. Aveston [52] has shown that high values of the work of fracture are possible by this mechanism.

Fiber pullout is promoted when the interfacial shear stress generated exceeds the shear resistance of the interface, and the stress transferred to the fibers is below the fiber fracture strength. The fiber pullout stress does not drop to zero after debonding since large frictional forces resist matrix sliding. Toughening results from the additional work required to pull the fibers out of the matrix against friction. Although this mechanism was originally developed for discontinuous fiber composites, it is also applicable to continuous fiber composites. In continuous systems, a statistical strength distribution generally exists along the fiber lengths. A fraction of the fibers, l_c/l, will not be loaded to their fracture stress and will pull out of the matrix. l_c is the minimum length of fiber which can be loaded to its fracture stress in the composite and is defined as $(\sigma_u r_f)/\tau$, where τ is the frictional restraining stress at the interface. The maximum value of fracture work due to fiber pullout occurs at $l = l_c$ and has been shown to be [63,64]:

$$\gamma_p = \frac{V_f \tau l_c^2}{12 r}$$

Matrix microcracking results from property mismatches between the fibers and matrix, especially thermal expansion mismatch. A positive thermal expansion mismatch ($\alpha_m > \alpha_f$) promotes microcracking in a strongly bonded system since an axial residual tensile stress develops in the matrix. Matrix microcracking also develops in weakly bonded composites due to effective load transfer, as indicated in the discussion of strengthening. Microcracking is a useful toughening mechanism only if it is selectively induced in the stress field of a primary crack. The development of a network of fine matrix microcracks in a direction perpendicular to the fiber axes results in a dissipation of energy which contributes to the work of fracture. However, the microcracking stress may serve as the useful limit of the material above which severe environmental degradation can occur.

The fracture toughness of brittle polymer matrix composites with multidirectional reinforcement has been related to the development of a damage zone at the crack or notch tip.(65) The damage zone consists primarily of matrix/interface cracks in each ply and delamination between plies. It effectively blunts the cracks, reducing stress concentrations in the fibers.

2.3 Factors Affecting Mechanical Behavior

Strengthening and toughening of ceramics by fiber reinforcement is not as straightforward as the above theories might suggest. Other interacting factors are involved which make designing these composites an engineering challenge. In addition to constitutive fiber and matrix properties, interfacial strengths, residual stresses and free edge effects must be considered. The development of damage, and subsequent failure are also influenced by laminate configuration and temperature. The synergistic effects of these parameters on mechanical response are highlighted below.

Where applicable, experimental findings for Nicalon fiber-reinforced glasses and glass-ceramics are presented. The majority of work to date has emphasized the unidirectional Nicalon/lithium aluminosilicate system (Nicalon/LAS), developed jointly by United Technologies Research Center (UTRC) and Corning Glass Works.(32) It serves as a model system and exhibits high temperature stability to temperatures approaching 1000°C. Most mechanical property evaluations reported in the literature employ three and four point flexure tests. Our laboratory has developed a tensile test which is useful to at least 1000°C.(66) Further details of advances in test methodology for these anisotropic materials can be found in several recent reviews.(59,60)

Fiber/Matrix Bond Strength

The characteristics of the fiber/matrix interface are critical in the effective design of *all* composite materials. Since the interface plays a major role in load transfer throughout the composite, most composite properties show some bond strength sensitivity. As noted above for CMC's, the interfacial bond strength controls toughness and flaw tolerance (i.e. resistance to matrix crack propagation). Composite off-axis and shear properties are also interface dependent, and expected to correlate with bond strength if other parameters remain unchanged. Schematics of these interface-dominated properties are given in Fig. 2-5.

The toughness of CMC's is enhanced by a weak interface.(5,8,29,35) A sufficiently low fiber/matrix bond strength will increase flaw tolerance by: i) allowing fiber debonding prior

to crack propagation through the fibers, and ii) deflecting matrix cracks (or cracks penetrating from off-axis plies) parallel to the fibers. For adequate composite strength, the interfacial strength level must permit matrix crack propagation without damage to a critical number of load bearing fibers. Off-axis and shear properties, as well as environmental stability, may be sacrificed if the bond is too weak. Contrary to polymer-matrix composites, maximization of the interfacial bond strength is not recommended in fiber-reinforced ceramics.[64] Alternatively, bond strength optimization is attempted to achieve a compromise between strength and toughness. Tough and strong CMC's may be possible by slight increases in interface strength, and suppression of microcracking to higher applied stress levels (e.g. by decreasing the fiber radius and/or decreasing V_f).[68] A large portion of the future research in this field will be directed towards achieving sufficient process control such that optimum fiber/matrix bond strengths are possible.

Until recently, estimates of interfacial integrity were based upon resultant composite properties or fractographic investigations of failed specimens. Although adequate for polymer matrix composites, this approach is unacceptable for CMC's where slight variations in bond strength can yield large changes in properties. A reliable, quantitative measure of fiber/matrix bond strength is needed and some progress has been made in development of experimental techniques.

Indentation tests are currently the most popular means of bond strength characterization. Several variations of this method are used to measure debonding strength [69] and/or the frictional sliding resistance of stiff fibers in brittle matrices [70-72]. Following debonding of the fiber/matrix interface in reinforced ceramics, stress transfer becomes entirely dependent on the resultant frictional forces between the fiber and matrix. Frictional stresses resist pullout and result in a non-catastrophic load drop which contribute to fracture toughness.

Although indentation tests have proven useful in quantifying interfacial strength, analysis has been very limited. Grande, et al. [67] used a detailed stress analysis to calculate interfacial shear strengths measured in a microdebonding test of carbon and Nicalon fiber-reinforced glasses and glass-ceramics. The results were correlated with composite longitudinal and interlaminar shear strength to explain the behavior. Further work along these lines is needed to establish the fundamental relationships between composite performance, bond mechanical properties, and bond chemistry and microstructure. The significance of the bond strength is addressed in the present work.

Some progress has been made in understanding the fiber/matrix bond chemistry of Nicalon fiber-reinforced glass-ceramics.[9,20,73-75] The weak interface which allows strong and tough behavior is related to an interfacial carbon layer. It forms upon composite consolidation at elevated temperatures due to an oxidation reaction between the Nicalon fibers and silicate matrices. The carbon-rich nature of the fiber/matrix interface was first determined by Brennan using scanning Auger electron microanalysis (SAM).[9] More recently, he found the interfacial region in LAS-III (lithium aluminosilicate) matrix composites to contain two reaction zones: an inner carbon rich layer (0.1-0.15 μm thick) next to the fiber, and an outer noncoherent NbC particulate layer (0.2-0.25 μm thick).[73] In-situ formation of NbC around the fibers is promoted by Nb_2O_5 particles in the LAS-III matrix.

Cooper and Chyung [74] also observed a 0.02 μm to 0.2 μm thick reaction-layer type fiber/matrix interface in both LAS and CAS (calcium aluminosilicate) matrix systems. Direct imaging of the interface by high resolution transmission electron microscopy (HRTEM) revealed 0.34 nm graphite crystallites as a primary interface constituent. Interface chemistry and morphology were found to be consistent with reaction layer formation by a SiC oxidation reaction, occurring at the Nicalon fiber surface. Formation of the carbon layer by this dynamic, diffusional process can be controlled by varying processing variables and/or matrix composition. Although these investigations have improved our understanding of the interfacial chemistry of Nicalon fiber-reinforced composites, additional studies are necessary to correlate composite performance with interfacial chemistry.

Test Temperature

CMC's are under development for high temperature structural applications. To guarantee acceptable performance, the strength and toughness of these materials must be maintained at elevated temperatures. As discussed earlier, extensive matrix cracking can occur under load. The matrix crack sites, in conjunction with weak fiber/matrix interfaces, provide an easy path for ingress of oxygen and other environmental constituents. Therefore, these high temperature composites must be designed such that the fibers and the interface can withstand oxidation and other chemical reactions which occur upon elevated temperature exposure.

It is likely that reinforced ceramics will experience thermal cycling in actual applications. Thus, knowledge of the effects of temperature on mechanical response is essential in

designing these structures. Several investigators [10-12,66] have characterized the mechanical behavior of Nicalon fiber-reinforced ceramics at ambient temperature, but few have investigated composite performance at elevated temperatures. Elevated temperature results are limited due to the inherent difficulties involved in high temperature testing. Further high temperature property evaluations are necessary before use of these materials can be optimized.

Room Temperature. The Nicalon/LAS composite system was reported to fail in several stages.[10-12] An idealized, tensile stress-strain curve of this system is depicted in Fig. 2-6; the general features are as expected from the theoretical discussion of strengthening. Initially, the curve is linear with an elastic modulus close to the rule of mixtures prediction, but becomes strongly non-linear as the matrix cracking strain (0.1 to 0.2 %) is approached. At high strain levels, the curve becomes linear again with a reduced elastic modulus close to that of the fibers. Failure occurs at a strain close to the fiber failure strain (~1 %). The behavior of the LAS-matrix system is representative of other Nicalon-reinforced glasses and glass-ceramics.[10,66]

Microstructural damage features correlated well with discontinuities in the stress-strain curve.[12] At the onset of matrix cracking, a single large crack spanned the entire specimen width and was bridged by intact fibers. Further load increases caused the formation of multiple, regularly-spaced matrix cracks away from the initial crack, and a marked deviation from linearity in the stress-strain behavior. The saturation matrix crack spacing approached 400 μm. Fiber fracture occurred at the peak load, followed by fiber pullout.

Differences in failure stresses and fracture modes occur in tensile vs. flexure tests. Marshall and Evans [12] found longitudinal flexure strengths to be approximately twice the tensile strength values as illustrated in Fig. 2-7. After matrix crack initiation, the flexure behavior is complicated by the stress gradient and shifting neutral axis of the specimen. Thus, the flexure test is inadequate for the measurement of ultimate strength.[10,12,66] It provides a useful measure of the first cracking stress and strain levels, and a qualitative idea of the stress-strain behavior.

High Temperature. Glass-ceramic matrix composites are more suited for extreme temperature applications than reinforced glasses owing to the difference in thermal stability of the matrix materials. To prevent fiber degradation, glasses which soften around 600°C are used. Crystalline glass-ceramic materials can endure temperatures exceeding 1000°C.

The general stress-strain behavior of a Nicalon fiber-reinforced aluminosilicate glass was found to undergo insignificant changes at temperatures up to 500°C.[66] Above 500°C, softening of the glass matrix caused decreases in both strength and modulus. (See Fig. 2-8.) Therefore, application of glass-matrix composites is aimed at "lower" temperature markets.

Other elevated temperature results have been reported for Nicalon/LAS [8,11,13,14] and, recently, in our laboratory for Nicalon/BMAS [15] (barium magnesium aluminosilicate). Both systems showed an initial increase in strength and strain to failure with temperature. However, significant embrittlement occurred upon testing in air at temperatures exceeding 800°C. This was accompanied by severe degradation of ultimate strength, as well as strain and modulus decreases. Both systems exhibited two distinct fracture surface regions: (i) an outer flat region of brittle failure, and (ii) an inner region showing fiber pullout. These are shown in Fig. 2-9 for the Nicalon/BMAS composite. In contrast to the room temperature fractures, no buildup of matrix cracking was found. Pullout lengths in the inner zone were shorter than at room temperature. The stress-strain curves remained linear to the onset of matrix cracking, beyond which catastrophic failure occurred at the point of sudden load drop.

Elevated temperature tests conducted in inert environments [11,16] and in vacuum [14,17] proved oxygen was the active species in embrittlement. An oxygen partial pressure of 10^3 Pa (10^{-2} atm) was sufficient for embrittlement of Nicalon/LAS at 900°C.[14] Long term thermal aging studies in air for Nicalon/LAS [11] and Nicalon/BMAS [20] demonstrated that the oxidation reaction is not initiated until the matrix cracks upon stressing, allowing penetration of high temperature air. Ingress of oxygen is also possible at ground surfaces prior to matrix crack initiation.[15] "Pipeline" oxidation can initiate at cut fiber ends which intersect the composite surface.

Although not yet fully understood, the elevated temperature embrittlement process has been linked to oxidation of the interfacial carbon layer, leading to: (i) fiber strength degradation and/or (ii) formation of a strong bond at the fiber/matrix interface.[17,19,20] Increased fiber matrix bond strengths have been measured in Nicalon/BMAS following elevated temperature exposure.[67] Strong bonding results when a bridging phase forms between the fibers and matrix following oxidation of the interfacial layer.[20] Nicalon/LAS appears to have less of a tendency to form a bridging interphase; extracted fiber studies showed the fibers are weakened and embrittled following high temperature exposure.[20,73] Thus,

fiber strength degradation is a contributing cause of embrittlement in the LAS system. Additional studies are needed to establish an increased understanding of the kinetics of the oxidation process.

In summary, the weak interfacial carbon layer which is essential for tough and strong composites at ambient temperature may prove detrimental at elevated temperatures. If oxidation of the carbon layer occurs, a strong interfacial bond forms and composite properties are degraded.

Laminate Configuration

Most theoretical and experimental treatments of brittle-matrix composites consider only unidirectional materials. Improvements in axial properties over the monolithic matrix materials are highlighted, but little coverage is given to the inferior transverse properties of these composites. The transverse properties of uniaxially reinforced ceramics are especially poor since they depend on the toughness of the matrix and interface directly, with no benefit of effects like fiber bridging.

The transverse tensile strength of unidirectional Nicalon/LAS was found to be substantially lower than the stress for matrix crack initiation in longitudinal tension.[11] Poor transverse tensile properties were also reported for a Nicalon fiber-reinforced glass composite; transverse failure strains as low as 0.03 to 0.04 % were measured.[66] Fracture was linear elastic in both cases. These results confirm the deleterious effect of weak bonding (required for optimum axial properties) on off-axis properties. The poor transverse properties of unidirectionally reinforced laminates limits their use since there are few engineering applications where transverse stresses are not encountered. To overcome this inadequacy, multidirectional laminates can be tailored to meet particular structural requirements. However, a thorough understanding of the damage development and failure processes of these materials is needed before they can be properly engineered.

Multidirectional CMC systems have not been widely characterized at either room or elevated temperatures. Except for early work at UTRC [11], little has been published. One preliminary investigation [18] studied crossplied Nicalon/LAS laminates at room temperature. (Failure analysis of multidirectional laminates is simplest for a crossply system.) Damage development occurred in several stages in the 0/90 LAS-matrix composite. Delamination cracks were the initial mode of stress-induced damage. These were followed by a succession of matrix cracking in the 90° plies, matrix cracking in the 0°

plies, and fiber fracture in the 0° plies. Catastrophic delamination caused ultimate composite failure. A typical room temperature stress-strain plot is illustrated in Fig. 2-10; discontinuities in the curve mark the onset of delamination and matrix cracking.

Additional studies of the mechanical behavior of other material systems and laminate configurations are necessary. Damage development must be better correlated with stress-strain behavior at both room and elevated temperatures. Improved experimental techniques, utilizing detailed microstructural investigations, will be required to better characterize the failure process of multidirectional laminates. A complete analysis of the mechanical behavior of multidirectional laminates must consider the effects of residual thermal stresses (due to fiber/matrix and ply/ply mismatch), and the possibility of delamination due to normal and shear stress concentrations at laminate edges.

Residual Stresses

Residual stresses are defined as those stresses remaining in a material in the absence of external loads or changes in temperature.[76] They vary in magnitude and can be either tensile or compressive, beneficial or detrimental. A compressive residual surface layer in glass is beneficial in preventing catastrophic failures. However, residual stresses can also initiate premature cracking which leads to ultimate failure of the material. The Eshelby [77] procedure is the most rigorous analysis for calculating microstructural residual stresses in homogeneous, isotropic materials.

Residual stresses often arise in composite materials due to differential thermal expansion/ contraction upon cooling from the fabrication temperature.[78] In metal and ceramic-matrix composites, residual stresses may also be related to unrelaxed volume changes associated with crystallization and phase changes. Resin shrinkage in the later stages of cure of polymer-matrix composites leads to microstresses which cannot be relieved.[51] The magnitude of residual stresses in composite materials may be sufficient to produce microcracking even in the absence of external loads. Premature failure is imminent if matrix residual stresses are a significant percentage of the matrix tensile strength.

In multidirectional laminates, residual stresses may also develop due to a property mismatch between adjacent plies (rather than the fiber and matrix). Thus, the residual stress distribution in the various plies of a laminate is dependent on ply stacking sequence and ply orientation. The distribution can be calculated using Classical Laminate Plate Theory (CLPT) [79] if the fiber and matrix thermal expansion coefficients and elastic

properties of the laminae are known. The temperature dependence of the thermal and elastic properties must be taken into consideration.

Residual thermal stresses are unavoidable in reinforced ceramics. Thermal stresses develop due to fiber/matrix thermal mismatch and substantial temperature drop after solidification. Thermal expansion mismatch is especially important in CMC's since fiber/matrix bonding is weak. Both longitudinal and radial residual stress components affect matrix fracture in CMC's. Radial residual stresses can have a significant influence on the frictional forces at the fiber/matrix interface. If the fiber expansion coefficient exceeds that of the matrix ($\alpha_f > \alpha_m$), separation of the fibers from the matrix is possible.[52] The frictional forces resisting fiber pullout decrease, accompanied by an increase in the debonding lengths. With respect to radial stresses, a small fiber expansion coefficient is beneficial.[78] However, if the expansion coefficient of the fiber is too small, large axial stresses develop in the matrix and cause cracking. Residual stresses parallel to the fibers superimpose directly on the applied stress and, therefore, control the opening of matrix cracks. A compromise must be achieved between a low α_f for beneficial interfacial stresses and a high α_f for axial properties. A small thermal mismatch is desirable, but if this is not possible $\alpha_f > \alpha_m$ is preferable because the fiber is better able to endure axial tensile strains.[68]

Most studies of residual stresses in composites have focused on metal and polymer matrix systems.[80-87] The effects of residual stresses have not been addressed adequately for reinforced ceramics. Marshall and Evans [12], and Sbaizero and Evans [18] alluded to residual stresses in their discussions of the failure mechanisms of undirectional and crossplied Nicalon/LAS laminates. However, further research is needed to establish a more thorough understanding of the effects of residual stress on damage development under both stressed and unstressed conditions.

Free Edge Effects

The in-plane failure modes already described are not the only means of fracture of laminated composites. In addition to longitudinal and transverse ply failure due to matrix cracking and ultimate fiber fracture, composite laminates can also fail by delamination. Failure of the thin matrix layer between plies can result in out-of-plane ply separations. Delamination failure should not be overlooked since it can occur at considerably lower loads than those which cause in-plane fracture. The onset of delamination may have a significant influence on the resulting failure process of the composite.

Delamination initiates at the free edges of composite laminates due to the effects of interlaminar stresses (σ_{zz}, σ_{2z}, and σ_{1z}). Analytical studies [88,89] have shown that the stress state in the vicinity of the free edge of laminated composites is fully three dimensional. Mechanical loading of the laminate causes interlaminar stresses to arise near the free edge. Residual thermal stresses formed upon cooling from the processing temperature also contribute to the development of out-of-plane stresses and associated edge cracking. In addition, the elastic property mismatch between adjacent plies must be considered in the development of interlaminar stresses at laminate free edges.

Interlaminar stresses are a result of the differences between CLPT, valid in the interior of the laminate, and the stress state at the free edge which must satisfy traction-free boundary conditions.[90] Fig. 2-11 illustrates the origin of these out-of-plane stresses for a simple $[0/90]_{nS}$ laminate under longitudinal loading. A tensile stress, σ_{zz}, exists at the edge and tends to peel the laminate apart. Delamination failure occurs at sufficiently large values of σ_{zz}. σ_{2z} is zero at the edge and the interior, with a maximum in between. σ_{22} rises from zero at the edge to its laminate theory value in the interior.

The out-of-plane stresses are localized and decrease to zero at the interior of the laminate. The magnitude of the interlaminar stresses is dependent upon the elastic properties of the laminae as well as the laminate configuration (i.e. ply stacking sequence, orientation, and thickness). The effect of free edges often extends into the laminate to a distance approximately equal to the thickness of the laminate. Thus, consideration of interlaminar stresses is most critical in finite width specimens. Free edge effects cannot be ignored in practical applications where holes and free edges are involved. An improved understanding of this insidious failure process is essential.

Numerous investigators [88-90,92-100] have studied the free edge delamination problem. Basic studies [88,89,93,94] have been directed towards understanding the nature of the free edge stresses. Analytical work [90,92,95-100] (including: finite difference and finite element methods, modified plate theory and energy methods) for predicting the initiation and growth of delamination is ongoing. All of the work to date has involved polymer-matrix composites.

A considerable free edge problem is expected in CMC's due to the large thermal residual stresses which result following processing. Delamination cracks have been observed as the initial form of stress-induced damage in a crossplied Nicalon/LAS laminate at room

temperature.[18] However, no studies have yet been conducted delineating the nature or extent of the problem. Further work (both experimental and analytical) is needed to examine this phenomenon in reinforced ceramics.

2.4 Theoretical Models of Brittle Cracking

The failure of CMC's is a progressive process dominated by matrix microcracking, and controlled by matrix flaws. The cracking process in unidirectional systems continues until the matrix has broken into fragments which are too small to be loaded to the breaking stress. In multidirectional composites, the damage development process is more complex and ply/ply load transfer must be considered, as well as fiber/matrix load transfer. Cracking of simple crossply laminates initially occurs in the transverse plies at strains considerably less than the failure strain of the longitudinal plies; longitudinal ply cracking follows. Several methods have been used to describe the cracking of composite laminates, including: energy-based approaches, statistical treatments and fracture mechanics analyses. The more relevant theories are described below.

Unidirectional Laminates

The mechanism of load transfer between fibers and matrix governs the degree of matrix cracking in unidirectional systems. If high strength fibers are employed, a saturation of microcracks can be achieved before fiber and ultimate composite failure.[55] The fibers remain intact and bridge the matrix cracks; fiber/matrix stress transfer occurs near to the crack face. At the crack position, the reinforcing fibers carry a maximum tensile strain since the matrix stress is reduced to zero. Differential movement occurs at the fiber/matrix interface as the matrix blocks relax elastically from their initial strain value upon cracking.

Energy-Based Models. The simplest stress transfer mechanism is frictional interaction, and assumes a constant interfacial shear stress, τ. The fibers and matrix are considered "unbonded" (i.e.there is no connection between the elastic displacements in the two components). Aveston, Cooper and Kelly (ACK) [55] established the theoretical framework of matrix cracking for this case. They derived an expression for the matrix crack separation using an energy-based analysis. The analysis considered the energy changes resulting when the matrix suddenly cracked on a plane normal to the fiber direction, leaving the fibers intact. The resultant crack spacing is between x' and 2x'. From a simple force balance, the lower limit is:

$$x' = \frac{V_m \sigma_{mu} r}{V_f 2\tau}$$

where, σ_{mu} = matrix failure stress
r = fiber radius
τ = interfacial shear stress due to friction.

If the specimen is unloaded after the formation of matrix cracks, a residual permanent extension of the composite remains due to the irreversible work dissipated by frictional losses.

The ACK theoretical model adequately describes the behavior if the interfacial bond is purely frictional. However, many reinforced ceramic systems exist in which chemical bonding and radial residual compression contribute to the interfacial bond. For these composites, little or no fiber sliding relative to the matrix may occur. Aveston and Kelly (101) revised the above model to account for purely elastic stress transfer, as well as partially debonded interfaces. For the case of purely elastic stress transfer with no fiber/matrix debonding, a shear lag analysis was employed to describe the enhanced stress carried by bridging fibers in the vicinity of matrix cracks. The stress enhancement decreases with increasing distance from a crack due to stress transfer to the matrix, and is expressed as:

$$\Delta\sigma = \Delta\sigma_o \exp(-\phi^{1/2} y)$$

where, $\Delta\sigma_o$ = stress enhancement (in a fiber) at the crack face
y = distance from the crack face
$\phi = \frac{2G_m E_c}{r^2 \ln(R/r) E_f E_m V_m}$
G_m = matrix shear modulus
$2R$ = distance between fiber centers
r = fiber radius.

The matrix cracks into blocks of length between l and $2l$ with:

$$l = \frac{-1}{\sqrt{\phi}} \ln\left(1 - \frac{\sigma_{mu} V_m}{\Delta\sigma_o V_f}\right)$$

If the appearance of the first matrix crack leads to partial debonding of the fiber/matrix interface, stress transfer takes place by frictional interaction over the debonded fiber length and by elastic effects at bonded locations. τ is not constant where the interface remains intact. Aveston and Kelly [101] predict a minimum crack spacing, L, for partially debonded fibers.

$$L = \frac{r\,\Delta\sigma_o}{2\tau'} - \frac{1}{\sqrt{\phi}}\left(\frac{\tau_u}{\tau'} + \ln\left(\frac{r\sqrt{\phi}\,(\Delta\sigma_o - \sigma_{mu}\,V_m/V_f)}{2\tau_u}\right)\right)$$

where τ' is the limiting shear stress at the fiber/matrix interface after debonding and τ_u is the shear stress at interfacial failure.

Fracture Mechanics Models. The energy-based analyses outlined above do not account for the dependence of matrix cracking on flaw distribution. Energy changes accompanying incremental changes in crack length are not considered. Recent work is directed towards developing a stress intensity criterion for fracture.[102] This approach should overcome the limitations of energy-based analyses, and provide greater insight into the processes involved in microcrack initiation and growth.

Marshall, Cox and Evans [102] developed a model which predicts a flaw size/failure stress relationship. They used a stress intensity fracture criterion to relate the applied stress to the size of a preexisting matrix crack. The theory predicts an increase in the stress for matrix microcracking as flaw size decreases for small flaw sizes. For cracks greater than a critical length, the matrix cracking stress is independent of flaw size and approaches the ACK value.

Current efforts are aimed at improving micromechanics treatment of cracking problems. Budiansky, Hutchinson and Evans [103] utilized a micromechanics analysis to describe the critical conditions for the onset of widespread matrix cracking in brittle-matrix composites with unbonded and partially debonded fibers. Their results generalize those of the ACK theory for unbonded fibers [55].

Multidirectional Laminates

Multiple cracking has been extensively characterized for crossply laminates of polymer-matrix systems.[104-109] Initial cracks develop in the transverse plies at strain levels considerably less than the failure strain of the longitudinal plies. Transverse ply cracking

represents the first phase of cumulative damage development in crossply laminates and must be accounted for in structural design. Although cracking of the transverse plies may render the laminate unsuitable for structural applications, the laminate continues to support an increasing load.

Cracks initiate in the transverse plies due to the brittle nature of the matrix, a lack of reinforcement in the loading direction, and stress concentration effects of the fibers. Transverse ply cracking continues as the load is increased. The crack development process is analogous to that of unidirectional composites with stress transfer occurring across the interply interface rather than the fiber/matrix interface Ply cracking may or may not result in debonding of the interply interface. Elastic stress transfer across the interply interface is possible when the interface remains intact. If the ply interface fails, stress transfer between plies occurs by frictional interaction if at all.

Although damage accumulation in crossplied CMC laminates has not been extensively characterized, the cracking processes described for crossplied polymer-matrix composites are expected to be applicable. However, some modifications are necessary to account for matrix brittleness. In CMC's, cracking occurs in both the longitudinal and transverse plies.[18] Interply load transfer shifts the load to the longitudinal plies following 90° ply cracking. The situation in the longitudinal plies resembles that outlined above for unidirectional laminates, and longitudinal ply cracking ensues due to the low matrix failure strain. Cracking of the longitudinal plies causes a reduction in stiffness. The decreased stiffness of the longitudinal laminae must be considered in analyzing the behavior of crossplied CMC's.

In polymer-matrix composites, transverse ply cracking continues with increasing strain until a limiting crack spacing is reached.[104,105] The saturation level of cracking is dependent on the geometry of the laminate. Generally, the limiting crack spacing increases as the transverse ply thickness increases, owing to more difficult stress transfer between plies.[105] Suppression of transverse cracking in crossply laminates has been observed for low transverse ply thicknesses.[106-108] When the transverse laminae are very thin, the onset of cracking is partially or completely suppressed because insufficient elastic strain energy is released by crack nucleation and growth. Similar behavior is also expected for CMC's. Transverse ply cracking in reinforced polymer laminates may also be inhibited due to longitudinal ply constraint. However, in CMC laminates, these constraints may be considerably reduced due to longitudinal ply cracking and/or residual stress effects.

Energy-Based Models. The energy-based approach is perhaps the simplest method of analyzing cracking in crossply laminates. Garrett and Bailey [104] were first to extend the multiple cracking theory of Aveston and Kelly [101] to crossply laminates. Based on experimental findings for a fiberglass/polyester system, they derived a relationship between the transverse crack density and the applied stress. A non-uniform redistribution of load between the plies, due to 90° ply failure, accounts for the increasing density of cracks with strain. [104,105]

The original Garrett and Bailey [104] theory underestimated the crack spacing for a given applied stress. Parvizi and Bailey [105] resolved this discrepancy by recalculating the value of the maximum additional stress, $\Delta\sigma_0$, carried by the longitudinal ply at a crack face. These theories [104,105] are based on shear lag analysis in which the plies remain elastically bonded. Shear lag theory was used to predict the redistribution of stress after formation of a transverse crack. Subsequent transverse cracks are assumed to occur midway between two existing cracks. However, this extreme situation cannot be guaranteed and flaw populations and statistics need to be considered.

Bailey, Curtis and Parvizi [109] later revised the above treatments to include the effects of thermal stresses developed during composite fabrication. Their energy constraint concept was used to predict both longitudinal splitting and transverse cracking behavior. They showed that the transverse ply cracking strain is reduced by an amount equal to the thermally developed tensile strain in the transverse ply.

The Garrett/Bailey/Parvizi analysis is based upon the existence of cracks spanning the entire thickness of the 90° ply (a fixed ply thickness) and does not consider the crack growth mechanism. A fixed fracture strain is utilized for a particular transverse ply thickness. This is invalid if flaw statistics are considered. The aforementioned theories proved useful in establishing a basic understanding of the cracking process in crossply laminates. However, a more generally applicable model, incorporating flaw statistics and crack growth mechanisms, is needed.

Recently, Han, Hahn and Croman [110] used the concept of a through-the-thickness inherent flaw, in conjunction with energy balance principles, to evaluate transverse crack initiation and multiplication in symmetric crossply laminates. Hahn and Johannesson [111] previously showed that the growth of a through-the-thickness flaw is stable since the

energy release rate associated with such a flaw is independent of its length. Using fracture mechanics, Han, et al.[110] determined the energy released due to transverse ply cracking and employed this to predict the increase in crack density. They proposed a resistance curve as a measure of the resistance to crack multiplication. The R-curve increased with increasing crack density. Although this model considers the effects of flaws, only a two dimensional stress analysis is applied. A three-dimensional analysis is necessary to fully describe the growth of cracks in crossply laminates.

Statistical Models. Transverse ply cracking in crossply laminates is believed to be sensitive to inherent flaws (e. g. voids, debonded fiber/matrix interfaces, microcracks, broken fibers). These microflaws act as local stress risers when external loading is applied or a temperature change is incurred. First cracking is governed by the most severe flaw. Further transverse cracking is dependent on the flaw distribution as well as the stress in the 90° ply. The energy-based analyses are deterministic and cannot fully account for the presence of flaws. A statistical approach is more realistic and has been attempted by several investigators.[112-115]

Peters [112] attempted to relate the thickness dependence of the transverse cracking strain to statistical phenomena (i.e. thicker 90° plies statistically contain more flaws and, therefore, crack growth is more likely at a low strain.) The transverse ply fracture strain was estimated by a two parameter Weibull model for different 90° ply thicknesses. For small transverse ply thicknesses, the Weibull shape factor was found to increase with decreasing ply thickness. Higher stresses are needed to initiate cracking in thin 90° plies. The shape factor for thick 90° plies is similar to that for unidirectional transverse laminates. The variation of the shape parameter with ply thickness precludes a description of the thickness effect by a Weibull shape parameter.

Other models have been developed to describe the statistical variation in strength of the transverse ply.[113,114] Manders et al.[113] showed that an analysis based on a unique value of strength for the 90° ply (i.e. Garrett/Bailey/Parvizi [104,105]) cannot fully account for the transverse crack spacings measured in a $[0/90]_S$ fiberglass/epoxy laminate. They considered the statistical variability of the 90° ply at a given stress level. A Weibull distribution of strength of the 90° plies was shown to adequately describe the crack spacings. The Weibull shape parameter was calculated based on the measured crack spacings.

Fukunaga, Chou, Peters and Schulte [114] further refined the approach of Manders, et al.[113] to study the failure characteristics of graphite/epoxy crossply laminates. In addition to the variability in 90° ply strength, thermal residual stresses and Poisson effects were considered. A two-parameter Weibull distribution of the 90° ply strength was also used, and the stress redistributions at transverse ply failure were analyzed by a shear lag model. Cracking was assumed to occur midway between any two adjacent cracks at a 50% failure probability. Formulae for determining first cracking, subsequent multiple cracking and ultimate fracture were derived. A good correlation between measured and calculated crack spacing was found. This analysis, like that of Manders, et al. [113], does not account for the flaw distribution of the laminate. Fracture mechanics concepts need to be combined with a better description of the flaw population to adequately describe cracking behavior.

Wang, et al.[115] introduced the concept of an effective flaw distribution as a basic ply property to replace the conventional constant ply strength criterion. Multiple transverse ply cracking was described by a stochastic procedure, incorporating the effective flaw distribution concept. Normal distributions were used to characterize the flaw size and spacing. Through-the-width flaws were assumed, in contrast to the through-the-thickness flaws [110] discussed earlier. Crack density was predicted as a function of laminate stress, using a simulation technique and fracture mechanics concepts. This approach has also been used for predicting the growth behavior of free edge delamination under both static and cyclic stresses.

The concept of an effective flaw distribution is progress towards the development of a better description of the flaw population. However, the assumption of a through-the-width flaw limits this model to two dimensions. A three-dimensional representation is needed. Then, the flaw population must be correlated with fracture-mechanics concepts to fully understand the mechanism of flaw growth.

Fracture Mechanics Models. Wang and coworkers [90,97,100] are responsible for most of the fracture mechanics analyses of crossply polymer laminates. They utilized an energy release rate approach to explain and predict the basic mechanisms of transverse ply cracking under monotonic loading. This approach has also been applied to model the various matrix crack interactions which occur during the later stages of loading.[116] The energy release rate, G, was obtained as a function of crack length by finite element methods. G for a specific laminate can also be calculated by a numerical procedure based on ply elasticity.[117]

The initiation of transverse ply cracking is predicted when the available energy release rate equals the critical energy release rate for the material. Good correlation was observed between experimental findings and the analytical prediction. The usefulness of the energy release method has also been established for predicting the growth behavior of free edge delamination.[90,97] Prediction of the initial mode of damage can be determined from a comparison of the stresses required to initiate transverse cracking and delamination.

The fracture mechanics model of Wang, et al.[90,97] requires knowledge of only one material parameter, the critical strain energy release rate. The critical strain energy release rate can be determined experimentally; the strain energy release rate curve for transverse cracking must be calculated. Unlike other treatments, the model is sufficiently general that it can be used to make predictions rather than just observations. However, it neglects flaw statistics and only utilizes a two-dimensional stress analysis. Real crack geometries are combinations of interlaminar and intralaminar components and, therefore, require a three-dimensional stress analysis for realistic modelling of the progressive cracking process in crossply laminates. Such a model should also incorporate flaw statistics, as well as residual stress effects.

A recent model proposed by Laws and Dvorak [118] comes closest to fulfilling these requirements. Their analysis, based on statistical fracture mechanics, provides a well-defined model of transverse cracking in crossply laminates. A shear lag parameter is introduced to account for sub-optimum shear stress transfer at the ply interfaces. All parameters used in the analysis can be determined by standard tests; no adjustable parameters are needed to fit a particular set of experiments. The shear lag parameter is inferred from standard data and knowledge of the first ply failure stress. The defining equation is:

$$\sigma_a^{fpf} = \left(\frac{\xi b E_l E_o G_c}{d(b+d)E_t}\right)^{1/2} - \frac{E_o}{E_t}\,\sigma_t^R$$

where, σ_a^{fpf} = applied stress at first ply failure

ξ = shear lag parameter

d, b = thickness of 90° and 0° plies, respectively

E_t,E_l = moduli of 90° and 0° plies, respectively

E_o = modulus of the uncracked laminate

G_c = critical strain energy release rate

σ_t^R = thermal residual stress in 90° plies.

The model delivers explicit formulae for stiffness loss as a function of crack density, and for crack density as a function of applied load. The main difference between this model and other treatments lies in consideration of the statistics of progressive cracking, as well as the existence of residual stresses. The approach supposes that a transverse crack will occur propagate when it is energetically favorable to do so. The location of this transverse crack is associated with a probability density function, chosen to be proportional to the stress in the transverse ply.

Since the Laws and Dvorak model most closely fits the criteria for an adequate model, it will be analyzed more closely later in this thesis. However, it will be necessary to modify the analysis to account for longitudinal ply cracking in crossplied CMC laminates.

3. EXPERIMENTAL PROCEDURE

3.1 Materials

Four developmental ceramic-matrix composite systems were investigated:

(1) Nicalon/1723 Glass

(2) Nicalon/CAS (calcium aluminosilicate)

(3) Nicalon/LAS-III (lithium aluminosilicate)

(4) Nicalon/BMAS-III (barium magnesium aluminosilicate)

These were supplied by Corning Glass Works in the form of unidirectional and crossplied laminate plates. Plates for high temperature testing measured 15.24 cm by 15.24 cm, while those for room temperature were 10 cm by 10 cm. All were fabricated by hot pressing of unidirectional tapes. The glass matrix composite (Nicalon/1723) was hot pressed at approximately 620°C. The other systems utilized glass-ceramic matrices and were given a subsequent crystallization treatment to increase matrix refractoriness. Ceraming temperatures exceeded 1000°C in all cases.

All of the composites studied were reinforced by continuous Nicalon fibers. The fibers are primarily silicon carbide, in an amorphous or crystalline form, with appreciable amounts of SiO_2 and free carbon. They are produced by the thermal conversion of a polycarbosilane precursor fiber [6], and are marketed by Nippon Carbon Company. Throughout this work, the term "Nicalon" will refer to the lower oxygen content version of the microcrystalline β-SiC, SiO_2, C mixture. The chemistry of this fiber, as reported by Simon and Bunsell [40], is 49 mole % SiC, 40 mole % C and 11 mole % SiO_2.

Four different matrices were examined: three crystalline glass-ceramic matrices (LAS-III, CAS-II, BMAS-III), and a non-crystalline glass matrix, Corning Code 1723. Lithium aluminosilicate (LAS) has been used extensively as a matrix material in these composites. The lithium aluminosilicate matrix studied in this work is LAS-III, developed jointly by Corning and UTRC.[32] When well-crystallized, the matrix phases are β-spodumene SS, mullite and NbC.[9] In the as-pressed condition, β-quartz is the primary microstructural constituent and the use temperature is lower than for well-crystallized systems. Some of the Nicalon/LAS laminates investigated contained β-quartz. Calcium aluminosilicate (CAS) and barium magnesium aluminosilicate (BMAS) offer improved matrix refractoriness. The BMAS-III matrix is based on barium osumilite and has a 100°C higher use temperature than LAS-III. CAS-II, composed primarily of stoichiometric anorthite, $CaAl_2Si_2O_8$, maintains excellent properties at temperatures approaching 1200°C. The Code 1723 glass is an

alkaline earth aluminosilicate composition which does not contain any alkali metal oxides. Composition and mechanical properties of the glass/glass-ceramic matrices and the Nicalon reinforcing fibers are summarized in Table 3-1.

The four composite systems were chosen such that the effects of varying interfacial strength and thermal expansion mismatch on mechanical behavior could be evaluated. The Nicalon/1723 and Nicalon/CAS systems have similar radial residual compressive stress fields due to a positive fiber/matrix thermal expansion mismatch (i.e. $\alpha_m > \alpha_f$). Radial residual compressive stresses can increase the resistance to debonding, and lessen the extent of fiber sliding after debonding. Although the thermal stability of the non-crystalline 1723 glass matrix is markedly inferior to the crystalline CAS matrix, it is a relatively reproducible system which is suited for experimental study. The thermal expansion coefficients of BMAS and LAS are smaller than that of the Nicalon fibers. In contrast to Nicalon/1723 and Nicalon/CAS, these composites exhibit a radial residual tensile stress at the fiber/matrix interface which assists debonding. The ply level residual stresses in crossplied laminates are also of opposite sense for the 1723 and CAS systems vs. BMAS and LAS.

Both unidirectional and multidirectional laminates were studied. The unidirectional composites served as a basis for analysis of the multidirectional systems which are more practical for structural applications. Crossply laminates were chosen for ease of analysis compared to angle-ply laminates. Specific laminate configurations varied depending on the materials supplied. However, in all cases, 10-20 μm diameter Nicalon fibers served as the reinforcing agent and fiber contents were approximately 35-45 vol %. Ply thicknesses were in the range of 0.2-0.3 mm. A typical 0/90 configuration is illustrated in Fig. 3-1.

3.2 Tensile Testing

Equipment

Initial System. Tensile tests were initially conducted on an Instron Model 1331 closed loop, servohydraulic dynamic test machine, equipped with a 10 kip load cell and a high temperature furnace system (Instron model SF375B). The furnace system is designed for testing to 1000°C. It includes a three-zone split furnace, microprocessor controller, water-cooled alignment rings, reverse stress pull rods, and an external axial quartz rod extensometer (Instron series 2632). Specimen heating was by radiation from Kanthal heating elements, and Type K chromel-alumel thermocouples were used to monitor temperature. The heating rate was microprocessor controlled to minimize overshoot and

smoothly ramp the temperature to the desired value. The entire test setup is described in more detail in Refs. 15 and 66.

Unidirectional and crossply laminates were tested in air at both ambient and elevated (>500°C) temperatures. Room temperature tests were performed on Nicalon/1723, Nicalon/BMAS and Nicalon/ CAS laminates using this facility. High temperature tests were also conducted on Nicalon/BMAS and Nicalon/CAS at 1000°C, and Nicalon/1723 at 500 and 600°C. Specimens were oriented with the tensile axis parallel to the fibers in the 0° plies. All tests were performed in stroke control using a displacement rate of 1.27 mm/min (0.05 in/min). Heatup for the high temperature tests was conducted in load control to prevent premature specimen failure due to stress generation as a result of thermal expansion of the specimen and grip system. Heatup times varied with test temperature, but generally 1 to 2 h was necessary to ensure stabilization.

Stress-strain data were obtained during each test run using X-Y recorders and computer acquisition. At room temperature, strain was monitored with SR-4 strain gages mounted back-to-back on the specimen surfaces with a cyano-acrylate adhesive. The high temperature, quartz rod extensometer was used on one specimen surface only. Use of the extensometer necessitated removal prior to specimen failure to prevent damage to the quartz contact rods. The rods rested in indents on the specimen surface which were machined with a carbide center drill to an approximate depth of 0.18 mm.

Primary System. An Instron 1361 servoelectric machine, equipped with a 20,000 lb load cell and water-cooled modular hydraulic grips (Instron series 2742), was acquired later in the test program. It is particularly suited to testing of brittle materials due to a highly accurate drive system which ensures long term stability. Precision alignment of the grips ensured against possible bending effects. All subsequent tensile tests and damage development studies were performed with this setup. The machine was outfitted with a specially designed front access furnace (Centorr Model S60). The 10.16 cm long furnace consists of a zirconia shell and is capable of attaining temperatures of 1600°C. Fig. 3-2 shows the elevated temperature test assembly.

Since the hydraulic grips were external to the furnace, at least 15 cm long specimens were necessary. Specimen heatup was accomplished by resistance heating from four super Kanthal elements. Temperature was monitored with a Type R, platinum-rhodium thermocouple; a Type W, tungsten-rhenium thermocouple was used to control the

overshoot. These were drawn through access ports in the furnace. An additional port was used for a high temperature extensometer (Instron series 3118). The extensometer has high purity alumina knife edges, enabling its use at temperatures up to 1500°C. It uses a capacitive transducer to monitor changes in axial strain and, therefore, only a minimal specimen contact force is necessary with no surface indentations. An amplifier unit linearizes the capacitance signal, and conditions the output such that strain may be read directly in volts. In contrast to the earlier model, removal of the extensometer was not required prior to specimen failure.

Specimen Design

Specimens were made from straight-sided coupons which were cut from the composite plates with a diamond cutting wheel. Plate edges were trimmed prior to cutting the specimens to ensure aligned microstructures. Three different specimen geometries were used, dependent upon test temperature and ply configuration. These are depicted in Fig. 3-3. For room temperature tests of unidirectional laminates, tapered aluminum tabs were adhesively bonded (with epoxy) to the ends of flat test coupons (Fig.3-3a). A thickness-tapered specimen (Fig. 3-3b), developed by Grande, et al. [15,66], was employed at high temperatures for unidirectional laminates.

The high temperature specimen has a constant width, but a reduced thickness in the gage section to ensure a gage section failure. The thickness at the center of the specimen was reduced by a two-stage grinding procedure. A 76 mm radius, 300 grit diamond wheel was used for grinding. First, 5° shoulder tapers were machined. This was followed by thickness reductions in the gage section to 1.02 mm. There is a smooth transition between the gage section and the tapered shoulders. The 5° shoulder tapers terminate in the end portion of the specimen which has parallel sides. Further details of the grinding procedure are given in Ref. 15.

The above designs proved unsatisfactory for tensile testing of crossply laminates. Many tabbed crossply laminates failed prematurely near the loading tabs in room temperature tests. In addition, surface grinding of a thickness-tapered specimen for high temperature work resulted in surface layers of varying orientations and a non-structurally symmetric specimen. A constant thickness, width-tapered specimen with double-pinned grips (Fig. 3-3c) was designed to overcome these problems. It was machined using a 51 mm diameter, 300 grit diamond grinding wheel. Holes (2.4 mm diameter) in the specimen ends were drilled with diamond-coated drill bits. This specimen has been utilized successfully for

both ambient and elevated temperature testing of crossply laminates. The design is ideally suited for multidirectional laminates since it precludes the need for surface grinding.

The gripping mechanism for tensile testing varied with specimen type. For tabbed or thickness-tapered specimens, a self-wedging grip was used. Gripping was accomplished with wedge blocks, machined to match the 5° tapers on the specimen shoulders or tabs. Thus, any tendency of the specimen to split longitudinally from the shoulder was suppressed by the generation of compressive forces in the shoulder regions during tensile loading. The wedge inserts were contoured to fit into the high temperature grips supplied by Applied Test Systems Inc. (4053A Wedge Couplings) as shown in Fig. 3-4. Both the ATS grips and the wedge inserts were made of Inconel to ensure use at temperatures up to 1000°C. For width-tapered specimens, a pinned-grip arrangement was utilized. Two 2.4 mm diameter Inconel pins were used at each end to align the specimen and wedge inserts, and provide initial load transfer between the wedge blocks and the specimen.

Fracture Surface Analysis

Fracture of the composites of interest was extensively characterized with the scanning electron microscope (SEM). Two models were used: (i) an AMR model 1500, and (ii) a Cambridge Stereoscan model 250, Mk 3. Both were operated at an accelerating voltage of 20 kV. The Cambridge was used more frequently for fractographic investigations since better resolution was possible with this instrument. Minimal specimen preparation was required. Fractured specimen halves were mounted without modification in the microscope stage. To minimize surface charging, specimens were gold coated prior to SEM examination.

The SEM was used to investigate the extent of matrix cracking, characteristics of fractured fibers and the degree of fiber pullout following tensile failure. Specimen surfaces were examined in the vicinity of the fracture to determine the degree of matrix cracking. Crack spacings and fiber pullout lengths were measured from SEM micrographs.

3.3 Damage Development Studies

To more accurately characterize the failure process, damage accumulation was monitored in unidirectional and crossply laminates. Damage development in the off-axis plies of the crossply laminates is of particular interest since cracking of these plies will constitute the first permanent damage in actual service applications. Matrix cracking in the longitudinal

plies, delamination, and fiber fracture were also investigated. Schematics of these damage types are given in Fig. 3-5.

Conventional methods used for monitoring damage in polymer-matrix composites were not directly applicable due to the opacity of ceramic-matrix composites and matrix crack closure problems. Other techniques explored, including: optical and stereomicroscopy, Nomarski interference, dilute hydrofluoric acid etching, ion milling and dye penetrant methods, were not successful for observing cracks apparently due to crack closure upon load release. Therefore, it was necessary to monitor damage development while specimens were under load. Two in-situ techniques (direct observation of flexure tests, and a replication method) were developed and are described below. Each requires careful specimen surface preparation.

Specimen Preparation and Polishing

Specimen geometries differed depending on the technique used to monitor damage development. For flexure tests, rectangular coupons were cut measuring up to 9.4 cm long and wider than 0.5 cm. A specimen span:depth ratio of 30:1 was used to minimize shear effects. For the replication procedure, room temperature tensile specimens measured 10 cm by 0.76 cm; specimens for high temperature tests were cut to 15.24 cm by 1.02 cm. Tapered, 1.6 mm thick Al tabs were attached to the ends of replication specimens with American Cyanamid FM-123 film adhesive. This required a 2 hour cure at 98°C. The adhesive proved adequate for high temperature testing (i.e 550°C) since the grips were water-cooled. Schutz [91] reported a temperature rise in the Al end tab of only 14°C during heating to 1200°C.

Polishing of the edge of replication tensile samples and the surface of flexure samples was necessary to clearly observe damage. The high pressures and long times necessary to polish ceramic-matrix composites to a smooth surface finish, in conjunction with large specimen sizes, made an automatic polishing method imperative. However, commercially available automatic machines are limited to smaller specimen geometries.

A semi-automatic polishing device was designed to overcome these problems. It consists of a rigid plate with cutouts for 3-10 cm long tensile (or flexure) specimens and 3 metallographic mounts. Two of the tensile cutouts can also accommodate 15.24 cm long, high temperature replication samples. The plate is situated atop a 20.32 cm diameter polishing wheel and attached to the polishing table by four stainless steel shafts. (See

diagram, Fig.3-6.) Sample holders equipped with weights were precision fit to the cutouts to minimize specimen rocking. The device did not decrease the polishing time required for a satisfactory surface finish, but process efficiency was greatly improved since several samples could be polished simultaneously.

All specimens were polished using this device. First, specimens were rough polished with a series of SiC papers (i.e. 240, 320, 400, 600, 800, 1000, 1200, 2400 and 4000 grit) and ethylene glycol as a lubricant. Several minutes of polishing time were required for each grit size. This was followed by diamond polishing (9, 6, 3 and 1 μm) on a silk cloth with lapping oil. Longer polishing times were necessary for each step in this series, thus mandating frequent replenishing of the diamond supply.

Nicalon/1723 and Nicalon/CAS composites were satisfactorily polished using this procedure. However, many difficulties were encountered with LAS and BMAS-matrix composites. The high radial residual tensile stress field at the interface (due to $\alpha_f > \alpha_m$) and the particular interphase characteristics of these two systems resulted in chipping and debonding near the interface during polishing. Polishing times of approximately 8 hrs/grit size were needed during diamond polishing to achieve a satisfactory surface for damage development studies.

Direct Observation of Flexure Tests

Although flexure testing of ceramic composites is unsatisfactory for design purposes, a better understanding of crack growth is possible by observing bend samples in-situ in the SEM. A four-point bend apparatus was designed and built for easy incorporation into the specimen chamber of the Cambridge SEM. (See sketch, Fig. 3-7) Prior to introduction into the SEM, flexure specimens were strained to the onset of matrix cracking while viewing the tensile surface under a stereomicroscope. Strain gages, mounted on the compression side of each sample, were used to monitor strain. After straining, the entire bend fixture and strained sample were gold-coated to minimize charging effects.

The flexure test samples were examined in-situ by mounting the gold-coated, four-point bend fixture in the SEM specimen chamber. Strain levels were maintained during SEM investigations by tightening the lock nut on the loading pin. Unidirectional Nicalon/1723 and Nicalon/BMAS laminates were studied. Specimens were investigated to uncover differences in fracture behavior related to the particular matrix material, and, thus, residual

stress state. It was of special interest to determine if fiber/matrix sliding was operative in specimens with different residual stress states at the fiber/matrix interface.

Replication

Replication techniques have proven useful in damage development studies of resin [119-123] and metal-matrix composites [124] where surface replicas were used to highlight transverse cracking. These techniques were adapted in the present study to investigate damage development in CMC laminates. Replication is especially advantageous since crack details can be captured while the specimen is loaded in tension and cracks remain open. Specimen removal or destruction is not necessary.

An edge replication technique was applied at room temperature to unidirectional and cross-plied Nicalon/1723, Nicalon/CAS, and Nicalon/LAS composites. Prepolished, tabbed samples were loaded in tension in the Instron 1361 servoelectric machine. During loading, each test was interrupted periodically to obtain replicas at a progression of strain levels (at least 5 different points along the stress-strain curve). An imprint of the damage accumulation was obtained at each loading step by applying cellulose acetate tape to the specimen edges, with acetone as a wetting agent. The procedure is illustrated in Fig. 3-8. At least several minutes drying time was necessary before removing the replica from the specimen edge and attaching it to a microscope slide.

All tests were conducted in stroke control at a very slow ramp speed (0.127 mm/min). During replication, the stroke ramp was switched to the hold position. Hold times of approximately 30 min. were required at each step in order to obtain several replicas (at least three/condition). A slight load drop and small strain increases were not uncommon during the replicating procedure since cracking continued even though the applied load was held constant. Strain was monitored during testing via strain gages which were carefully mounted to the specimen surfaces to minimize damage to the polished edges. To ensure a high level of accuracy, especially at low strains, data were acquired continuously during testing using the computer and ASYST data acquisition system.

The replication technique was also adapted for damage development investigations at high temperatures. 550°C was chosen as the high temperature of interest since the 1723 glass matrix softens at approximately 600°C, and a comparison of damage accumulation in the CAS, LAS and 1723 composite systems was desired. This temperature should be sufficient to allow release of residual stresses which may exist at room temperature

following high temperature processing. Thus, the effects of residual stresses on damage development were investigated by comparing room temperature results with those obtained at 550°C.

Each specimen was first mounted in the hydraulic grips and heated to 550°C. Before heatup and testing, replicas were taken of the as-polished surface both before and after gripping. Gripping and heating were performed in load control to prevent accidental overloading. Heatup times were typically 2 h with an additional 0.5 h hold to ensure temperature stabilization. Following heatup, the grips were retightened to prevent slippage during testing, the machine was switched to stroke control (for loading) and the high temperature extensometer positioned against the specimen. Specimens were loaded to a selected strain level at a displacement rate of 0.127 mm/min. The applied load was removed before cooling to room temperature, and the machine returned to load control. The cooldown period was approximately the same duration as the heatup (2 h) to prevent thermal shock. A low tensile stress (~ 20 MPa) was maintained during heating and cooling to ensure against accidental compressive load excursions.

Replicas were taken after the specimen and chamber returned to ambient temperature. Each specimen was then reloaded slightly (to a strain level beneath which matrix cracking initiates at room temperature) and replicas taken as described for the room temperature case. Specimens were reloaded to approximately 0.02-0.03 % using a slow stroke ramp. Reloading was necessary to open the cracks enough so that they could be clearly imprinted on the replicas. If additional replicas were desired at higher strains, specimens were reheated and successively reloaded to higher strain levels. The same heatup/load/ cooldown/reload/replication cycle was repeated until the failure strain of the composite was reached. At least two cycles were performed on each high temperature specimen.

Replicas were examined by scanning electron microscopy since it was found to yield clearer images of damage accumulation than optical or stereomicroscopy. Individual replicas, mounted on microscope slides, were gold coated to improve conductivity and prevent excessive charging. The sequence of replicas was then examined in the SEM to determine the extent of cracking. Low accelerating voltages (5 kV) and large beam diameters (spot size = 3) were necessary to prevent excessive damage to the cellulose acetate replicas. Representative photographs were taken at each strain level for subsequent crack spacing measurements.

Image Analysis

Crack spacings from replicas were measured in each SEM photograph using an MOP-Videoplan image analysis system. The system, manufactured by Kontron Electronics, is designed for data acquisition and computation of geometric characteristics by tracing structures of images on a digitizer tablet. After inputting the appropriate scaling factors, crack spacings were readily calculated by guiding a magnetic cursor over each photograph when placed on the digitizer tablet. Measurements were only made for cracks which extended across the entire ply thickness. A standard measuring program was used to compute crack spacing statistics for each individual ply as well as an average for all plies in the laminate. Gaussian distributions were obtained for each data set based on absolute and cumulative frequency.

3.4 Bond Strength Measurements

Fiber/matrix bond strengths of the various composite systems were measured using a microdebonding test method developed by Mandell, et al.[69,125]. Originally developed for polymer-matrix composites, this indentation technique has also been applied to metal, glass and glass-ceramic matrix composites [15,67,126,127]. The microdebonding test yields a quantitative measurement of the shear strength at the fiber/matrix interface. The apparatus and loading scheme are illustrated in Fig. 3-9. Details of the test assembly, experimental procedure and analysis are described in Refs. 67, 126 and 127.

The microdebonding test involves compressively loading the ends of individual fibers in composite specimens. Specimens are oriented such that the fibers of interest are aligned normal to the polished surface. The selected fiber is incrementally loaded, with the bond viewed optically between steps, until debonding is observed. The average applied compressive stress on the fiber end at debond initiation is the quotient of the measured debonding force and the fiber cross-sectional area. The interfacial shear strength at debonding is then calculated using a finite element model.

Well-polished specimens are required for the microdebonding test. A smooth, flat surface, free of interface discontinuities, is essential so that debond initiation is clearly visible. Differential wear of the fibers and matrix during polishing must be avoided. For the ceramic composite systems of interest, this was accomplished using the polishing procedures described earlier. All specimens were polished to a 1 μm diamond finish.

Fiber/matrix bond strengths were measured on several types of specimens. To determine the effects of bond strength on damage initiation and bond strength changes associated with damage development, microdebonding was performed on damage development samples both before and after testing and replication. Non-destructive measurements were possible in the 90° plies of crossply samples by mounting the tensile specimens on edge in a fixture designed for this purpose. Most microdebonding tests were conducted near the sample ends since only minimal variations in bond strength were observed between the end and mid sections of the samples. Bond strength measurements of unidirectional samples or the 0° plies of crossplied specimens required cutting, sectioning and mounting the specimens in bakelite or epoxy. Some tensile test samples were also sectioned and mounted for microdebonding following tensile loading. Bond strength variability was investigated by performing microdebonding tests at various locations throughout the cross-section. A series of microdebonding tests at increasing depths beneath the specimen surface were performed on oxidation samples. (See following section for more experimental details.) These were mounted, polished and debonded in a holder designed for easy specimen manipulation.

The microdebonding test was run on individual selected fibers in a polished sample. At least 10 fibers per sample were evaluated, and the results averaged to obtain an adequate measure of bond strength. The diameter of the tested fiber and the distance to the nearest-neighbor fiber were measured in each test using the scale in the microscope eyepiece. These were incorporated in the finite element analysis for calculation of the shear strength of the fiber/matrix interface. A very simplified axisymmetric (cylinder) geometry was employed to model the stress field generated by the probe loading. The cylindrical model consisted of the fiber, surrounding matrix material of constant thickness, and averaged composite properties beyond the matrix. Linear elastic behavior is assumed; residual thermal stresses are included in some cases. The analysis is described in detail in Refs. 15, 67, 69, and 125-127.

3.5 Oxidation Studies

Interface oxidation governs the behavior of ceramic matrix composites at elevated temperatures. The Nicalon/CAS-IIb system was investigated to increase our understanding of the kinetics of the oxidation reaction. The CAS-IIb matrix is generally similar to the CAS-II matrix described earlier. The effect of oxygen tunnelling from exposed fiber ends was examined by determining variations in bond strength at specific depths below an oxidized surface.

Small unidirectional samples of Nicalon/CAS-IIb (< 1 cm^2) were exposed in air to temperatures of 800°C, 1000°C and 1200°C for differing durations (0.5h, 5h and 50h). All sample ends were polished to a 1 μm diamond finish prior to elevated temperature oxidation to guarantee exposure of fiber ends and to ease the burden of polishing following oxidation. Other edges of the samples were ground by Corning Glass. To prevent thermal shock, specimens were exposed during furnace heatup. An older tube furnace, heated by glowbars, was utilized for the 800°C and 1000°C exposures; a 6 h heatup time was required. Only a 2 h heatup was necessary for the 1200°C exposures since a newer Lindbergh box furnace was used. Thus, heatup times were not identical for all cases.

Following oxidation, all samples were ground and repolished to a 1 μm diamond finish. This was accomplished using a sample holder specifically designed for this application and noting the grinding depth. Bond strengths were then measured on all samples at specific depths below the oxidized surfaces. (See sketch, Fig. 3-10.) More extensive grinding was necessary for measurements at large depths into the samples. Bond strength vs. depth (along the fiber axis) profiles were determined at each exposure temperature. Microdebonding tests were performed along the specimen periphery, as well as the interior. Hence it was possible to measure the bond strength gradient inward from the exposed sample ground edges, perpendicular to the fibers.

4. RESULTS AND DISCUSSION

The results of the experiments outlined in the previous chapter are discussed below. First, the ambient and elevated temperature tensile behavior of the composite systems is reported. The fracture resistance of unidirectional and crossply laminates is explained on the basis of fractographic investigations, and the magnitude of residual stresses and fiber/matrix bond strengths. Second, interface oxidation studies of Nicalon/CAS-IIb are discussed. Interfacial bond strengths have been correlated with oxidation kinetics in an effort to increase the current level of understanding of the elevated temperature embrittlement process. Findings from the damage development studies are included in the final section of this chapter. Measured crack spacings compare favorably with a theoretical model which was developed for predicting crack density as a function of applied stress. Theoretical modelling details are reported in Chapter 5.

4.1 Tensile Behavior

Room and elevated temperature tensile test results are summarized in Tables 4-1, 4-2 and 4-3. Ultimate stress and strain, and initial composite modulus are given for each test specimen. Specimens are identified by a code: the number corresponds to the composite plate from which the specimen was taken and the letter distinguishes the particular test run. Appendix A enumerates the composite plates obtained from Corning during the course of this investigation. Tensile properties were derived from a single test of each specimen, except for specimens marked with an asterisk (*). These specimens were used in damage development studies and loaded in a series of steps. The failure stresses and strains reported for the damage development specimens are from the final loading step, and the modulus from the initial cycle.

The mechanical properties listed in the tables are for less than optimal materials, and may not be useful for design predictions. However, mechanical property measurements are not the intent of this thesis. It is directed towards establishing a better understanding of the damage development and failure process of ceramic matrix composites. Fulfillment of this objective was possible by damage development studies and fractographic investigations. These were conducted on the specimens listed in the tables, as well as additional specimens tested by the previous student on this project.

The low failure stresses and strains, and composite moduli are attributed to poorly processed composite plates, testing procedures, and the presence of cracks prior to testing.

Matrix cracking can arise before loading due to specimen preparation procedures (e.g. grinding and polishing) and excessive gripping forces. In addition, some bending may occur during testing due to imperfect specimen alignment. Premature specimen failures frequently initiated in the shoulder regions apparently due to stress concentrations at the aluminum tabs. The growth of delamination cracks also resulted in premature failures in the grip region. Delamination initiated in the specimen shoulders of both longitudinal and crossplied specimens when Cyanamid FM-123 adhesive was used for bonding end tabs. Thermal mismatch stresses, generated between the Al tabs and the composite specimens during curing at 98°C, caused the onset of delamination. Tabs on some unidirectional specimens debonded prior to composite failure; the fiber failure strain could not be reached. The footnotes in the tables indicate the incidence of premature failure and the specimen design utilized.

Effect of Matrix Material

The room temperature tensile behavior of unidirectional laminates varied with matrix composition. SEM fractographic investigations revealed differences in fracture surface appearance among the composite systems, and these were correlated with fracture resistance. The overall fracture surface appearance is governed by the relative amounts of interface failure and the magnitude of the interfacial stresses. Axial residual stresses in the matrix, resistance to fiber slippage relative to the matrix, and matrix toughness influence matrix cracking resistance. Hence, it was possible to ascertain the effect of matrix material (and, thus, residual stress fields) on tensile behavior. The effects of different processing conditions for each composite system must also considered.

Nicalon/1723. Under optimal test conditions, the unidirectional Nicalon/1723 system exhibited a three part longitudinal stress-strain curve at room temperature. A representative curve is shown in Fig. 4-1. Specimens which failed prematurely in the grip region did not exhibit a third regime, and failure strains were less than optimal. The general features of the curve are as expected from the theoretical discussion of Section 2.2. The initial linear behavior is closely predicted by the rule of mixtures. Beyond 0.1 to 0.15 % strain, the onset of matrix cracking caused the curve to deviate from linearity. A saturation of matrix cracks was achieved at strains approaching 0.4 %, and the response became linear again. The reduced modulus in the final portion of the curve is approximated by $E_f V_f$. The cracked matrix contributes little to the composite strength and modulus in this regime. The behavior of the Nicalon/1723 system, as depicted in Fig. 4-1, can be considered optimal since the composite failure strain approached the average fiber failure

strain (1%). The ultimate composite strength averaged 690 MPa, approximately $\sigma_f V_f$. A more detailed description of the room temperature tensile behavior of Nicalon/1723 is given in Refs. 15 and 66.

Room temperature fractures of unidirectional Nicalon/1723 were characterized by extensive matrix cracking and short fiber pull-out. A saturation matrix crack spacing of ~80 to 100 μm was measured. The high matrix crack density correlates well with the three-stage stress-strain curve of Fig. 4-1 where only fibers contributed to the strength at high strains. The short pullout lengths (< 10 fiber diameters) are indicative of a high interfacial friction which resists fiber pullout and debonding. Pullout lengths were considerably shorter than those reported for systems with similar failure strains but lower expansion matrices (e.g. Nicalon/LAS).[12,33] The difference is related to interfacial bond strength differences. Grande, et al. [67] reported the interfacial shear strength of Nicalon/1723 to be roughly four times that of LAS and BMAS-matrix composites.

Nicalon/CAS. The room temperature tensile behavior of unidirectional Nicalon/CAS was generally similar to the 1723-matrix system. However, stress-strain plots were often limited to two regimes. (See Fig. 4-2.) The characteristic knee in the curve occurred at a slightly higher strain level, 0.2 %. Room temperature properties were somewhat inferior to Nicalon/1723: UTS = 300 MPa, ε_u = 0.6% and E_{init} = 126 MPa, but are in close agreement with tensile data reported by Corning Glass Works.[128] Short fiber pull-out lengths (approximately 50 fiber diameters) were commonly observed; saturation matrix crack spacings approached 250 μm.

The difference in fracture surface features must be related to the different matrix materials since the interfacial shear strengths and longitudinal residual tensile stresses in the matrices of these composites do not differ significantly. The higher matrix crack initiation strain is attributed to the higher toughness of the CAS matrix versus 1723. The lower toughness of the glass matrix may also account for a greater degree of matrix cracking in the Nicalon/1723 system. In addition, the higher temperatures required for processing the glass-ceramic matrix composite may cause some fiber and, thus, property degradation. Low ultimate strains in early LAS-matrix composites were attributed to fiber degradation during processing.[11] Prewo, et al.[11,17] have related the axial strength of fiber-reinforced glass-ceramic matrix composites to in-situ fiber strength. Significantly lower strengths were reported for Nicalon fibers extracted from LAS glass-ceramic matrix composites relative to as-received fibers.

Nicalon/BMAS. At room temperature, unidirectional Nicalon/BMAS composites failed at lower strains than either Nicalon/1723 or Nicalon/CAS, and were not as strong. Fig. 4-3 illustrates a typical room temperature response curve. Like Nicalon/CAS, the characteristic knee in the curve occurred at approximately 0.2 %; average failure strains were less than 0.4%. A saturation of matrix cracks was not achieved in this system since specimens failed before the nonlinear region of the curve was exceeded. The suboptimal behavior may be related to the poor quality of this particular material batch. In addition, high processing temperatures could lead to fiber degradation.

Fibrous fractures were generally observed at room temperature with fiber pullout lengths approaching 100 fiber diameters. Similar behavior has also been reported for Nicalon/LAS glass-ceramic matrix composites [8], and is typical of low expansion matrix systems. The frictional resistance to sliding of debonded fibers is minimal. Matrix crack spacings for the BMAS-matrix composite measured 200 to 300 μm at room temperature, in agreement with reported spacings for LAS-matrix composites.[10,12] Mah, et al.[10] observed crack spacings of 300 μm; Marshall, et al.[12] measured spacings closer to 400 μm.

The tensile response of Nicalon/LAS and Nicalon/BMAS composites was similar. This is not unexpected since the two systems are processed at similar temperatures and the matrix thermal expansion coefficients do not differ substantially. Hence, the residual thermal stress fields are similar. The frictional sliding resistance of Nicalon/BMAS [15,67] was previously found to be of the same magnitude as that reported for Nicalon/LAS [70]. It was often possible to analyze only one of these systems for a particular condition since the material supply was limited, and polishing was difficult.

Effect of Fiber/Matrix Bond Strength and Residual Stresses

The effect of fiber/matrix bond strengths and residual stresses were alluded to in the above discussion. A more detailed account follows. The magnitude of these stresses strongly influences matrix crack initiation and saturation. The extent of fiber pullout and resistance to fiber slippage is also affected. Residual stresses due to fiber/matrix mismatch as well as ply/ply mismatch must be considered.

Bond strengths of the four composite systems of interest were previously measured, [15,67,127] and are summarized in Table 4-4. The low interfacial strengths of LAS and BMAS-matrix composites are promoted by a thick interfacial carbon layer (up to 500 nm)

which forms upon processing. The carbon layer provides a weak interface which allows strong and tough behavior in Nicalon fiber-reinforced CMC's. The low expansion coefficients of the LAS and BMAS matrices cause radial residual tensile stresses to develop at the fiber/matrix interface upon cooling from processing temperatures. The radial stresses may also contribute to the low measured bond strengths. Accordingly, the frictional resistance to fiber slippage and the fiber/matrix load transfer rate are low. Extensive fiber pullout and debonding occurred. Matrix crack densities were less than for Nicalon/1723 and Nicalon/CAS. Crack opening occurred by matrix sliding along the fiber/matrix interface, as shown in Fig. 4-4 for Nicalon/BMAS; fibers remained intact. The low expansion matrix systems are flaw tolerant since debonding occurs readily enough to allow matrix crack deflection and fiber sliding prior to fiber fracture. However, low bond strengths may lead to poor off-axis properties.

Nicalon/1723 and Nicalon/CAS-I exhibited four times greater bond strengths than LAS and BMAS composites.[67] (See Table 4-4.) The bond strength of the Nicalon/CAS-II system utilized in the present investigation was slightly lower than that of composites with CAS-I and 1723 matrices. The higher measured bond strengths of Nicalon/CAS and Nicalon/1723 are related to a thinner interfacial carbon layer. In addition, high matrix expansion coefficients cause radial residual compressive stresses to develop at the interface, and these contribute to the high interfacial strengths. Fiber/matrix load transfer is facilitated; frictional sliding resistance is increased. Thus, a saturation of matrix cracks was achieved, and pullout lengths were shortened relative to Nicalon/LAS and Nicalon/BMAS composites. The saturation crack density of Nicalon/1723 was found to exceed that of Nicalon/CAS. The smaller crack spacing in the 1723 system is apparently due to the lower fracture toughness of the glass matrix, as well as a slightly higher bond strength which enhances fiber/matrix load transfer.

The pullout lengths and matrix crack spacings of the composite systems are compared in Figs. 4-5 and 4-6. The degree of fiber pullout and extent of matrix cracking were commensurate with the fiber/matrix interfacial strengths in Table 4-4. Fiber pullout lengths of Nicalon/CAS were between those of Nicalon/1723 and Nicalon/BMAS, in agreement with the bond strength measurements. Matrix crack spacings followed the same order.

Axial residual stresses due to thermal expansion mismatch also affected fracture behavior. The residual strain in each unidirectional system was calculated from the difference in the composite and matrix strains. The results are summarized in Table 4-5; Appendix B and C

include essential data and details of the calculations. For unidirectional Nicalon/1723 and Nicalon/ CAS composites, axial residual tensile stresses developed in the matrices and contributed to the matrix cracking behavior, as shown in Fig. 4-5. The extent of these residual stresses is evident in Fig. 4-7 in the vicinity of the fiber ends. Axial residual compressive stresses were generated in the BMAS and LAS matrix composites. Accordingly, matrix cracking was delayed in these systems and lower crack densities were observed. The magnitude of the residual stresses varied with processing conditions, as shown in the table for as-pressed vs. ceramed Nicalon/LAS.

In multidirectional laminates, residual stresses due to ply/ply mismatch are also present. If the mismatch and/or the temperature change is large, substantial residual stresses can develop and strongly influence the damage development process. Composite laminated plate theory (CLPT) was used to calculate the thermal residual stresses due to ply/ply mismatch in Nicalon/1723, Nicalon/CAS and Nicalon/LAS crossply laminates. The residual strains in the 0° and 90° plies were determined from the difference in laminate and ply dimensional changes. The calculations are outlined in Appendix C.

The results, summarized in Table 4-5, indicate residual tensile stresses occur in the transverse plies of crossplied Nicalon/CAS and Nicalon/1723. The residual stress (and strain) is slightly larger in the Nicalon/CAS composite. The 90° plies of Nicalon/LAS and Nicalon/ BMAS crossply laminates experienced residual compressive stresses of substantial magnitude. These delayed cracking in the transverse plies of Nicalon/LAS and Nicalon/BMAS to higher strain levels. Conversely, residual tensile stresses in the transverse plies of Nicalon/CAS and Nicalon/1723 crossply laminates caused the initiation of transverse cracks at very low strain levels (i.e. 0.03-0.05 %). Details of the damage development process are described in Section 4.3.

Effect of Laminate Configuration

Room temperature stress-strain curves of Nicalon/1723, Nicalon/CAS and Nicalon/BMAS crossply laminates are included in Figs. 4-1, 4-2 and 4-3, respectively. These plots are typical of "well-behaved" test specimens. In contrast to the unidirectional systems, the stress-strain curves of crossplied Nicalon/1723 and Nicalon/CAS composites remained linear to strains of only 0.03 to 0.05 %. Transverse ply cracks were found to initiate at these low strains using the replication technique described earlier. The curves became nonlinear upon increasing the strain beyond 0.05 %. The deviation from linearity was

more pronounced at approximately 0.1-0.2 % strain due to the onset of matrix cracking in the longitudinal plies.

Nicalon/LAS and Nicalon/BMAS crossply laminates did not undergo transverse ply cracking until approximately 0.1 % strain; longitudinal ply cracking ensued at slightly higher strains. In contrast, Sbaizero and Evans [18] reported delamination cracking between plies as the first damage in the Nicalon/LAS crossply system. They linked delamination to the initial deviation from linearity in the stress-strain curve. Delamination was not observed in the crossply laminates of interest in this study until higher strain levels were attained. The spread of delamination resulted in ultimate failure in most specimens.

The low transverse ply cracking strains of Nicalon/1723 and Nicalon/CAS crossply laminates correlate with the inherently low transverse tensile properties of analogous unidirectional systems. Transverse failure strains in the 0.03 to 0.04 % range (and approximate transverse strengths of 25 to 30 MPa) have been reported for Nicalon/1723 [15,66] and Nicalon/LAS [11]. The presence of fibers in the transverse direction creates stress concentrations and flaws which are not present in the unreinforced matrix. Poor transverse properties result, and these may be inferior to the unreinforced matrix properties. If there is little or no interfacial bonding, the fibers can be regarded as holes in the matrix and transverse strength reductions occur due to stress concentrations around the holes. The higher observed transverse ply cracking strains of Nicalon/LAS and Nicalon/BMAS crossply laminates are related to the residual compressive stresses in the 90° plies which delay transverse ply cracking.

The composite moduli and ultimate strengths of the four crossply laminates were similar, but lower than that of their unidirectional counterparts. (See Figs. 4-1, 4-2 and 4-3.) Altering the laminate configuration from 0° to 0/90° caused a degradation of composite mechanical properties. The Nicalon/1723 system underwent the most drastic property changes. The ultimate failure stress decreased from 690 MPa to approximately 250 MPa. If adjustments are made to account for the smaller volume fraction of axial reinforcing fibers, the crossply laminate strength approaches $\sigma_f V_f$. Thus, the transverse plies contribute little to the ultimate composite strength. The ultimate failure strain dropped below that of the fibers, and a twenty-five percent reduction in composite modulus was noted (from 140 to 103 GPa).

Nicalon/CAS and Nicalon/ BMAS crossply laminates generally exhibited failure strains in the 0.5 to 0.6 % range. Although these values are similar to those measured for the corresponding unidirectional composites, they are still less than expected. The optimum failure strain of unidirectional and crossply composites should ideally approach the Nicalon fiber failure strain (1%). Considerable strength and modulus reductions occurred relative to the unidirectional systems. The maximum measured strengths of the crossply laminates were: 285 MPa (Nicalon/CAS), 227 MPa (Nicalon/BMAS), and 200 MPa (Nicalon/LAS). When normalized by the percentage of 0° material, the strengths of all four composite systems should be similar. However, differences remained and these may result from processing difficulties and/or poor specimen design. Experimentally measured moduli were often less than those calculated from micromechanics. Composite moduli decreased below 100 GPa and, in some instances, approached the modulus of the unreinforced matrix. Unless the fibers completely debond from the matrix, the modulus should not decrease relative to the unreinforced matrix. The low moduli may be associated with regions of localized cracking in these materials and is further discussed in the next chapter.

Tensile behavior of the crossply laminates was better understood through fractographic investigations. All systems experienced extensive fiber pullout in the longitudinal plies. In analogy with their unidirectional counterparts, pullout lengths were longer for the Nicalon/BMAS and Nicalon/LAS crossply laminates. This is indicative of a low fiber/matrix bond strength (relative to residual stresses) and low frictional resistance. The progression of edge delamination between plies was evident in some cases, but was more clearly observed in polished cross-sections taken from fractured specimens. Fig. 4-8 depicts a delamination crack which initiated at a 0/90 ply interface, and subsequently extended across a 0° ply in a Nicalon/1723 laminate.

The less-than-optimal failure strains of crossplied Nicalon/1723 composites may be related to the presence of "embrittled zones" in this material. Embrittled zones are regions of flat fracture, depicted in Fig. 4-9, found in the longitudinal plies following room temperature fracture. The regions occurred regularly across the fracture surface, but were most prevalent near delaminations. It is likely that delamination altered the residual stress field in adjacent plies and the change was manifested as embrittled regions. No association of the embrittled zones with locally higher bond strengths was found. Entire 0° plies were not always embrittled. Fiber pullout occurred at the 0/90 ply interfaces as shown in Fig. 4-9. Embrittlement zones were not observed in the 0° surface plies, except in matrix-rich regions; fiber pullout was extensive.

Fibers in the embrittled zones exhibited typical mirror-mist-hackle regions. The direction of crack advance was not easily determined since the mirrors were oriented in various directions. (See Fig. 4-9b, which is an enlargement of the 0° ply in Fig. 4-9a.) However, observation of the fibers at high magnifications seems to indicate that cracks moved from the center of the 0° plies towards the 0/90 interfaces.

The embrittlement zones are attributed to residual stress effects. The lack of embrittlement zones in the surface plies (where only one 90° ply is restrictive, versus two in the inner plies) indicates that a residual stress effect is operative on a macroscale due to ply/ply mismatch. Microscale residual stresses due to fiber/matrix thermal expansion mismatch may also influence behavior. The absence of embrittlement zones in samples fractured at 600°C lends credence to the residual stress explanation. Since embrittled zones were also found in fractured unidirectional Nicalon/1723 composites, the effect is more likely due to fiber/matrix thermal expansion mismatch rather than ply/ply mismatch. However, other effects (e.g. bending during fracture, crack velocity, etc.) may also contribute to this phenomenon.

The embrittled zones are unique to the Nicalon/1723 system. Examination of crossplied Nicalon/CAS and Nicalon/BMAS composites, fractured at room temperature, did not reveal any embrittlement zones. Instead, fiber pullout dominated in the longitudinal plies. Pullout lengths for Nicalon/CAS were much shorter than the corresponding unidirectional material (10 fiber diameters vs. 50 fiber diameters). The shorter pullout lengths in the 0/90 system may be indicative of a lower failure strain created by ply residual stresses.

Extensive matrix cracking and fragmentation occurred in crossplied Nicalon/BMAS, as evidenced by the lack of matrix material remaining in the vicinity of the fracture. See Fig. 4-10. The fiber/matrix bond strength was apparently insufficient to allow cracked matrix regions to cling to the fibers. Fibers in the longitudinal plies remained intact and provided the dominant load carrying capacity. Pullout lengths in the 0° plies were longer than for the glass-matrix system since the frictional resistance was minimal. Crack opening in these plies occurred by matrix sliding along the interface. The weak bonding in Nicalon/BMAS may be detrimental to transverse ply strength and, thus, composite properties. Similar behavior is expected for the 0/90 Nicalon/LAS system.

Effect of Temperature

Limited elevated temperature test results generally indicated that composite properties were not significantly affected by temperatures up to 500°C. Failure stress and strain, and composite modulus declined substantially with increasing temperature. The limiting temperature beyond which property degradation occurred was higher for the glass-ceramic matrix composites than for Nicalon/1723 (700°C vs. 500°C). Degradation of composite properties at elevated temperatures was accompanied by a change in fracture appearance, related to high temperature oxidation and embrittlement. The ensuing discussion relates the elevated temperature tensile behavior of Nicalon/1723, Nicalon BMAS, and Nicalon/CAS to the fracture surface appearance.

Unidirectional Composites. Brittle fracture of Nicalon/1723 occurred at temperatures in the vicinity of 600°C. Essentially no fiber pullout or matrix cracking was observed. Specimen failure occurred by the advance of a single matrix crack. These features correspond with the lower measured failure strains at 600°C.

Although the thermal expansion behavior of CAS and 1723 are similar, the elevated temperature performance of the Nicalon/CAS composite was superior due to the higher thermal stability of the glass-ceramic matrix. At 600°C, properties of Nicalon/CAS were similar to those observed at room temperature. The 600°C stress-strain curve remained essentially unchanged from the room temperature curve, as illustrated in Fig. 4-11. Both curves exhibited the characteristic knee associated with matrix cracking at approximately 0.2 % strain; failure strains were comparable (0.6 %). Matrix cracking was less extensive at 600°C. Some matrix cracks extended through the fibers, as shown in Fig. 4-12. Other fibers remained intact following matrix crack opening. Fiber pullout lengths were shorter, and may be indicative of a strengthening of the interfacial bond. However, the degree of strengthening was not sufficient to cause embrittlement at 600°C.

Significant embrittlement of the Nicalon/CAS composite occurred at 1000°C, and the composite failure strain decreased to 0.23 %. (See Fig. 4-11.) The stress-strain curve remained linear to failure since the matrix cracking strain was not exceeded. The fracture surface appearance was characteristic of brittle fracture, in accord with the low measured failure strain. Two distinct failure regions were apparent, as shown in Fig. 4-13a. Similar features have also been observed in elevated temperature fractures of Nicalon/LAS [8,11,14] and Nicalon/BMAS [15]. Fig. 4-13b depicts the embrittlement of Nicalon/BMAS at 1000°C.

The brittle fracture region extended around the specimen periphery in both cases. The thickness of the embrittled region measured approximately 500 μm in Nicalon/CAS and 300 μm in the Nicalon/BMAS composite. The larger penetration in the Nicalon/CAS composite is attributed to a greater tendency for matrix cracking prior to failure. Matrix cracks provided an additional path for ingress of oxygen. Fiber pullout lengths in the central region were substantially reduced relative to those measured at lower temperatures. Pullout lengths did not exceed 200 μm. The shorter pullout lengths may indicate a lower strain in the fibers at failure, due to the lower composite strength and strain to failure at elevated temperature. Nicalon/CAS specimens exposed to 1000°C prior to room temperature testing also exhibited a two zone fracture. However, the embrittlement zone covered a larger percentage of the specimen.

Elevated temperature embrittlement has been linked to oxidation of the interfacial carbon layer [17,19,20], as discussed in Chapter 2. A high matrix reactivity complicates the interfacial oxidation process. In the Nicalon/CAS system, fiber fusion was observed in the embrittlement zone of a Nicalon/CAS specimen exposed to 1000°C prior to room temperature testing. (See Fig. 4-14a.) A semi-quantitative EDS analysis showed Al and Ca to be the active species since they were found in the affected fibers. Other areas of the same specimen revealed fibers to cleanly debond from the matrix as shown in Fig. 4-14b. Similar fusion reactions were also observed in the embrittlement zones of Nicalon/CAS and Nicalon/BMAS composites, following fracture at 1000°C. However, the extent of fusion was greater in the Nicalon/CAS composite. The presence of Ca in the matrix appears to increase the activity at the fiber/matrix interface.

Elevated temperature exposure also affected the fibers in the CAS-matrix composites. Although most fibers pulled out cleanly, some were swollen at the ends as illustrated in Fig. 4-14c. After fracture at 1000°C, continued elevated temperature exposure (during the 2 h cooldown) may cause melting of some fibers which then fuse upon cooling. The exact nature of these reactions has not yet been established, but some additional experiments were conducted to correlate bond strength and interfacial oxidation. The results are presented in the next section of this chapter.

Nicalon/BMAS exhibited similar behavior to Nicalon/CAS over a range of elevated temperatures. At test temperatures below 650°C fiber pullout and debonding prevailed. In analogy with Nicalon/CAS, pullout lengths following 600°C fracture were slightly less than

those measured at room temperature (approximately 100 fiber diameters). Matrix crack spacings decreased from 200-300 μm at 25°C to approximately 140 μm at 600°C. The minimal decrease in crack spacing and pullout length implies only a small increase in interfacial bond strength at 600°C, or may be due to reduced residual stresses.

At higher test temperatures, the fracture surface features of Nicalon/BMAS changed more dramatically in accord with the lower measured composite failure strains. Pullout lengths decreased with temperature as shown in Fig. 4-15. The short pullout lengths (approximately 10 fiber diameters) at 800°C are characteristic of brittle fracture. The pullout lengths at 800°C were similar to those in the central pullout region of the 1000°C fractures. The absence of matrix cracking indicates composite failure occurred by the advance of a single matrix crack. This correlates with the stress-strain curve (Ref. 15) which terminates in the initial linear region, prior to the onset of multiple matrix cracking.

To determine the extent of the embrittlement in Nicalon/CAS and Nicalon/BMAS laminates, a composite with strong interfacial bonding was examined following short beam shear testing (tensile failure mode). The brittle fracture surface of this specimen resembled the outer region of the 1000°C Nicalon/BMAS and Nicalon/CAS test specimens. Thus, it appears embrittlement is related to strong fiber/matrix bonding. Microdebonding tests have confirmed this finding.[15]

Multidirectional Composites. Several crossply laminates were tested at temperatures in the 550-600°C range. Representative stress-strain plots are shown in Figs. 4-16a and 4-16b for crossplied Nicalon/1723 and Nicalon/LAS composites. Nicalon/LAS exhibited a two part stress-strain curve. The characteristic knee in the curve occurred at a similar strain level to that observed at room temperature. Thus, cracking in the longitudinal plies initiated at 0.2 % strain, and substantial matrix cracking occurred prior to failure (0.32 %). Fibers in the transverse plies of Nicalon/LAS debonded at very low strains (< 0.1 %) following elevated temperature exposure. The Nicalon/1723 stress-strain curve was essentially linear to failure. This system failed soon after the initiation of longitudinal ply cracking at a lower strain than the LAS composite. Transverse ply cracks in the 1723 system initiated upon thermal cycling (even without loading), but this was not readily apparent from the stress-strain curve. The failure sequence was verified with the replication technique; details follow in the damage development section.

The pictured stress-strain curves were obtained under optimal test conditions. Load fluctuations in these plots are attributed to mechanical vibrations from the furnace transformer, and were observed in all high temperature tests using the primary test setup. Most data were obtained with tabbed, straight-sided 15.24 cm long specimens. Premature failures were common due to the spread of delamination from the specimen end. Delamination initiated during curing of the FM-123 adhesive used for bonding the tabs.

Exposure to 550°C caused a small degradation in composite properties from those measured at room temperature. Strength and modulus reductions were minimal. Nevertheless, experimental moduli were consistently less than theoretically predicted. (Compare moduli in Tables 4-1, 4-2 and 4-3 with the predicted values in Appendix B.) At 550°C, failure strains of the crossply laminates decreased substantially. The maximum measured strains for Nicalon/1723 and Nicalon/LAS composites were 0.28 % and 0.32 %, respectively, as shown in Figs. 4-16a and 4-16b. The low failure strains were not delamination-induced, since the curves shown were obtained from specimens which failed in the gage section. Fig. 4-17 gives an overall view of the gage section failures.

The degradation in properties at 550°C was accompanied by a change in fracture surface appearance. Shorter pullout lengths (200 μm) were observed in the longitudinal plies of both systems. The Nicalon/LAS laminate showed some embrittlement (i.e. a flat fracture region) at one end of the specimen. No spalling of the matrix material occurred, and the composite remained more intact than at room temperature. Thus, elevated temperature exposure appears to have strengthened the interfacial bond in Nicalon/LAS or, more likely, reduced the residual stresses. The Nicalon/1723 fracture surface was similar to the LAS-matrix composite. No obvious "embrittled zones" were found, in contrast with the room temperature behavior of this system.

4.2 Interface Oxidation Studies

The effect of oxidation tunnelling from exposed fiber ends in Nicalon/CAS-IIb was investigated by determining bond strength variations at specific depths below an oxidized surface. The bond strength results are compiled in Table 4-6. Bond strength versus depth (along the fiber axis) profiles are plotted in Fig. 4-18 for exposure temperatures of 800°C, 1000°C and 1200°C, and 0.5 h, 5 h and 50 h exposure times. The data were taken in the central regions of each specimen (i.e. away from the exposed edges). The transverse penetration of oxygen was also examined at various depths below the exposed surface. Gradients in bond strength were determined inward from the exposed, ground edges of the

samples and are summarized in Table 4-7. The measurements described herein are the first known attempt at relating the kinetics of the oxidation process to variations in bond strength over a range of times and temperatures.

Bond strengths increased relative to the control after exposure at all temperatures, as shown in Table 4-6. No reductions in bond strength were observed, although these might be expected if oxidative removal of the carbon layer occurred without any subsequent reactions. The increase in bond strength was most pronounced close to the exposed surface. At large depths beneath the surface, the bond strength reverted to that of the unexposed material and the oxidation process sealed off. This trend is depicted in Fig. 4-18. The decrease in bond strength with depth (along the fiber axis) is indicative of an oxygen tunnelling effect.

The largest bond strength increases occurred after 800°C exposure, and were most pronounced near the exposed surface. This is evident in Fig 4-18 where each 800°C data point represents an average bond strength for fibers which could be debonded. In some regions of samples exposed for 5 h or more, the interfacial bond strength showed a threefold increase over the control. Little change was noted after 0.5 h exposure at 800°C. Thus, it appears that an incubation period is required at 800°C before oxidation effects become evident.

Fibers in some regions of the 800°C samples, exposed for 5 or more hours, could not be debonded. The bond strengths were extremely high and exceeded the measurement capacity of the microdebonding apparatus (>1000 MPa). This is indicated by an arrow in Fig. 4-18. Lower bond strength regions were also found in the same samples. Bond strengths were lower in high fiber density regions; high bond strengths were measured in areas of low fiber content. The boundary between the two regions was very distinct. Careful measurements indicated the high/low bond strength regions were associated with tow boundaries.[127]

Only a moderate increase in bond strength was noted for the 1000°C and 1200°C exposures. Bond strengths increased by less than a factor of two even at shallow depths below the exposed surfaces. For the 1200°C samples, the increase was maintained to a depth of 6 to 7 mm, as shown in Fig. 4-18. The bond strength of the 1000°C samples dropped to the control value at this depth. However, transverse penetration studies for these samples showed very high bond strengths (>1000 MPa) for fibers near the oxidized

surface. This could also have been the case for the fiber ends on the exposed cross-section, but measurements were not taken closer than 0.4 mm below the surface.

Transmission electron microscopy studies of oxidized glass-ceramic matrix composites at Corning have revealed three different interphase conditions: [74,128]

(i) A gap between fiber and matrix due to complete oxidative removal of the interfacial carbon layer with no subsequent reactions.

(ii) Replacement of the oxidized carbon layer with a new interfacial phase which is strongly bonded to the fiber, causing extensive embrittlement.

(iii) A partially intact interphase region.

The differences between the higher temperature exposures and those at 800°C appear to be related to these interphase changes. At 800°C, the extremely high bond strengths can be accounted for by formation of a new, strongly bonded interphase upon oxidation of the interfacial carbon layer. A similar phenomenon has been reported previously for Nicalon/BMAS.[15] Partially intact interphase regions could correspond to the moderate bond strength increases observed at 1000°C and 1200°C. Oxidation appears to spread along the interface from the exposed fiber ends (at 800, 1000 and 1200°C), rather than reflecting a local fiber-matrix interaction. Control bond strength is retained at a great enough distance from the exposed surface. The apparent presence of two interphase oxidation processes complicates interpretation of the data, and a more extensive study is required to define the details of each process.

Longer exposure times at temperature do not appear to enhance embrittlement. Bond strengths following 50 h exposure were not significantly different from those measured at 5 h. Although longer times and higher temperatures may increase oxygen diffusion, the kinetics of other interfacial reactions are also enhanced. Creation of another interfacial region may occur rapidly, filling in the gap between the fiber and matrix caused by oxidative removal of the carbon layer. This interfacial layer is believed to thwart further oxidation down the fibers.

In addition to oxygen tunnelling from exposed fiber ends, the effect of oxygen diffusion transverse to the fibers was examined. The transverse penetration of oxygen depends on the depth below the exposed surface at which it is measured. Table 4-7 lists approximate transverse penetration depths at various distances beneath the surface. At shallow depths, the 800°C exposure exhibited the greatest transverse penetration. The width of the embrittlement zone after 50 h at 800°C approached 0.5-0.8 mm, an order of magnitude

larger than measured under comparable conditions at 1000°C and 1200°C. Further down from the exposed surface, at approximately 6 mm, little difference was found in the extent of penetration for the various times and temperatures. All transverse penetration depths were less than 0.08 mm. The data are more meaningful at this depth since the effects of axial tunnelling are greatly reduced. The low penetration depths at 6 mm imply that the transverse penetration of oxygen is insignificant for Nicalon/CAS-IIb. Fig. 4-18 shows an axial penetration depth of approximately 1.5 mm along the fiber axis. Thus, the oxidation process is dominated by oxygen tunnelling via a "pipeline mechanism".

The penetration depths for Nicalon/CAS-IIb are less than those reported by Grande, et al.[15,67] in similar experiments for Nicalon/BMAS-III. Transverse penetration depths of approximately 0.5 mm were measured for the BMAS system following 12 h exposure at 1000°C. The Nicalon/BMAS composite also exhibited similar penetrations following high temperature tensile fracture. Fig. 4-13 shows approximate penetration depths of 0.5 mm and 0.3 mm for Nicalon/CAS and Nicalon/BMAS, respectively. Thus, embrittlement is much more extensive in the Nicalon/CAS tensile specimen. This can be related to a network of matrix cracks which form before or during testing, and serve as additional paths for the ingress of oxygen. Such cracking appears to be necessary for significant transverse penetration of oxidation in the CAS-IIb system.

4.3 Damage Development Studies

Current understanding of the micromechanisms of failure of glass and glass-ceramic matrix composites is based primarily on analysis of fractured samples. Most studies to date have been limited to optical and scanning electron microscopy for determination of matrix crack spacings and fiber pullout lengths. Some insight into the fracture process was gained from fractographic investigations similar to those described in Section 4.1. Except for some recent optical studies [12,18], there have been no reported attempts at monitoring damage development during loading. The techniques described in the experimental procedure (i.e. replication, and SEM observation of loaded flexural specimens) were utilized to monitor damage initiation, accumulation and interactions during loading of Nicalon/1723, Nicalon/CAS, Nicalon/LAS and Nicalon/BMAS laminates. To more accurately describe the failure process, the events leading to failure were correlated with discontinuities in the stress-strain curve.

Direct Observation of Flexure Tests

Loaded flexural specimens were examined in the SEM to highlight differences in the fracture behavior of CMC's related to thermal expansion mismatch. Unidirectional Nicalon/1723 and Nicalon/BMAS composites were chosen as representative systems with high and low matrix expansion coefficients. The results may be generally applicable to other systems with similar residual stress fields.

The Nicalon/1723 system underwent extensive matrix cracking, as shown in Fig. 4-19a. The cracks were regularly spaced (~60-80 μm) and, in some cases, extended through the Nicalon fibers. These findings agree with earlier observations of tensile fracture of Nicalon/1723. Matrix cracking is promoted in CMC's with high matrix expansion coefficients. As described earlier, the positive mismatch generates axial residual tensile stresses in the matrix and radial residual compressive stresses at the interface. The radial residual compressive stresses add to the interfacial bond strength, facilitating fiber/matrix load transfer and matrix crack saturation.

The BMAS-matrix composite exhibited irregular matrix cracking. See Fig. 4-19b. However, the crack opening displacements were larger than observed in the glass-matrix composite. Matrix cracks did not extend through the fiber reinforcement. High magnification microscopy work revealed the fibers remained intact beneath surface cracks in the BMAS matrix. Fig. 4-19c shows that matrix crack opening occurs by sliding along the interfaces. This agrees with reported findings for Nicalon/LAS.[12] The Nicalon/BMAS and Nicalon/LAS systems exhibit a lower resistance to matrix sliding than the 1723 composite due to lower fiber/matrix bond strengths and radial residual tensile stresses at the interface. It is not clear from this work whether any relative sliding of fiber and matrix occurs with Nicalon/1723; none could be observed within the matrix cracks.

Replication

Room Temperature:

Replicas were taken at a progression of strain levels during tensile loading of Nicalon/1723, Nicalon/CAS and Nicalon/LAS crossply laminates. Replicas of as-polished samples served as controls. In addition, some results were obtained for unidirectional Nicalon/1723 and Nicalon/LAS composites. Tensile properties from these experiments are included in Tables 4-1, 4-2 and 4-3.

Nicalon/1723. Four crossplied Nicalon/1723 specimens were investigated: two $[0/90]_{2S}$ laminates and two $[0/90]_{4S}$ laminates. The measured properties were less than optimal due to premature specimen failures as a result of delamination of the end tabs. Although the individual specimens failed at different ultimate stresses and strains, the damage development process prior to failure was consistent. Representative stress-strain plots of the 8 and 16 ply laminates, obtained during the replication procedure, are shown in Fig. 4-20. Serrations in the curves represent the strain levels at which replicas were taken when the loading was interrupted.

SEM examination of replicas revealed matrix cracking in the transverse plies as the initial form of damage. Transverse ply cracking initiated at very low strains (approximately 0.025 to 0.05 %), in agreement with the deviations from linearity noted in the stress-strain curve of Fig. 4-1. Damage is associated with tensile loading since no cracks were observed on replicas of as-polished samples, as shown in Fig. 4-21. Matrix cracks in the longitudinal plies initiated at approximately 0.1 % strain, but did not extend across each 0° ply until higher strain levels were reached (> 0.130 %). Fig. 4-22 illustrates this phenomenon at a strain level of 0.23 %. Some cracks in the 90° plies are also not fully extended through the ply thickness. Thus, cracking is controlled by propagation, not initiation. Higher magnification (Fig. 4-23) shows that the 90° ply cracks grow preferentially in the fiber/matrix interface where possible, and are primarily interface cracks.

Transverse ply cracks were observed in one Nicalon/1723-$[0/90]_{2S}$ laminate prior to tensile loading. Replicas taken following gripping of the specimen in the hydraulic grips, but prior to tensile loading, revealed cracks in the 90° plies with an average spacing of 750 μm. The gripping force was believed to cause cracking and subsequent tests were conducted with lower gripping pressures.

Increased loading beyond that required for crack initiation caused further cracking in both the longitudinal and transverse plies. Cracking of the 0° and 90° plies continued until saturation crack spacings were achieved. The accumulation of damage is illustrated in the sequence of replicas in Fig. 4-24. Except for one specimen, no delamination between plies was observed at low strain levels. When delamination occurred, it commenced at strain levels close to the failure strain and caused ultimate failure. This contrasts with previous findings for Nicalon/LAS [18] where delamination was reported at strains less than the matrix cracking strain.

Cracking of the transverse plies is controlled by the resistance to crack growth parallel to the fibers under transverse tensile loading. In addition, the residual stress state in the 90° ply influences cracking. Longitudinal ply cracking is governed by the same factors as matrix cracking in unidirectional composites, namely: axial residual thermal stress in the matrix, resistance to fiber slippage and matrix toughness. The effects of ply residual stresses on longitudinal cracking must also be considered. After the initiation of damage in crossply laminates, further damage development in specific plies is influenced by the damage state in adjacent plies and changes in the residual stress pattern. The physical presence of a crack tip near the ply interface, as well as a decrease in the modulus of cracked, adjacent plies could affect the damage development process.

An image analyzer was used to statistically analyze the crack spacings recorded on SEM micrographs. These measurements are summarized for each specimen in Appendix D. Crack spacings are plotted as a function of applied strain in Fig. 4-25. The curve includes damage development results for four different Nicalon/1723-0/90 specimens; crack spacings reflect the overall average for all plies. Although matrix cracking in the 0° plies initiated at a higher strain level than in the 90° plies, the two curves cross and smaller crack spacings were measured in the longitudinal plies at high strains. An approximate saturation spacing of 200 μm was attained in the transverse plies, versus only 50 μm in the longitudinal plies. The small saturation spacing in the 0° plies is due to a low matrix toughness and a high shear stress transfer at the fiber/matrix interface. The high stress transfer results from the high fiber/matrix bond strength and radial residual compressive stresses at the interface.

Fig. 4-25 does not account for the dependence of transverse cracking strain on ply thickness, since the 90° ply crack spacings are averaged for all plies. Transverse cracking theories [104,106,108,115] predict cracking at lower strains in thick 90° plies, and this has been experimentally observed for crossply polymer matrix composites. Thick 90° plies (vs. thin plies) are statistically more likely to contain a critical flaw which leads to crack growth at low laminate strains; thin plies experience more constraint from the 0° plies. The limiting crack spacing is also dependent on transverse ply thickness. At a given strain, the saturation crack spacing increases with transverse ply thickness. This is an expected consequence of the operation of a stress transfer mechanism at the 0/90 ply interface.

Analysis of transverse ply cracking on a ply-by-ply basis in the Nicalon/1723 system yielded consistent spacings in each 90° ply. As expected, the saturation crack density was lower in the central 90° plies (i.e a double thickness ply) due to the greater effective ply thickness. This is illustrated in Fig. 4-26 for a $[0/90]_{2S}$ laminate. However, the thinner plies did not consistently exhibit a greater resistance to transverse ply crack initiation. The initiation of transverse ply cracks was observed at similar strains in all plies, as shown in Fig. 4-26.

Damage development was also investigated in a $[90/0]_{2S}$ laminate to determine the effects of altering the ply stacking sequence. The free edge ply residual stresses are reversed in this configuration. However, this change had little effect on damage development. Transverse ply cracking remained the initial form of damage. Cracking initiated in the longitudinal and transverse plies at similar strains (0.1% and 0.025 %, respectively) to those observed in the [0/90] laminates. A crack spacing versus strain plot for the [90/0] laminate is presented in Fig. 4-27. Limiting crack spacings were comparable to those in [0/90] laminates (Fig. 4-25). Thus, free-edge effects do not appear to significantly affect these results. The effects of the free edge on the transverse tensile strain is not generally significant.

The strains at which longitudinal ply cracking were found to initiate in the crossply laminates are similar to matrix cracking strains determined from the characteristic knee in room temperature tensile curves of unidirectional Nicalon/1723 laminates. Crack spacings in the longitudinal plies of crossply laminates (measured from replicas) were comparable with those reported earlier for unidirectional composites. Replication studies of a unidirectional laminate confirmed these findings. Crack spacings for the unidirectional laminate are overlayed on the plot in Fig. 4-28 for the 0/90 composites. Although the unidirectional specimen failed in the grip region prior to matrix crack saturation, the unidirectional crack spacing data follow the same trend as the 0° plies of the crossply laminate. Matrix cracking initiated at a somewhat lower strain in the unidirectional laminate (approximately 0.06 %).

Nicalon/CAS. Damage development behavior of a Nicalon/CAS crossply laminate was similar to that of the Nicalon/1723 composite, as expected from the similar residual stress states. Transverse ply cracking was the initial form of damage, but did not commence until 0.055 % strain. Matrix cracking in the 0° plies initiated at approximately 0.1 % strain, in agreement with Nicalon/1723. The crack spacing versus strain plots for

Nicalon/CAS and Nicalon/1723 show similar trends. (Compare Figs. 4-25 and 4-29.) However, the limiting spacings are slightly larger for the CAS system. This difference may be due to the higher fracture toughness of the CAS matrix, as discussed later. Fig. 4-30 illustrates a well-developed crack pattern for Nicalon/CAS at high strains. Delamination was not observed.

The spacings in Fig. 4-29, like those of Fig. 4-25, are overall average ply spacings. The Nicalon/CAS composite also showed a difference in crack spacings when analyzed on a ply-by-ply basis. The saturation crack density was again lower in the central 90° plies (i.e a double thickness ply) due to the greater effective ply thickness.

Replicas were obtained from one unidirectional Nicalon/CAS specimen, loaded in tension at 25°C. Premature specimen failure at the tabs prevented a complete replica sequence. However, sufficient replicas were taken to determine the strain level at the onset of matrix cracking. Matrix cracking initiated at 0.15 % strain, in agreement with the crossply laminate replication findings and room temperature tensile test results.

Nicalon/LAS. Two Nicalon/LAS-$[0/90]_{3S}$ specimens were investigated. Replicas were not as clear as those for the 1723 and CAS systems. Polishing problems made it difficult to achieve an adequate surface finish and, consequently, the accuracy of the crack spacing measurements was reduced. Transverse ply cracking remained the initial form of damage, but did not commence until approximately 0.1 % strain. Thus, the first ply cracking strain of Nicalon/LAS was increased threefold relative to Nicalon/1723. Matrix cracks in the 0° plies were not as apparent and initiated at approximately 0.15 to 0.2 % strain. At low strains, crack spacings in the 0° plies were slightly larger than those in the 90° plies. This is evident in the crack spacing versus strain plot in Fig. 4-31. Crack saturation was achieved in both the 0° and 90° plies, and the limiting crack spacings were similar (~200 μm). Crack branching occurred at strain levels approaching the failure strain in all three composite systems, but was most extensive in Nicalon/LAS. (See Fig. 4-32.) No delamination was observed until failure was imminent. Delamination then was observed by pullout of fibers in the longitudinal plies.

Table 4-8 compares the first 90° ply cracking strains of the three composite systems. The calculated residual thermal strains in the 90° plies at the test temperature (25°C) are also included. The residual strains are slightly different from those reported in Table 4-5 since experimental, rather than theoretical, parameters were utilized in the calculations. The

results indicate the LAS system can withstand significantly higher applied mechanical strains before cracking initiates in the transverse plies. Transverse ply cracking is delayed in Nicalon/LAS due to a residual compressive stress in the 90° plies. When the residual and measured strains are added, the first 90° ply cracking strains are similar for the LAS and CAS crossply laminates (approximately 0.07 %). This strain level is in the range of published unidirectional transverse failure strain for Nicalon/LAS.[11]

The low first cracking strain for the 1723 system (total strain = 0.042 %) is attributed to an inherently low crack resistance of the glass matrix for cracks growing parallel to the fibers. The strain value compares with that reported from transverse tension tests of unidirectional Nicalon/1723.[15,66] The resistance to transverse cracking in brittle polymer-matrix composites is proportional to the fracture toughness of the neat matrix.[129] If a similar relationship holds for CMC's, the low fracture toughness of glass relative to glass-ceramics accounts for the decreased resistance to transverse cracking.

Several replicas obtained during loading of a unidirectional Nicalon/LAS laminate revealed similar behavior to the longitudinal plies in the corresponding crossply laminate. Crack spacing versus strain data for the unidirectional laminate are overlayed on the plot for the Nicalon/LAS crossply laminate in Fig. 4-33. The unidirectional crack spacing data follows the same trend as the 0° plies of the crossply laminate. Matrix cracking initiated at similar strains (approximately 0.15 %) and comparable saturation spacings were achieved (200 μm).

Elevated Temperature (550°C):

Damage development studies were also conducted at elevated temperatures (550°C) to determine the effects of residual stress on the damage development process. The replication technique was adapted for high temperature studies, as described in the experimental procedure. Specimens were exposed at 550°C to release (or reduce) residual stresses remaining in the material due to high temperature processing. Two datasets each were obtained for Nicalon/1723-$[0/90]_{2S}$ and Nicalon/LAS-$[0/90]_{2S}$ laminates following 550°C tensile loading to particular strain levels. In addition, some results were obtained for Nicalon/CAS-$[0/90]_{2S}$. Tensile data from these experiments are included in Tables 4-1, 4-2 and 4-3. Measured properties were less than optimal since many specimens failed prematurely due to the spread of delamination which initiated upon bonding the Al end tabs at 98°C. Representative stress-strain curves are shown in Fig. 4-16 for crossply laminates of Nicalon/1723 and Nicalon/LAS at 550°C.

Nicalon/1723. Cracks were observed in both the longitudinal and transverse plies following loading at 550°C to strains as low as 0.025 %. Initial crack spacings of approximately 100 μm and 300 μm were measured in the longitudinal and transverse plies, respectively. No additional damage occurred with further straining at 550°C. Crack densities remained approximately constant, as illustrated in Fig. 4-34. The 550°C crack spacings are slightly larger than the room temperature saturation crack spacings for the 0° and 90° plies. Compare Figs. 4-34 and 4-25.

Crack saturation occurs at very low strains following loading at 550°C. The findings contradict the expectation of delayed cracking in the transverse ply due to release of residual tensile stresses at high temperature. A detailed series of control samples was subsequently investigated to determine the origins of premature cracking. Longitudinal and transverse ply cracking were found to occur prior to loading at high temperature, indicating that the cracks did not form due to straining at elevated temperature. Cracks formed due to thermal cycling even before the samples were tightened in the grips. The initial crack spacings were close to saturation levels. Thus, elevated temperature exposure lowers the threshold for room temperature cracking. The flatness of the curve in Fig. 4-34 indicates Nicalon/1723 is resistant to further cracking at elevated temperature. Straining at 550°C has little effect on damage development after initial cracking.

The crack spacings in Fig. 4-34 are overall average ply spacings. When crack spacings in the 90° plies were considered on a ply-by-ply basis, the effect is similar to that observed at room temperature. The central 90° plies (i.e a double thickness ply) exhibited a low saturation crack density due to the greater effective ply thickness. Cracks were more closely spaced in the thinner, outer 90° plies, as illustrated in Fig. 4-35. Exposure to 550°C caused transverse ply cracks to initiate prior to loading in all 90° plies, regardless of thickness.

Replicas taken after specimen exposure to 550°C were much clearer than those obtained following room temperature testing. Fibers in the transverse plies of Nicalon/1723 were easily distinguished, and cracks were observed to progress around the fibers. Fibers in the transverse plies were not visible on replicas obtained after room temperature loading: white cracks were observed on a dark background. The difference is illustrated in Fig. 4-36. Replicas of the high temperature samples prior to exposure resembled the earlier replicas obtained at room temperature. Therefore, the change is attributed to etching of the glass

matrix at high temperature which creates a height differential between the fibers and matrix. This is highlighted on the replicas and photographed as varying shades of gray. The effect is further evidence that 550°C exposure damages the 1723 system, at least on the surface.

Nicalon/LAS. No cracking was observed in either the longitudinal or transverse plies following repeated loadings at 550°C. Instead, fibers in the transverse plies debonded at strains as low as 0.03 %. Debonded fibers were characterized by a white ring around the fiber periphery and are shown in Fig. 4-37. Fiber debonding was not observed following room temperature loading of Nicalon/LAS crossply laminates until the failure strain (> 0.3 %) was approached. Final failure occurred at both temperatures by delamination.

The observation of debonding at low strains in samples exposed to 550°C suggests that debonding was induced by thermal cycling, rather than straining. It is unknown whether debonding occurred at 550°C or upon cooling to room temperature. However, it is likely that 550° exposure caused the release of residual compressive stresses in the transverse plies, and debonding occurred at 550°C prior to cooldown. Fibers were completely debonded from the LAS matrix, as evidenced by replicas obtained at room temperature. Reloading at 25°C to strains of 0.03 % and 0.08 % did not change the damage structure. Similar structures were also observed in replicas taken at room temperature without any reloading. The debonds did not close in the absence of stress and, thus, stress relaxation does not occur.

Debonding of fibers in the 90° plies altered the residual stress pattern and the cracking conditions in the transverse plies. Consequently, neither transverse nor longitudinal ply cracking occurred. Limited transverse cracking was observed in the vicinity of the delamination. The cracks did not extend very far into the sample and were not regularly spaced, precluding any crack spacing measurements.

Correlation with Fiber/Matrix Bond Strength

The effect of fiber/matrix bond strength on damage development in crossply laminates was investigated. Tables 4-9, 4-10 and 4-11 summarize the bond strengths of Nicalon/1723, Nicalon/CAS and Nicalon/LAS damage development specimens. Although some results were obtained after tensile testing and replication, most measurements were taken prior to testing. Bond strengths were obtained for fibers from several plies in each sample.

The results indicate minimal variation in bond strength through the laminate thickness in most cases. Consistent fiber/matrix bond strengths were measured for individual 90° plies in most samples. However, a significant fluctuation in bond strength was observed through-the-thickness of Nicalon/1723-$[90/0]_{2S}$ laminates (Plate 25), possibly due to a change in prepreg lot during stacking of the plate.

Bond strengths for a particular composite system varied with the material batch. Table 4-9 shows the overall bond strength of the Nicalon/1723-$[0/90]_{2S}$ laminates (Plates 24,30) exceeds that of the Nicalon/1723-$[0/90]_{4S}$ laminates (Plate 13). A similar discrepancy was also observed in the Nicalon/CAS system (Table 4-10) for laminates of similar configuration. The bond strength of the 15.24 cm long laminates (Plate 29) was almost double that of the shorter 10.16 cm laminates (Plate 18). These variations indicate a serious problem in material consistency.

Comparison of Tables 4-1 and 4-9 shows that the more weakly bonded Nicalon/1723 crossply laminate (Plate 13) experienced higher ultimate stresses and strains prior to failure. The lower strength of the strongly bonded material (Plate 24) is attributed to bond strengths which are high enough to cause some longitudinal embrittlement.[67] Strong fiber/matrix bonding was expected to improve off-axis properties and increase the cracking resistance of the transverse plies. However, Fig. 4-25 shows that transverse ply cracks initiated at similar strains in Nicalon/1723 crossply laminates irrespective of bond strength. Table 4-12 summarizes the results for the Nicalon/1723 crossply laminates tested. It suggests the transverse tensile behavior of brittle CMC's is controlled by the fracture toughness in the transverse direction and inherent flaw population, rather than the onset of debonding.

The bond strength of Nicalon/1723-$[0/90]_{2S}$ did not change significantly after tensile testing to failure at 600°C. See Table 4-9, Spec. 24E. Short time exposure to elevated temperatures does not appear to significantly embrittle the 1723 composite.

5. THEORETICAL MODELLING

Theoretical modelling of the damage development process in fiber-reinforced ceramics is necessary to aid in the design of these materials. Suitable models should incorporate microstructural and statistical parameters to predict fracture. Models are needed which can relate fracture predictions to actual service life. Design methodology will only be as accurate as the model used.

Most attempts at modelling the fracture process have involved unidirectional laminates. Considerable progress has been made toward understanding the influence of material properties on cracking of unidirectional brittle matrix composites. [55,58,102,103,130,131] The classical theory of Aveston, Cooper and Kelly [55] predicts the limiting crack spacing and the failure strain of the reinforced matrix based on a simple energy balance. Budiansky, Hutchinson and Evans [103] employed a more rigorous fracture mechanics approach, but current models still involve great simplification in geometric and materials parameters. More detailed descriptions of these models are included in the modelling section of Chapter 2.

Multiple cracking of crossply laminates has been extensively characterized for polymer-matrix composites.[104-110,112-118] However, little theoretical or experimental work has yet been directed toward modelling damage development in multidirectional ceramic-matrix composites. A predictive model is crucial since multidirectional laminates are more likely to be used in design applications.

Two distinct damage models for crossply CMC laminates have been developed in this thesis. The theoretical models were adapted from existing models for polymer-based composites. Modifications were necessary for ceramic-matrix composites to account for residual stresses and longitudinal ply cracking, and are described in the ensuing discussion. The validity of the two theories was verified with experimental data from the replication studies (section 4.3). The models are capable of predicting the development of transverse cracking at room temperature in the crossplied composites of interest, and should be generally applicable to similar fiber-reinforced crossply laminates. Modelling of transverse cracking in these composites is of particular importance since it represents the first phase in the cumulative damage development process.

The energy-based model is an extension of the ACK [55] theory. It was adapted from the work of Garrett and Bailey [104], and Parvizi and Bailey [105] for a $[0/90]_S$ fiberglass/ polyester laminate. This simplified model assumes that cracks develop midway between two existing cracks and is based on a shear lag analysis in which the plies remain elastically bonded. The modified fracture mechanics model of Laws and Dvorak [118] is more realistic. It is useful for predictions, as well as observations. Residual stress effects and progressive cracking statistics are incorporated in this model. In addition, a shear lag parameter, ξ, is introduced to account for sub-optimum stress transfer at the 0/90 ply interfaces.

5.1 Fracture-Mechanics Model

This model was derived from the statistical fracture mechanics theory of Laws and Dvorak [118], summarized in Chapter 2. The theory is based on monotonic simple tensile loading of symmetric crossply laminates and considers the growth of an inherent flaw which is both partially through the thickness and partially through the width of the laminate. Their approach supposes that transverse crack propagation occurs when it is energetically favorable to do so; the location of a developing crack is associated with a probability density function. Specific formulae are developed for stiffness loss as a function of crack density, and crack density as a function of applied load.

Parameters

The model is well-defined since no adjustable parameters were used to fit a particular set of experiments. All parameters used in the analysis were readily determined by standard tests or calculations except for the shear lag parameter, ξ. This parameter is a critical factor in the analysis, and was inferred from standard data and knowledge of the first ply failure stress. The defining equation [118] is essentially a first ply failure criterion:

$$\sigma_a^{fpf} = \left(\frac{\xi b E_l E_o G_c}{d(b+d)E_t}\right)^{1/2} - \frac{E_o}{E_t}\,\sigma_t^R \qquad \text{(A)}$$

where, σ_a^{fpf} = applied stress at first ply failure

ξ = shear lag parameter

d, b = thickness of 90° and 0° plies, respectively

E_t, E_l = transverse and longitudinal moduli, respectively

E_o = modulus of the uncracked laminate

G_c = critical strain energy release rate for cracks parallel to the fibers

σ_t^R = thermal residual stress in 90° plies.

Knowledge of the above parameters was necessary for calculation of ξ. σ_a^{fpf} was determined experimentally from the replication studies; d and b were readily measured. E_t (E_{22}) and E_l (E_{11}) were determined from micromechanics and are included in Appendix B. Experimental measurements were also made in some cases. Calculation of E_o was possible using CLPT once E_{22} and E_{11} were known. σ_t^R was calculated as described in Appendix C. However, the critical strain energy release rate for transverse cracking in the composite, G_c, was unknown. Experimental determination of G_c has been accomplished with polymer composites [132,133], and may be possible with CMC's using a modified double cantilever beam (DCB) test method [134]. Such testing is suggested for a true measure of G_c. For the present analysis, G_c was initially estimated as G_c of the neat matrix. Thus,

$$G_c\,(\text{matrix}) = \frac{K_c^2}{E_m}\,(1 - \nu_m^2) \qquad (B)$$

E_m and ν_m are given in Appendix B; the K_c values for each matrix were obtained from Corning Glass. K_c and the corresponding G_c values are listed in Table 5-1 for the 1723, CAS and LAS matrices. The assumed equivalence of G_c (matrix) and G_c (composite) was considered a reasonable approximation since the fiber volume content of the composites was low (35 %). It was thought to be a conservative estimate since G_c of polymer-matrix composites exceeds G_c (matrix).

Discrepancies between theory and experiment were observed when G_c (matrix) was substituted in the modelling equations. An alternative method was sought for determination of G_c. Although experimental determination of G_c is the most accurate, tests of this type have not yet been sufficiently developed for ceramic composites. Alternatively, G_c was calculated based on the experimentally observed first ply cracking stress. The method employs an energy criterion for first ply cracking, based on the work of Han, et al.[110]. Eqn. 18 in their paper gives the stress in the 90° ply required for first cracking of the transverse ply. Rearrangement of the equation and adjustment for residual stress effects yields the following expression for G_c:

$$G_c = 2\,\gamma_f = 2\,d\left(\left(\frac{\sigma_a^{fpf}}{E_o} + \varepsilon_t^R\right)E_t\right)^2\left(\frac{b\,E_l + d\,E_t}{12\,b\,E_l\,E_t\,G_{23}}\right)^{1/2} \qquad (C)$$

where, γ_f = fracture surface energy

$\frac{\sigma_a^{fpf}}{E_o}$ = average composite strain at first ply failure

ε_t^R = thermal residual strain in 90° plies

$E_t\left(\frac{\sigma_a^{fpf}}{E_o} + \varepsilon_t^R\right)$ = stress in 90° ply at first ply failure

G_{23} = transverse shear modulus

and the other parameters are as defined above. The results of these alternative G_c calculations are also included in Table 5-1. The parameters used in the calculations and the theoretical modelling equations are summarized in Appendix E. Four different datasets ((a) through (d)) are given for Nicalon/LAS, as a function of thermal expansion coefficient.

This was necessary since the crossplied Nicalon/LAS composite used in the room temperature replication studies was not a well-controlled material and exhibited considerable microstructural variability. The laminate was as-pressed at approximately 725°C, and consisted of a mixture of β-quartz and glass. The thermal stability of this system is less than that of a fully crystallized, LAS glass-ceramic matrix composite. Experimentally measured thermal expansion coefficients (2.95 X 10^{-6}/°C) [128] differed from theoretical predictions for the as-pressed condition. Therefore, the theoretical analysis for Nicalon/LAS was conducted with several different laminate thermal expansion coefficients (and, consequently, several residual stresses).

A comparison of Appendices B and E shows differences in the Young's moduli of the longitudinal and transverse plies for each composite system. The E_{11} (E_l) and E_{22} (E_t) values listed in Appendix B were obtained from micromechanics calculations. However, these calculated values and the resultant composite moduli do not agree with experimentally measured moduli. See Tables 4-1, 4-2 and 4-3 for individual modulus measurements.

The longitudinal moduli, measured from tensile tests of unidirectional composites, were slightly higher than the calculated value (E_l = 127.2 GPa). Composite moduli of Nicalon/ 1723, Nicalon/ CAS and Nicalon/LAS crossply laminates, measured in longitudinal tension tests, were significantly less than the CLPT calculated value (E_o = 121.5 GPa). The low composite moduli also suggest low transverse moduli, E_{22}. Experimentally measured transverse moduli were often less than the corresponding micromechanics value (E_t = 115.7 GPa). Transverse tension tests of unidirectional composites yielded approximate

transverse moduli of 101 GPa and 117 GPa for Nicalon/1723 [15,66] and Nicalon/CAS-II [128], respectively. UTRC utilized three different techniques to measure an average transverse modulus of 41 GPa for ceramed Nicalon/LAS and 83 GPa for as-pressed Nicalon/LAS.[11,17]

To obtain a more accurate prediction of the behavior of these composite systems, the experimental moduli were utilized in the theoretical analysis. The moduli listed in Appendix E are averages of the experimentally measured Young's moduli, and were used in calculating residual thermal stresses. Therefore, the residual thermal stresses in Appendix E differ from those in Table 4-5 which are calculated using theoretical moduli. The shear moduli (G_{12} and, thus, G_{23}) reported in Appendix E are calculated values. These were employed in the model since only a minimal difference between theoretical and experimental values was expected.

The exact cause of the discrepancy between experimental and theoretical moduli is unknown. Transverse modulus reductions are unlikely unless fiber/matrix debonding has occurred. This is not inconceivable for the weakly bonded Nicalon/LAS system. The transverse modulus of Nicalon/LAS is inherently low due to a thick interfacial carbon layer (300-500 nm) which contributes to a low bond strength. If the thickness of the carbon layer is considered in the micromechanics calculations, a much lower transverse modulus is predicted. Prewo, et al. [17] found the transverse modulus of Nicalon/LAS to be strongly dependent on matrix condition. Low transverse moduli were measured for LAS composites in the ceramed condition. The transverse moduli of as-pressed composites were closer to the theoretical prediction, but still less than expected. Therefore, the low transverse modulus of ceramed Nicalon/LAS-III is most likely due to fine microcracking in the LAS matrix. The as-pressed modulus value was used for the materials in this study.

The differences between theoretical and calculated moduli were not as substantial for Nicalon/1723 and Nicalon/CAS. The debonding explanation is not feasible for these composites since the fiber/matrix bond strength exceeds that of Nicalon/LAS owing to a thinner interfacial carbon layer. Low measured moduli may be related to non-uniformities in the composite plates due to processing. Specimen condition also affects the modulus measurements. The presence of localized cracking regions may cause localized reductions in modulus. Therefore, the low composite modulus of these materials is attributed to the buildup of damage which occurs during testing. Replication studies revealed extensive damage in both the transverse and longitudinal plies.

Modelling Equations

The stresses in the transverse and longitudinal plies are referred to in the subsequent discussion of transverse cracking. Laws and Dvorak [118] derived expressions for these stresses using shear lag theory. For the ply configuration and crack spacing shown in Fig. 5-1, the stresses are:

$$\sigma_t = \left(\sigma_a \frac{E_t}{E_0} + \sigma_t^R\right)\left(1 - \frac{\cosh \frac{\xi x}{d}}{\cosh \frac{\xi h}{d}}\right) \qquad (D)$$

$$\sigma_l = \sigma_a \frac{E_l}{E_0}\left(1 + \frac{dE_t}{bE_l} \frac{\cosh \frac{\xi x}{d}}{\cosh \frac{\xi h}{d}}\right) + \sigma_l^R\left(1 - \frac{\cosh \frac{\xi x}{d}}{\cosh \frac{\xi h}{d}}\right) \qquad (E)$$

The experimental findings reported in Section 4.3 showed crack density to increase with applied stress. Crack development appears to be related to the inherent flaw population. Transverse ply cracking initiated at low strains in high fiber density regions due to the presence of large inherent flaws. Smaller flaws controlled the damage behavior at higher strains and a saturation crack density was attained. An ideal theoretical model should consider the relationship between microstructure and flaw population. However, no suitable flaw distribution function exists, and determination of an explicit function is difficult. Most existing crack development models employ deterministic methods which are inadequate for predicting the locations of cracks. The Laws and Dvorak model [118] provides the most realistic description of transverse cracking in crossply laminates since it utilizes a statistical analysis, though not a statistical flaw distribution. The statistics of progressive cracking are considered and the location of developing transverse cracks is described by a probability density function, p(y).

The analysis is based on the laminate configuration shown in Fig. 5-2 with an average initial crack separation of 2h and a crack density parameter, β. ($\beta = d/h$.) Crack density is expressed directly as 1/2h. The next crack which appears in the ligament AB occurs at location C. The location of C is random; p(y) is assumed to be proportional to the stress in the transverse ply, $\sigma_t(y)$. From Eqn. (D) with x = y - h:

$$p(y) = \frac{1}{2h}\left(1 - \frac{\cosh\frac{\xi(y-h)}{d}}{\cosh\frac{\xi h}{d}}\right)\left(1 - \frac{\tanh\frac{\xi h}{d}}{\frac{\xi h}{d}}\right)^{-1} \qquad (F)$$

The applied stress needed to produce a crack at C, $\sigma_a(h_1)$, is determined from the critical energy release rate for crack propagation across the ply. The Laws and Dvorak model gives an explicit expression for $\sigma_a(h_1)$.

$$\sigma_a(h_1) = \left(\sigma_a^{fpf} + \frac{E_o}{E_t}\sigma_t^R\right)\left(\tanh\frac{\xi h_1}{2d} + \tanh\frac{\xi h_2}{2d} - \tanh\frac{\xi h}{d}\right)^{-1/2} - \frac{E_o}{E_t}\sigma_t^R \qquad (G)$$

The expected value of applied stress to cause additional cracking in a laminate which already contains cracks of density β is:

$$E[\sigma_a(\beta)] = \int_0^{2h} \sigma_a(y)p(y)dy \qquad (H)$$

Application of numerical methods was necessary to evaluate this integral.

The stiffness loss of the crossply laminate due to transverse cracking was also modelled. An explicit formula was presented for the decrease in stiffness as a function of crack density. Thus, the Young's modulus of a laminate containing transverse cracks is:

$$E(\beta) = E_o\left(1 + \frac{\beta}{\xi}\frac{dE_t}{bE_l}\tanh\frac{\xi}{\beta}\right)^{-1} \qquad (I)$$

The variation in stiffness at high and low crack densities can be obtained by cycling through various values of the crack density parameter, β.

Solutions and Modifications

A computer program was devised to evaluate Eqns. (H) and (I), and is included in Appendix F. To determine the relationship between stiffness loss and crack density (1/2h), a wide range of crack densities was considered. β values ranging from 0.1 through 4 were substituted in Eqn. (I). The results were plotted as a theoretical curve of stiffness vs. crack density for each composite system.

Crack density (1/2h) was also correlated with the expected value of the applied stress to cause additional cracking, described by Eqn. (H). The integral was solved using Simpson's Rule and disciplined mathematical manipulations. The following substitutions were made in Eqn. (G):

$$h_1 = y$$
$$h_2 = 2h - y$$
$$h = d/\beta$$

β was cycled from 0.1 through 4 in increments of 0.1; h varied accordingly. $\beta = 0$ was neglected to avoid division by zero in the expression for h. For each value of β, Eqns. (F) and (G) were evaluated for y ranging from 0 through 2h. The integral, Eqn. (H), was also evaluated from 0 to 2h for each β, and the results plotted. The (0,2h) range was divided into approximately 300 equal intervals to ensure a high level of accuracy in the Simpson's Rule calculation.

Representative plots of p(y) and $\sigma_a(y)$ versus y are shown in Figs. 5-3 and 5-4 for $\beta = 2$. The abscissa on each plot ranges from 0 to 2h, and is analogous to the AB ligament in Fig. 5-2. The probability density function, p(y), indicates that the location of the next crack is most likely to occur near the center of the uncracked ligament. The applied stress for cracking is also lowest near the ligament center. Thus, the likelihood of additional cracking is low in the vicinity of existing cracks.

The solution described above does not consider the effect of the adjacent 0° plies on the transverse cracking process. It was derived for reinforced polymer composites where matrix cracking of the longitudinal plies is prevented due to the high failure strain of the polymer matrix relative to the fibers. The 0° plies remain intact and have a constraining effect on the cracking process in the transverse plies. In ceramic-matrix composites, development of a network of transverse ply cracks is succeeded by longitudinal ply cracking. Cracking of the longitudinal plies causes a decrease in 0° ply stiffness and, thus, composite stiffness. The crack development process in the transverse plies may be altered due to a change in shear stress transfer at the 0/90 interface. For high expansion matrix systems, the decrease in modulus causes a reduction in ply/ply stress transfer, and transverse cracking is retarded. The situation is reversed for Nicalon/LAS due to the opposite residual stress pattern. After matrix cracking occurs in the 0° plies, the cracks close; stress transfer is enhanced.

The Laws and Dvorak theory [118] was modified to account for longitudinal ply cracking and the accompanying stiffness decrease. In addition to the solution outlined above, a second case was considered in which the longitudinal plies were cracked at the outset (i.e. prior to transverse cracking). The parameters used in the above analysis were adjusted to account for the presence of longitudinal ply cracks. Both sets of parameters are included in Appendix E. The parameters for the undamaged laminates are denoted "initial"; adjusted parameters are designated as "cracked".

The decrease in E_l was quantified by examining longitudinal stress-strain curves of analogous unidirectional composites. Secant modulus measurements at various locations along the curve showed minimal differences until a saturation of microcracks was achieved. Thus, a 5 % reduction in longitudinal modulus (E_l) was thought to be sufficient to account for the initial stiffness loss due to longitudinal ply cracking. A corresponding reduction of 5 % was also made to the composite modulus (E_o) of each system. The transverse and shear moduli were presumed to be unaffected by longitudinal ply cracking and no adjustments were made to these parameters.

Some local fiber debonding occurs in the longitudinal plies after matrix cracking initiates. Except for some frictional resistance to sliding (for Nicalon/CAS and Nicalon/1723), the longitudinal fibers are free to move. The 0° plies conform to the strain dictated by the 90° plies, and residual stress and strain decline. In the limit, σ_t^R approaches zero. Therefore, $\sigma_t^R = 0$ was substituted in the revised model.

The applied stress at first ply failure (σ_a^{fpf}) was also adjusted. If the 0° plies are initially cracked, the transverse plies experience a higher load than if there was no preexistent damage. Thus, cracking of the transverse plies initiates at a lower σ_a^{fpf} (i.e. ignoring residual stresses and assuming the 90° ply has some inherent strength). To account for the lower transverse cracking stress, σ_a^{fpf} was adjusted based on the revised moduli. The stress at first ply failure was represented as: $\sigma_a^{fpf} \frac{E_{new}}{E_o}$. No changes were made to the critical energy release rate, G_c. Longitudinal ply cracking was thought to have little effect on G_c. The change in stress transfer at the ply interface was reflected in the shear lag parameter. ξ was recalculated for each composite system using the revised parameters. Table 5-2 summarizes ξ and σ_a^{fpf} for the unadjusted, as well as the cracked conditions.

Comparison with Experiment

For each composite system, the stiffness loss and the applied stress for additional cracking were computed as a function of crack density in the 90° plies. Two cases were considered:

(i) transverse crack development in an undamaged laminate

(ii) transverse crack development in a laminate with preexisting longitudinal ply cracks.

Theoretical curves of crack density (in the transverse plies) vs. applied stress were obtained for both cases. The curves are compared with experimental findings from replication studies in Figs. 5-5 through 5-7. The solid curves in the figures represent Case (i); the dotted curves predict the transverse cracking behavior for Case (ii). Each symbol represents an average crack density for a particular specimen. Since the model was developed for central transverse plies, the experimental crack densities are based on the central 90° plies of each laminate. The predicted stiffness loss due to transverse cracking is plotted in Fig. 5-8 for each composite system, and compared with experimentally measured modulus changes in Figs. 5-9, 5-10 and 5-11.

The theoretical curves were computed using calculated G_c values. Table 5-1 lists G_c's for each composite system, calculated using the two methods described earlier. Several G_c's are given for Nicalon/LAS, dependent upon the laminate thermal expansion coefficient. The predicted crack density was found to be extremely sensitive to the value of G_c. When G_c (matrix) was used in the modelling equations, a large discrepancy was observed between theory and experiment. The slope of the theoretical curve was too shallow, but was found to increase as G_c decreased (i.e. for a given load, crack density decreased with toughness). The strong G_c dependency is evident in Fig. 5-7, (a) through (d). Laws and Dvorak [118] also reported similar findings for E-glass/epoxy crossply laminates. Better agreement was obtained when G_c was calculated using the analysis of Han, et al. [110]. The curves in Figs. 5-5 through 5-11 were computed using these calculated values. Although a better fit between theory and experiment was obtained, the calculated G_c values are much lower than G_c (matrix).

The low G_c values needed to attain conformity are disturbing. They are considerably less than expected, and suggest composite transverse toughness is inferior to that of the unreinforced matrix materials. Experimental measurements of G_c for each composite system are needed to determine the accuracy of the calculated values; the modified DCB test method [134] should prove useful. The low G_c values are indicative of a low fracture energy, and must be related to the weak interface in these composites. The weak interface does not provide much resistance to developing cracks. Cracks can readily propagate along

the fiber/matrix interface, as shown in Fig. 5-12 for Nicalon/BMAS. (See also Fig. 4-23 for Nicalon/1723.) The situation is more severe for low expansion matrix systems (i.e. Nicalon/LAS) since the interface may debond due to a lower fiber/matrix bond strength. A more detailed investigation is needed to determine the effect of interface strength and toughness on composite crack growth and toughness.

The experimental data in Figs. 5-5 through 5-7 show a general trend which is reasonably approximated by the theoretical crack density vs. stress plots. At low stresses, the experimental findings follow the theoretical curve for Case (i). Some deviation occurs as the stress level is increased for each composite system, and is associated with the initiation of longitudinal ply cracking. Once initiated, longitudinal ply cracking is assumed to occur instantaneously. This is reflected in Figs. 5-5, 5-6 and 5-7 by the instantaneous shift in behavior, as indicated by the dashed line between the theoretical curves for Case (i) and (ii). At higher stress levels, the transverse crack density is more accurately predicted by the Case (ii) theoretical curve. The transition associated with the onset of 0° ply cracking is most apparent for the Nicalon/1723 system (Fig. 5-5) since a wide range of experimental data is available. Limited test results were obtained for Nicalon/CAS (Fig. 5-6) and Nicalon/LAS (Fig. 5-7) due to testing and polishing difficulties, as well as a limited material supply. Nevertheless, the data appear to follow a similar trend: agreement with curve (i) until longitudinal ply cracking initiates and the behavior shifts instantaneously to curve (ii).

Nicalon/1723 and Nicalon/CAS crossply laminates demonstrated similar behavior owing to similar residual stress fields. Initially, both composites followed the theoretically predicted curve for the undamaged case. The crack density was slightly lower for the Nicalon/CAS composite at a given load, owing to the higher toughness of the CAS matrix relative to 1723 glass. Longitudinal ply cracking initiated at similar stresses and strains in both systems as indicated in Table 5-3. Accordingly, deviations from the theoretical curve for the undamaged case occurred at similar stress levels (60-70 MPa). Nicalon/1723 then followed the theoretical curve corresponding to a laminate with longitudinal ply cracks, and the transverse crack density levelled off. Nicalon/CAS is expected to exhibit similar behavior at higher applied stresses.

The damage development process of the three composite systems is strongly influenced by residual stresses. Axial residual compressive stresses in the 90° plies of the Nicalon/LAS system delayed the onset of transverse ply cracking until approximately 0.1 % strain.

Longitudinal ply cracking was also delayed relative to 1723 and CAS-matrix composites. Thus, deviations from the initial theoretical curve occurred at a higher stress level, approximately 120 MPa. (See Table 5-3.) Like Nicalon/1723 and Nicalon/CAS, once longitudinal ply cracks initiated, the behavior was more accurately characterized by the adjusted theoretical curve. However, the transverse crack density of Nicalon/LAS did not stabilize after cracking of the 0° plies, but continued to increase with stress. This trend is best illustrated in Figs. 5-7b and 5-7c.

The theoretical curves in Fig. 5-7a were calculated using the experimentally measured laminate expansion coefficient, $\alpha_{lam} = 2.95 \times 10^{-6}/°C$. These curves do not adequately describe the experimental behavior. Thus, a parametric study was conducted to determine the most appropriate α (and σ_t^R and G_c). The data imply a lower expansion coefficient than experimentally measured. This is not unexpected due to the variability of this particular Nicalon/LAS laminate. Figs. 5-7b, 5-7c and 5-7d correspond to expansion coefficients of $2.5 \times 10^{-6}/°C$, $2.0 \times 10^{-6}/°C$, $1.5 \times 10^{-6}/°C$. Fig. 5-7c provides the best fit between theory and experiment. Thus, the behavior of Nicalon/LAS is most accurately described for low α_{lam} and G_c, and high residual stresses.

As discussed in the previous section, cracking of the longitudinal plies causes a decrease in 0° ply stiffness. Thus, shear stress transfer between the 0° and 90° plies is reduced and transverse ply cracking is retarded. This is reflected by a decrease in the calculated shear lag parameter. (See Table 5-2.) A horizontal shift occurred from the "undamaged" to the "cracked" theoretical curves in Figs. 5-5 and 5-6, and the density of 90° ply cracks levelled off. The shift in the Case (i) versus Case (ii) curves was found to be most sensitive to residual stress. Variations in parameters such as moduli, G_c, and shear lag parameter, did not cause significant changes relative to those which resulted from altering the residual stress magnitude.

The shear lag parameter of the Nicalon/LAS composite increased when longitudinal ply cracking was considered (See Table 5-2 and Fig. 5-7). Stress transfer was enhanced since both 0° and 90° ply cracks close upon unloading. Although cracking of the 0° plies initiated at a much higher stress in the LAS system versus Nicalon/1723 and Nicalon/CAS, 90° ply cracking was not retarded. The transverse ply crack density increased dramatically as shown is Fig. 5-7b and 5-7c. Longitudinal ply cracking generates more transverse cracks since the benefit of a compressive residual stress field no longer exists in the 90° plies.

When modified to account for longitudinal ply cracking, the shear lag theory of Laws and Dvorak is a reasonable predictor of transverse cracking behavior in Nicalon fiber-reinforced ceramics. The agreement between theory and experiment is encouraging considering the assumptions made and the complexities of the mathematical formulations. Also, the theory is based on a [0/90/0] laminate with various ply thicknesses. Some differences may result since the experimental results presented in Figs. 5-5, 5-6 and 5-7 were for $[0/90]_{nS}$ laminates with $n \geq 2$.

Transverse ply cracking also cause composite stiffness reductions. The decrease in modulus of the three crossply laminates due to transverse ply cracking is shown in Fig. 5-8. The theoretical curves were predicted from Eqn. (I), assuming no prior damage. The Nicalon/LAS curve represents $\alpha_{lam} = 2.0 \times 10^{-6}/°C$, although little difference was found for the various α's reported in Appendix E. This value was employed since it provided the best fit between theory and experiment in Fig. 5-7. The theory predicts a stiffness decline for each composite system until a transverse crack density of approximately 3 cracks/mm is reached, and the modulus stabilizes at a constant fraction of the initial modulus. For Nicalon/1723 and Nicalon/CAS, a 35-40% stiffness reduction is predicted. The loss is slightly larger for the CAS composite owing to its higher toughness. The smallest decrease in composite modulus is predicted for Nicalon/LAS. The delay in transverse crack initiation for Nicalon/LAS may account for this behavior.

Figs. 5-9, 5-10 and 5-11 show reasonable agreement between theory and experiment for the three composite systems at low transverse crack densities. However, the measured moduli continue to decrease with crack density, and do not stabilize. The continuous moduli reductions are attributed to longitudinal ply cracking, which is not included in the Dvorak and Laws analysis. The initial deviation between theory and experiment occurs at crack densities corresponding to the onset of longitudinal ply cracking. (Compare Figs. 5-5, 5-6, 5-7 with Figs. 5-9, 5-10, and 5-11.) For Nicalon/1723 and Nicalon/CAS, 0° ply cracking initiates at a transverse crack density of 2 to 3 cracks/mm. Longitudinal ply cracking and, thus, significant reductions in the modulus of Nicalon/LAS do not commence until a transverse crack density of 5 cracks/mm is reached. Further work is required to incorporate the effects of longitudinal ply cracking into the stiffness loss predictions.

5.2 Energy-Based Model

A second model was examined to determine if similar transverse ply crack densities can be predicted as a function of applied stress using a different approach. It was adapted from the early transverse cracking theory of Garrett and Bailey [104], with later revisions by Parvizi and Bailey [105]. The model is rather simplistic compared to the statistical fracture mechanics analysis of Laws and Dvorak [118]. The Garrett/Bailey/Parvizi (GBP) theory accounts for the increasing crack density in terms of a non-uniform redistribution of load after transverse cracking; shear lag theory is used to describe the stress state. Cracks are assumed to develop midway between existing cracks and the plies are assumed to remain elastically bonded after cracking. Although the model is deterministic and does not consider an inherent flaw population or the statistics of progressive cracking, it has proven useful in predicting transverse cracking in fiberglass/epoxy crossply laminates. Thus, some consideration of this model for crossplied CMC's is warranted. Modifications were necessary for ceramic-matrix composites to account for residual stresses and longitudinal ply cracking.

Parameters

The parameters utilized in this model were readily measured or calculated from standard data. Many of the parameters (e.g. moduli, ply thicknesses, residual stresses) are the same as those employed in the statistical fracture mechanics model. The stresses and strains in the 90° ply at first ply failure were calculated using the following relationships:

$$\varepsilon_{tu} = \frac{\sigma_a^{fpf}}{E_o} \tag{J}$$

$$\sigma_{tu} = \left(\varepsilon_{tu} + \varepsilon_t^R\right) E_t \tag{K}$$

The σ_{tu} equation is modified from that used in the Garrett and Bailey model to include the effect of residual thermal strain in the transverse plies, ε_t^R. The other parameters remain the same as defined earlier.

A modified shear lag analysis was employed throughout the model. The parameters used in the shear lag analysis have not been defined previously. When a laminate experiences an applied stress, σ_a, transverse cracking initiates at a strain, ε_{tu}. Transverse cracking causes an additional stress, $\Delta\sigma$, to be placed on the longitudinal plies. This additional stress has a maximum value, $\Delta\sigma_o$, in the plane of the transverse crack and decays with distance from

the crack surface as some load is transferred back to the 90° plies by shear transfer. For crossply laminates:

$$\Delta\sigma = \Delta\sigma_o \exp(-\phi^{1/2} y) \tag{L}$$

where

$$\phi = \frac{E_o G_{23}}{E_l E_t}\left(\frac{b + d}{bd^2}\right) \tag{M}$$

and y represents distance in the direction of the applied load. The laminate configuration used for the Garrett/Bailey/Parvizi model is illustrated in Fig. 5-13. As shown in the diagram, the y direction is parallel to the longitudinal plies. Appendix E includes all of the parameters used in the analysis.

Modelling Equations

Energy balances governing load transfer between the longitudinal and transverse plies, and the shear lag equation (Eqn. (L)) are the basis of this model.[104,105] Cracking of the transverse plies is dictated by the load redistribution between the 0° and 90° plies. The first crack occurs when the load carried by the transverse plies reaches $2\,\varepsilon_{tu} E_t\,dc$; this load is then shifted to the longitudinal plies. Further loading of the transverse plies occurs by shear load transfer. The load transferred back to the 90° plies from the 0° plies is:

$$F = 2bc\,\Delta\sigma_o\,[1 - \exp(-\phi^{1/2} y)] \tag{N}$$

where c is the width of the laminate, as shown in Fig. 5-13. Subsequent cracking occurs when the applied stress σ_a (and, thus, $\Delta\sigma_o$) is sufficient for F to reach $2\,\varepsilon_{tu} E_t\,dc$. The next series of cracks occurs midway between existing cracks when the transverse plies are again loaded to $2\,\varepsilon_{tu} E_t\,dc$.

The applied stress (σ_a) is related to the maximum additional stress in the longitudinal plies ($\Delta\sigma_o$) by:

$$\sigma_a = \frac{\Delta\sigma_o}{\frac{b + d}{b} - \frac{E_l}{E_o}} \tag{O}$$

This expression was obtained upon rearrangement of Eqn. (5) in the Parvizi and Bailey paper [105].

For a specimen of length s, first cracking occurs at :

$$\begin{aligned} \sigma_a &= \varepsilon_{tu} E_o \\ \Delta\sigma_o &= \varepsilon_{tu} E_t \frac{d}{b} = \sigma_{tu} \frac{d}{b} \end{aligned} \qquad (P)$$

If initial cracking is assumed to occur in the middle of the specimen, the second and third cracks occur simultaneously at the specimen ends when $\Delta\sigma_o$ becomes large enough. The crack spacing is s/2 and:

$$\Delta\sigma_o = \sigma_{tu} \frac{d}{b} [1 - \exp(-\phi^{1/2} s/2)]^{-1} \qquad (Q)$$

σ_a is readily obtained by substitution of $\Delta\sigma_o$ in Eqn. (O).

The next series of transverse cracks occurs midway between existing cracks and the resultant spacing is s/4

$$\Delta\sigma_o = \sigma_{tu} \frac{d}{b} [1 + \exp(-\phi^{1/2} s/2) - 2\exp(-\phi^{1/2} s/4)]^{-1} \qquad (R)$$

The applied stress for cracking is expressed by Eqn. (O) using the above relation for $\Delta\sigma_o$. The value of $\Delta\sigma_o$ necessary for further cracking is also given by Eqn. (R) with the necessary adjustments for crack spacing. According to the premises of the model, the crack spacing diminishes by 50% for each subsequent cracking event. σ_a is obtained upon substitution of the revised expressions for $\Delta\sigma_o$ into Eqn. (O). The transverse ply cracking sequence continues until a saturation spacing is attained. This may be precluded by delamination or longitudinal ply failure.

Solutions and Modifications

The applied stress necessary for transverse ply cracking was calculated as a function of crack spacing, and the results correlated with experimental findings from room temperature damage development studies of crossplied CMC's. A Fortran program was written to compute the applied stresses for given set of crack spacings. An initial specimen length

was input; transverse crack spacings were automatically calculated based on the premise that developing cracks formed midway between existing cracks. The applied stress was calculated using Eqns. (O), (P) and (Q) during the early stages of cracking. For subsequent cracking and, thus, smaller spacings, repeated application was made of Eqn. (R) in conjunction with Eqn. (O).

Plots of 90° crack spacings versus applied stress were constructed for each composite system. The theoretical analysis [104] predicts a stepped curve: the transverse crack spacing remains unchanged until a specific applied stress is attained and the spacing is reduced by 50%. The stepped curve indicates the crack spacings when the first crack initiates in the middle of a specimen of a particular length. The envelope formed around the stepped curve represents the range of possible crack spacings for specimens of any length with an arbitrary position of the first crack.

The Garrett/Bailey/Parvizi model [104,105] does not account for residual stresses. The replication studies discussed earlier highlighted the major effect these stresses have on the damage development process of ceramic-matrix composites. Therefore, it was necessary to revise the model to include residual stress effects. Residual strain in the transverse plies was already input in the calculation of σ_{tu} (Eqn. (K)). The residual stress in the longitudinal plies must also be included in the analysis, and the expressions for $\Delta\sigma_o$ were altered to include a residual stress term. Hence:

$$\Delta\sigma_o^R = \Delta\sigma_o + \sigma_l^R \qquad (S)$$

where, $\Delta\sigma_o^R$ = revised $\Delta\sigma_o$

$\Delta\sigma_o$ = maximum additional stress in 0° plies due to shear stress transfer

σ_l^R = residual thermal stress in the 0° plies.

Eqns. (P), (Q) and (R) must be revised, and the modified expressions used to calculate σ_a according to the defining Eqn. (O). Values of the residual thermal stresses in the longitudinal plies of the three composite systems of interest are listed in Appendix E.

Further modifications were necessary to include the effects of longitudinal ply cracking. As discussed in the previous section, cracking of the 0° plies caused a stiffness reduction (for the longitudinal plies, and the composite) and a change in the residual stress field. The shear stress transfer was altered and the applied stress at first ply failure decreased. To

account for these changes, the "cracked" parameters listed in Appendix E were utilized in the analysis. In addition, the decreased value of σ_a^{fpf} was represented by $\sigma_a^{fpf} \frac{E_{new}}{E_o}$. The values were previously calculated and are included in Table 5-2.

The effects of longitudinal ply cracking were considered separately from the above cases. The computer program was run with reduced values of E_0, E_l, and σ_a^{fpf}. The same values of E_t and G_{23} were used. Although the above changes should result in a change in the value of ϕ, 5 % reductions in *both* E_0 and E_l negated the effect. The residual stresses were assumed to diminish with cracking. In analogy with the assumptions used in the statistical fracture mechanics model, the residual stresses (σ_t^R and σ_l^R) were assumed to approach zero after the onset of longitudinal ply cracking. Thus, σ_{tu} (see Eqn. (K)) changed due to decreases in both ε_{tu} and ε_t^R. Corresponding changes also occurred in $\Delta\sigma$, $\Delta\sigma_0$ and σ_a. Thus, Eqns. (O), (P), (Q) and (R) were revised accordingly. Applied stress was recalculated as a function of crack spacing and the results plotted.

Comparison with Experiment

The applied stress necessary for transverse cracking was determined as a function of 90° crack spacing for each composite system. Three cases were considered:

(i) transverse crack development in an undamaged laminate (GBP model)

(ii) transverse crack development , including residual stress effects

(iii) transverse crack development in a laminate with preexisting longitudinal ply cracks

Theoretical curves of crack spacing vs. applied stress were obtained for each case. The stepped curves are compared with experimental findings from replication studies in Figs. 5-14, 5-15 and 5-16. Only case (i) and case (ii) are plotted since little difference was found between case (i) and case (iii) for each composite system. As shown previously, the effect of longitudinal ply cracking is substantial. However, it is not adequately described by the Garrett/Bailey/Parvizi model. The envelope formed around the curves represents the range of possible crack spacings. Each symbol represents an average crack spacing for a particular specimen. To comply with the conventions of the model, the experimental crack spacings were based on the central 90° plies of each laminate.

Figs. 5-14 and 5-15 show reasonable agreement between the theoretical curves and the experimental measurements for crossplied Nicalon/1723 and Nicalon/CAS. The data fall within the predicted range of possible crack spacings. At low applied stresses, the transverse cracking behavior is best predicted by the original GBP model, along with

revisions for residual thermal stresses. Some deviation from the theory is evident at high applied stress levels. The behavior at high stresses was more accurately described by the Laws and Dvorak model [118] when modifications were made for longitudinal ply cracking. However, such modifications did not prove effective with the Garrett and Bailey model.

The transverse cracking behavior of Nicalon/LAS is close to the Garrett and Bailey prediction. (See Fig. 5-16.) However, the delay in the onset of transverse ply cracking and the effect of longitudinal ply cracking is not evident with this theory. Additional work is needed to determine the shortcomings of this model before it can be used to effectively describe the behavior of these CMC crossply laminates.

6. CONCLUSIONS

The major contribution of this thesis is an increased understanding of the failure process of fiber-reinforced, ceramic matrix composites. A generalized treatment of mechanical behavior was accomplished by investigating a range of Nicalon fiber-reinforced materials with varying bond strengths, residual stress fields and laminate configurations at both ambient and elevated temperatures. The investigations reported herein have expanded the knowledge base since most of the work to date has been limited to the unidirectional Nicalon/LAS system.

The damage development studies are the first known attempt at monitoring damage accumulation during loading. The onset of damage, as well as saturation and failure, are readily detected with an edge replication technique. The behavior was more easily understood by correlating fiber/matrix bond strength measurements with the damage. Such experiments are an initiative towards establishing a quantitative relationship between damage development behavior and interfacial bond strength. Theoretical modelling of transverse cracking in crossply CMC laminates also represents a pioneering effort. Although cracking of unidirectional brittle-matrix composites has received widespread attention, no models exist for multidirectional CMC's. Thus, a model of transverse cracking based on crossplied polymer-matrix composites was adapted.

Further insight into the high temperature embrittlement process is an additional outcome of this work. The measurements described herein are the first to relate the kinetics of the oxidation process to variations in fiber/matrix bond strength over a range of times and temperatures.

Specific conclusions, based on experimental findings, are related in the subsequent discussion. These are grouped in three sections: (1) Tensile Behavior, (2) Oxidation and High Temperature Embrittlement, and (3) Damage Development. Highlights of the theoretical modelling work are included in a fourth section. Finally, implications of this work and possible solutions are reported.

6.1 Tensile Behavior

Room temperature tensile behavior of unidirectional CMC's is readily determined from stress-strain curve features. Generally, a three stage curve is observed, corresponding to elastic, matrix cracking and post cracking regimes. Composite properties in the initial

linear portion of the curve are adequately described by the rule of mixtures. The curve becomes non-linear when matrix cracking initiates at strains close to the matrix failure strain. Upon reaching a saturation of matrix cracks, the fibers dominate the behavior. Failure occurs at the fiber failure strain when the fibers can no longer endure the applied load.

The performance of unidirectional Nicalon/1723 laminates is near optimal since all three regimes of behavior are demonstrated, and the ultimate failure strain is close to that of the fibers (1 %). However, use of these composites may be restricted to the elastic regime since matrix cracking (initiation strain $\cong$ 0.2 %) allows enhanced oxygen penetration, and causes reductions in composite stiffness and toughness. The extent of matrix cracking can be reduced with higher toughness matrix materials, such as glass-ceramics. CAS and BMAS-matrix composites exhibit similar stress-strain behavior to Nicalon/1723, but the strain to failure is considerably less than the fiber failure strain. The low failure strains of the glass-ceramic matrix composites are attributed to degradation of the reinforcing fibers during elevated temperature processing.

At ambient temperatures, the development of matrix cracks normal to the loading axis dominates the tensile behavior of unidirectional laminates. Matrix cracking is controlled by: axial residual stresses in the matrix, resistance to fiber slippage, and matrix toughness. High fiber/matrix interfacial strengths and axial residual matrix tensile stresses (e.g. Nicalon/1723 and Nicalon/CAS composites) facilitate fiber/matrix load transfer and promote matrix cracking. The opening of matrix cracks is prevented by a high frictional resistance. Excessive matrix cracking occurs if the matrix toughness is too low, as observed by the smaller saturation spacings of unidirectional and crossply Nicalon/1723 laminates relative to similar CAS-matrix systems. Crack saturation cannot be achieved in less strongly bonded, low expansion matrix systems (e.g Nicalon/BMAS) since load transfer is more difficult. The onset of microcracking is delayed by axial residual compressive stresses in the matrices of these composites. When cracking occurs, the low fiber/matrix interfacial strength allows debonding and matrix crack deflection. Sliding of debonded fibers is possible and matrix cracks are bridged by reinforcing fibers.

The degree of fiber/matrix bonding is critical to achieving optimal mechanical performance. In contrast to reinforced polymers and metals, CMC's require bond strength optimization rather than maximization. A moderate level of bonding is preferred for adequate composite toughness. Toughness may be achieved at the expense of composite off-axis strength if the

bond strength is too low; strong bonding causes catastrophic failure. Fiber/matrix bond strength and, hence, toughness of Nicalon-reinforced ceramics is governed by the interfacial carbon layer which forms upon processing. A thick, pure carbon layer is associated with weak bonding.

Bond strength also influences off-axis properties. Low interfacial strength in composites is generally associated with poor off-axis and shear properties. However, strong bonding may not improve the off-axis properties of CMC's. The transverse ply cracking strain of Nicalon/1723 crossply laminates showed minimal change with bond strength. This suggests that flaw population and matrix toughness control transverse cracking, rather than the onset of debonding.

The longitudinal stress-strain curve of crossply laminates contains a fourth damage regime. This regime is not readily apparent from the loading curve. However, correlation of damage development studies with tensile response indicates the initial elastic regime is limited to very low strains due to transverse ply cracking. For Nicalon/1723 and Nicalon/CAS composites, transverse cracking occurs at strains considerably less than the matrix cracking strain. Residual compressive stresses in the 90° plies of low expansion matrix systems (e.g. Nicalon/LAS) delay transverse cracking to higher strain levels. Thus, the failure process of crossply laminates is controlled by ply residual stresses, as well as fiber/matrix bond strength and matrix toughness.

6.2 High Temperature Embrittlement and Interface Oxidation

The elevated temperature tensile properties of Nicalon fiber-reinforced glasses and glass-ceramics (in air) are generally good. Mechanical performance is not significantly affected up to a limiting temperature. The limiting temperature for unidirectional Nicalon/1723 composites is approximately 500°C. Glass-ceramic matrix systems have greater thermal stability, and the decline in properties does not occur until approximately 700°C. Property degradation is accompanied by changes in fracture surface appearance due to reduced residual stresses and/or strengthening of the interfacial bond. Matrix crack spacings and fiber pullout lengths decrease relative to room temperature.

At 1000°C, embrittlement of unidirectional glass-ceramic matrix composites (Nicalon/CAS, Nicalon/BMAS and Nicalon/LAS) is extensive. The behavior is characterized by a two zone fracture: an inner region of short pulled-out fibers, surrounded by an embrittled zone around the specimen periphery. The width of the embrittlement zone corresponds to the

transverse penetration depth of oxygen. Based on these measurements, oxygen penetration is substantial (approximately 30 to 50 % of the specimen thickness) for high temperature tensile samples tested in air. Matrix cracks which form upon loading provide additional paths for ingress of oxygen. Such cracking is necessary for significant transverse penetration of oxygen in the Nicalon/CAS-IIb system. Unstressed samples exposed at 800, 1000 and 1200°C exhibit only limited transverse penetration at various depths below the exposed surface.

Elevated temperature embrittlement is linked to oxidation of the interfacial carbon layer, and is accompanied by an increase in bond strength. The carbon layer is essential for flaw tolerance and its loss causes a significant loss in toughness. Correlation of interfacial bond strength with high temperature embrittlement of Nicalon/CAS-IIb suggests two different interphase oxidation processes. At 800°C, the carbon layer apparently oxidizes away and is replaced by a new, strongly bonded interphase. Moderate increases in bond strength at 1000°C and 1200°C could reflect a partially intact interphase region. Moderate bond strength increases were also observed at 800°C at large depths below the exposed surface; very high bond strengths were observed at 1000°C and 1200°C very close to the exposed (transverse) surfaces. In all cases, oxidation appears to spread along the interface from exposed fiber ends rather than by local fiber-matrix interactions. Decreasing bond strength with depth below the oxidized surface is evidence of an oxygen tunnelling mechanism.

6.3 Damage Development

SEM examination of loaded flexure specimens and an edge replication method are useful for monitoring damage accumulation during loading of unidirectional and crossply laminates. The replication technique is preferred since crack details can be preserved during tensile loading. Hence, a systematic study of the failure process is possible. This procedure was also adapted for damage development studies at 550°C. Although crack patterns are clear, the method is ineffective since thermal cycling to high temperatures causes damage initiation prior to loading.

At room temperature, transverse ply cracking is the initial form of damage for each of the three systems studied (1723, CAS and LAS). Cracks in the 90° plies initiate at strains as low as 0.025 % in Nicalon/1723 crossply laminates. Such cracks grow preferentially in the fiber/matrix interface and are primarily interface cracks. The onset and development of damage in crossply laminates is strongly influenced by residual stresses. Transverse ply cracking is controlled by the resistance to crack growth parallel to the fibers under

transverse loading, as well as residual stresses in the 90° plies. Compressive residual stresses are desirable and delay transverse ply cracking. The LAS system can withstand significantly higher applied mechanical strain than 1723 or CAS crossply laminates prior to transverse ply cracking due to compressive residual stresses in the 90° plies (0.1 % vs. 0.025 % and 0.055 %, respectively). When residual strains are considered, crossplied Nicalon/LAS and Nicalon/CAS composites crack at similar values of 90° ply strain. The low fracture toughness of glass relative to glass-ceramics accounts for the lower first cracking strain of Nicalon/1723.

Matrix cracks in the longitudinal plies of all three composites initiate at higher applied strains than transverse ply cracking, but achieve a higher saturation density. The level of cracking in the 0° plies corresponds with unidirectional test measurements. Stress transfer at the fiber/matrix interface is high for the high expansion matrices (1723 and CAS), and the saturation crack densities exceed those of less strongly bonded systems (Nicalon/LAS). The low fracture toughness of the 1723 glass matrix relative to CAS results in smaller saturation spacings for the Nicalon/1723 crossply laminate. Thus, the initiation strain for longitudinal ply cracking of crossply laminates is dependent on the same factors as matrix cracking in unidirectional laminates, as well as the ply residual stress. Delamination does not occur until the failure strain is approached.

Contrary to expectation, strong fiber/matrix bonding may not improve off-axis properties. A strongly bonded Nicalon/1723 crossply laminate had a lower ultimate tensile strength than a weakly bonded composite. The bond strength difference did not cause any significant change in 90° ply cracking resistance of the two laminates. Equivalent 90° ply crack initiation strains, and similar saturation crack densities were measured. This suggests transverse tension behavior is controlled by inherent flaws and fracture toughness rather than the onset of debonding.

The damage development process is limited by crack propagation, rather than initiation. Large flaws cause damage initiation at low stresses and strains. Smaller flaws dominate the cracking behavior at higher stresses. However, crack propagation does not proceed until the energetics are favorable.

Damage development is not easily characterized at elevated temperatures. Although the adapted replication procedure is ineffective for investigating residual stress and elevated temperature loading effects, the effects of high temperature exposure can be determined.

For Nicalon crossply laminates, thermal cycling to 550°C (prior to gripping and loading) causes longitudinal and transverse ply cracking. Elevated temperature exposure decreases the resistance to cracking at room temperature; subsequent tensile loading at elevated temperatures does not exacerbate the problem. Therefore, application of Nicalon/1723 is limited by temperature rather than stress effects. Use of crossplied Nicalon/LAS at elevated temperatures may also be limited since off-axis properties are degraded. High temperature loading causes fiber debonding in the transverse plies; no 90° ply cracking occurs. Ply residual stresses appear to be the most influential parameter since similar effects were not observed in unidirectional laminates.

6.4 Theoretical Modelling

Experimental findings from the replication studies have been employed in developing a theoretical model to describe the damage behavior. Investigations of several different crossply systems made it possible to develop a generalized model which includes residual stress and bond strength effects. Models of damage development for CMC's are limited, partly due to a shortage of reliable experimental data. Prior to the present work, Nicalon/LAS was the only fiber-reinforced, advanced CMC that had been characterized sufficiently for comparison with existing brittle cracking theories for unidirectional laminates [55,101,103]. No theories exist for damage development in multidirectional ceramic-matrix composites.

The damage model developed herein is based on a statistical fracture mechanics model by Laws and Dvorak [118] for polymer-matrix composites. The merit of this model lies in its treatment of the statistics of progressive cracking and residual stress effects. Most earlier models of transverse cracking in crossply polymer laminates are deterministic and neglect statistics. Well-defined matrix and fiber fracture stresses and strains are assumed. Such models cannot fully account for the flaw dependent behavior of glasses and glass-ceramics. Inclusion of residual stresses is also desirable since they strongly influence the damage development behavior of CMC's.

The empirical model derived from the Laws and Dvorak theory [118] reasonably predicts transverse ply cracking as a function of applied load at room temperature. In addition to residual stresses and progressive cracking statistics, it incorporates a shear lag parameter, ξ, which accounts for sub-optimum shear stress transfer at the fiber/matrix interface. Adjustments have been made for stiffness reductions and decreased stress transfer due to longitudinal ply cracking. The model also delivers an explicit formula for stiffness loss as

a function of crack density. Although derived for specific composite systems, it should be generally applicable to crossplied CMC's.

The statistical fracture mechanics model requires knowledge of the critical strain energy release rate for transverse cracking in the composite, G_c. The G_c values predicted from the analysis of Han, et al.[110] are less than those of the corresponding monolithic matrix materials, suggesting that fiber reinforcement may not enhance toughness parallel to the fibers. The low calculated composite G_c values suggest a low interface fracture energy.

The energy-based models of Garrett and Bailey [104], and Bailey and Parvizi [105] for transverse cracking in polymer-matrix crossply laminates are also valid for CMC's. The models were modified for crossplied ceramic-matrix composites to include residual thermal stresses and reductions in composite stiffness due to longitudinal ply cracking. The revised model provides an alternative approach for determining transverse crack density as a function of applied load. However, the Laws and Dvorak model gives a more accurate description of the transverse cracking behavior.

6.5 Implications

The development of damage in Nicalon fiber-reinforced glass and glass-ceramics is more extensive than preliminary investigations suggest. The promise of these materials for high temperature structural applications is based on early reports that addition of high modulus fibers may enhance the matrix cracking strain of brittle matrices. If a moderate level of interfacial bonding can be attained, the flaw tolerance of unidirectional Nicalon composites is improved relative to the unreinforced matrix and near optimal behavior is possible (i.e. the composite failure strain approaches that of the fibers). Strongly bonded composites are not feasible since matrix crack deflection and fiber debonding cannot occur, and brittle cracking results.

Multidirectional laminates are more likely candidates for actual applications than unidirectional composites. However, damage initiation in crossply laminates can occur at strains considerably less than the matrix failure strain (0.025 %). Transverse cracking at these low strain levels may render the composite unsuitable for potential structural applications due to significant reductions in composite stiffness. In addition, the presence of matrix cracks provides additional paths for oxygen penetration. High temperature embrittlement is likely.

Transverse ply cracking can be delayed with low expansion matrix composites which have a moderate level of fiber/matrix bond strength. The generation of residual compressive stresses in the 90° plies delays the onset of damage. However, release of the residual compressive stresses with loading causes a dramatic increase in transverse crack density. An alternative solution is hybrid composites with fiber and whisker reinforcements. Addition of high aspect ratio whiskers has been found to increase the damage initiation strain threefold relative to fiber-reinforced systems.[128]

Elevated temperature embrittlement is another area which requires further attention before these materials can be successfully employed in demanding environments. Oxidation of the interfacial carbon layer causes a substantial decrease in flaw tolerance. The process is self-propagating since it easily proceeds by oxidation tunnelling from exposed fiber ends. Tailoring of the interphase region of Nicalon fiber-reinforced composites is necessary to limit the oxidation process. In-situ modification of the fiber surface and matrix additions which segregate to the fiber surface are two possibilities.[9,73,135] Although fabrication is not difficult, such modifications may degrade fiber strength. Coating of the fibers with an oxidation resistant material (for example, B_3N_5) is a logical remedy. However, the coating must provide both a flaw tolerant and an oxidation resistant interphase. Most of the work to date has involved SiC-based fibers where an interfacial carbon layer is essential for adequate toughness. Recent developments in high temperature fibers may lead to a more suitable oxidation-resistant fiber.

7. RECOMMENDATIONS FOR FURTHER WORK

Although this study has increased the current level of knowledge of the failure mechanisms of advanced ceramic-matrix composites, further work is required before the damage development process is completely understood. This thesis has created additional questions which must be answered before these materials can be employed in high temperature structural applications.

Determination of the composite strain energy release rate parallel to the fibers, G_c, is of primary importance. The G_c values predicted from the analysis of Han, et al. [110] for cracks parallel to the fibers are less than those of the corresponding unreinforced matrix materials, suggesting fiber reinforcement in the transverse direction may degrade toughness. Experimental determination of composite G_c is needed for a true measurement. G_c for polymer-matrix composites has been obtained using a double cantilever beam (DCB) test method.[132,133] Use of this procedure requires modifications for ceramic-matrix composites. An applied moment double cantilever beam (AMDCB) test has been shown to yield accurate G_c measurements for ceramics.[134] Other test methods for determining fracture toughness of advanced ceramics have been summarized by Anderson [136]. These may require adaptations for composites.

The low calculated composite G_c values parallel to the fibers are indicative of a low interface fracture energy, and must be related to the weak interface in CMC's. A more direct study is necessary to determine crack growth as a function of interface toughness. This should include a systematic study, correlating damage development with interfacial bond strength and toughness. Application of a double torsion test method [136] for obtaining crack velocity vs. toughness data may be useful in comparing crack growth rates.

Further work is also needed in correlating fiber/matrix bond strength with high temperature performance. The oxidation studies of Nicalon/CAS-IIb reported in Section 4.2 are the first known attempt at relating interfacial strength to composite properties over a range of times and temperatures. A more extensive investigation of the elevated temperature embrittlement process is required. Correlation of interfacial structure with bond strengths at various depths from an oxidized surface will aid in understanding the complex interfacial reactions which occur at high temperature. Work should combine high resolution TEM with systematic property evaluations. Kinetics of the oxidation process must be clarified.

Extension of this work to a lower expansion matrix composite may prove useful in highlighting bond strength effects.

Elevated temperature performance is of particular interest since these composites will ultimately be used in demanding high temperature environments. Some high temperature properties were measured in tensile tests of both unidirectional and crossply laminates of all four composite systems. Most data were based on single tests for each condition. Hence, additional high temperature property investigations are needed. These are required to expand the database of high temperature properties, as well as to substantiate earlier tensile test results. A variety of laminate configurations should be examined since it unlikely that unidirectional laminates will be utilized in potential applications.

Mechanical property evaluations should be conducted at test temperatures closer to the targeted use temperatures of the composites (> 1000°C). If the water-cooled hydraulic gripping system is utilized for future elevated temperature testing, modifications to the current specimen design will be necessary. Alternatively, design of a gripping fixture or inserts for the hydraulic grips may allow use of the thickness-tapered specimen [15,66] which proved useful in earlier high temperature property evaluations. Although the water-cooled grips may provide sufficient cooling for the use of tabbed specimens at high temperature, the occurrence of delamination upon curing renders such specimens unsuitable for either room or elevated temperature mechanical property evaluations.

The elevated temperature damage development process requires more detailed characterization and analysis. First, a fundamental study is necessary to determine if high temperature exposure alone causes transverse cracking and/or debonding. An exposure series similar to that for crossplied Nicalon/1723 should also be conducted for Nicalon/CAS and Nicalon/LAS crossply laminates. The procedure involves exposing well-polished specimens to elevated temperatures prior to loading and gripping, and subsequent exposures with small increasing applied loads. Damage development can be determined from replicas of the surfaces taken after exposure. Exposure temperatures in excess of 550°C may be required to cause damage in the CAS and LAS glass-ceramic matrix composites due to their higher thermal stability.

The adapted replication technique, as described above, provides some useful information on high temperature damage. However, this method has inherent deficiencies and better methods for monitoring damage development at elevated temperatures must be established.

A technique developed by researchers at Drexel University [137] may be useful in determining the onset of damage at elevated temperatures. It relates damage events to changes in electrical resistance of surface Au films. An incremental strain test (IST) [138] may also have some application in high temperature damage development studies. An indication of the onset, duration and degree of damage can be determined by measuring the load relaxation at each increment of applied constant strain. Both methods will aid in determining the stress and/or strain levels at which damage develops. However, visual inspection is the only true indicator of the extent of damage, and innovative techniques must be devised for high temperature detection.

Most of the mechanical property evaluations of fiber-reinforced, ceramic-matrix composites have involved flexure testing of unidirectional materials. The present program was undertaken to overcome some of the deficiencies associated with flexure tests and determine the tensile behavior of CMC's. Some progress was made in understanding damage development and failure of unidirectional and crossply laminates in tension. However, it is likely that potential applications of these composites will involve various orientations with differing imposed stress fields and these must be considered.

Composites must be evaluated in various orientations under tensile, shear and compressive loading, as well as combined loading. Transverse tension tests of unidirectional materials are needed to more accurately determine the transverse moduli and failure strains of the various systems, and for comparison with transverse ply failure conditions in crossply laminates. Careful attention to detail will be necessary to obtain accurate measurements since the transverse failure stresses and strains are known to be low. In addition, compression and shear property determinations are needed both at ambient and elevated temperatures. Further development of such test methods are necessary since there are presently none available for CMC's. Compression and shear test methods for polymer-matrix composites must be adapted. Standardization will be required once test methodologies have been established.

Finally, more theoretical work is needed to establish a framework for the experimental investigations. Micro and macro stress and strain field calculations are necessary for a thorough understanding of the failure process. A more extensive treatment of thermal and edge effects should help to explain the experimental findings. Theoretical modelling of the damage development process also requires further attention. An improved model for predicting design stresses at various temperatures is needed. An adequate model must

incorporate fracture mechanics, fracture statistics and residual stresses. Although the statistics of the cracking process were included in the model of Section 5.1, a more accurate treatment must include flaw statistics. Further work is needed to devise a flaw distribution function which adequately describes the inherent flaw population. Additional damage development and replication studies may be required to provide the necessary data.

REFERENCES

1. G. Fisher, "Advanced Ceramics Continue Progress to Products", *Am. Cer. Soc. Bull.*, 63 [2], p. 249 (1984).

2. R.A. Sambell, D. Bowen and D.C. Phillips, "Carbon Fiber Composites with Ceramic and Glass Matrices, Part 2, Continuous Fibers", *J. Mat. Sci.*, 7(7), pp. 676-681 (1972).

3. S.R.Levitt, "High Strength Graphite Fiber-Lithium Aluminosilicate", *J. Mat. Sci.*, 8, pp. 793-806 (1973).

4. D.C. Phillips, R.A. Sambell and D.H. Bowen, "The Mechanical Properties of Carbon Fiber Reinforced Pyrex", *J. Mat. Sci.*, 7, pp. 1454-1464 (1972).

5. D.C. Phillips, "Interfacial Bonding and Toughness of Carbon-Fiber Reinforced Glass and Glass-Ceramics", *J. Mat. Sci.*, 9, pp. 1847-1854 (1974).

6. S. Yajima, K. Okamura, J. Hayashi and M. Omori, "Synthesis of Continuous SiC Fibers with High Tensile Strength", *J. Am. Cer. Soc.*, 59 [7-8], pp. 324-327 (1976).

7. K.M. Prewo and J.J. Brennan,"High Strength Silicon Carbide Fiber Reinforced Glass Matrix Composites", *J. Mat. Sci.*, 15 (2), pp. 463-468 (1980).

8. J.J. Brennan and K.M. Prewo, "Silicon Carbide Fiber Reinforced Glass-Ceramic Matrix Composites Exhibiting High Strength and Toughness", *J. Mat. Sci.*, 17, pp. 2371-2383 (1982).

9. J.J. Brennan, "Additional Studies of SiC Fiber Reinforced Glass-Ceramic Matrices", ONR Contract No. N0014-82-C-0096, Project No. NR32-616/10-30-81 (430), United Technologies Research Center, East Hartford, CT, April 1, 1984.

10. T. Mah, M.G. Mendiratta, A.P. Katz, R. Ruh, K.S. Mazdiyasni, "Room Temperature Mechanical Behavior of Fiber-Reinforced Ceramic-Matrix Composites", *J. Am. Cer. Soc.*, 68 [1], pp. C27-C30 (1985).

11. K.M. Prewo, "Advanced Characterization of SiC Fiber-Reinforced Glass-Ceramic Matrix Composites", ONR Report No. R83-915939-1 under ONR Contract No. N0014-81-C-0571, United Technologies Research Center, East Hartford, CT, June 1983.

12. D.B. Marshall and A.G. Evans, "Failure Mechanisms in Ceramic-Fiber Ceramic Matrix Composites", *J. Am. Cer. Soc.*, 68 [5], pp. 225-231 (1985).

13. E.Y. Luh and A.G. Evans, "High-Temperature Mechanical Properties of a Ceramic Matrix Composite", *J. Am. Cer. Soc.*, 70 [7], pp. 466-469 (1987).

14. T. Mah, M.G. Mendiratta, A.P. Katz, R. Ruh, K.S. Mazdiyasni, "High Temperature Mechanical Behavior of Fiber-Reinforced Glass-Ceramic Matrix Composites", *J. Am. Cer. Soc.*, 68 [1], pp. C248-C251 (1985).

15. D.H. Grande, "Testing and Properties of High Temperature Glass-Ceramic Matrix Composites", Ph.D. Thesis, Massachusetts Institute of Technology, Dept. of Materials Science and Engineering, Cambridge, MA (1987).

16. T. Mah, NASA Conf. Publ. 2357 on Metal Matrix, Carbon and Ceramic Matrix Composites, Proc of NASA/DOD Conf., Cocoa Beach, FL (1984).

17. K.M. Prewo, "Tension and Flexural Strength of Silicon Carbide Fiber-Reinforced Glass-Ceramics", *J. Mat. Sci.*, 21, pp. 3590-3606 (1986).

18. O. Sbaizero and A.G. Evans, "Tensile and Shear Properties of Laminated Ceramic Matrix Composites", *J. Am. Cer. Soc.*, 69 [6], pp. 481-486 (1986).

19. T. Mah "Environmental Effects on Ceramic Matrix Composites at Elevated Temperatures", presented at Am. Cer. Soc. 88th Annual Mtg., Chicago (1986).

20. R.L Stewart, K. Chyung, M.P. Taylor and R.F. Cooper, "Fracture of SiC Fiber/Glass-Ceramic Composites as a Function of Temperature", in Fracture Mechanics of Ceramics, Vol. 7, ed. by R.C. Bradt, A.G. Evans, D.P.H. Hasselman and F.F. Lange, Plenum Publishing Corp. (1986).

21. P.F. Becher and G.C. Wei, "Toughening Behavior in SiC-Whisker-Reinforced Alumina", *Comm. Am. Cer. Soc.*, 67 [12], pp. C267-C269 (1984).

22. G.C. Wei and P.F.Becher, "Development of SiC-Whisker-Reinforced Ceramics", *Am. Cer. Soc. Bull.*, 64 [2], pp. 298-304 (1985).

23. P.D. Shalek, J.J. Petrovic, G.F. Hurley and F.D. Gac, "Hot Pressed SiC Whisker/ Si_3N_4 Matrix Composites", *Am. Cer. Soc. Bull.*, 65 [2], pp. 351-356 (1986).

24. K.P. Gadkaree and K. Chyung, "Silicon-Carbide-Whisker-Reinforced Glass and Glass-Ceramic Composites", *Am. Cer. Soc. Bull.*, 65 [2], pp. 370-376 (1986).

25. R.A. Sambell, D. Bowen and D.C. Phillips, "Carbon Fiber Composites with Ceramic and Glass Matrices, Part 1, Discontinuous Fibers", *J. Mat. Sci.*, 7 (7), pp. 663-675 (1972).

26. K.M. Prewo, "A Compliant High Failure Strain Fiber Reinforced Glass Matrix Composite", *J. Mat. Sci.*, 17, pp. 3549-3563 (1982).

27. K.T. Faber and A.G. Evans, "Crack Deflection Processes - I. Experiment", *Acta. Met.*, 31, pp. 565-576 (1983).

28. D.C. Phillips, "Fibre Reinforced Ceramics", Chapter 6 of Fabrication of Composites, A. Kelly and S.T. Mileiko, eds., North-Holland Publishers, Amsterdam (1983).

29. D.C. Phillips,"High Temperature Fibre Composites", *Proc. 6th Intl. Conf. on Comp. Matls.*, ICCM-VI, Vol. 2, ed. by F.L. Matthews, J.M. Hodgkinson and J. Morton, pp. 1-32 (1987).

30. Advances in Ceramics, Vol. 12, Science and Technology of Zirconia II, ed. by N. Claussen, M. Ruhle and A.H. Heuer, Am. Cer. Soc., Columbus, OH (1984).

31. T. Mah and H.A. Lipsitt, "Silicon Carbide Fiber-Reinforced Magnesium Aluminosilicate Glass-Ceramic Composites", Proc. of a Joint NASA/DOD Conf., Cocoa Beach, FL, NASA Conf. Publ. No. 2291, pp. 153-171, Jan. 20, 1983.

32. J.J. Brennan, K. Chyung and M.R. Taylor, "Reaction-Inhibited Silicon Carbide Fiber Reinforced High Temperature Glass-Ceramic Composites and a Method of Manufacture of the Same", European Pat. Application 0 095 433, June 17, 1983.

33. K.M. Prewo and G.K. Layden, "Advanced Fabrication and Characterization of SiC Fiber-Reinforced Glass-Ceramic Matrix Composites", ONR Report No. R84-916175-1 under ONR Contract No. N0014-81-C-0571, United Technologies Research Center, East Hartford, CT, June 1983.

34. K.M. Prewo, J.J. Brennan and G.K. Layden, "Fiber Reinforced Glasses and Glass-Ceramics for High Performance Applications", *Am. Cer. Soc. Bull.*, 65 [2], pp. 305-313 (1986).

35. K.M. Prewo, "Fiber Reinforced Metal and Glass Matrix Composites", Chapter 6 in Frontiers in Materials Technology, M.A. Meyers and O.T. Inal, eds., Mat. Sci. Monographs #26, Elsevier Publishers, NY, pp. 201-232 (1985).

36. T. Mah, N. Hecht, D. McCullum, J. Hoenigman, H. Kim, H. Lipsitt and A. Katz, "Thermal Stability of SiC Fibers (NICALON)", *J. Mat. Sci.*, 19, pp. 1191-1201 (1984).

37. T.J. Clark, M. Jaffe, J. Rabe, and N.R. Langley, "Thermal Stability Characterization of SiC Ceramic Fibers: I, Mechanical Property and Chemical Structure Effects", *Cer. Eng. Sci. Proc.*, 7 [7-8], pp. 901-913 (1986).

38. L.C. Sawyer, R.T. Chen, F. Haimbach, IV, P.J. Harget, E.R. Prack, and M. Jaffe, "Thermal Stability Characterization of SiC Ceramic Fibers: II, Fractography and Structure", *Cer. Eng. Sci. Proc.*, 7 [7-8], pp. 914-930 (1986).

39. G. Simon and A.R. Bunsell, "The Creep of Silicon Carbide Fibres", *J. Mat. Sci. Lett.*, 2, pp. 80-82 (1983).

40. G. Simon and A.R. Bunsell, "Mechanical and Structural Characterization of the Nicalon Silicon Carbide Fibre", *J. Mat. Sci.*, 19 [11], pp. 3649-3657 (1984).

41. G. Simon and A.R. Bunsell, "Creep Behavior and Structural Characterization at High Temperatures of Nicalon SiC Fibres", *J. Mat. Sci.*, 19 [11], pp. 3658-3670 (1984).

42. A.R. Bunsell and G. Simon, "Mechanical and Structural Characterization of Nicalon SiC Fibres up to 1300°C", *Comp. Sci. and Tech.*, 27, pp. 157-171 (1986).

43. T. Mah, M.G. Mendiratta, A.P. Katz, and K.S. Mazdiyasni, "Recent Developments in Fiber-Reinforced High Temperature Ceramic Composites", *Am. Cer. Soc. Bull.*, 66 [2], pp. 304-308 (1987).

44. J.A. Cornie, Y.-M. Chiang, D.R. Uhlmann, A. Mortensen, and J.M. Collins, "Processing of Metal and Ceramic Matrix Composites", *Am. Cer. Soc. Bull.*, 65 [2], pp. 293-304 (1986).

45. A.J. Caputo and W.J. Lackey, "Fabrication of Fiber-Reinforced Ceramic Composites by Chemical Vapor Infiltration", *Cer. Eng. Sci. Proc.*, 5 [7-8], pp. 654-667 (1984).

46. A.J. Caputo, W.J. Lackey and D.P. Stinton, "Development of a New, Faster Process for the Fabrication of Ceramic Fiber-Reinforced Ceramic Composites by Chemical Vapor Infiltration", *Cer. Eng. Sci. Proc.*, 6 [7-8], pp. 694-706 (1985).

47. D.P. Stinton, A.J. Caputo and R.A. Lowden, "Synthesis of Fiber-Reinforced SiC Composites by Chemical Vapor Infiltration", *Am. Cer. Soc. Bull.*, 65 [2], pp. 347-350 (1986).

48. J.W. Warren, "Fiber and Grain-Reinforced Chemical Vapor Infiltration (CVI) Silicon Carbide Matrix Composites", *Cer. Eng. Sci. Proc.*, 5 [7-8], pp. 684-693 (1985).

49. M.S. Newkirk, A.W. Urquhart and H.R. Zwicker, "Formation of Lanxide™ Ceramic Composite Materials", *J. Mat. Res.*, 1 [1-2], pp. 81-89 (1986).

50. Y.-M. Chiang, J.S. Haggerty, R.P. Messner and C. Demetry, "Reaction-Based Processing Methods for Ceramic-Matrix Composites", *Am. Cer. Soc. Bull.*, 68 [2], pp. 420-428 (1989).

51. D. Hull, "Strength of Unidirectional Laminae", in An Introduction to Composite Materials, Cambridge University Press, Cambridge (1981).

52. J. Aveston, "Strength and Toughness in Fibre-Reinforced Ceramics", in Properties of Fiber Composites, Conf. Proc., Nat. Phys. Lab., I.P.C. Science and Technology Press, Guildford, pp. 63-73, Nov. 1971.

53. D.K. Shetty, "Ceramic Matrix Composites", Current Awareness Bulletin, Metals and Ceramics Information Center, Battelle Columbus Labs, 118 [12] (1982).

54. A. Kelly, Strong Solids, 2nd edition, Oxford University Press, Oxford (1973).

55. J. Aveston, G.A. Cooper and A. Kelly, "Single and Multiple Fracture" in Properties of Fiber Composites, Conf. Proc., Nat. Phys. Lab., I.P.C. Science and Technology Press, Guildford, pp. 15-26, Nov. 1971.

56. P.J. Romauldi and G.B.Batson, "Mechanics of Crack Arrest in Concrete", *Proc. Amer. Soc. Civil Eng.*, 89, pp. 146-168 (1963).

57. J. Aveston, R.A. Mercer, and J.M. Silwood, "Fiber Reinforced Cements - Scientific Foundations for Specifications" in *Proc. of the Conf. of Comp. - Standards, Testing and Design*, I.P.C. Science and Technology Press, Guildford, p. 93, April 1974.

58. G.A. Cooper and J.M. Silwood, "Multiple Fracture in a Steel Reinforced Epoxy Resin Composite", *J. Mat. Sci.*, 7, p. 325 (1972).

59. D.C. Larsen, S.L. Stuchly, S.A. Bortz and R. Ruh, "Test Methodology for Ceramic Fiber Composites: Results for SiC/LAS, SiC/SiC and C/SiC Composites", paper presented at DOD/NASA Advanced Composites Working Group, 9th Conf. on Composite Materials, Cocoa Beach, FL, Jan. 1985.

60. J.J. Mecholsky, "Evaluation of Mechanical Property Testing Methods for Ceramic Matrix Composites", *Am. Cer. Soc. Bull.*, 65 [2], pp. 315-322 (1986).

61. R.W. Rice, "Mechanisms of Toughening in Ceramic-Matrix Composites", *Cer. Eng. Sci. Proc.*, 2 [7-8], pp. 661-701 (1981).

62. R.W. Rice, "Ceramic-Matrix Composite Toughening Mechanisms: An Update", *Cer. Eng. Sci. Proc.*, 6 [7-8], pp. 589-607 (1985).

63. A.H. Cottrell, "Strong Solids", *Proc. R. Soc. Lond.*, A 282, pp. 1-9 (1964).

64. A. Kelly, "Interface Effects and the Work of Fracture of a Fibrous Composite", *Proc. R. Soc. Lond.*, A 319, pp. 95-116 (1970).

65. J.F. Mandell, "Fatigue Behavior of Short Fiber Composite Materials", Chapter 9 in The Fatigue Behavior of Composite Materials, K.L. Reifsnider, ed., (in press).

66. J.F. Mandell, D.H. Grande and B. Edwards, "Test Method Development for Structural Characterization of Fiber Composites at High Temperatures", *Cer. Eng. Sci. Proc.*, 6 [7-8], pp. 524-535 (1985).

67. D.H. Grande, J.F. Mandell and K.C.C. Hong, "Fiber/Matrix Bond Strength Studies of Glass, Ceramic and Metal Matrix Composites", *J. Mat. Sci.*, 23 (1), pp. 311-328 (1988).

68. R.W. Davidge, "Fibre-Reinforced Ceramics", *Composites*, 18 (2), pp.92-98 (1987).

69. J.F. Mandell, D.H. Grande, T.-H. Tsiang and F.J. McGarry, "Modified Microdebonding Test for Direct In-Situ Fiber/Matrix Bond Strength Determination in Fiber Composites" in Composite Materials: Testing and Design , ASTM STP 893, ed. by J.M. Whitney, ASTM, Philadelphia, PA, pp. 87-108 (1986).

70. D.B. Marshall, "An Indentation Method for Measuring Matrix-Fiber Frictional Stresses in Ceramic Composites", *Comm. Am. Cer. Soc.*, 67, pp. C259-C260 (1984).

71. D.B. Marshall and W.C. Oliver, "Measurement of Interface Properties in Ceramic Composites", *J. Am. Cer. Soc.*, 70 , p. 542 (1987).

72. T.P. Weihs and W.D. Nix, "Direct Measurement of the Frictional Resistance to Sliding of a Fiber in a Brittle Matrix", *Scripta Met.*, 22, p. 271 (1988).

73. J.J. Brennan, "Interfacial Studies of SiC Fiber Reinforced Glass-Ceramic Matrix Composites", ONR Contract No. N0014-82-C-0096, United Technologies Research Center, East Hartford, CT, Sept 30, 1986.

74. R.F. Cooper and K. Chyung, "Structure and Chemistry of Fibre-Matrix Interfaces in Silicon Carbide Fibre-Reinforced Glass-Ceramic Composites: An Electron Microscopy Study", *J. Mat. Sci.*, 22, pp. 3148-3160 (1987).

75. B.A. Bender, D. Lewis III, W.S. Coblenz and R.W. Rice, "Electron Microscopy of Ceramic Fiber-Ceramic Matrix Composites - Comparison with Processing and Behavior", *Cer. Eng. Sci. Proc.*, 5 [7-8], pp. 513-529 (1984).

76. A.S. Argon and F.A. McClintock, eds., Mechanical Behavior of Materials, Chapter 12, Addison-Wesley Publishing Co., Reading, MA, pp. 420-432 (1966)

77. J.D. Eshelby, "The Determination of the Elastic Field of an Ellipsoidal Inclusion and Related Problems", *Proc. R. Soc. Lond.*, A 241, pp. 376-396 (1957).

78. M.R. Piggott, Load Bearing Fiber Composites, Pergamon Press, Elmsford, NY (1980).

79. R.M. Jones, Mechanics of Composite Materials, Scripta Book Co., Washington, D.C. (1975).

80. I.M. Daniel and T. Liber, "Effect of Laminate Construction on Residual Stresses in Graphite/Polyimide Composites", *Exptl. Mech.*, 17 (1), p. 21 (1977).

81. R.A. Schapery, "Thermal Expansion Coefficients of Composite Materials Based on Energy Principles", *J. Comp. Mat.*, 2, p. 380 (1968).

82. H.T.Hahn and N.J. Pagano, "Curing Stresses in Composite Laminates", *J. Comp. Mat.*, 9, p. 91 (1975).

83. H.T.Hahn, "Residual Stresses in Polymer Matrix Composite Laminates", *J. Comp. Mat.*, 10, p. 266 (1976).

84. G.Jeronimidis and A.T. Parkyn, "Residual Stresses in Carbon Fibre-Thermoplastic Matrix Laminates", *J. Comp. Mat.*, 22, pp. 401-415 (1988).

85. M. Vedula, R.N. Pangborn and R.A. Queeney, "Fibre Anisotropic Thermal Expansion and Residual Thermal Stress in a Graphite/Aluminium Composite", *Composites*, 19 (1), pp. 55-60 (1988).

86. R.J. Arsenault and M. Taya, "The Effects of Differences in Thermal Coefficients of Expansion in SiC Whisker 6061 Aluminum Composites", *Proc. 5th Intl. Conf. on Comp. Matls*, ICCM-V, ed. by W.C. Harrigan, Jr., J. Strife and A.K. Dingra, pp. 21-36 (1985).

87. O.B. Pedersen, "Residual Stresses and the Strength of Metal Matrix Composites", *Proc. 5th Intl. Conf. on Comp. Matls*, ICCM-V, ed. by W.C. Harrigan, Jr., J. Strife and A.K. Dingra, pp. 1-36 (1985).

88. R.B. Pipes and N.J. Pagano, "Interlaminar Stresses in Composite Laminates under Axial Extension", *J. Comp. Mat.*, 4, pp. 538-48 (1970).

89. A.S.D. Wang and F.W.Crossman, "Some New Results on Edge Effects in Symmetric Composite Laminates", *J. Comp. Mat.*, 11, pp. 92-106 (1977).

90. A.S.D. Wang and F.W. Crossman, "Initiation and Growth of Transverse Cracks and Edge Delamination in Composite Laminates", Part 2, Experimental Correlation, *J. Comp. Mat. Suppl.*, 14, pp. 88-108 (1980).

91. J.B. Schutz, "Failure Criteria for Ceramic Matrix Composite Laminates", Ph.D. Thesis Proposal, Massachusetts Institute of Technology, Dept. of Materials Science and Engineering, Cambridge, MA (1988).

92. J.B. Brewer, "Failure of Graphite/Epoxy Induced by Delamination, Ph.D. Thesis, Massachusetts Institute of Technology, Dept. of Aeronautics and Astronautics, Cambridge, MA (1988).

93. S.S. Wang, "Delamination Crack Growth in Unidirectional Fiber-Reinforced Composites under Static and Cyclic Loading", in Composite Materials: Testing And Design, ASTM STP 674, ASTM, Philadelphia, PA, pp. 642-663 (1979).

94. C. Kassapoglou, "Interlaminar Stresses at Straight Free Edges of Composite Laminates", M.S. Thesis, Massachusetts Institute of Technology, Dept. of Aeronautics and Astronautics, and Dept. of Mech. Engineering, Cambridge, MA (1984).

95. P. Lagace, J. Brewer and C. Kassapoglou, "The Effect of Thickness on Interlaminar Stress and Delamination in Straight-Edged Laminates", *J. Comp. Tech. and Research*, 9 (3) pp. 81-87 (1987).

96. A.S.D. Wang and F.W. Crossman, "Edge Effects on Thermally Induced Stresses in Composite Laminates", *J. Comp. Mat.*, 11, pp. 300-312 (1977).

97. A.S.D. Wang and F.W. Crossman, "Initiation and Growth of Transverse Cracks and Edge Delamination in Composite Laminates", Part 1, An Energy Method, *J. Comp. Mat. Suppl.*, 14, pp. 71-87 (1980).

98. E.F. Rybicki, D.W. Schmueser, and J. Fox, "An Energy Release Rate Approach for Stable Crack Growth in the Free-Edge Delamination Problem", *J. Comp. Mat.*, 11, pp. 470-487 (1977).

99. T.K. O'Brien, "Characterization of Delamination Onset and Growth in a Composite Laminate", in Damage in Composite Materials, ASTM STP 775, ed. by K.L. Reifsnider, ASTM, Philadelphia, PA, pp. 140-167 (1982).

100. F.W. Crossman and A.S.D. Wang, "The Dependence of Transverse Cracking and Delamination on Ply Thickness in Graphite/Epoxy Laminates", in Damage in Composite Materials, ASTM STP 775, ed. by K.L. Reifsnider, ASTM, Philadelphia, PA, pp. 118-139 (1982).

101. J. Aveston and A. Kelly, "Theory of Multiple Fracture of Fibrous Composites", *J. Mat. Sci.*, 8 , pp. 352-362 (1973).

102. D.B. Marshall, B.N. Cox and A.G. Evans, "The Mechanics of Matrix Cracking in Brittle-Matrix Fiber Composites", *Acta Met.*, 33 (11), pp. 2013-2021 (1985).

103. B. Budiansky, J.W. Hutchinson and A.G. Evans, "Matrix Fracture in Fiber-Reinforced Ceramics", *J. Mech. Phys. Solids*, 34 (2), pp. 167-189 (1986).

104. K.W. Garrett and J.E. Bailey, "Multiple Transverse Fracture in 90° Cross-Ply Laminates of a Glass Fibre-Reinforced Polyester", *J. Mat. Sci.*, 12 pp. 157-168 (1977).

105. A. Parvizi and J.E. Bailey, "On Multiple Transverse Cracking in Glass Fiber Epoxy Cross-Ply Laminates", *J. Mat. Sci.*, 13 pp. 2131-2136 (1978).

106. A. Parvizi, K.W. Garrett and J.E. Bailey,"Constrained Cracking in Glass Fibre-Reinforced Epoxy Cross-Ply Laminates", *J. Mat. Sci.*, 13 pp. 195-201 (1978).

107. Y. Korczynskyj and J.G. Morley, "Constrained Cracking in Cross-Ply Laminates", *J. Mat. Sci.*, 16, pp. 1785-1795 (1981).

108. P.W.M. Peters, "Constrained 90° Ply Cracking in 0/90/0 and ±45/90/+45 CFRP Laminates", in Composite Materials: Fatigue and Fracture, ASTM STP 907, ed. by H.T. Hahn, ASTM, Philadelphia, PA, pp. 84-99 (1986).

109. J.E. Bailey, P.T. Curtis and A. Parvizi, "On the Transverse Cracking and Longitudinal Splitting Behaviour of Glass and Carbon Fibre Reinforced Epoxy Cross Ply Laminates and the Effect of Poisson and Thermally Generated Strain", *Proc. R. Soc. Lond.*, A 366, pp. 599-623 (1979).

110. Y.M. Han, H.T. Hahn and R.B. Croman, "A Simplified Analysis of Transverse Ply Cracking in Cross-Ply Laminates", *Comp. Sci. and Tech.*, 31, pp. 165-177 (1988).

111. H.T. Hahn and T. Johannesson, "Fracture of Unidirectional Composites: Theory and Applications, in Mechanics of Comp. Matls., AMD, 58, ASME, New York, pp. 135-42 (1983).

112. P.W.M. Peters, "The Strength Distribution of 90° Plies in 0/90/0 Graphite-Epoxy Laminates", *J. Comp. Mat.*, 18, pp. 545-556 (1984).

113. P.W. Manders, T.W. Chou, F.R. Jones, J.W. Rock, "Statistical Analysis of Multiple Fracture in 0°/90°/0° Glass Fibre/Epoxy Resin Laminates", *J. Mat. Sci.*, 18, pp. 2876-2889 (1983).

114. H. Fukunaga, T.W. Chou, P.W.M. Peters, K. Schulte, "Probabilistic Failure Strength Analyses of Graphite/Epoxy Cross-Ply Laminates", *J. Comp. Mat.*, 18, pp. 339-356 (1984).

115. A.S.D. Wang, P.C. Chou and S.C. Lei, "A Stochastic Model for the Growth of Matrix Cracks in Composite Laminates", *J. Comp. Mat.*, 18, pp. 239-254 (1984).

116. A.S.D. Wang, N.N. Kishore and C.A. Li, "Crack Development in Graphite-Epoxy Cross-ply Laminates under Uniaxial Tension", *Comp. Sci. and Tech.*, 24, pp. 1-31 (1985).

117. A.S.D. Wang, "Fracture Mechanics of Sublaminate Cracks in Composite Materials", *Comp. Tech. Review*, 6, p. 45 (1984).

118. N. Laws and G.J. Dvorak, "Progressive Transverse Cracking in Composite Laminates", *J. Comp. Mat.*, 22, pp. 900-916 (1988).

119. J.E. Masters and K.L. Reifsnider, "An Investigation of Cumulative Damage Development in Quasi-Isotropic Graphite/Epoxy Laminates", in Damage in Composite Materials, ASTM STP 775, ed. by K.L. Reifsnider, ASTM, Philadelphia, PA, pp. 40-62 (1982).

120. R.D. Jamison, K. Schulte, K.L. Reifsnider and W.W. Stinchcomb, "Characterization and Analysis of Damage Mechanisms in Tension-Tension Fatigue

of Graphite/Epoxy Laminates", in Effects of Defects in Composite Materials, ASTM STP 836, ASTM, Philadelphia, PA, pp. 21-55 (1984).

121. M.G. Bader and L. Boniface, "Damage Development During Quasi-Static and Cyclic Loading in GRP and CRFP Laminates Containing 90° Plies", *Proc. 5th Intl. Conf. on Comp. Matls*, ICCM-V, ed. by W.C. Harrigan, Jr., J. Strife and A.K. Dingra, pp. 221-232 (1985).

122. D. Liu, L.S. Lillycrop, L.E. Malvern and C.T. Sun, "The Evaluation of Delamination - An Edge Replication Study", *Exptl. Tech.*, Society for Exptl. Mech., 11(5), pp. 20-25 (1987).

123. S.E. Groves, C.E. Harris, A.L. Highsmith, D.H. Allen and R.G. Norvell, "An Experimental and Analytical Treatment of Matrix Cracking in Cross-ply Laminates", *Exptl. Mech.*, pp. 73-79 (1987).

124. D.A. Ulman and E.G. Henneke II, "Nondestructive Evaluation of Damage in FP/Al Composites", in Composite Materials: Testing And Design, ASTM STP 787, I.M. Daniel, ed., ASTM, Philadelphia, PA, pp. 323-342 (1982).

125. J.F. Mandell, J.H. Chen and F.J. McGarry in *Proc. 35th Conf. of Reinf. Plastics/ Composite Institute,* Society of the Plastics Industry, New York (1980).

126. D.H. Grande, "Microdebonding Test for Measuring Shear Strength of the Fiber/ Matrix Interface in Composite Materials", S.M. Thesis, Massachusetts Institute of Technology, Dept. of Materials Science and Engineering (1983).

127. S.-H. Jao, "Interface Studies in Composite Materials", S.M. Thesis, Massachusetts Institute of Technology, Dept. of Materials Science and Engineering, Cambridge, MA (1988).

128. Corning Glass Works, Personal Communication, 1988.

129. D.L. Hunston, "Characterization of Interlaminar Crack Growth in Composites with the Double Cantilever Beam Specimen", in Tough Composites - Recent Developments, Noyes Publishers, Park Ridge, NJ, pp. 2-14 (1985).

130. L.N. McCartney, "Mechanics of Matrix Cracking in Brittle-Matrix Fibre-Reinforced Composites", *Proc. R. Soc. Lond.,* A 409, pp. 329-350 (1987).

131. M.D. Thouless and A.G. Evans, "Effects of Pull-Out on the Mechanical Properties of Ceramic-Matrix Composites", *Acta Met.*, 36 (3) pp. 517-522 (1988).

132. J.M. Whitney, C.E. Browning, and W. Hoogsteden, "A DCB Test for Characterizing Mode I Delamination of Composite Materials", *J. Reinf. Pl. and Comps.*, 1, pp. 297 (1982).

133. P.E. Keary, L.B. Ilcewicz, C. Shaar and J. Trostle, "Mode I Interlaminar Fracture Toughness of Composites using Slender Double Cantilevered Beam Specimens", *J. Comp. Mat.*, 19, p. 154 (1985).

134. C. Cm. Wu, J. Cunnif and K.R. McKinney, "Modified DCB Method for Measurement of High Toughness Ceramic Composites", *Cer. Eng. Sci. Proc.*, 6 [7-8], pp. 550-557 (1985).

135. J.J. Brennan, "Interfacial Characterization of Glass and Glass-Ceramic Matrix/ Nicalon SiC Fiber Composites" in Tailoring Multiphase and Composite Ceramics, ed. by R.E. Tressler, G.L. Messing, C.G. Pantano and R.E. Newnham, Plenum Press, NY, pp. 549-560 (1986).

136. R.M. Anderson, "Testing Advanced Ceramics", *Adv. Mat. & Processes*, 135 (3), pp. 31-36 (1989).

137. M. Barsoum and O.Z. Zhou, "Microcracking in Ceramic/Ceramic Composites", presented at 89th Annual Meeting, Am. Cer. Soc., Pittsburgh, PA (1987).

138. R.E. Swain, K.L. Reifsnider and J. Vittoser, "The Investigation of Damage in Composite Laminates Using the Incremental Strain Test", in Composite Materials: Testing and Design (9th Conf), ASTM STP to be published.

TABLES

TABLE 2-1 *

New Ceramic Fibers

Manufacturer	Designation	Composition (wt %)	Tensile Strength (MPa)	Tensile Modulus (GPa)	Density (g/cc)	Diameter (mm)
UBE	Tyranno	Si,Ti,C,O	>2970	>200	2.3 - 2.5	8 - 10
Avco/Textron		Si,C	>2800	280-315		6 - 10
Dow Corning/ Celanese	MPDZ	47Si,30C,15N,8O	1750-2100	175-210	2.3	10 - 15
Dow Corning/ Celanese	HPZ	59Si,10C,28N,3O	2100-2450	140-175	2.35	10
Dow Corning/ Celanese	MPS	69Si,30C,1O	1050-1400	175-210	2.6 - 2.7	10 - 15
3M	Nextel440	$70Al_2O_3,28SiO_2,2B_2C_3$	2100	189	3.05	10 - 12
3M	Nextel480	$70Al_2O_3,28SiO_2,2B_2O_3$	2275	224	3.05	10 - 12
Du Pont	PRD-166	Al_2O_3, 15-25 ZrO_2	2100-2450	385	4.2	20

* reproduced from Ref. (43)

All data were provided by fiber manufacturers and their distributors. Mechanical property data are for room temperature. Fiber gage lengths tested may differ, making direct comparison of tensile strength data questionable.

TABLE 3-1 *
Fiber/Matrix Compositions and Properties

	Nicalon™ Fibers	Code 1723 Aluminosilicate	BMAS Glass-Ceramic	CAS Glass-Ceramic	LAS Glass-Ceramic
Major Constituents	β-SiC, SiO_2, C	Al_2O_3,MgO,CaO, SiO_2	BaO, MgO, Al_2O_3, SiO_2	CaO,Al_2O_3,SiO_2	Li_2O,Al_2O_3,MgO, SiO_2,Nb_2O_5
Primary Crystalline Phase	β-SiC	—	Ba-osumilite $BaMg_2Al_6Si_9O_3$	stoichiometric anorthite $CaAl_2Si_2O_8$	β-spodumene
Fiber Diameter (μm)	10-20				
Density (g/cc)	2.55	2.64	2.77		
Coeff. Therm Expansion (10^{-7}/°C)	32 (0 - 600°C) 39.3 (0-1200°C)	50 (0-600°C)	27 (0-1150°C)	52 (0-1250°C)	15 (0-1000°C)
Young's Modulus(GPa)	200	88	106	88	88
Shear Modulus (GPa)	77	36	43	36	36
Tensile Strength(GPa)	2.07				
Poisson Ratio	0.299	0.222	0.222	0.222	0.222
Solidification Temp (°C)		620	1130	1230	1030

* Properties supplied by Dr. K. Chyung (Corning Glass Works) and from Refs. 20,74.

TABLE 4-1

Longitudinal Tensile Test Data
Nicalon/1723

Spec. No.	Configuration	Test T (°C)	UTS (MPa)	E (GPa)	ε_u (%)
23A[i]	$[0]_8$	25	479	149.51	0.355+
23B[i]	$[0]_8$	25	460	139.36	0.332
23C[i]	$[0]_8$	25	331	144.21	0.231
* 23D2[i]	$[0]_8$	25	462	163.80	0.294
33A[ii]	$[0]_{12}$	550	356	142.00	0.366
* 13G[ii]	$[0/90]_{4S}$	25	242	98.80	0.574
* 13H[ii]	$[0/90]_{4S}$	25	268	85.32	0.950
24A[iii]	$[0/90]_{2S}$	25	169	90.14	0.320
24B[ii]	$[0/90]_{2S}$	25	171	111.90	0.299
* 24C[ii]	$[0/90]_{2S}$	25	124	102.90	0.381
* 24F[ii]	$[0/90]_{2S}$	25	171	113.89	0.330
* 25A[ii]	$[90/0]_{2S}$	25	222	77.03	0.600
24D[iii]	$[0/90]_{2S}$	600	196	121.67	0.425
24E[iv]	$[0/90]_{2S}$	600	105	88.73	0.120
* 30A3[ii]	$[0/90]_{2S}$	550	129	87.27	0.220
* 30B6[ii]	$[0/90]_{2S}$	550	117	92.47	0.190
30C[ii]	$[0/90]_{2S}$	550	120	96.47	0.220
30D[ii]	$[0/90]_{2S}$	550	146	83.00	0.278

i) Tab failure - specimen remained intact
ii) Tabbed specimen
iii) Width-tapered, pinned-grip specimen
iv) Straight-sided, pinned-grip specimen

TABLE 4-2

Longitudinal Tensile Test Data
Nicalon/CAS

Spec. No.	Configuration	Test T (°C)	UTS (MPa)	E (GPa)	ε_u (%)
15B[i]	$[0]_{12}$	25	201	141.18	0.136
15C[i]	$[0]_{12}$	25	153	125.00	0.125
15D[ii]	$[0]_{12}$	25	326	150.00	0.701
28C[iii]	$[0]_{12}$	25	209	133.12	0.166
15E2[ii]	$[0]_{12}$	25 but preheated to 1000°C	205	116.78	0.237
15A[i]	$[0]_{12}$	600	311		0.290
18A[iv]	$[0/90]_{2S}$	25	155	85.72	0.632
18B[v]	$[0/90]_{2S}$	25	106	92.91	0.290
18C[iv]	$[0/90]_{2S}$	25	142	95.35	0.393
* 18D[v]	$[0/90]_{2S}$	25	133	79.00	0.525
29B[iii]	$[0/90]_{2S}$	25	285		0.350
29C[iii]	$[0/90]_{2S}$	800	95	114.23	0.480
29D1[v]	$[0/90]_{2S}$	550	88	94.55	0.105

i) Thickness tapered specimen - shoulder failure
ii) Thickness-tapered specimen
iii) Tabbed specimen - delamination-induced failure
iv) Width-tapered, pinned-grip specimen
v) Tabbed specimen

TABLE 4-3

Longitudinal Tensile Test Data
Nicalon/LAS

Spec. No.	Configuration	Test T (°C)	UTS (MPa)	E (GPa)	ε_u (%)
26A[i]	$[0]_{12}$	25	316	125.00	0.265
37A[ii]	$[0]_{12}$	550	202	137.47	0.160
* 37B[i]	$[0]_{12}$	550	190	139.15	0.142
37D[ii]	$[0]_{12}$	550	201	117.54	0.171
27A[i]	$[0/90]_{3S}$	25	181	97.50	0.365
* 27B3[i]	$[0/90]_{3S}$	25	159	82.77	0.503
36E[ii]	$[0/90]_{2S}$	25	156	89.43	0.264
36F[iii]	$[0/90]_{2S}$	25	199	96.13	0.566
* 36A2[ii]	$[0/90]_{2S}$	550	203	91.90	0.520
* 36B4[ii]	$[0/90]_{2S}$	550	127	100.00	0.278
36C[ii]	$[0/90]_{2S}$	550	169	90.41	0.310
36D[iv]	$[0/90]_{2S}$	550	168	89.67	0.317

i) Tab failure - specimen remained intact
ii) Tabbed specimen - delamination-induced failure
iii) Tabbed, width-tapered specimen
iv) Tabbed specimen

TABLE 4-4 *

Average Bond Strengths
Nicalon Fiber-Reinforced Glass and Glass-Ceramics

Composite System	τ_{deb} (MPa) Interfacial Shear Strength		
	Thermal Residual	Mechanical	Mechanical + Thermal Residual
Nicalon/1723	- 31.16	236	204.84
Nicalon/CAS-I	- 24.59	249	224.41
Nicalon/CAS-IIb	-22.48	204	181.52
Nicalon/BMAS-III	45.70	60	105.70
Nicalon/LAS-III	63.11	56	119.11

* Data from Refs. 15, 67 and 128.

TABLE 4-5

Calculated Axial Residual Thermal Stresses and Strains
Nicalon Fiber-Reinforced Glass and Glass-Ceramics

	Nicalon/1723	Nicalon/CAS	Nicalon/LAS	
			Ceramed	As-Pressed
Unidirectional: Axial Residual Matrix Strain (%)	+ 0.052	+ 0.057	- 0.109	- 0.018
Unidirectional: Axial Residual Matrix Stress (MPa)	+ 45.822	+ 50.254	-95.575	- 15.400
Laminate Coeff. of Thermal Exp. (10^{-6}/°C)	4.33	4.54	2.56	2.95
Crossply Laminate Thermal Strain (%)	- 0.259	- 0.557	- 0.264	- 0.207
Ply Thermal Strain (%)				
0° Ply	- 0.0134	- 0.0147	+ 0.0280	+ 0.0047
90° Ply	+ 0.0145	+ 0.0159	- 0.0302	- 0.0050
Laminate Thermal Stress (MPa) *laminate coordinates*				
0° Ply	- 13.68	-15.034	+28.552	+ 4.759
90° Ply	+ 13.68	+15.034	-28.552	- 4.759

TABLE 4-6

Bond Strengths following Oxidation
Nicalon/CAS-IIb

Exposure Temp (°C)	Depth beneath Exposed Surface (mm)	τ_{deb} (MPa) 0.5h	5h	50h
800	0.65	294.69 (62.72)	~483-621	~483-621
	1.4	294.69 (62.72)	588.04 (117.41) low V_f 269.26 (56.34) high V_f	1071.70 (135.63) 384.42 (66.98)
	6.1	220.12 (24.40)	195.74 (17.01)	264.94 (26.87)
1000	1.55	245.11 (28.66)	312.82 (32.10)	250.55 (42.54)
	7.1	210.69 (14.72)	203.25 (13.64)	201.68 (15.23)
1200	0.4	261.02 (31.83)		313.61 (23.16)
	1.6	246.66 (26.91)		294.82 (23.39)
	6.7	276.22 (32.91)		294.93 (25.28)

CONTROL 1. τ_{deb} = 177.04 (34.21) MPa
2. 203.75 (29.98) MPa

Standard deviations are given in parentheses.

TABLE 4-7

Transverse Penetration Depths of Oxidation
Nicalon/CAS-IIb

Exposure Temp (°C)	Depth beneath Exposed Surface (mm)	Transverse Penetration Depth (mm) 0.5h	5h	50h
800	0.65			
	1.4	0	0.1-0.2	0.5-0.8
	6.1			
1000	1.6	0.03-0.06	0.04-0.08	0.04-0.08
	7.1			
1200	0.4	0.06-0.08		0.06-0.08
	1.6	0.02-0.04		0.02-0.04
	6.7	0.02-0.05		0.03-0.04

TABLE 4-8

First 90° Ply Cracking Strain
[0/90] Laminates - 25°C

MATRIX	OBSERVED STRAIN at 1st 90° Ply Cracking (%)	THERMAL RESIDUAL 90° Ply STRAIN (%)	OBSERVED + RESIDUAL STRAIN (%)
1723	.026	(+) .0158	.0418
CAS-II	.055	(+) .0162	.0712
LAS-III	.094	(-) .0219	.0720

TABLE 4-9

Bond Strengths of Tensile Test Specimens
Nicalon/1723

Spec. No.	Condition	Ply	τ_{deb} (MPa) Avg.	S.D.
$[0]_8$:				
23	as polished (transverse section)	unidirectional	408.964	48.151
$[0/90]_{2S}$:				
13	as polished (transverse section)	1st 0	298.246	37.562
		2nd 0	304.673	36.583
		3rd 0	334.374	25.150
		4th 0	381.935	56.418
13A	AFTER TESTING end of sample	1st 90	508.050	43.563
		2nd 90	472.162	73.734
		3rd 90	386.625	64.611
		4th 90	474.288	79.068
13G	AFTER TESTING end of sample	1st 90	366.119	77.628
		2nd 90	364.556	63.730
		3rd 90	374.413	82.049
		4th 90	343.070	75.034
13H	BEFORE TESTING end of sample	1st 90	350.958	23.567
		2nd 90	347.876	24.252
		3rd 90	388.325	39.987
		4th 90	433.310	99.794
$[0/90]_{2S}$:				
24C	BEFORE TESTING	?	492.435	48.179
24C	AFTER TESTING end of sample	1st 90	614.411	67.248
		central 90's	632.670	62.373
		4th 90	621.413	99.181
24E	BEFORE TESTING end of sample	1st 90	500.867	40.619
		central 90's	555.056	83.298
		4th 90	650.800	64.093
24E	AFTER 600°C TESTING mid region of sample (end oxidized)	1st 90	522.289	82.932
		central 90's	506.104	48.772
		4th 90	540.578	91.696

TABLE 4-9 (cont'd)

Bond Strengths of Tensile Test Specimens
Nicalon/1723

Spec. No.	Condition	Ply	τ_{deb} (MPa) Avg.	S.D.
$[0/90]_{2S}$:				
24F	BEFORE TESTING	1st 90	558.003	79.498
	end of sample	central 90's	539.844	42.284
		4th 90	478.493	28.298
30A	BEFORE TESTING	1st 90	462.890	105.375
	end of sample	central 90's	349.425	97.584
	15.24 cm sample	4th 90	407.073	38.013
30B	BEFORE TESTING	1st 90	593.566	44.961
	end of sample	central 90's	414.045	64.326
	15.24 cm sample	4th 90	561.521	87.008
$[90/0]_{2S}$:				
25A	BEFORE TESTING	1st 90	613.120	143.373
	end of sample	2nd 90	563.182	61.673
		3rd 90	306.301	78.354
		4th 90	368.584	35.672

TABLE 4-10

Bond Strengths of Tensile Test Specimens
Nicalon/CAS

Spec. No.	Condition	Ply	τ_{deb} (MPa) Avg.	S.D.
$[0/90]_{2S}$:				
18D	BEFORE TESTING	1st 90	213.734	29.904
	end of sample	central 90's	216.904	43.729
		4th 90	255.517	26.295
29D	BEFORE TESTING	1st 90	578.022	81.109
	end of sample	central 90's	419.328	41.457
	15.24 cm sample	4th 90	373.958	30.927

TABLE 4-11

Bond Strengths of Tensile Test Specimens
Nicalon/LAS

Spec. No.	Condition	Ply	τ_{deb} (MPa) Avg.	S.D.
$[0]_8$:				
26	as polished (transverse section)	unidirectional	105.027	17.843
$[0/90]_{3S}$:				
27A	BEFORE TESTING	1st 90	101.926	20.565
	end of sample	2nd 90	157.599	29.725
		3rd 90	112.961	16.818
		4th 90	110.658	8.650
27B	BEFORE TESTING	1st 90	93.686	10.643
	end of sample	2nd 90	93.053	21.602
		central 90's	104.136	17.782
36A	BEFORE TESTING	1st 90	166.238	14.615
	end of sample	central 90's	154.896	13.058
	15.24 cm sample	4th 90	170.312	17.228
36B	BEFORE TESTING	1st 90	135.520	5.567
	end of sample	central 90's	138.716	23.079
	15.24 cm sample			

TABLE 4-12

Bond Strength Variation
Nicalon/1723 - [0/90] Laminates
25°C

Spec No.	Laminate Configuration	Avg τ_{deb} (MPa)	Observed Strain at 1st 90° Ply Cracking (%)
24C	$[0/90]_{2S}$	623	0.031
24F	$[0/90]_{2S}$	525	< 0.026
13H	$[0/90]_{4S}$	380	0.028

TABLE 5-1

Calculated G_c Values

System	K_c - matrix (MPa $\sqrt{m}$)	G_c - matrix (J/m^2)	G_c - composite Han analysis (J/m^2)
Nicalon/1723	1.0	10.7	3.24
Nicalon/CAS	2.2	51.5	8.12
Nicalon/LAS	1.9	38.4	
$\alpha_{lam} = 2.95 \times 10^{-6}/°C$			6.41
$\alpha_{lam} = 2.5 \times 10^{-6}/°C$			4.94
$\alpha_{lam} = 2.0 \times 10^{-6}/°C$			3.50
$\alpha_{lam} = 1.5 \times 10^{-6}/°C$			2.34

TABLE 5-2

σ_a^{fpf} and ξ Values
Initial and Cracked Conditions

	σ_a^{fpf} (MPa)		ξ	
	Initial	Cracked	Initial	Cracked
Nicalon/1723 (calc G_c = 3.24 J/m^2)	22.64	21.51	1.148	0.441
Nicalon/CAS (calc G_c = 8.12 J/m^2)	40.00	38.00	1.150	0.613
Nicalon/LAS	71.00	67.45		
(calc G_c = 6.41 J/m^2)			1.703	1.979
(calc G_c = 4.94 J/m^2)			1.774	2.570
(calc G_c = 3.50 J/m^2)			1.887	3.622
(calc G_c = 2.34 J/m^2)			2.054	5.426

TABLE 5-3

First 0° Ply Cracking Stress and Strain
[0/90] Laminates - 25°C

System	Observed Cracking Strain (%)	Observed Cracking Stress (MPa)
Nicalon/1723	0.088	63.53
Nicalon/CAS	0.094	60.98
Nicalon/LAS	0.174	116.45

FIGURES

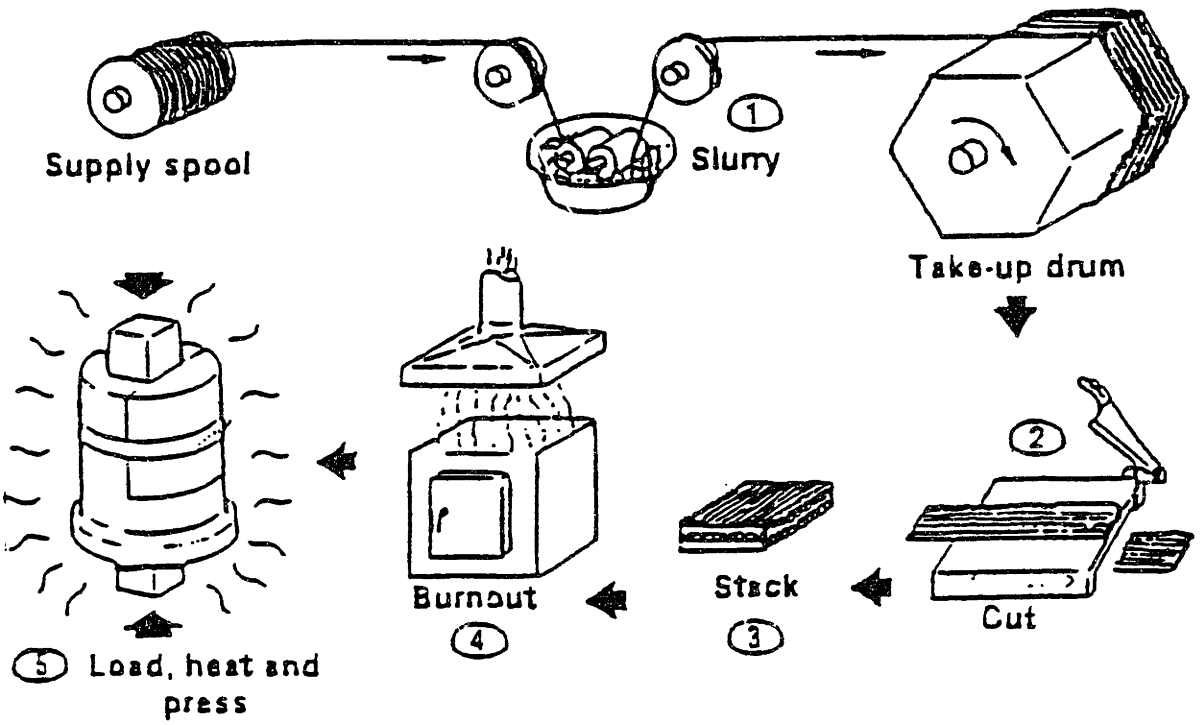

Fig. 2-1 Steps in processing of continuous fiber-reinforced, glass-matrix composites by a slurry infiltration/hot pressing technique (Ref. 34).

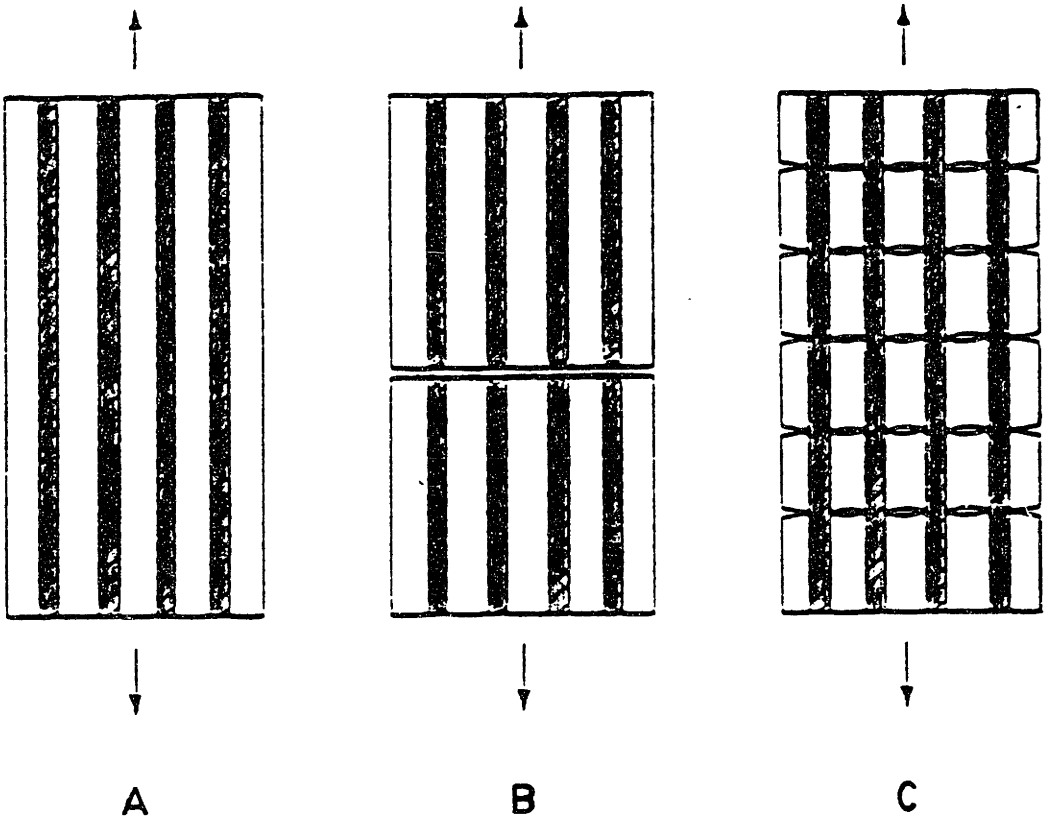

Fig. 2-2 Failure processes in CMC's (adapted from Ref. 51):
(A) Before fracture
(B) Simultaneous matrix and fiber fracture in a strongly bonded system
(C) Multiple matrix cracking prior to fiber failure in a weakly bonded system

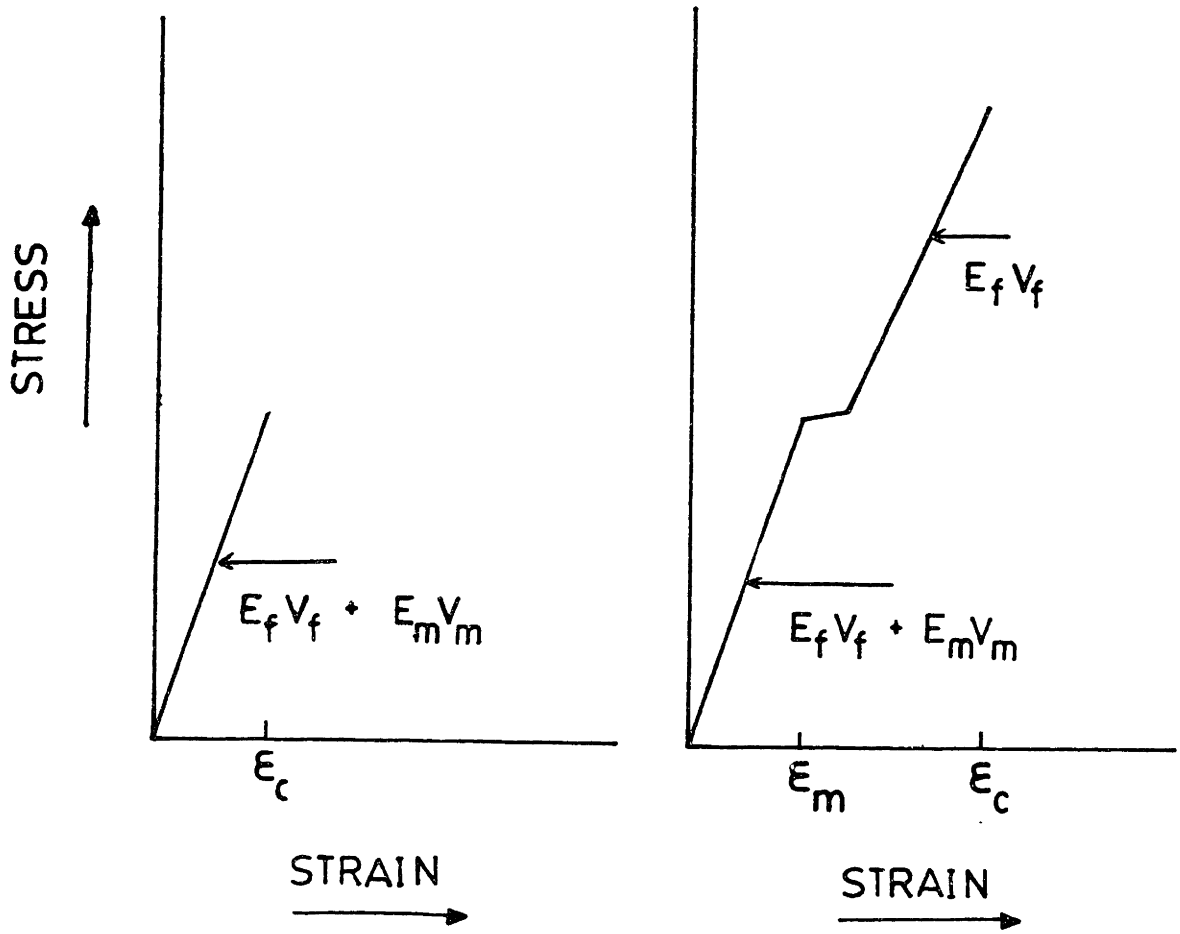

Fig. 2-3 Model stress-strain behavior for fiber reinforced CMC's:
a) Strongly bonded system
b) Weakly bonded system

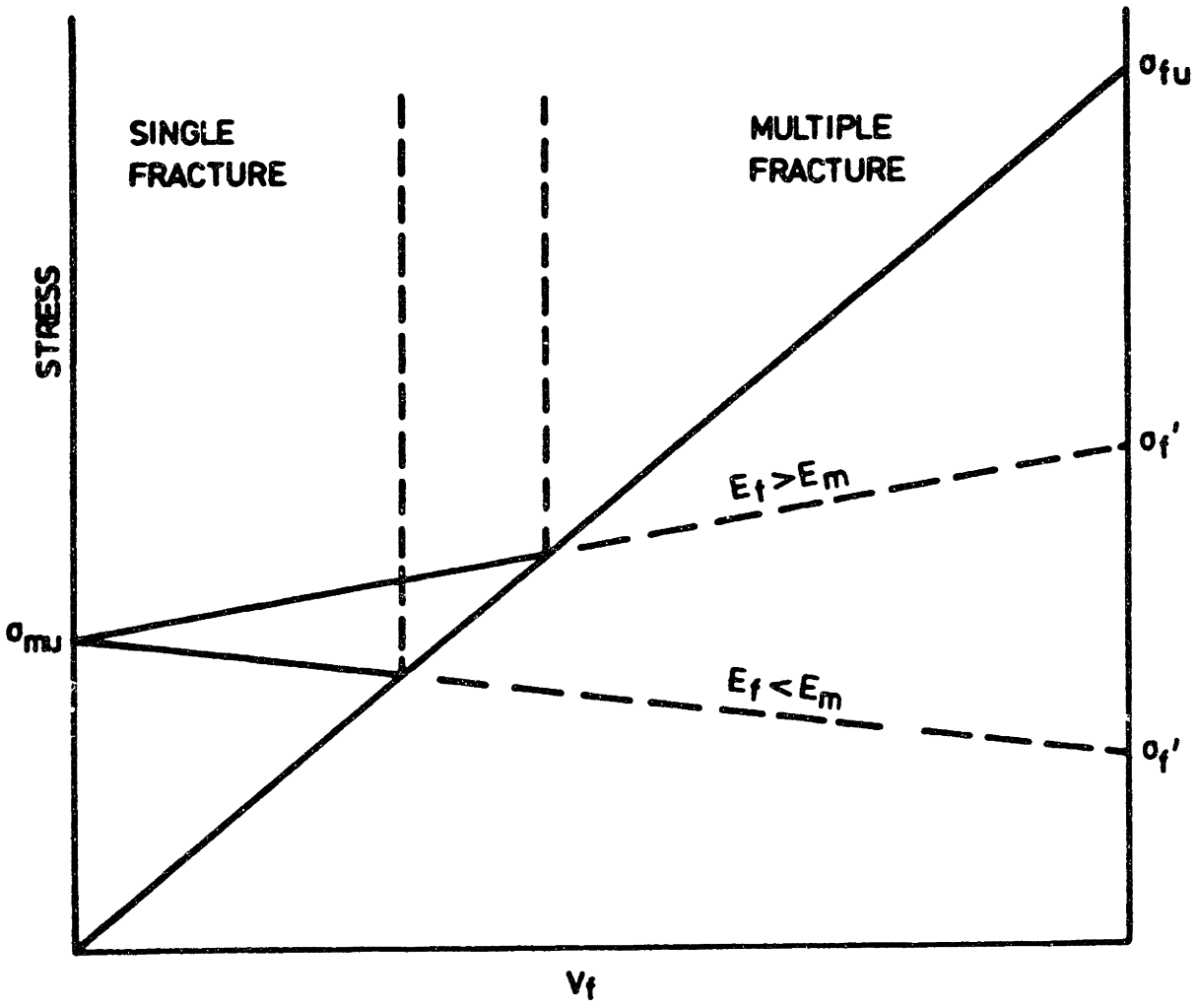

Fig. 2-4 Dependence of composite strength and modulus on fiber content (Ref. 54).

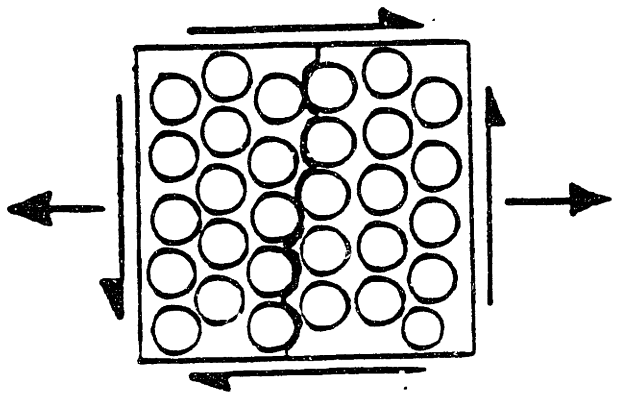

(a) OFF-AXIS AND SHEAR PROPERTIES

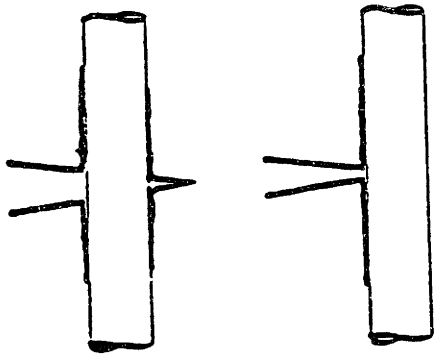

(b) FLAW TOLERANCE

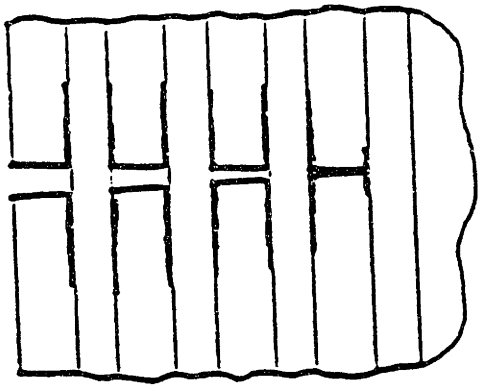

(c) RESISTANCE TO MATRIX CRACK OPENING

Fig. 2-5 Interface-dominated properties (Ref. 67):
a) Off-axis and shear strength
b) Flaw tolerance
c) Resistance to the onset of macroscopic matrix cracking in longitudinal tension

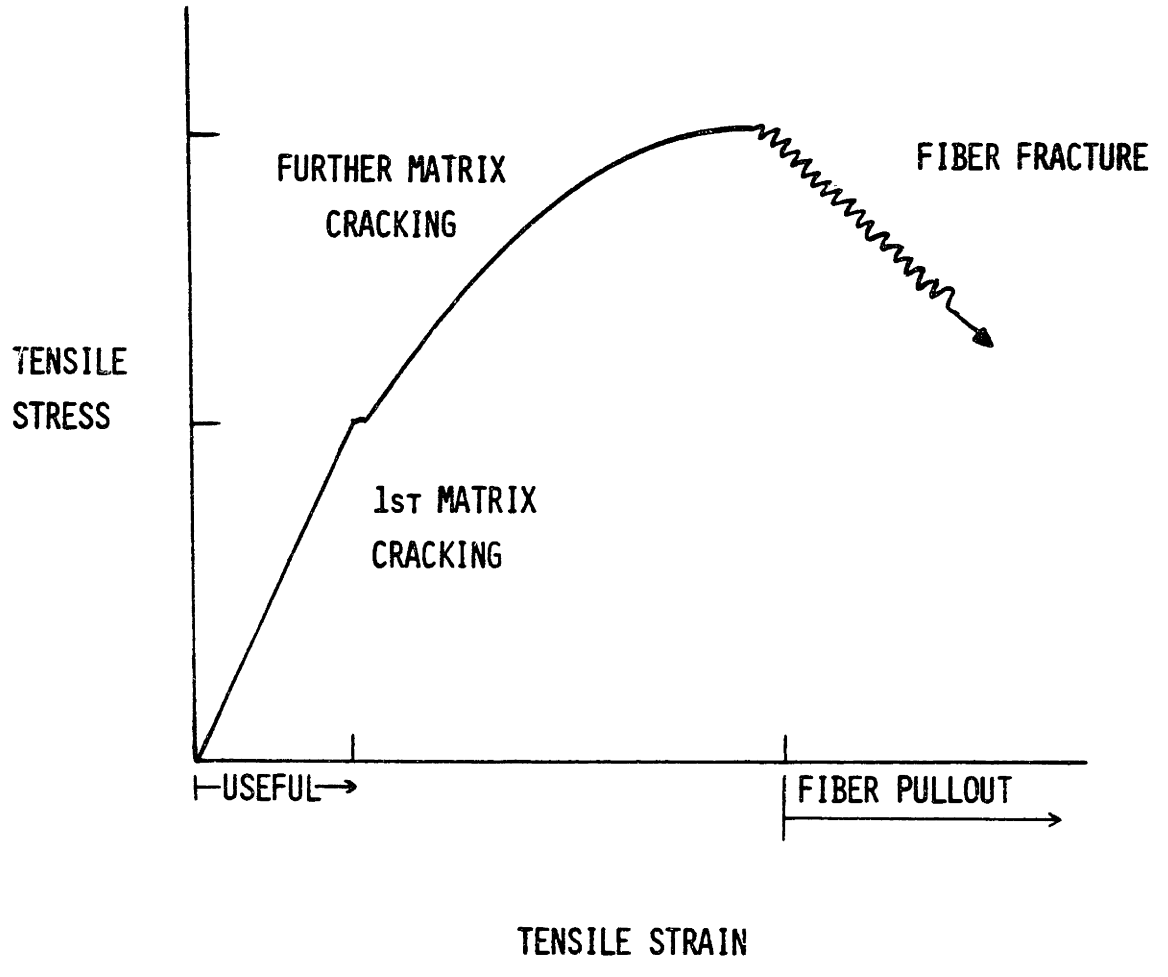

Fig. 2-6 Idealized tensile stress-strain curve for CMC's (adapted from Ref. 59).

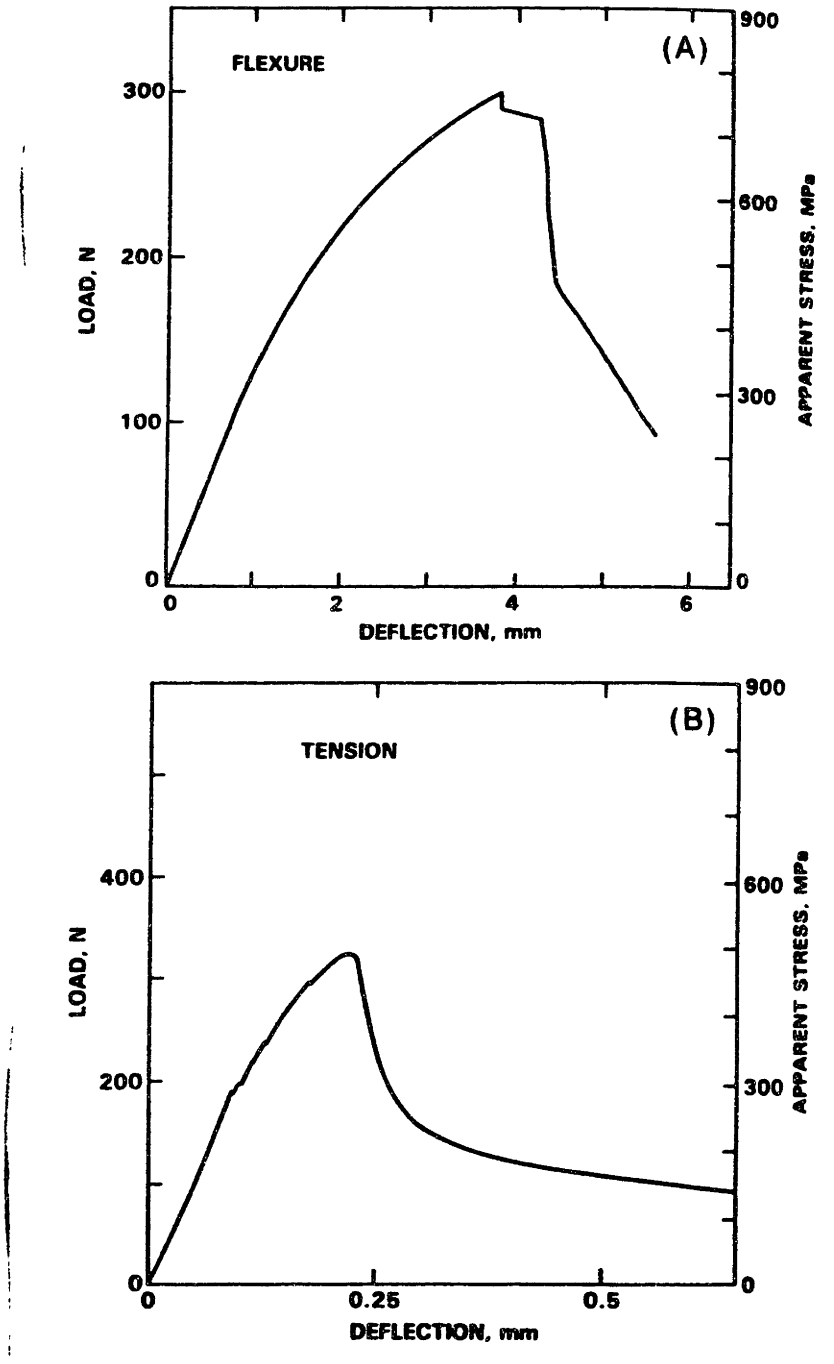

Fig. 2-7 Load-deflection curves for: (A) flexure and (B) tension tests (Ref. 12). For flexure tests, the apparent stress was calculated from measured load assuming a uniform linear elastic beam in bending. For tensile tests, it was obtained from measured load/cross-sectional area.

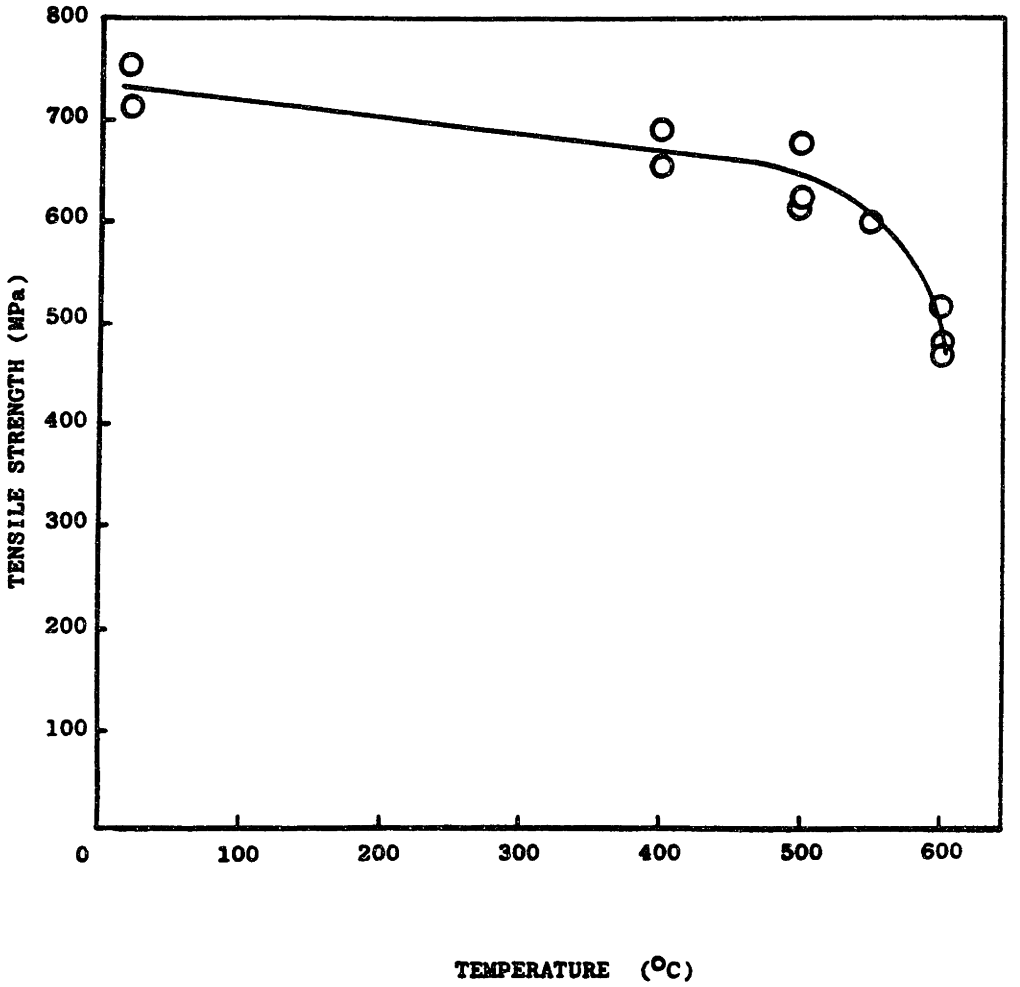

Fig. 2-8 Effect of temperature on the tensile strength of a unidirectional Nicalon/1723 composite (Ref. 66).

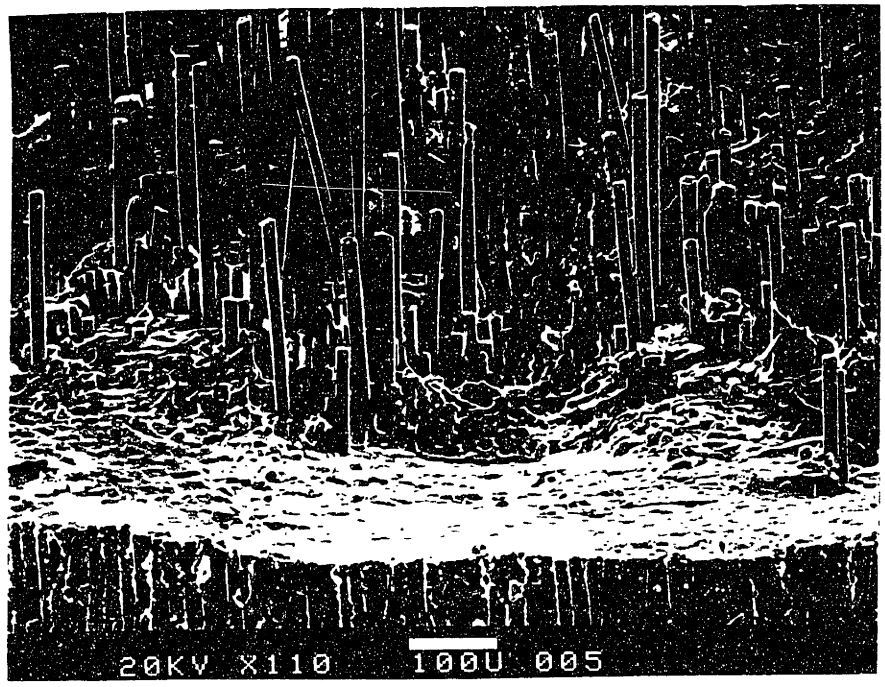

Fig. 2-9 Two distinct fracture surface regions in a unidirectional Nicalon/ BMAS composite following tension testing in air at 1000°C.

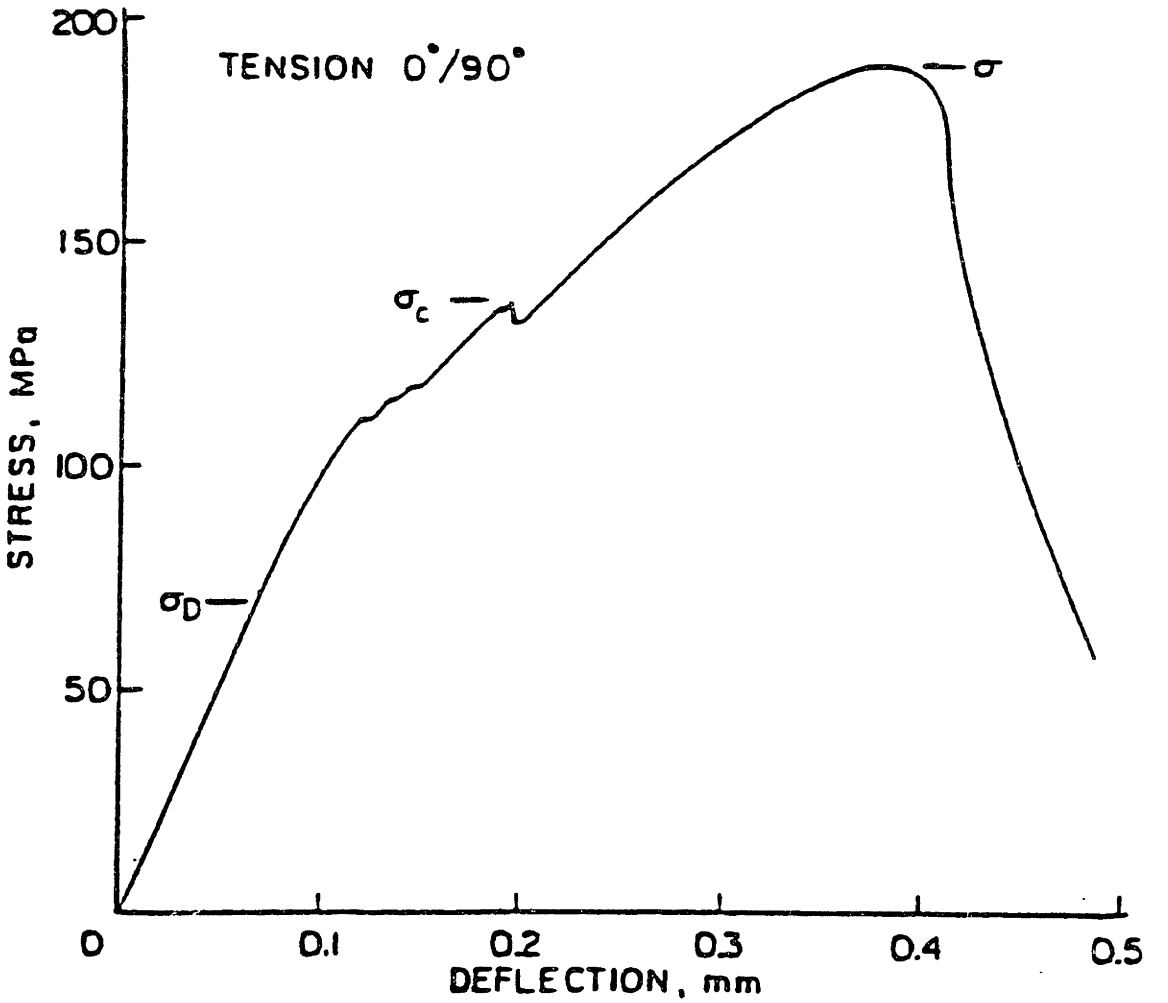

Fig. 2-10 Typical 25°C tensile stress-strain curve for a Nicalon/LAS crossply laminate (Ref. 18).

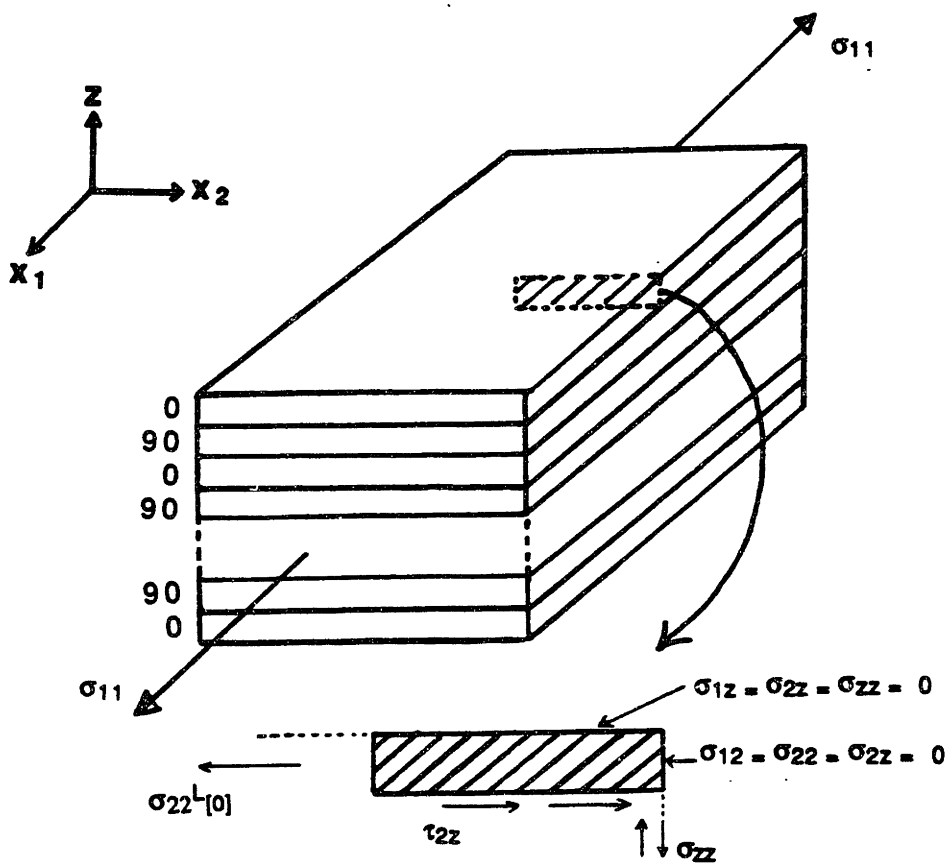

- Surfaces must be stress free
- CLPT predicts that $\sigma_{22}^{L}{}_{[0]}$ exists
- Force balance in x_2 direction requires τ_{2z} to exist
- Moment balance requires σ_{zz}
- σ_{zz} must be self-equilibrating to satisfy z-direction force balance

Fig. 2-11 Origin of free edge stresses in composite laminates (adapted from Ref. 91).

Fig. 3-1 A typical 0/90 laminate configuration.

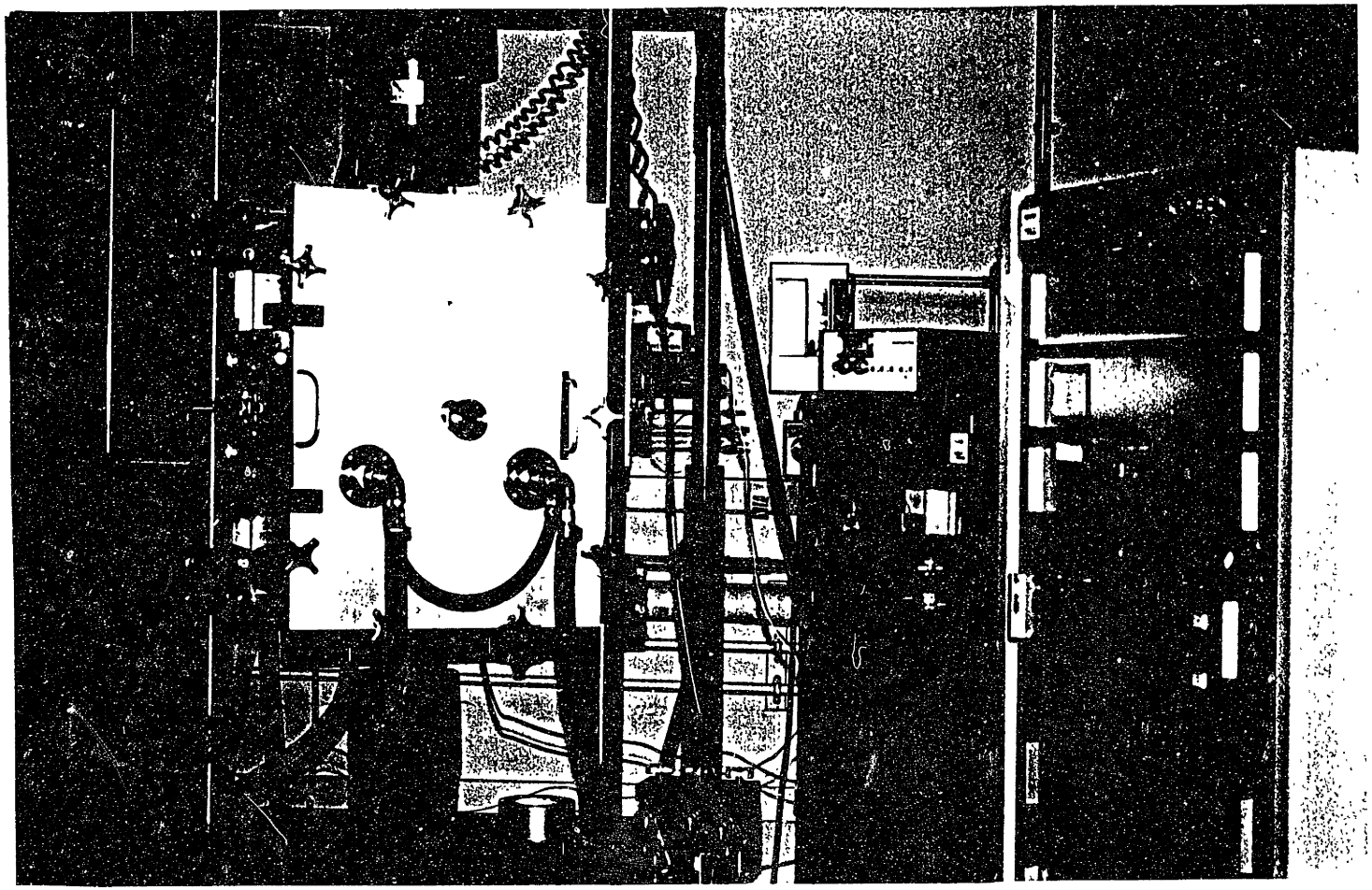

Fig. 3-2 Test setup for primary tensile tests and damage development studies.
(a) High temperature (1500°C) test facility

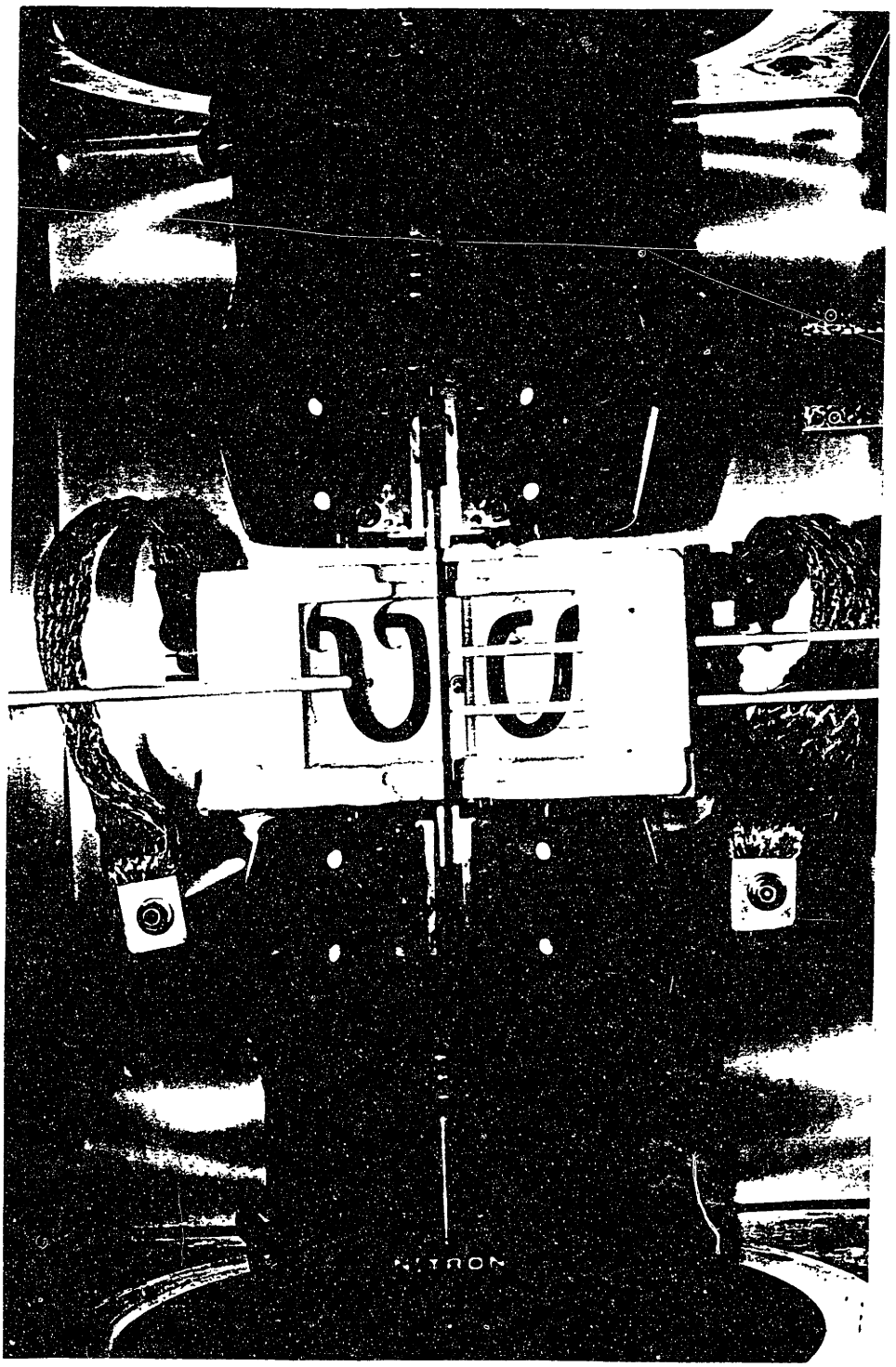

Fig. 3-2 Test setup for primary tensile tests and damage development studies. (b) Specimen situated in water-cooled hydraulic grips. Note the access ports in the furnace shell for the high temperature extensometer (right) and thermocouples (left and rear).

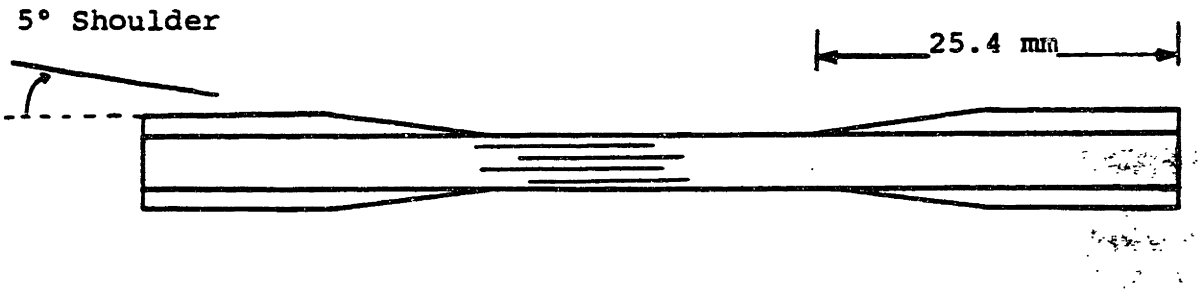

(a)

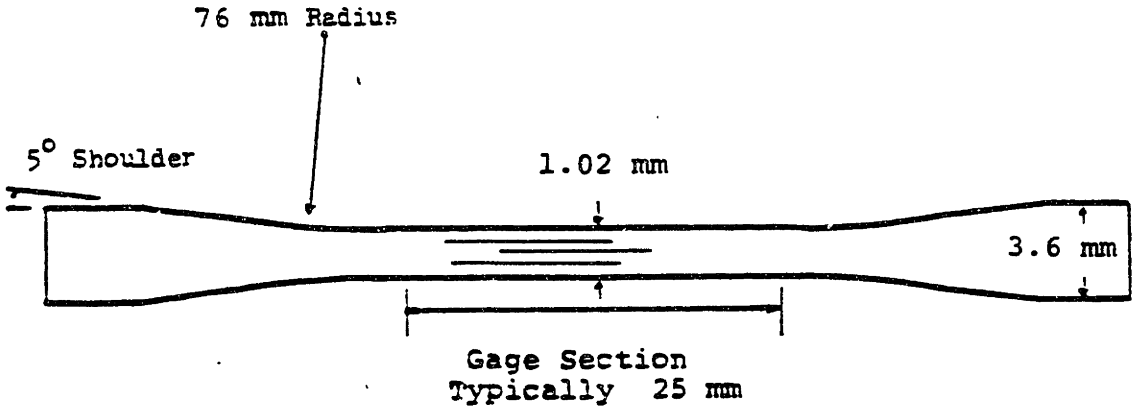

(b)

Fig. 3-3 Specimen geometries:
a) Tabbed specimen for room temperature tests of unidirectional laminates
b) Thickness-tapered specimen for elevated temperature tensile tests of unidirectional laminates

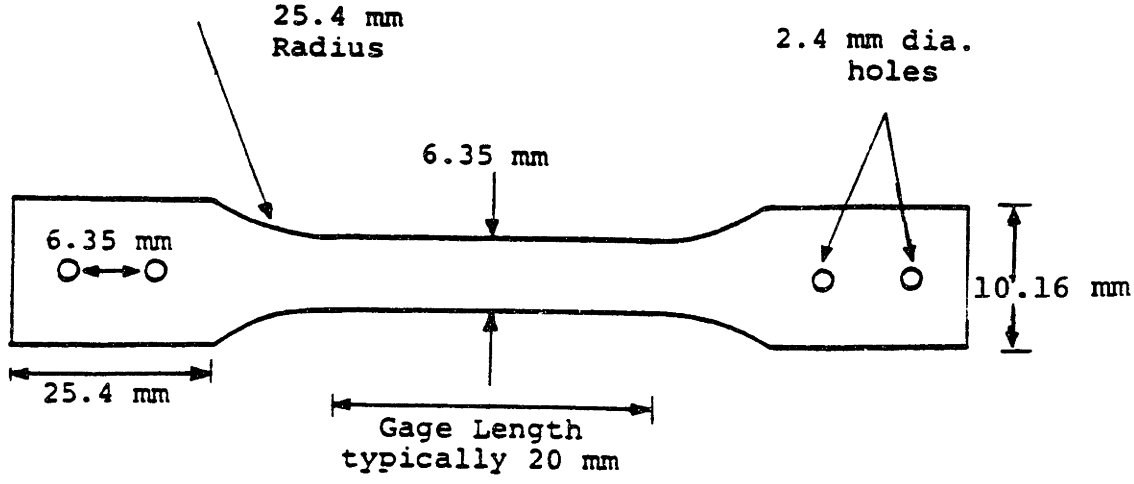

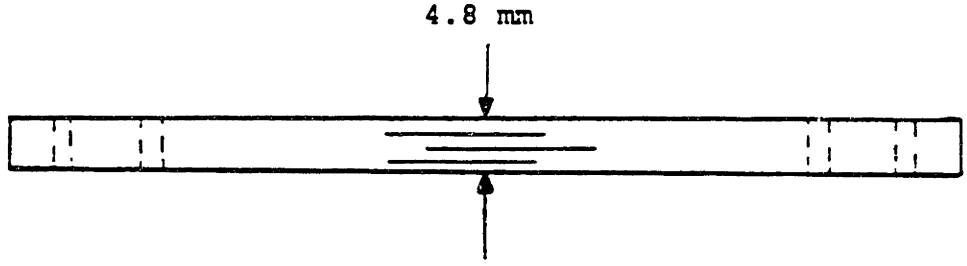

(c)

Fig. 3-3 c) Width-tapered specimen for room and elevated tensile test of multi-directional laminates.

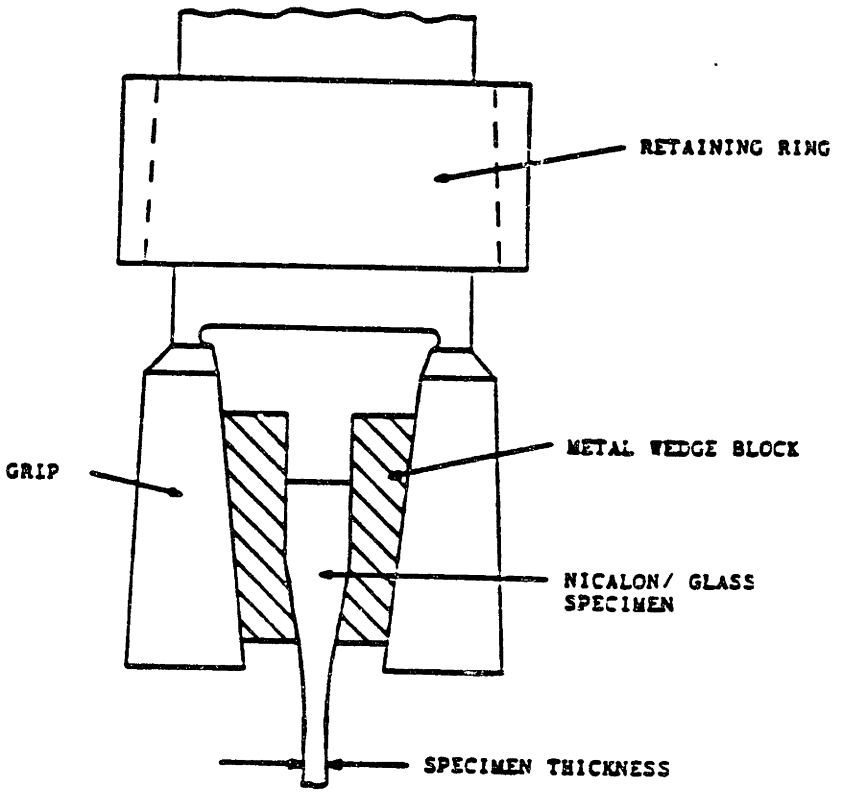

Fig. 3-4 Gripping assembly for tensile testing of thickness-tapered unidirectional specimens. The wedge blocks are contoured to fit between the grips and the tapered specimen shoulders.

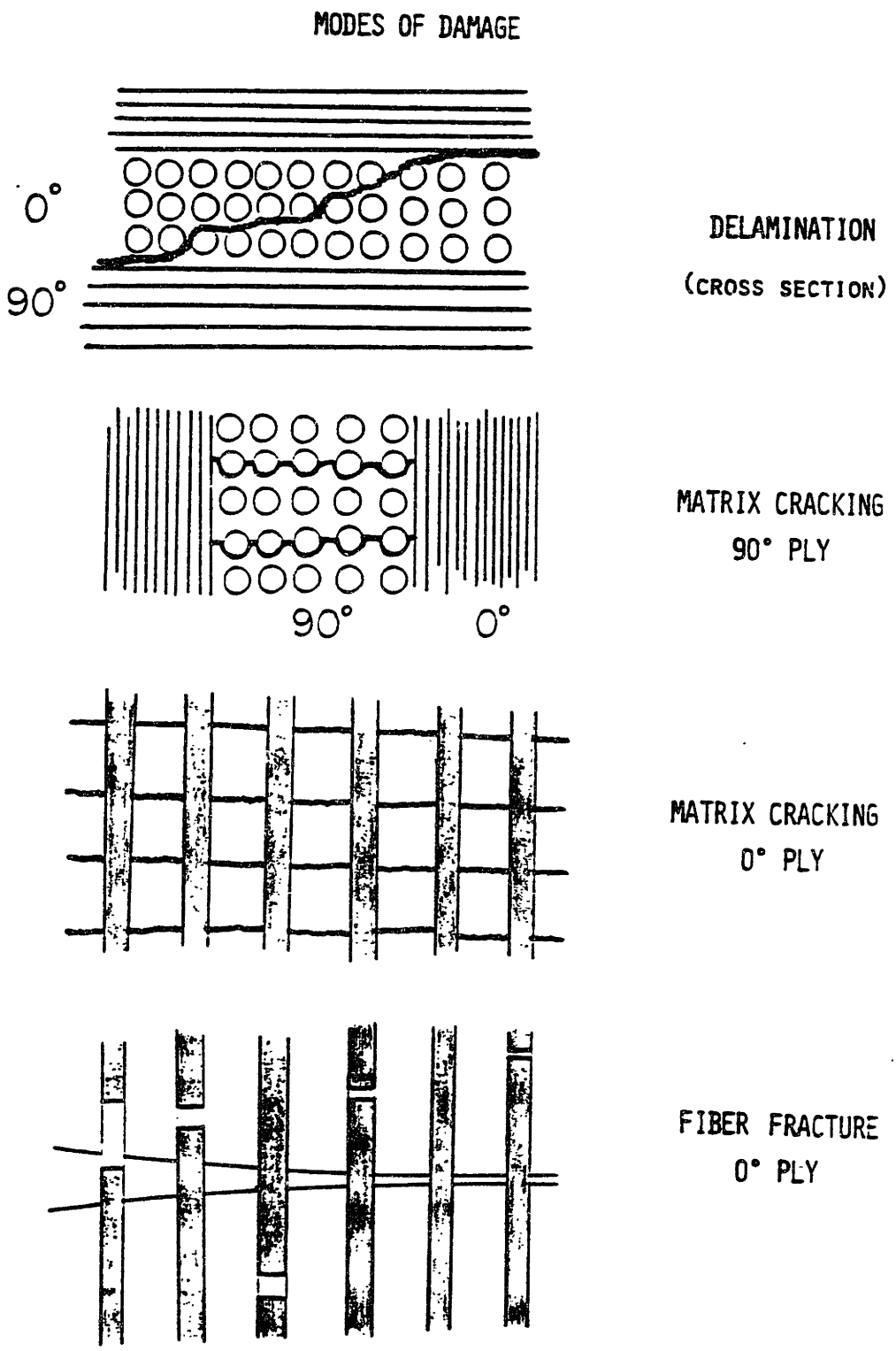

Fig. 3-5 Modes of damage in crossply laminates.

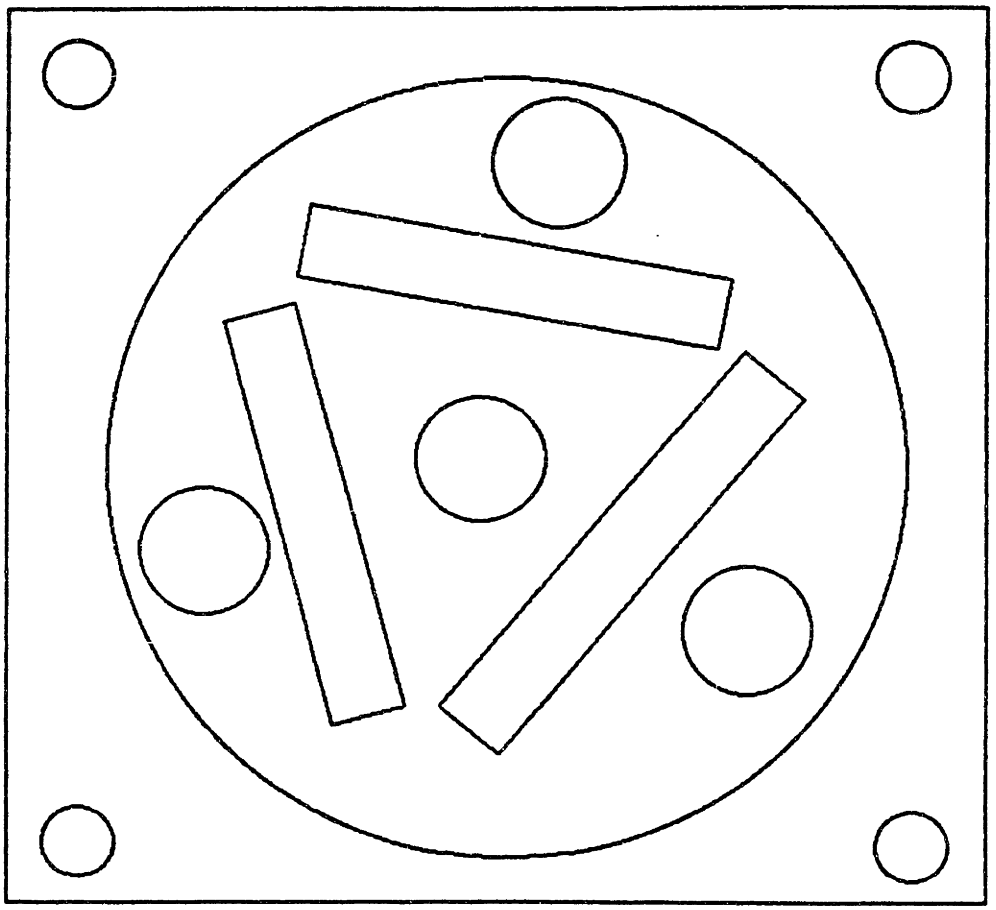

Fig. 3-6 Semi-automatic polishing design. This rigid plate is mounted atop a polishing wheel and attached to the polishing table by stainless steel shafts.

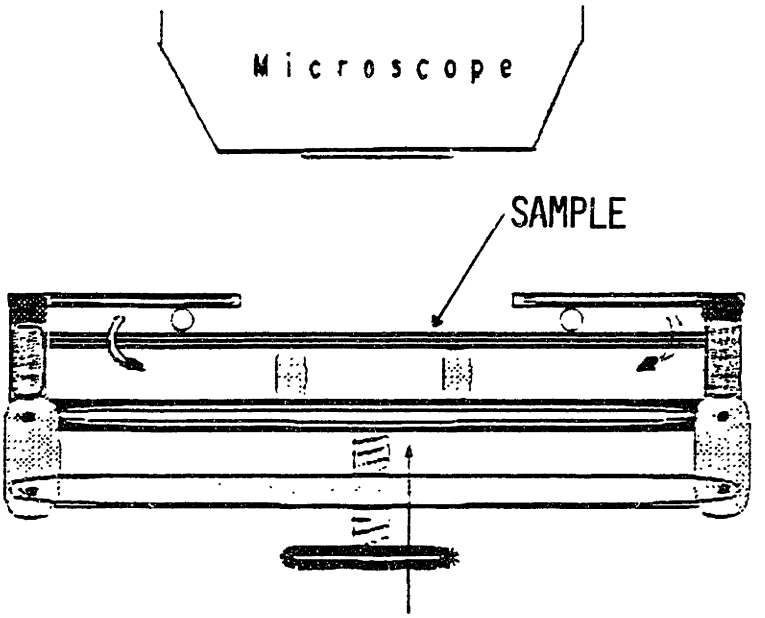

Fig. 3-7 Four-point bend apparatus, designed for incorporation in the SEM specimen chamber. In-situ observation of flexure samples is possible with this device.

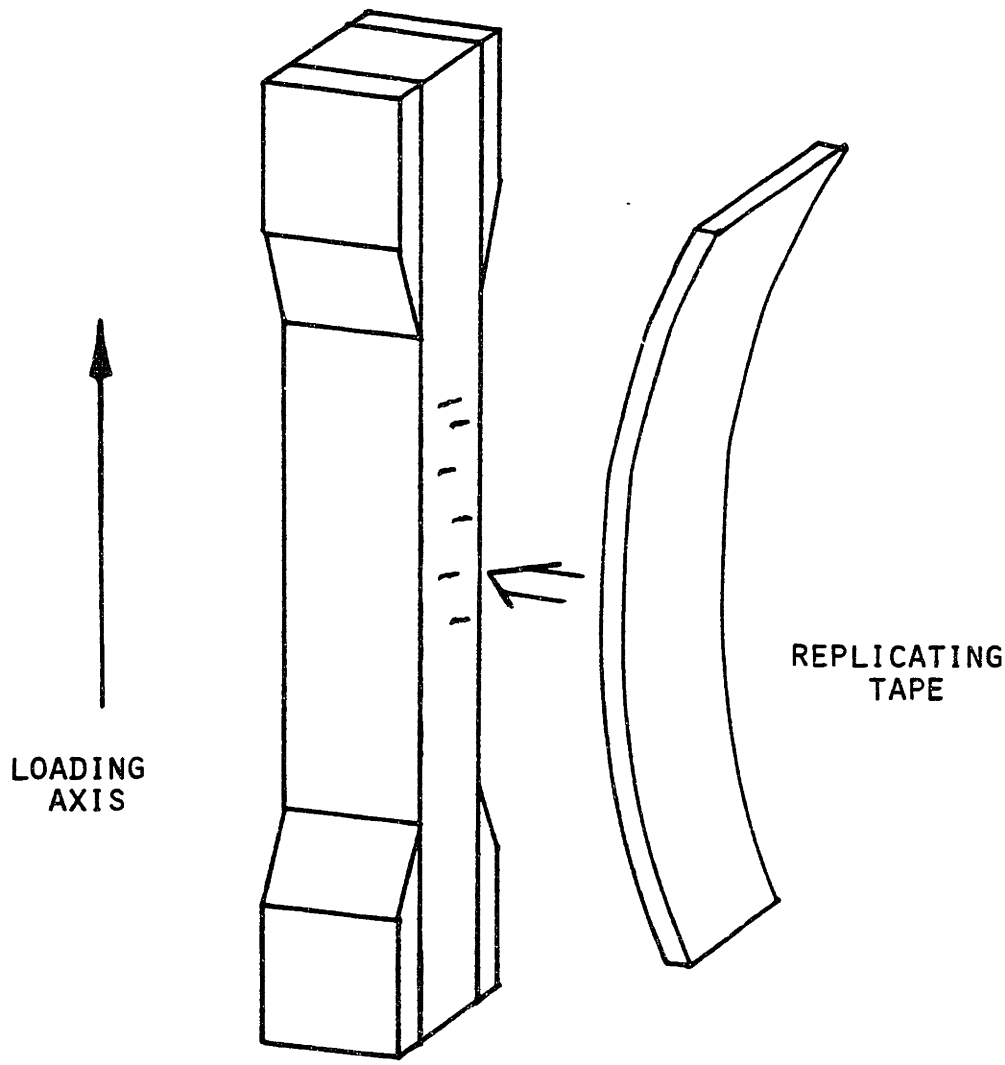

Fig. 3-8 The replication procedure involves taking an imprint of a specimen edge using cellulose acetate tape and acetone, as a wetting agent.

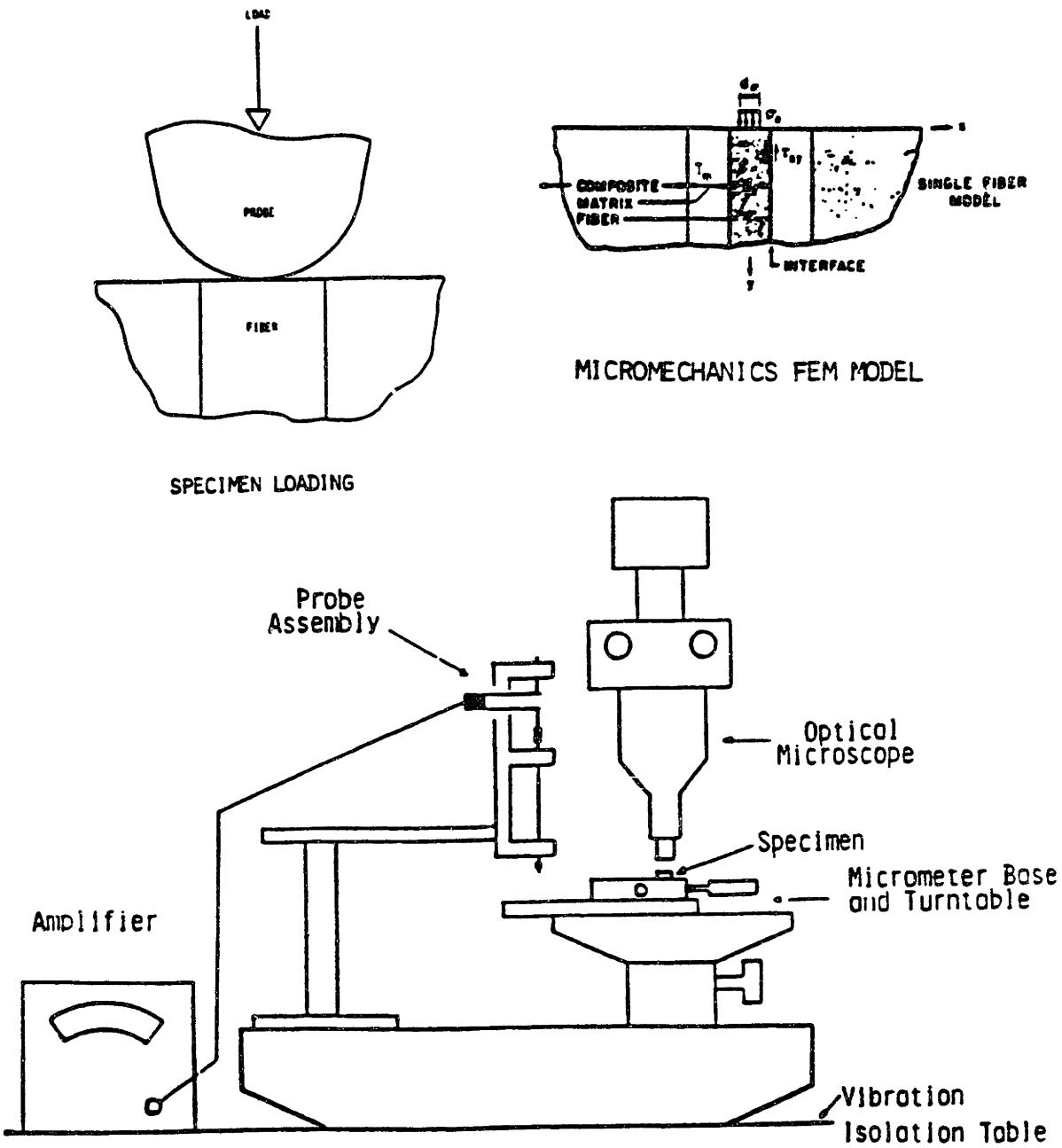

Fig. 3-9 Microdebonding apparatus.

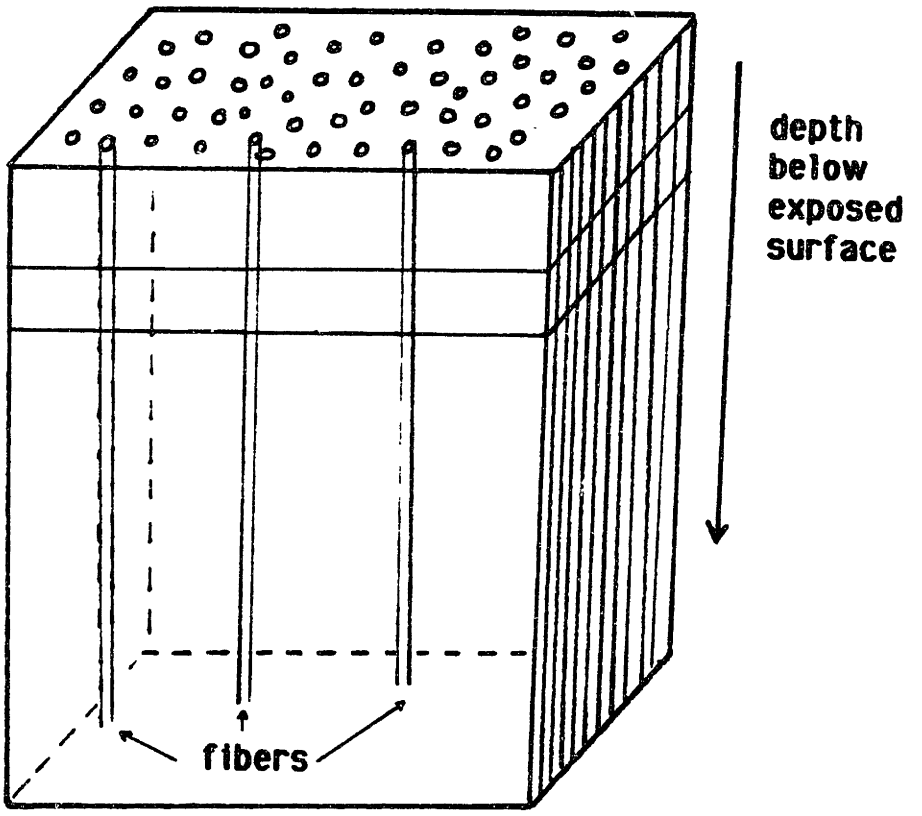

Fig. 3-10 Orientation of oxidized Nicalon/CAS-IIb samples for the microdebonding test. Bond strength variations were determined at various depths below the exposed surfaces.

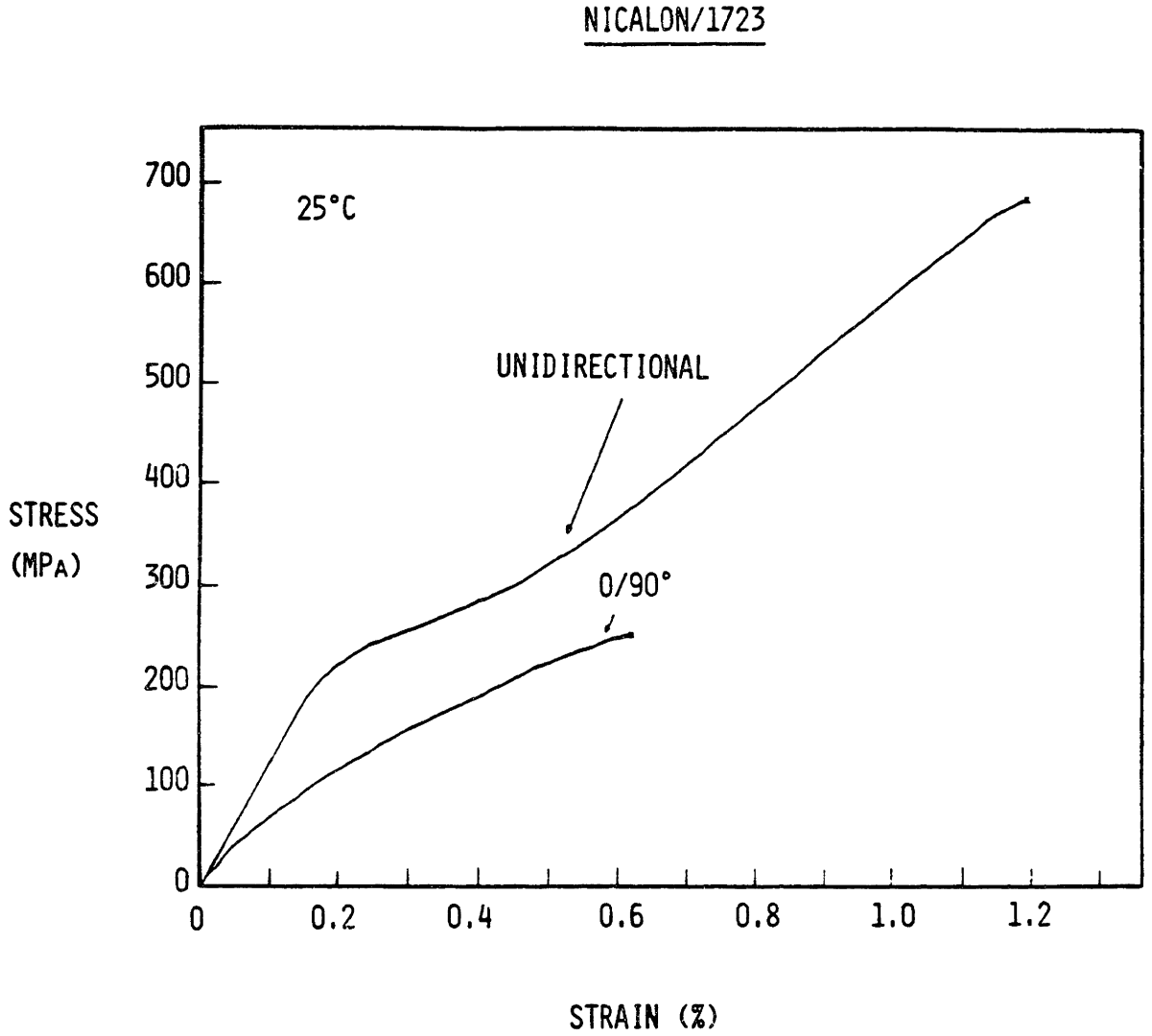

Fig. 4-1 Room temperature stress-strain curves for unidirectional and crossplied Nicalon/1723. The unidirectional laminate shows three regimes of tensile behavior.

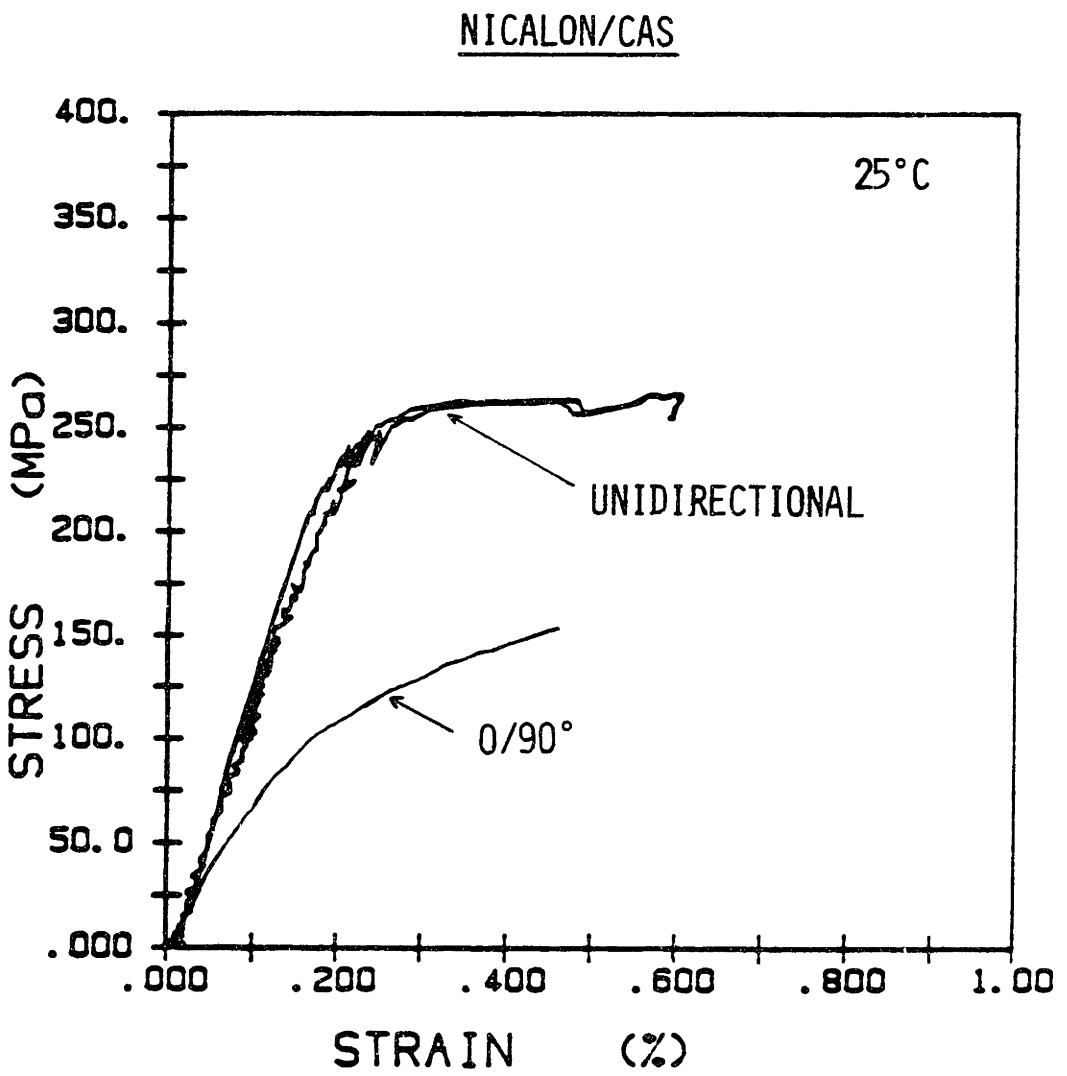

Fig. 4-2 Typical longitudinal stress-strain curves for unidirectional and crossplied Nicalon/CAS at 25°C.

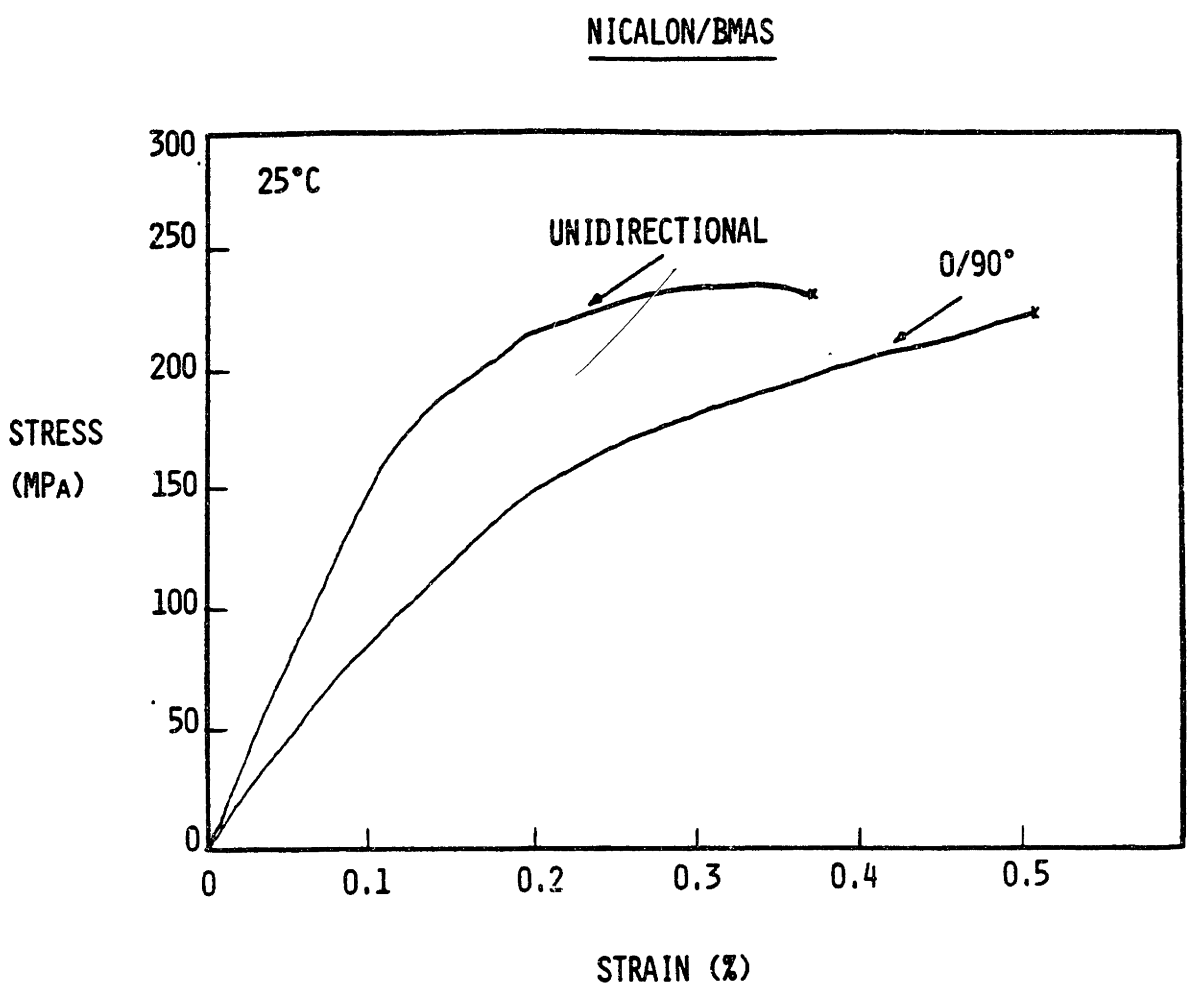

Fig. 4-3 Room temperature stress-strain curves for unidirectional and crossplied Nicalon/BMAS.

NICALON/BMAS

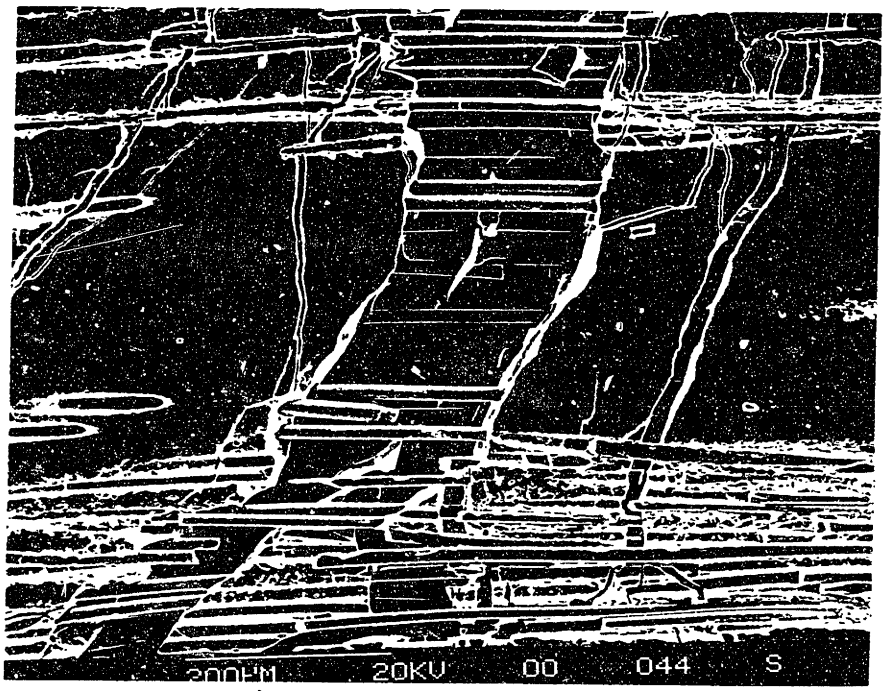

Fig. 4-4 Matrix crack opening by sliding along the interface in a Nicalon/BMAS composite. Fibers remained intact.

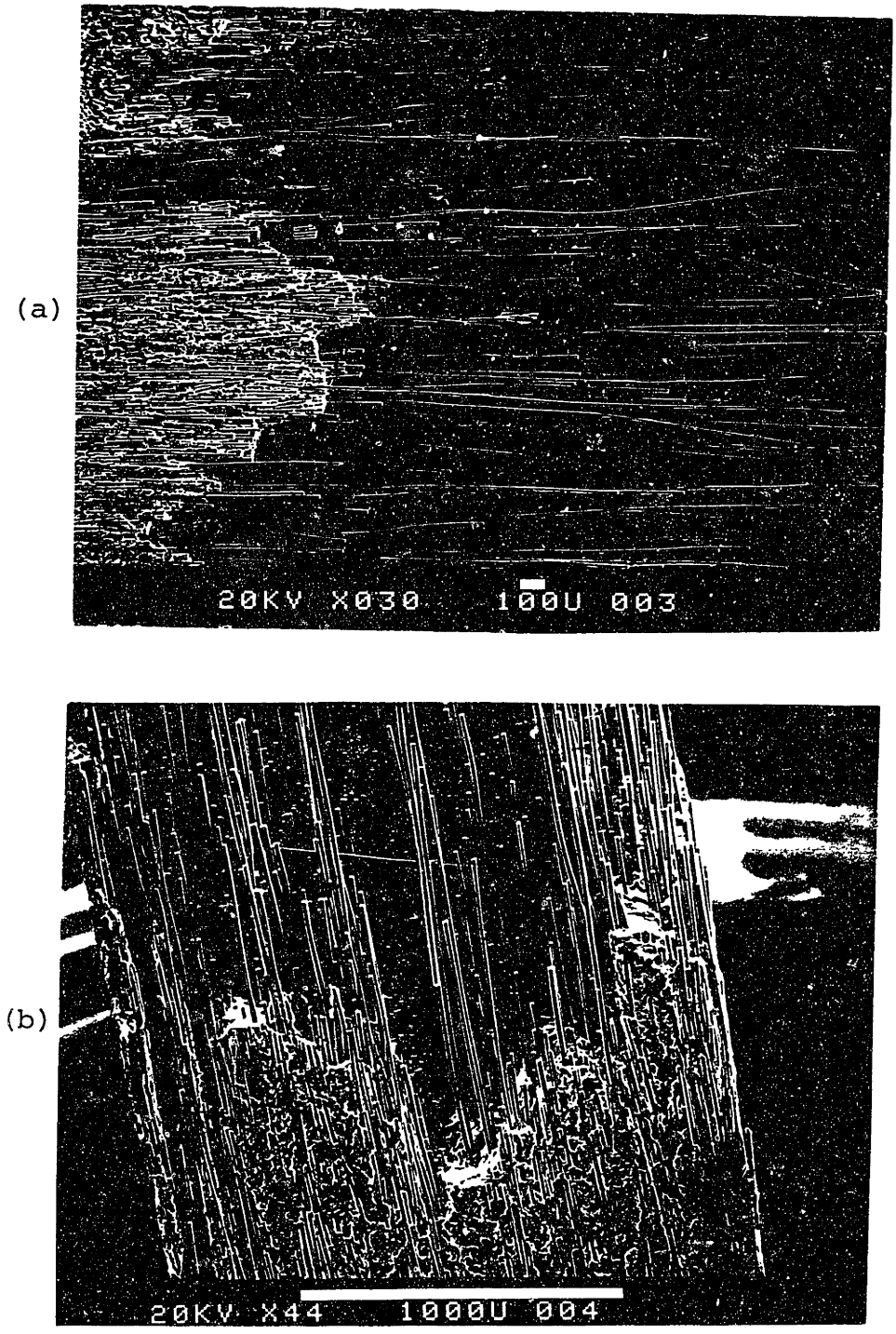

Fig. 4-5 Comparison of pullout lengths following room temperature tensile fracture of unidirectional: (a) Nicalon/BMAS, (b) Nicalon/CAS and (c) Nicalon/1723.

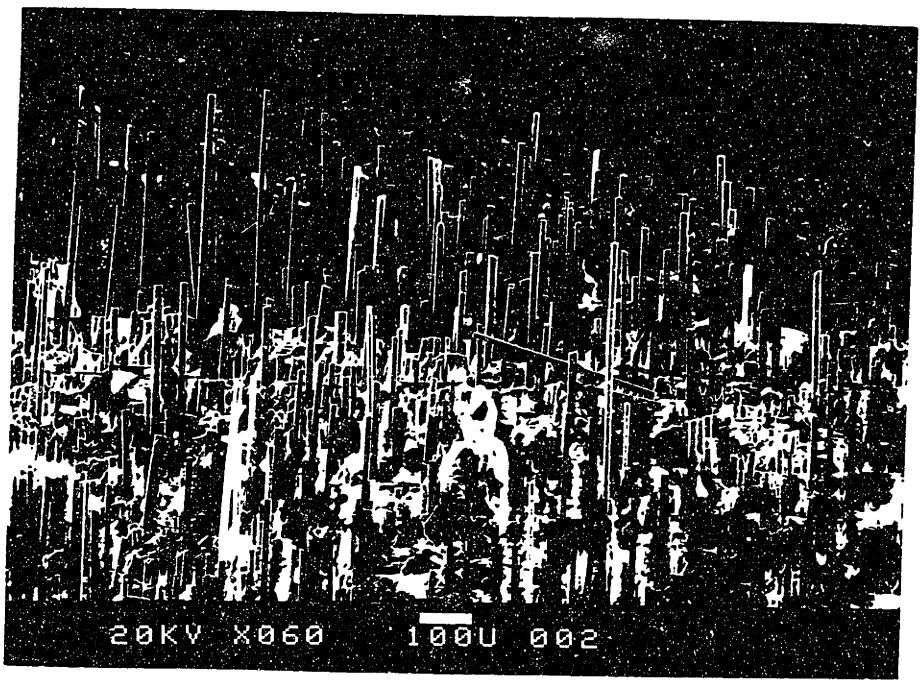

(c)

Fig. 4-5 (c) Nicalon/ 1723.

(a)

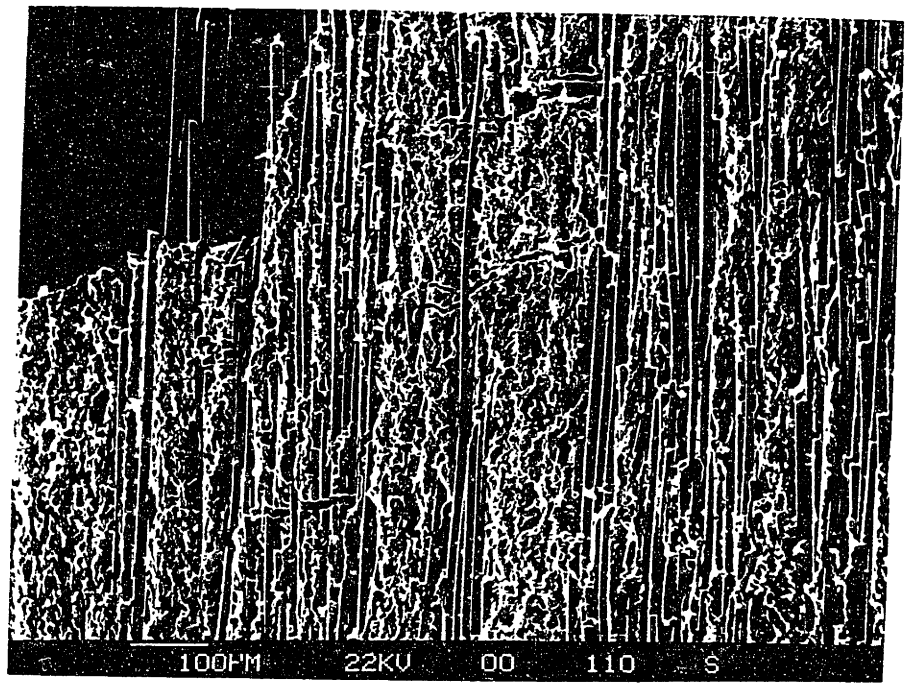

(b)

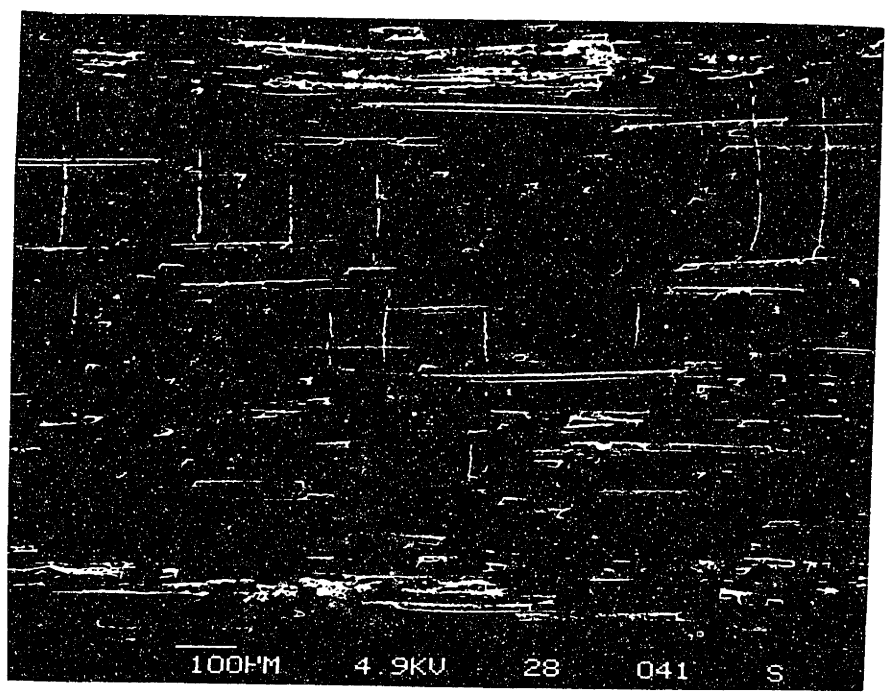

Fig. 4-6 Comparison of matrix crack spacings following room temperature tensile fracture of unidirectional: (a) Nicalon/BMAS, (b) Nicalon/CAS and (c) Nicalon/1723.

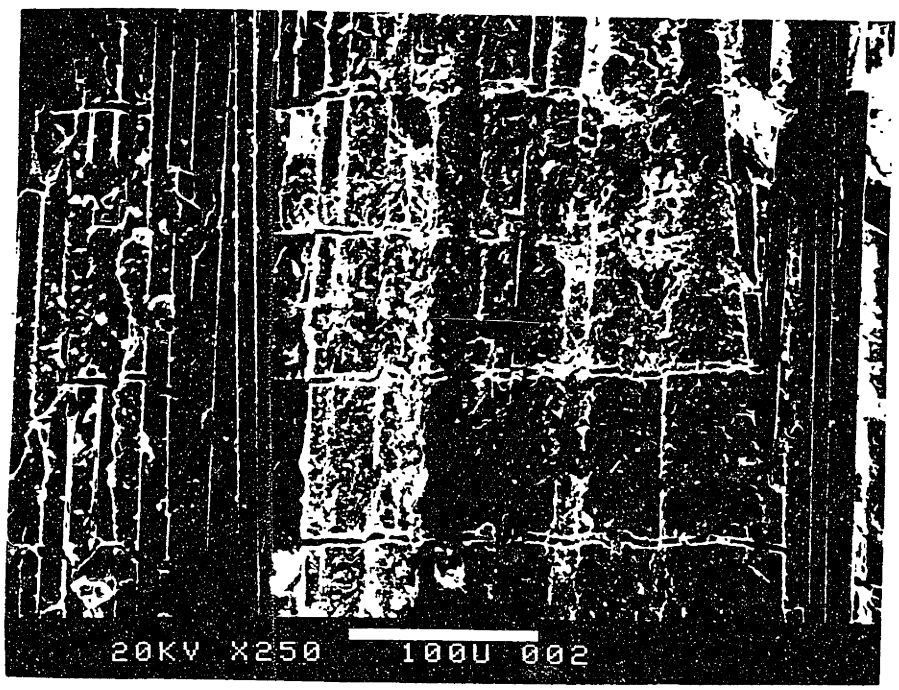

(c)

Fig. 4-6 (c) Nicalon/1723.

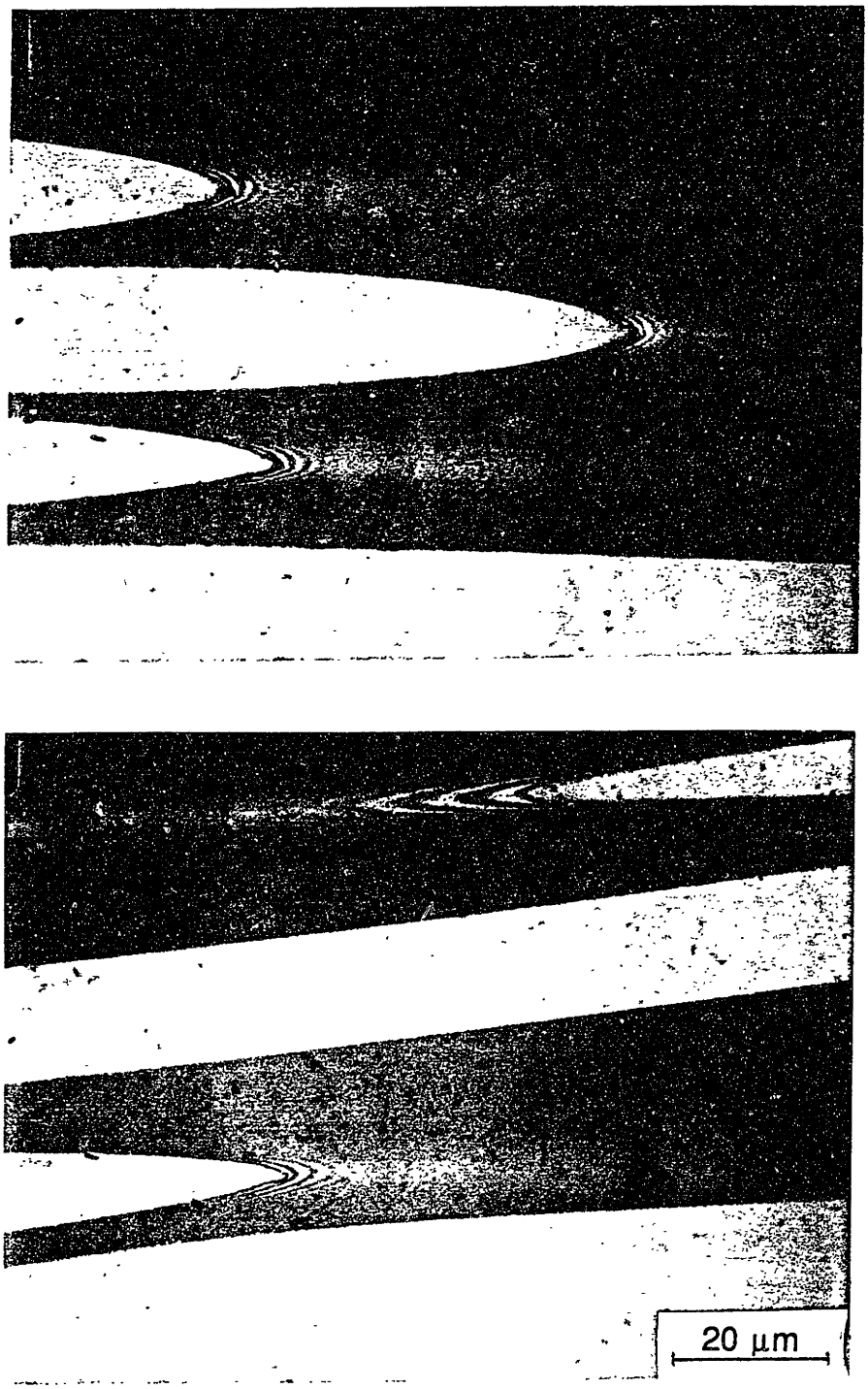

Fig. 4-7 The presence of residual stresses in a unidirectional Nicalon/CAS composite is evident in the vicinity of the fiber ends.

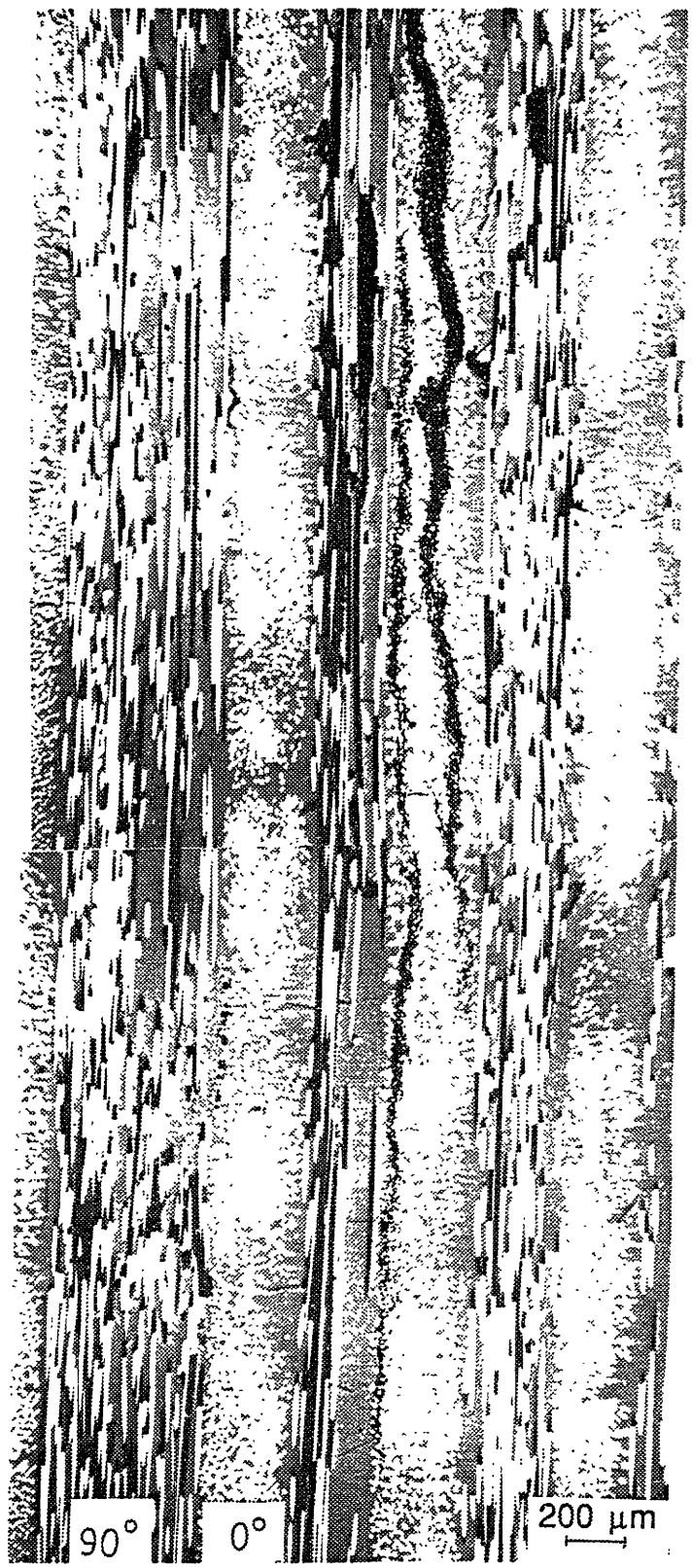

Fig. 4-8 Delamination crack in a crossply Nicalon/1723 composite, tested at room temperature. (Cross-sectional view)

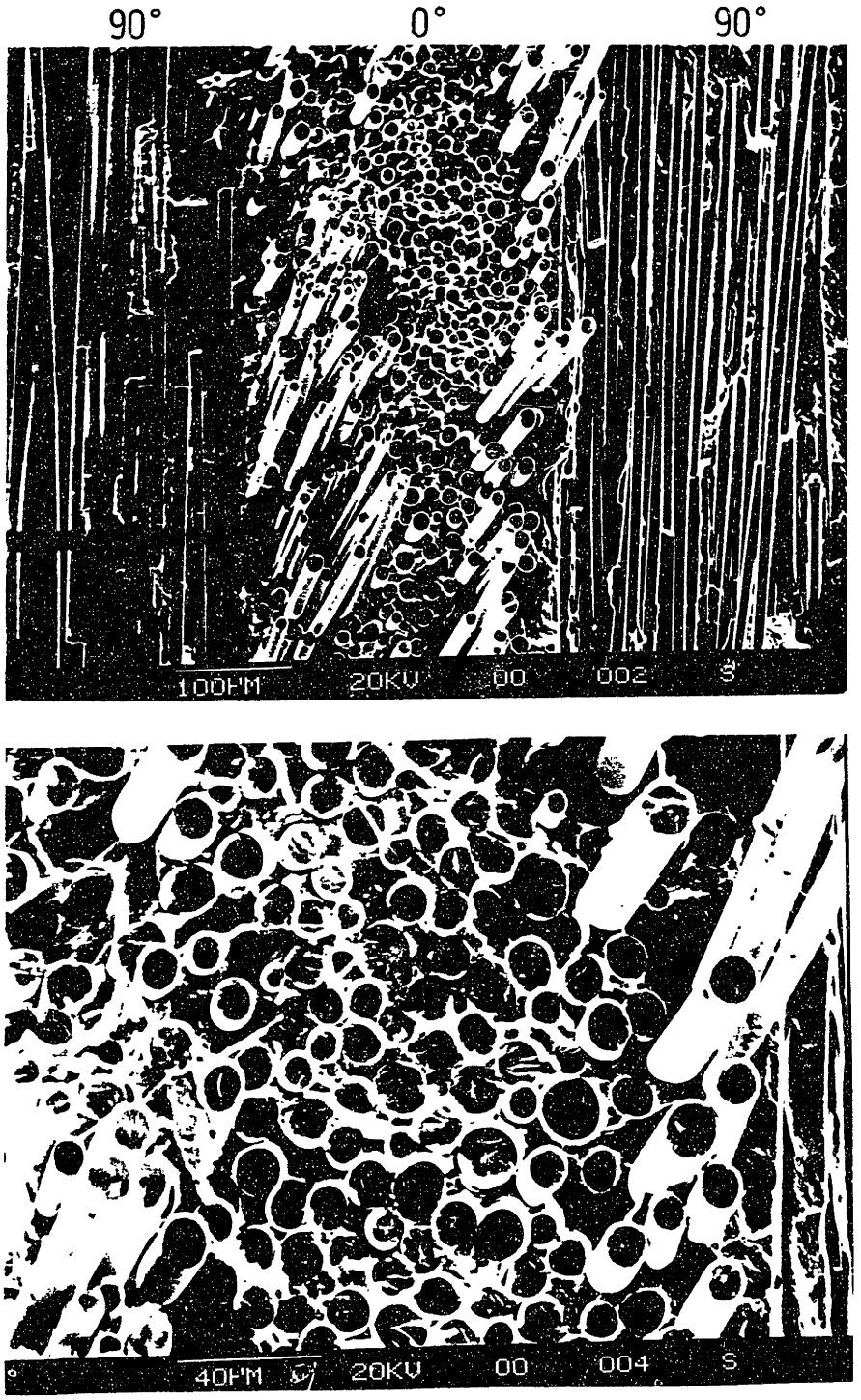

Fig. 4-9 Embrittled zone in a 0° ply of a Nicalon/1723 crossply laminate. Note the fiber pullout at the 0/90 interfaces.

(a)

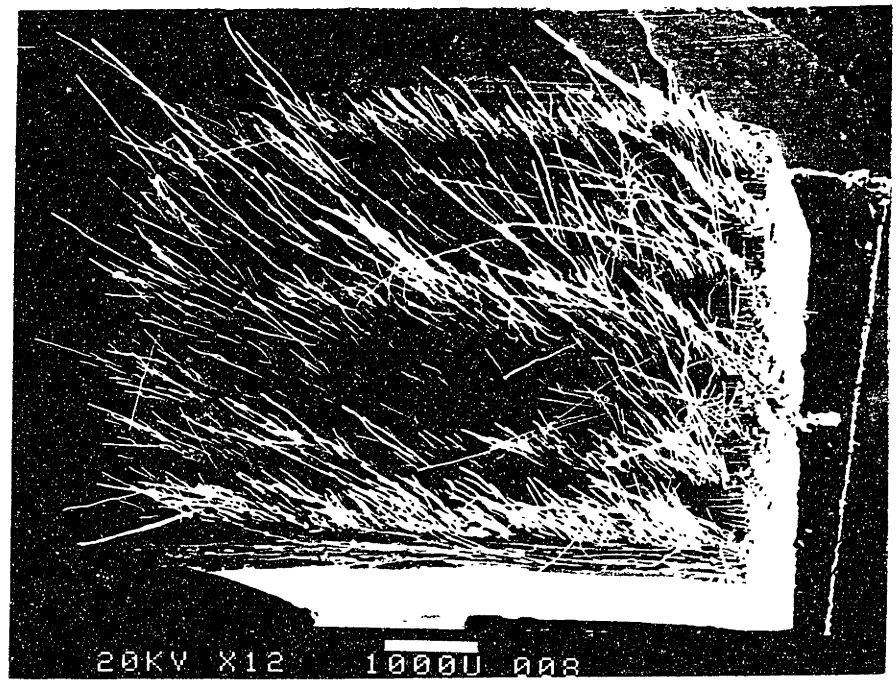

(b)

Fig. 4-10 A Nicalon/BMAS crossply laminate following room temperature fracture:
(a) Overall fracture surface
(b) Side view

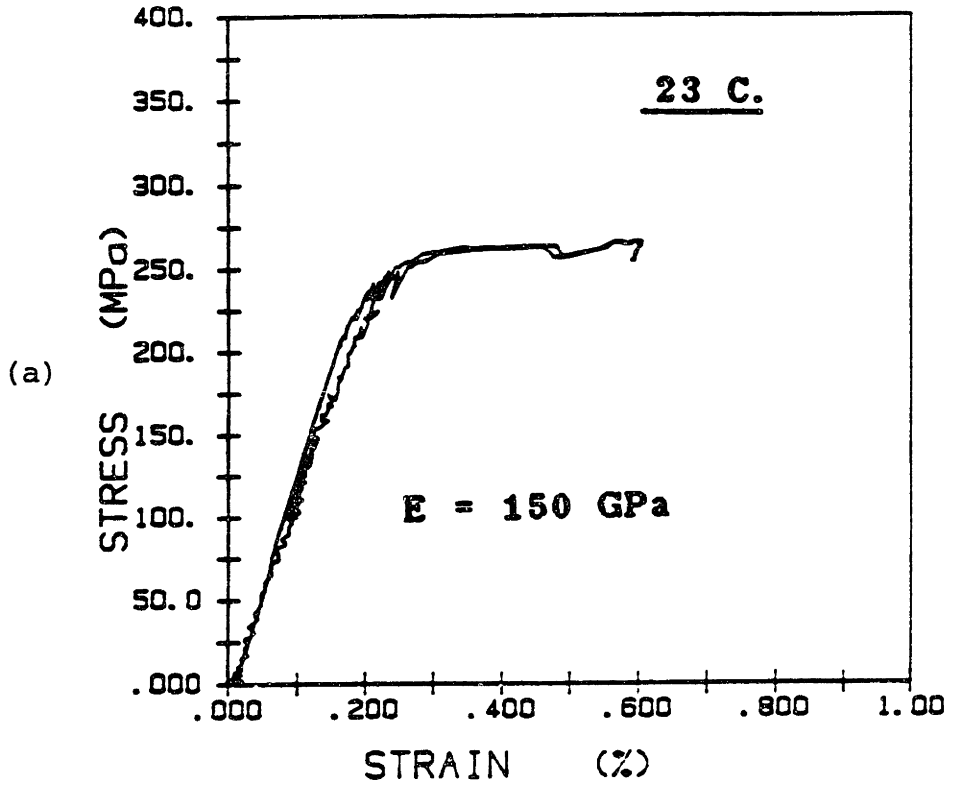

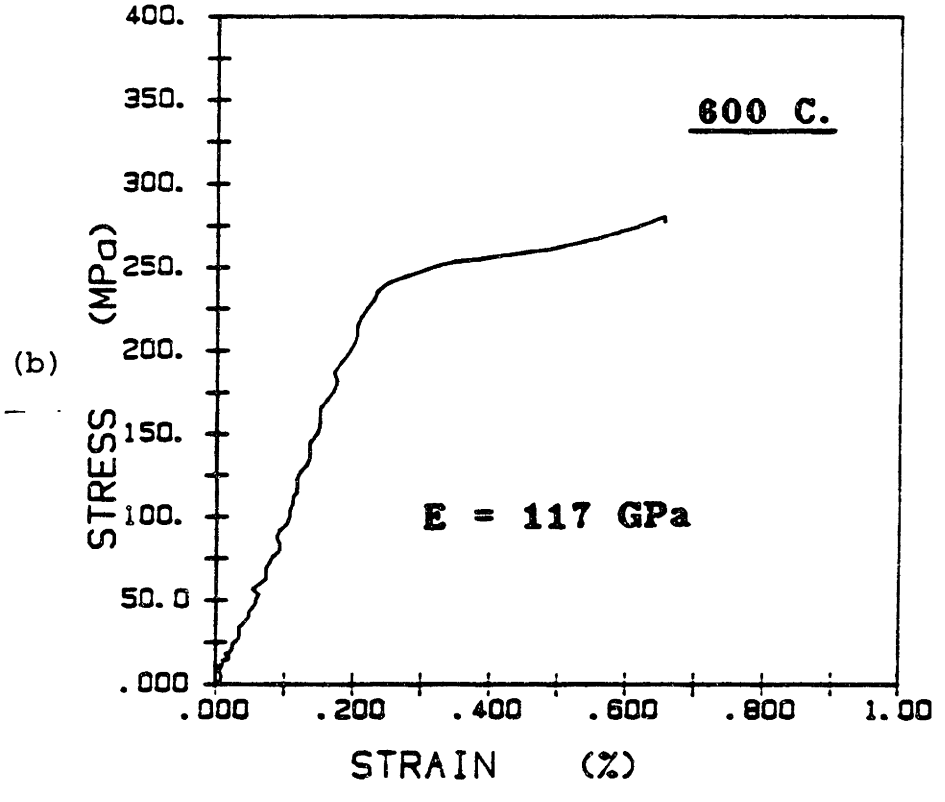

Fig. 4-11 Tensile stress-strain curves of undirectional Nicalon/CAS composites tested at: (a) 23°C, (b) 600°C and (c) 1000°C. (Ref. 91)

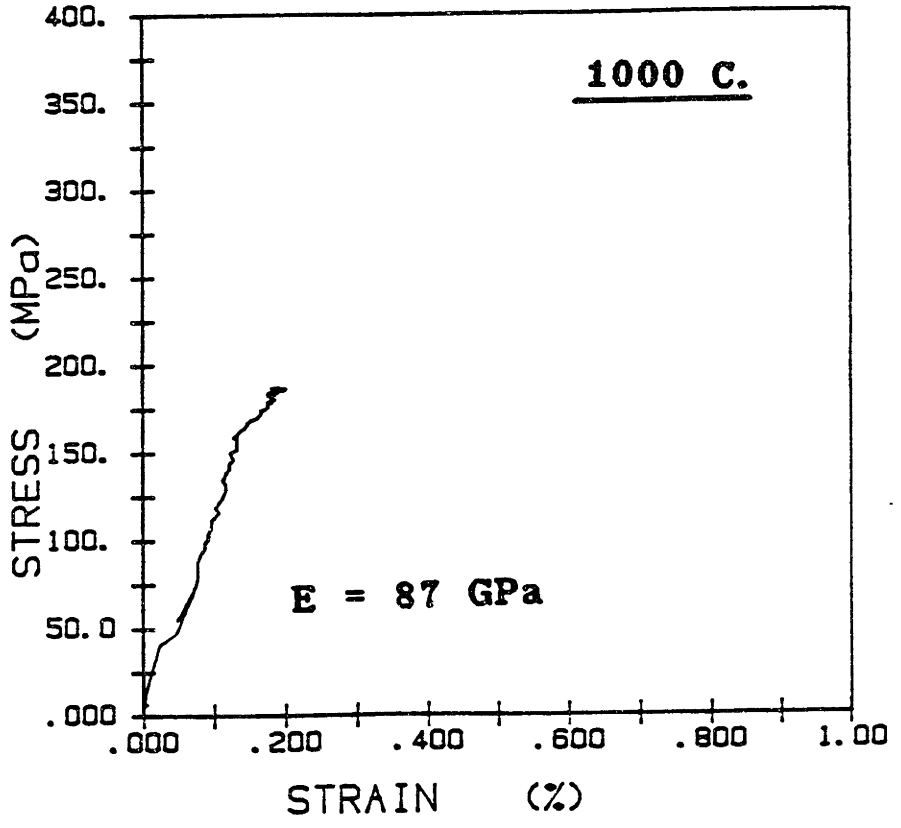

(c)

Fig. 4-11 Tensile stress-strain curve of undirectional Nicalon/CAS (c) 1000°C.

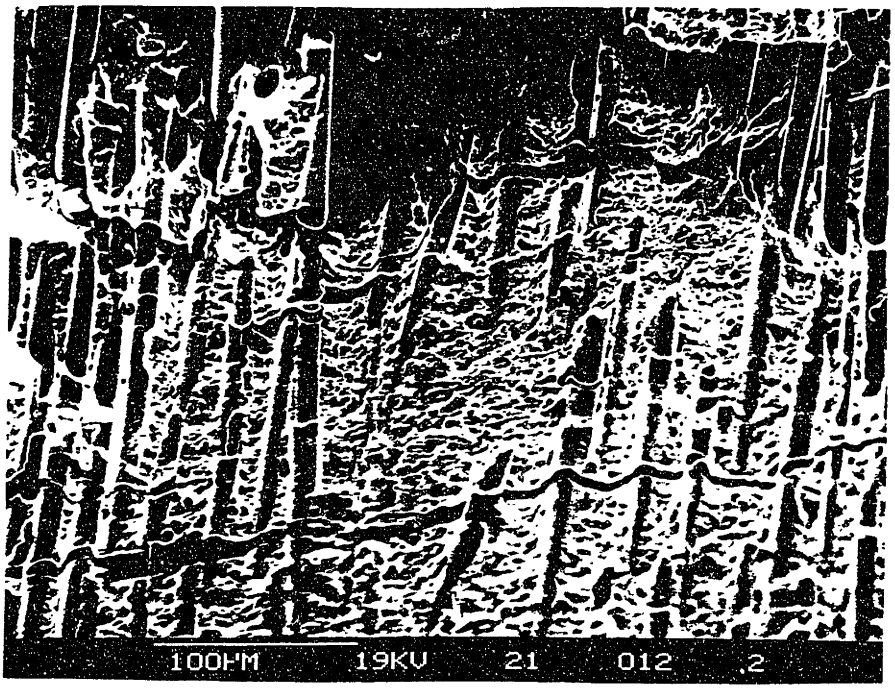

Fig. 4-12 Matrix cracks in the vicinity of the fracture surface of a Nicalon/CAS composite after tensile testing at 600°C. Some cracks have extended through the fibers.

(a)

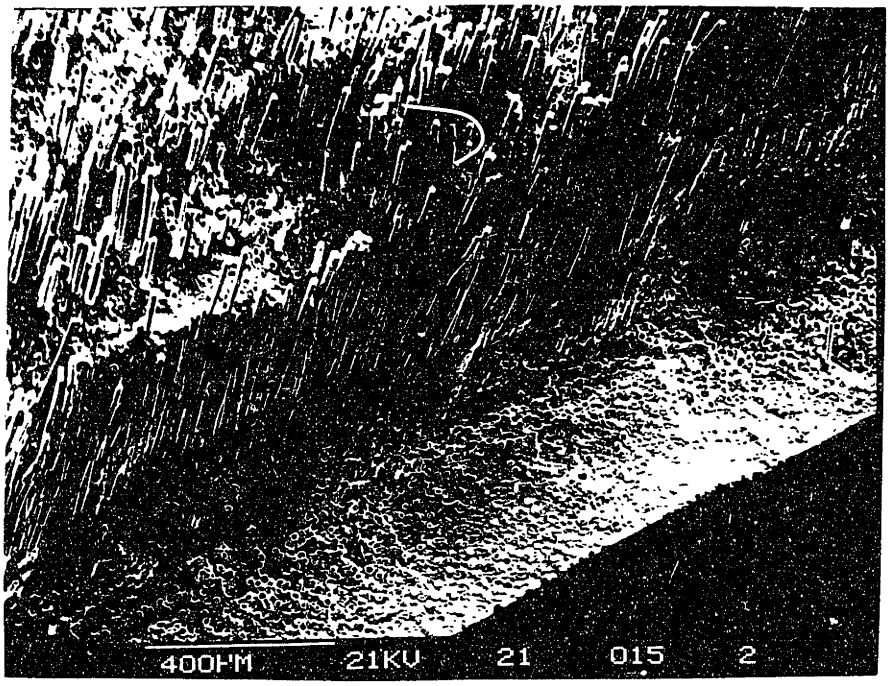

(b)

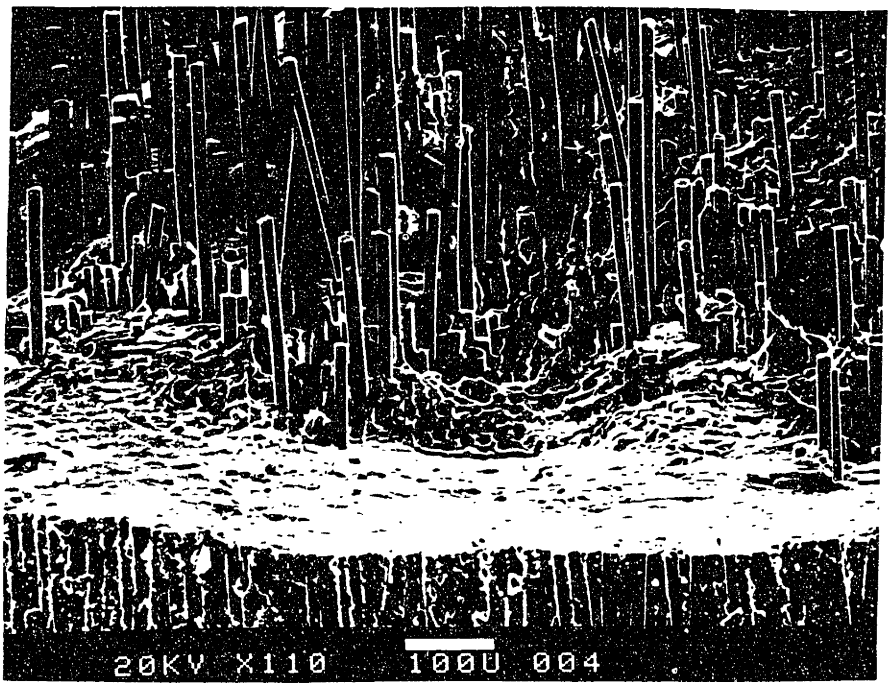

Fig. 4-13 Embrittled region around the specimen periphery of unidirectional glass-ceramic matrix composites tested at 1000°C:
(a) Nicalon/CAS
(b) Nicalon/BMAS

(a)

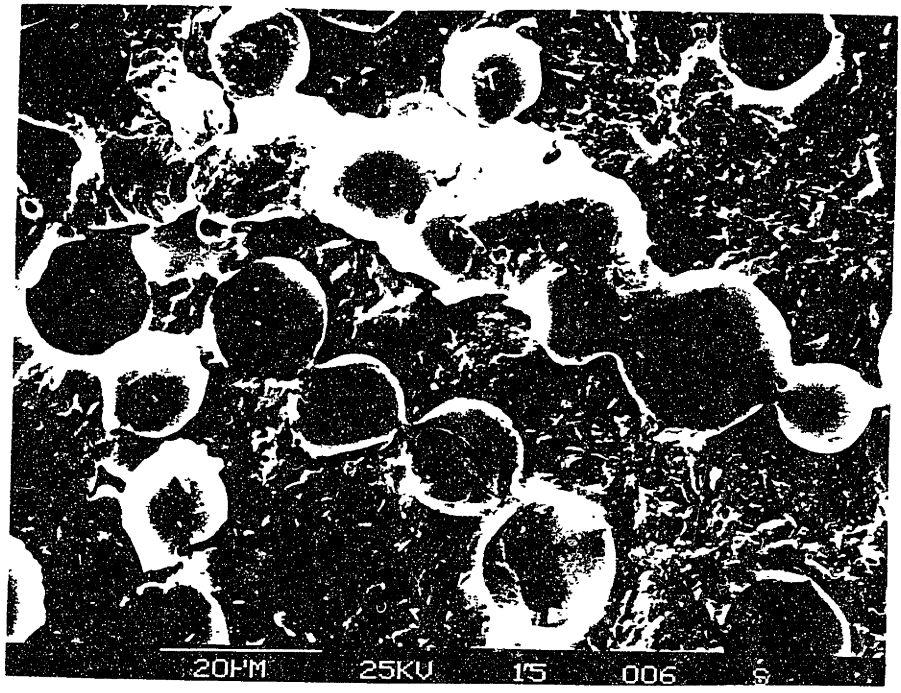

(b)

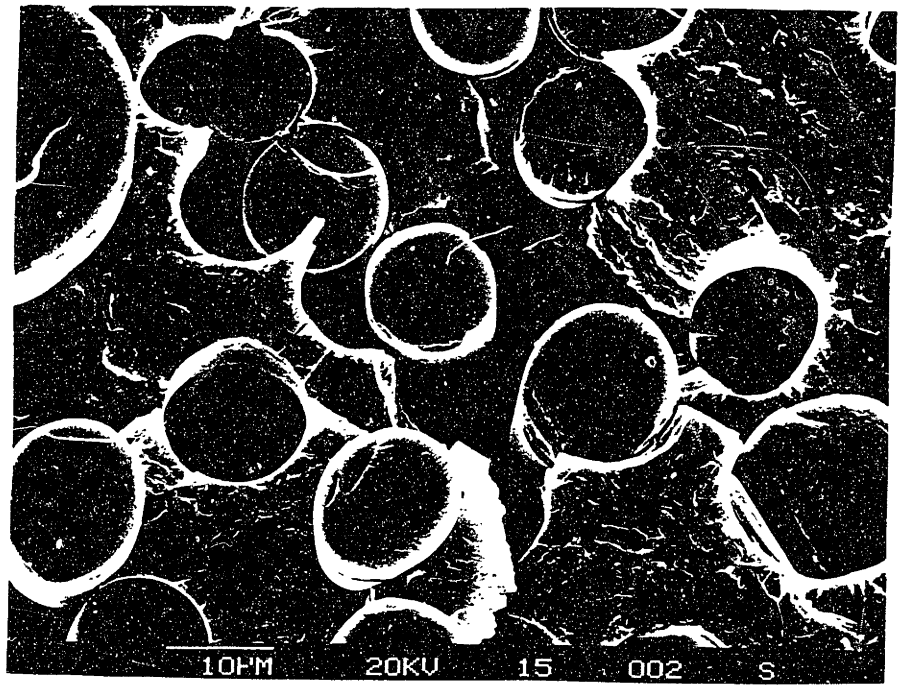

Fig. 4-14 Elevated temperature phenomena in a unidirectional Nicalon/CAS composite following 1000°C exposure:
(a) Fiber fusion in the embrittlement zone
(b) Fiber/matrix debonding

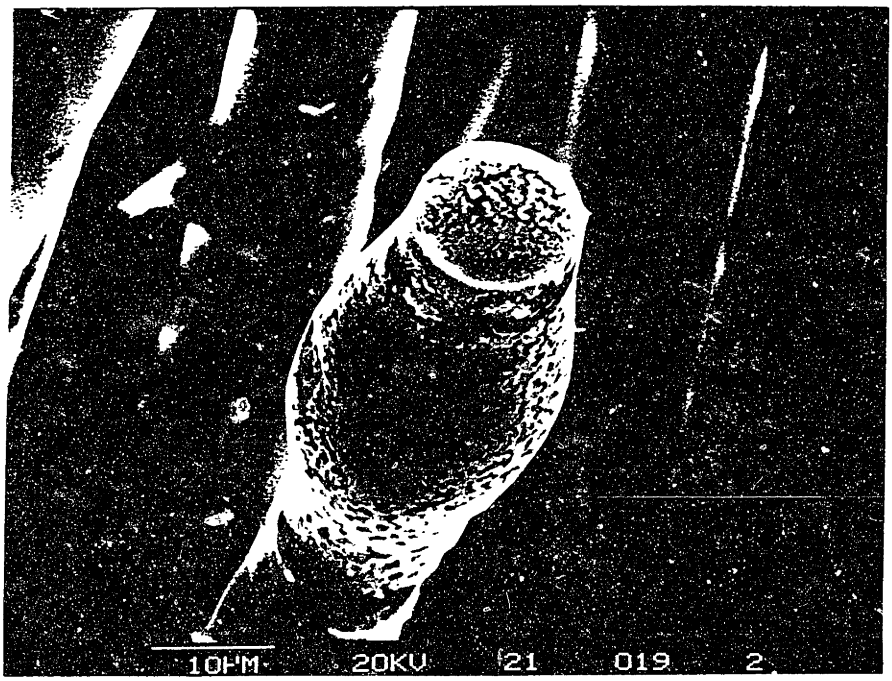

(c)

Fig. 4-14 Elevated temperature phenomena in a unidirectional Nicalon/CAS composite following 1000°C exposure:
(c) Swelling of a Nicalon fiber

(a)

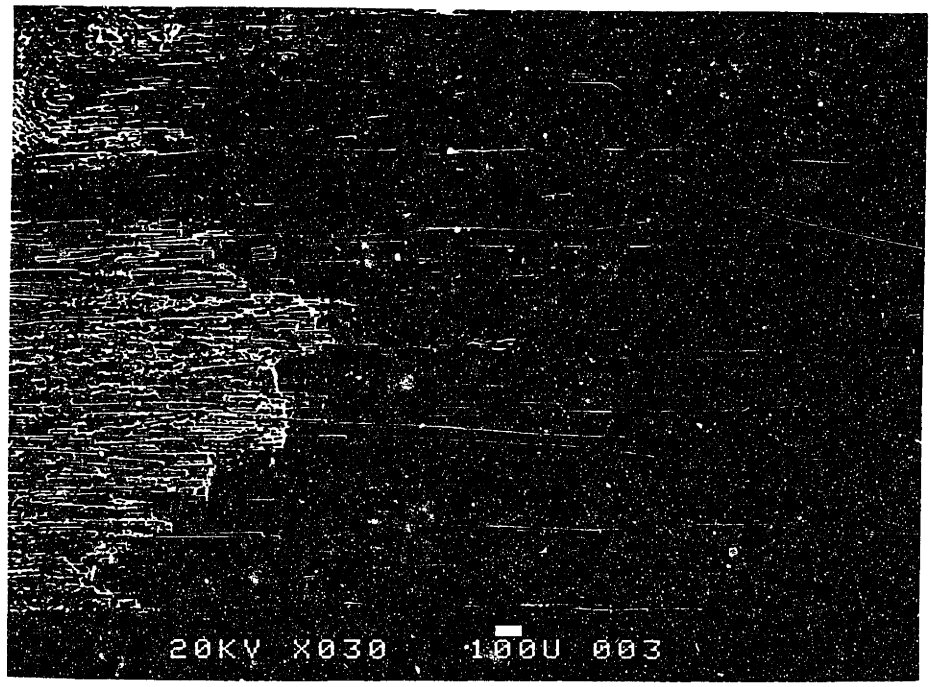

(b)

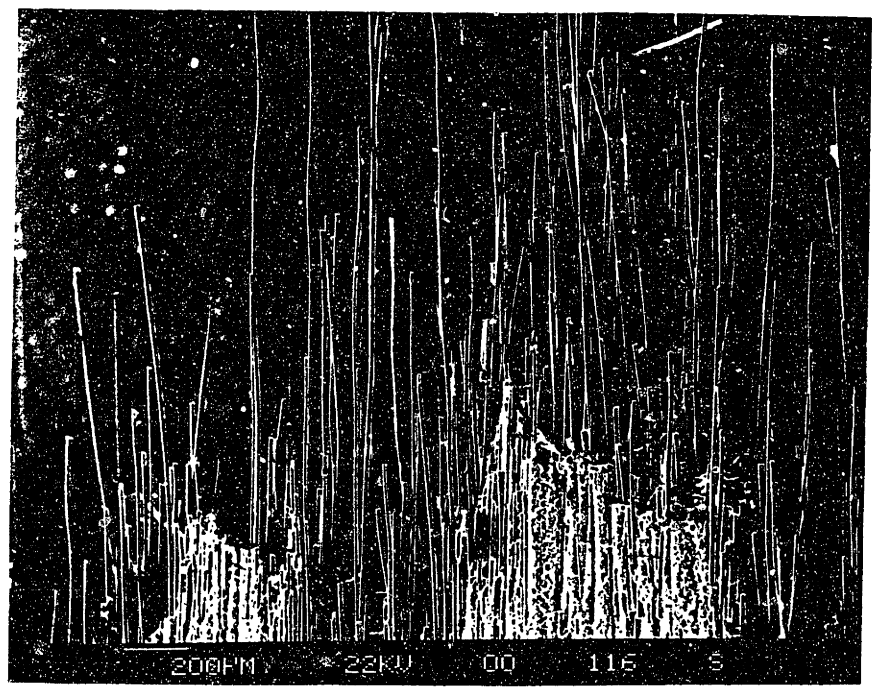

Fig. 4-15 Fracture surfaces of unidirectional Nicalon/BMAS composites after tensile testing at: (a) 23°C, (b) 600°C and (c) 800°C. Note the decrease in fiber pullout lengths with increasing temperature.

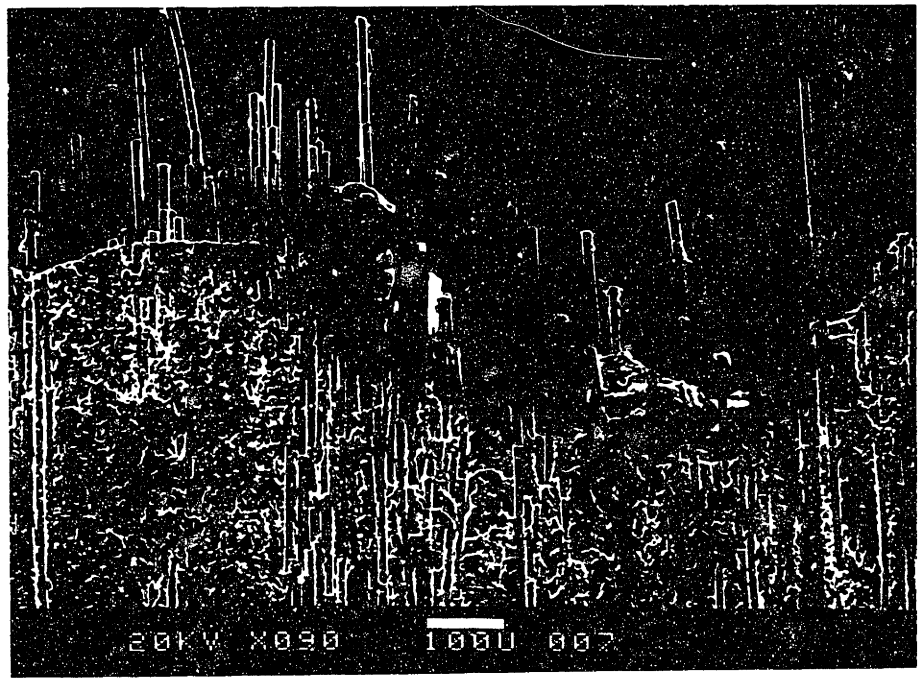

(c)

Fig. 4-15 (c) 800°C.

(a)

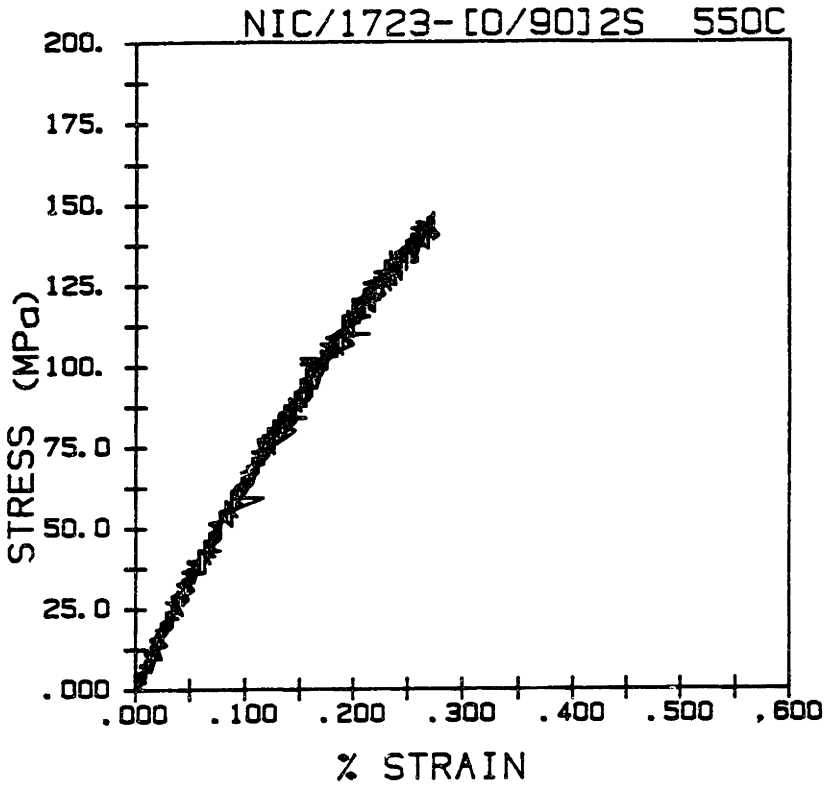

(b)

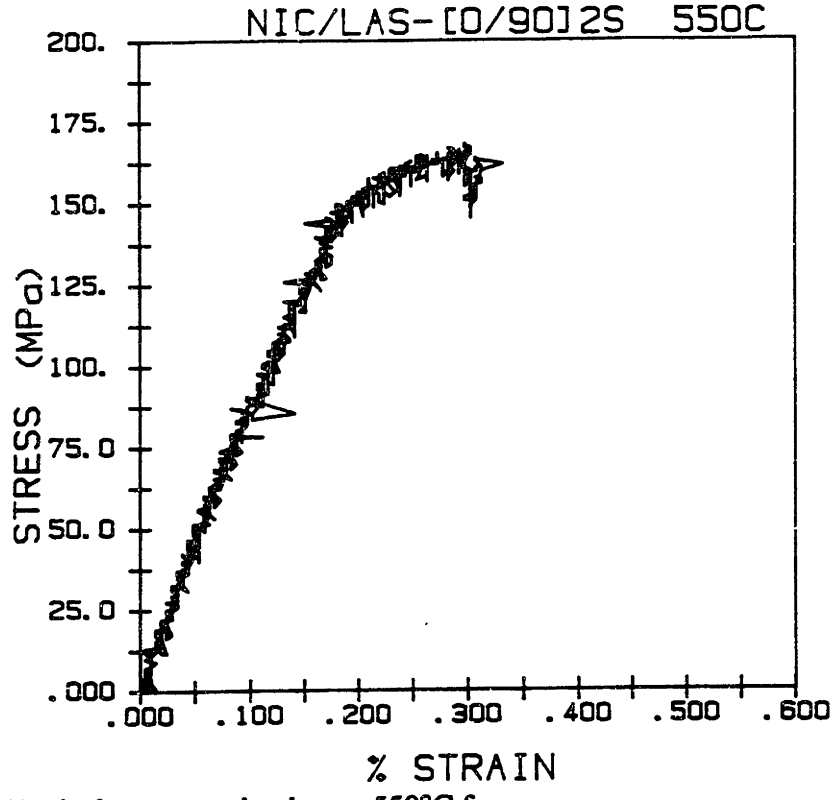

Fig. 4-16 Typical stress-strain plots at 550°C for:
(a) Nicalon/1723-$[0/90]_{2S}$
(b) Nicalon/LAS-$[0/90]_{2S}$

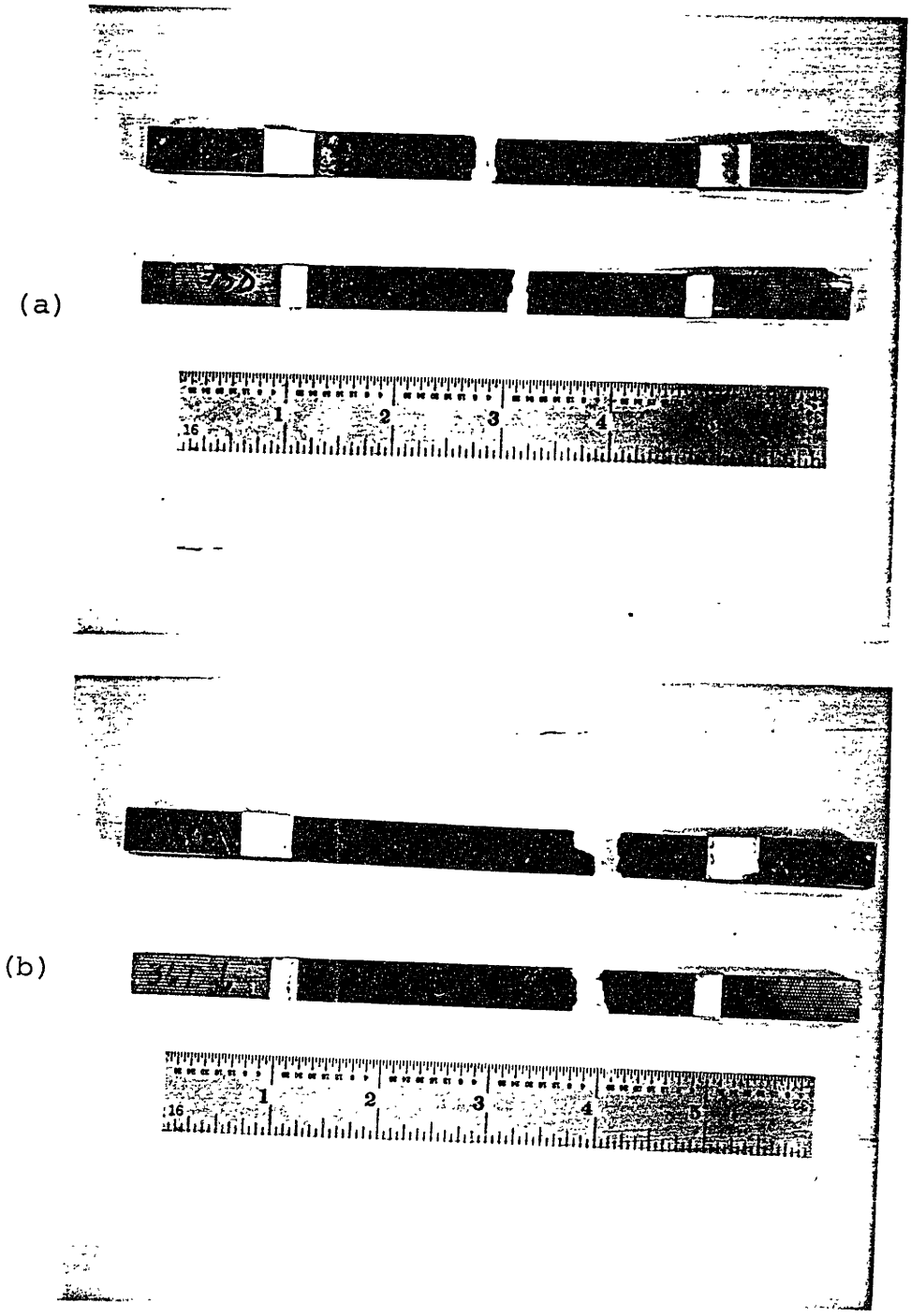

Fig. 4-17 Overall view of gage section failures of (a) Nicalon/1723 and (b) Nicalon/LAS following fracture at 550°C.

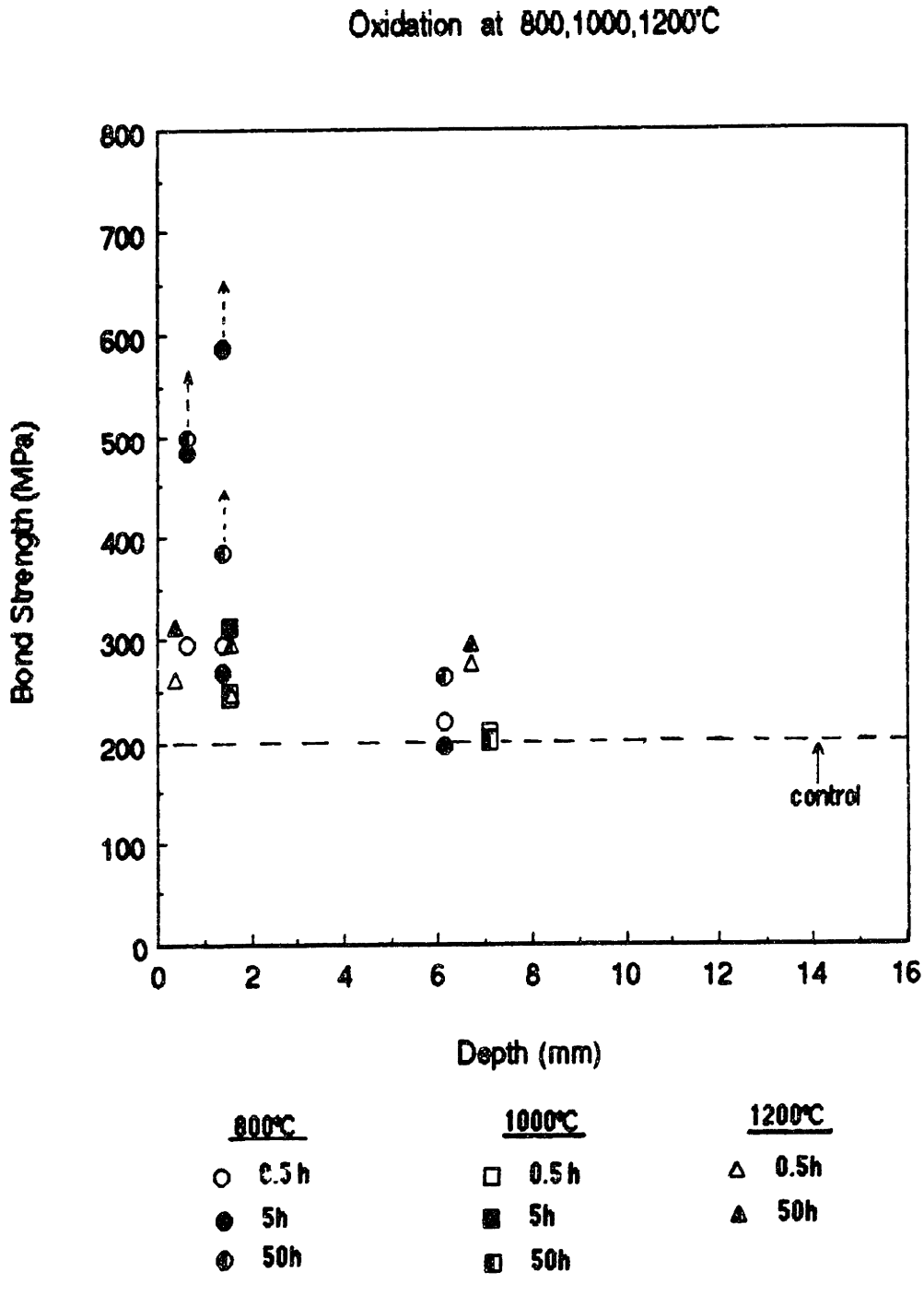

Fig. 4-18 Bond strength (τ_{deb}) versus depth below the exposed surface for Nicalon/ CAS-IIb samples oxidized at 800, 1000 and 1200°C for various times.

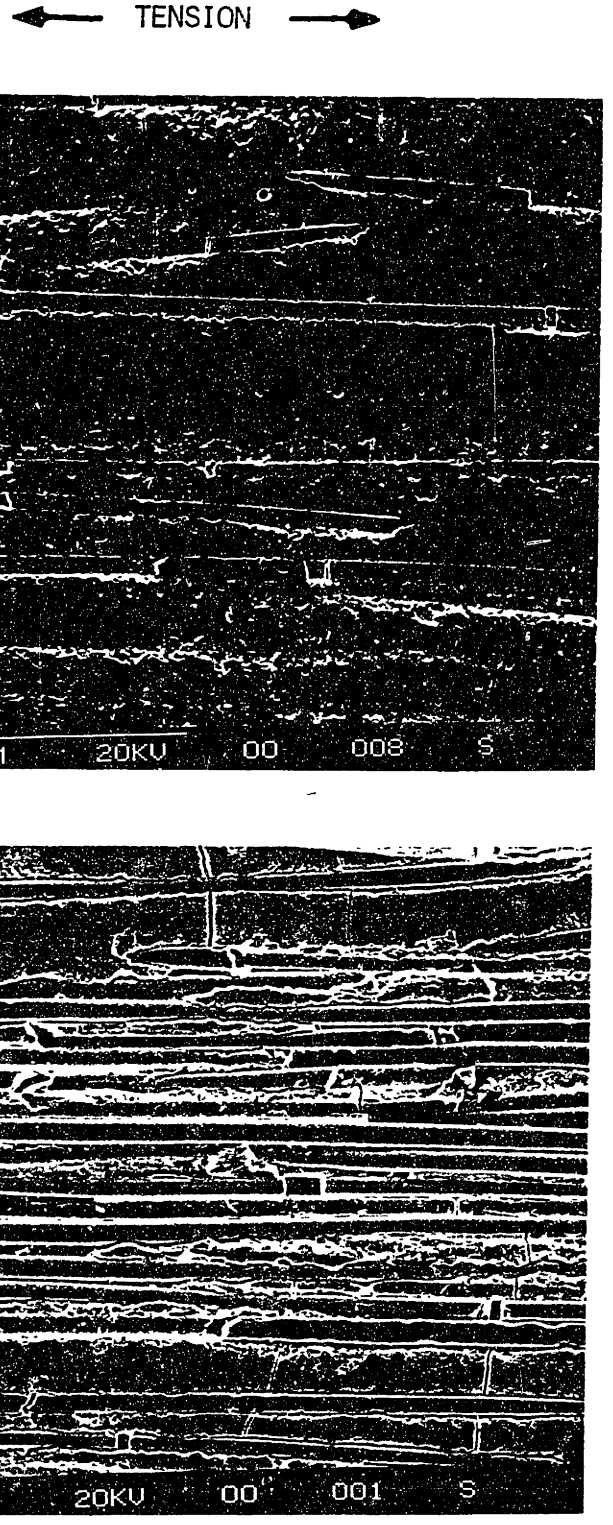

Fig. 4-19 Cracking in unidirectional laminates after straining in four-point bending.
a) Regularly spaced matrix cracks in Nicalon/1723 at 0.5 % strain.
b) Irregular matrix cracking in Nicalon/BMAS at 0.45 % strain.

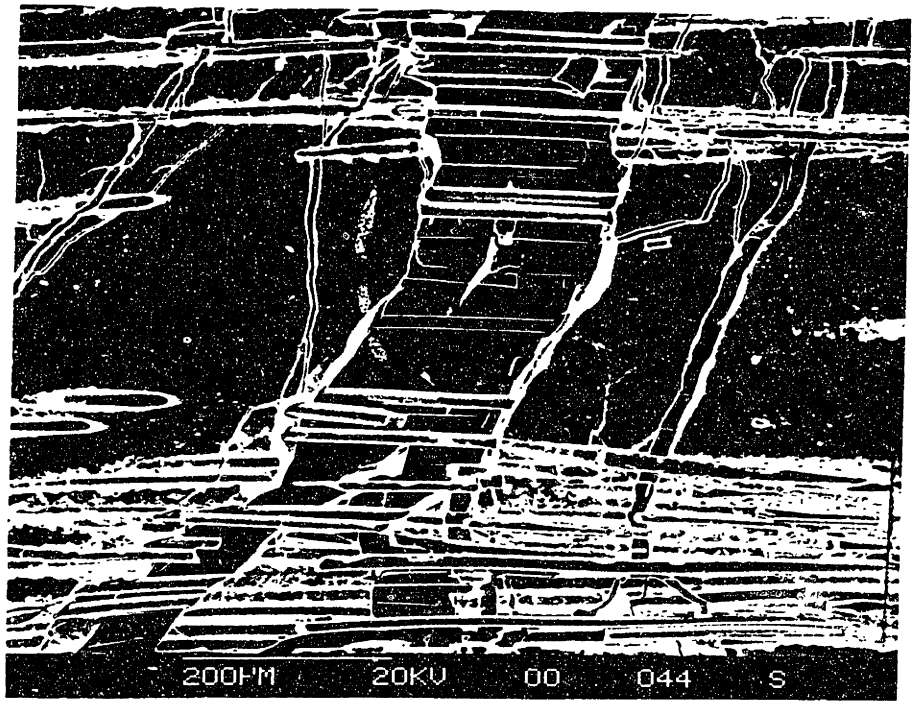

(c)

Fig. 4-19 c) Matrix sliding in Nicalon/BMAS at strains exceeding 0.45 % strain.

(a)

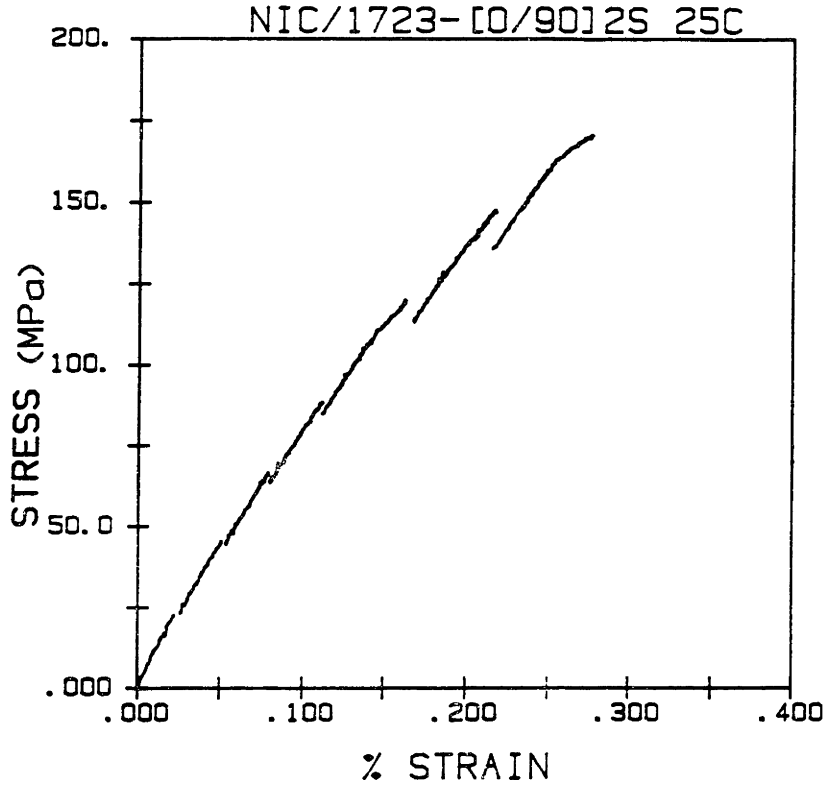

(b)

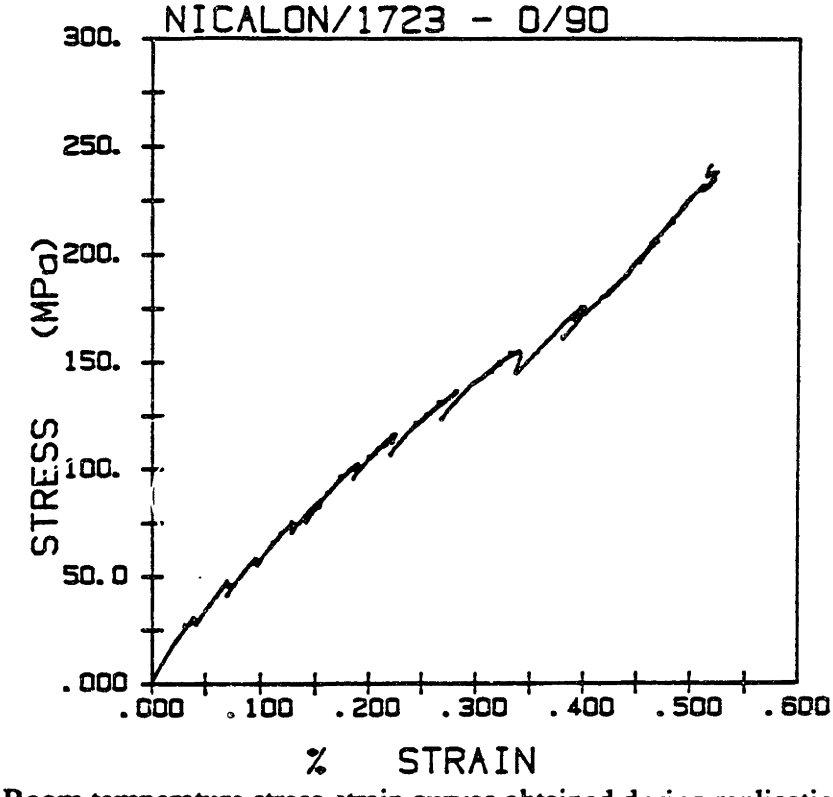

Fig. 4-20 Room temperature stress-strain curves obtained during replication studies of: a) Nicalon/1723-$[0/90]_{2S}$
b) Nicalon/1723-$[0/90]_{4S}$

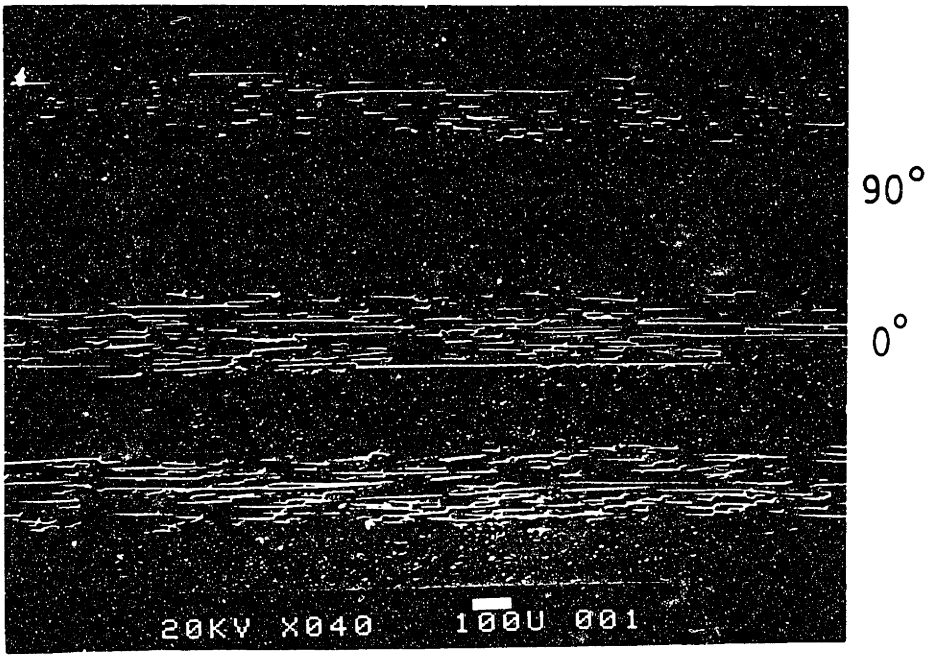

Fig. 4-21 Replica of an as-polished Nicalon/1723 crossply laminate. No cracks are evident prior to loading.

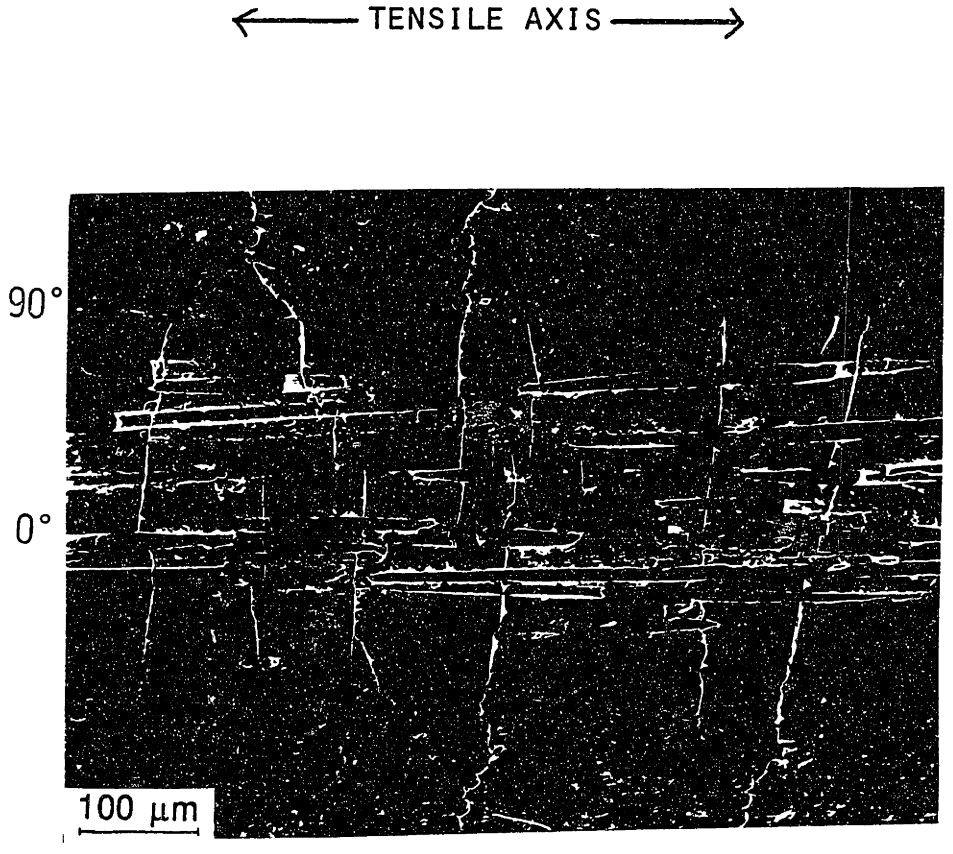

Fig. 4-22 Longitudinal and transverse ply cracking in crossplied Nicalon/1723 at 0.231 % strain. Some cracks have not fully extended across the entire ply thickness.

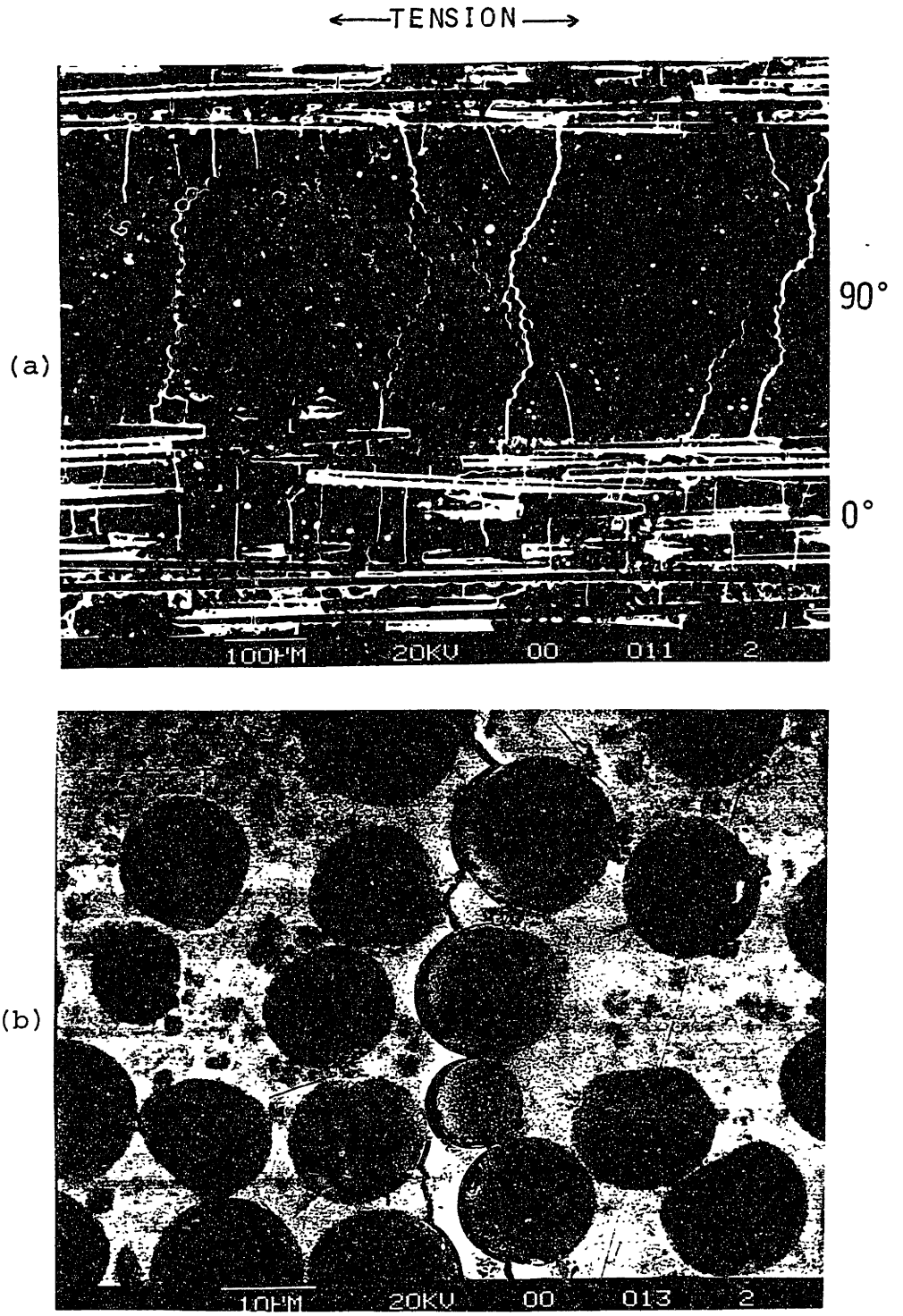

Fig. 4-23 Preferential growth of 90° ply cracks along the fiber/matrix interface in a crossplied Nicalon/1723 laminate. (b) is an enlarged view of (a).

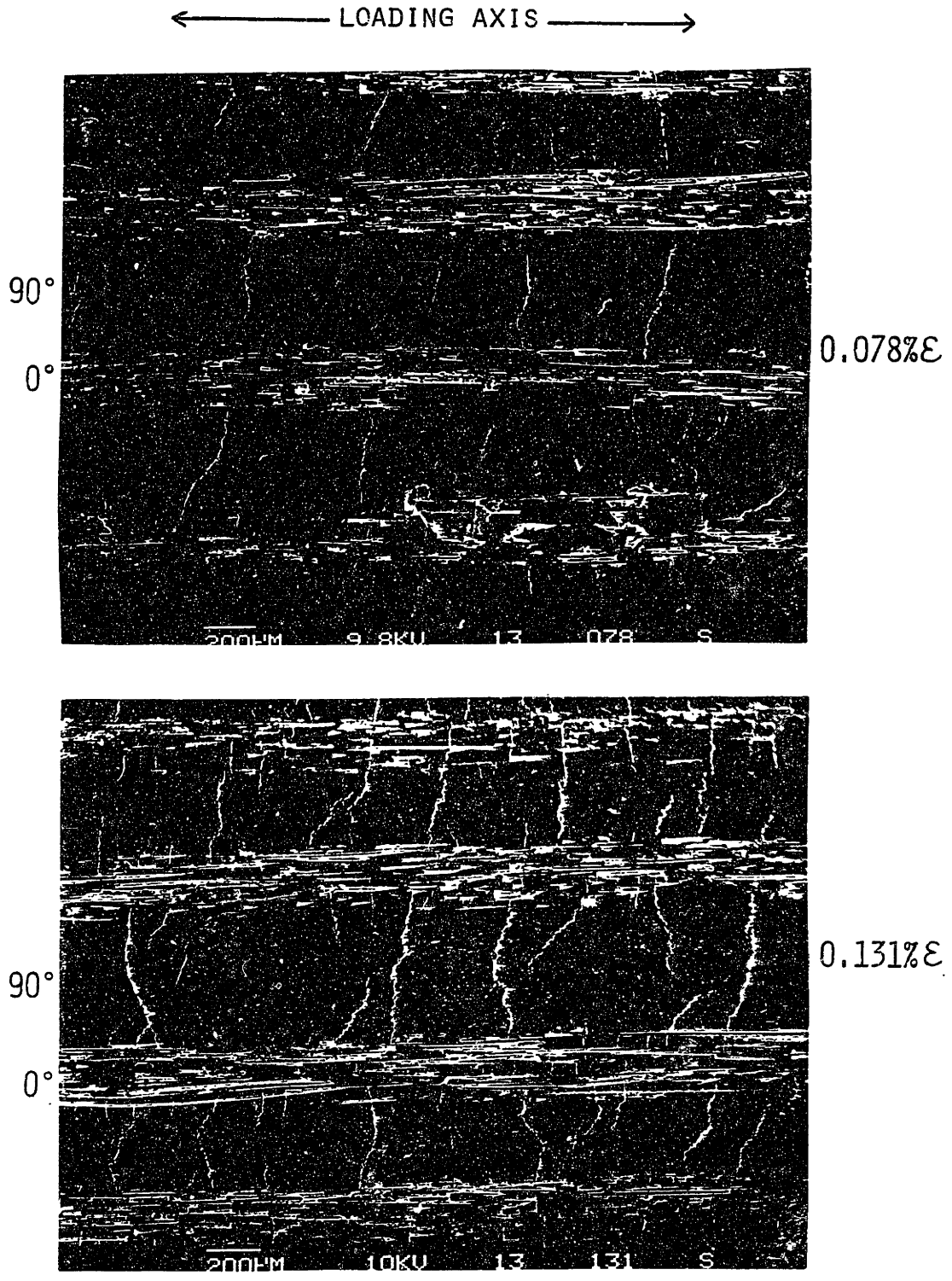

Fig. 4-24 Damage development in Nicalon/1723-$[0/90]_{4S}$ at a progression of strain levels.

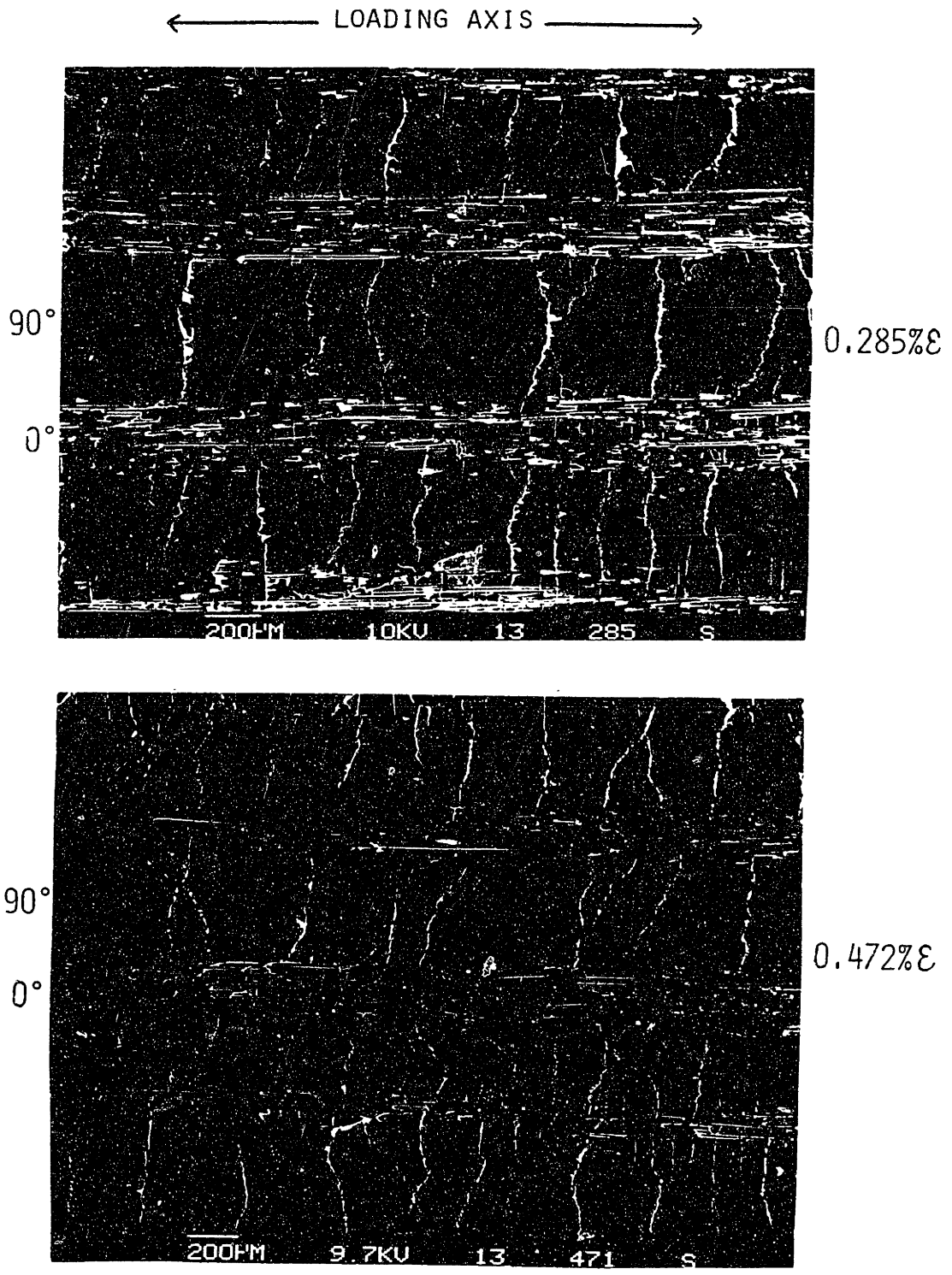

Fig. 4-24 Damage development in Nicalon/1723-$[0/90]_{4S}$ at a progression of strain levels.

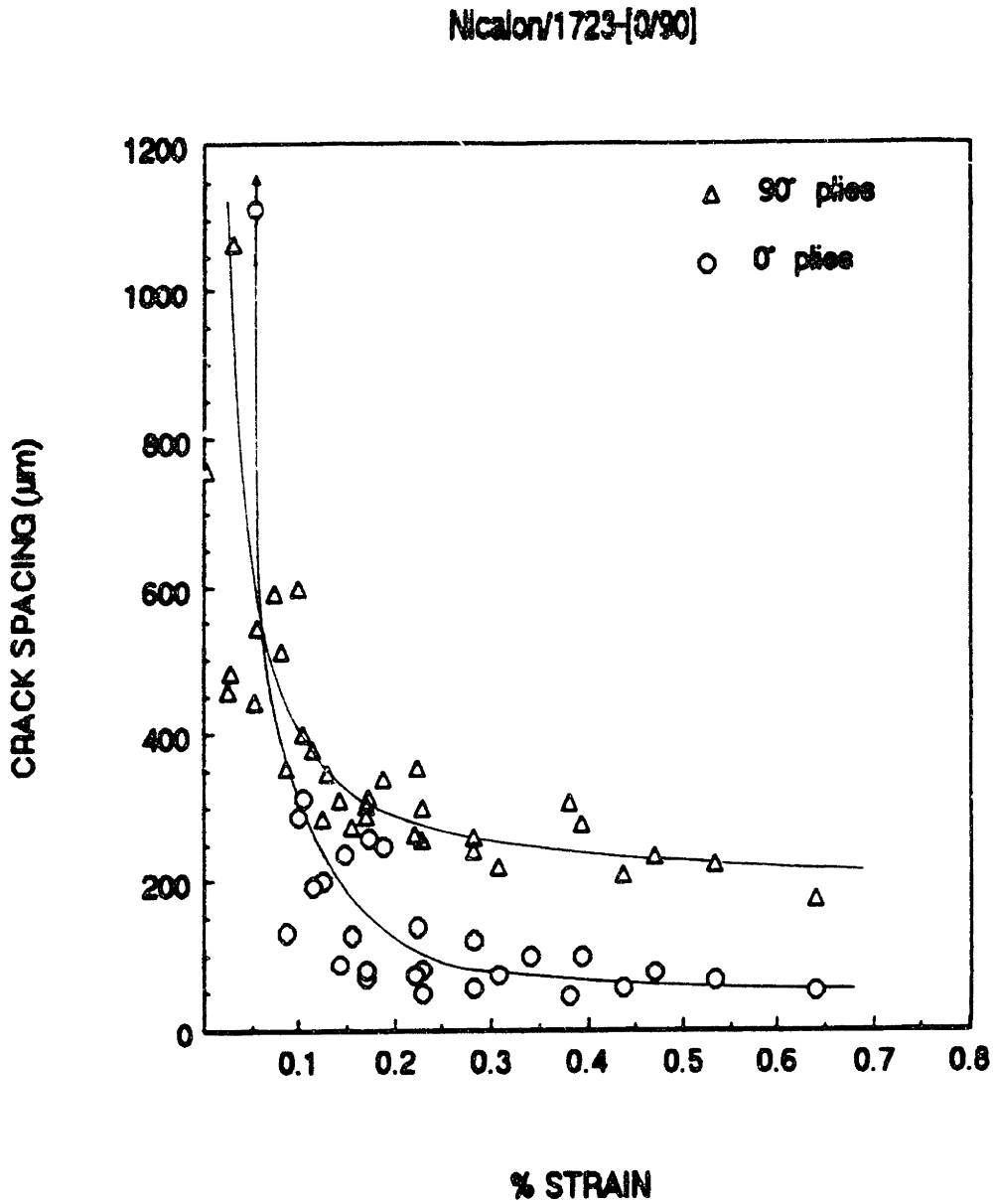

Fig. 4-25 Crack spacing vs. applied strain in the longitudinal and transverse plies of Nicalon/1723 crossply laminates after room temperature loading.

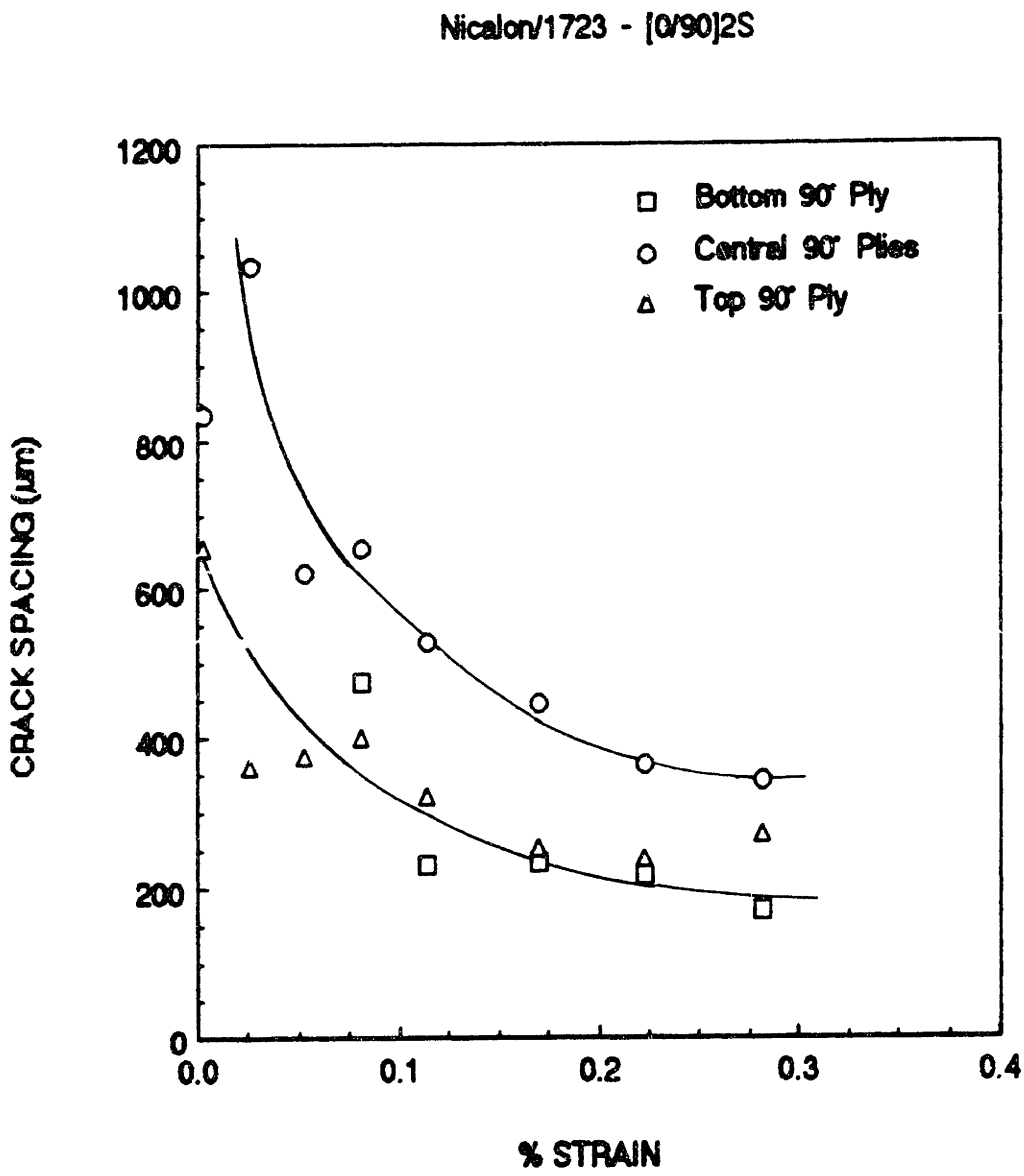

Fig. 4-26 Crack spacing vs. applied strain for each 90° ply in a Nicalon/1723-$[0/90]_{2S}$ laminate. The thickness of the central 90° plies is twice that of the outer 90° plies.

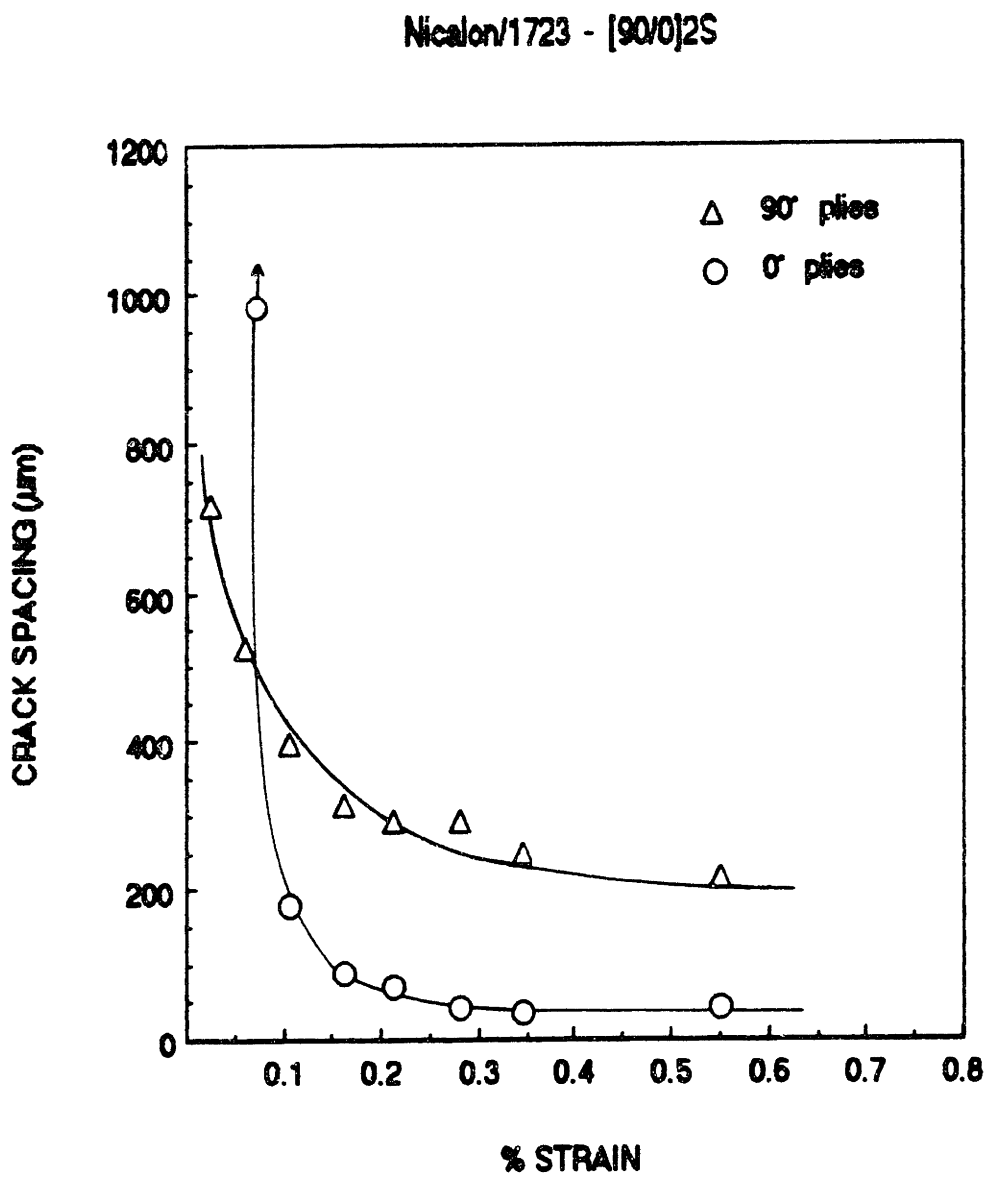

Fig. 4-27 Crack spacing vs. applied strain for a Nicalon/1723-$[90/0]_{2S}$ laminate after tensile loading at 25°C.

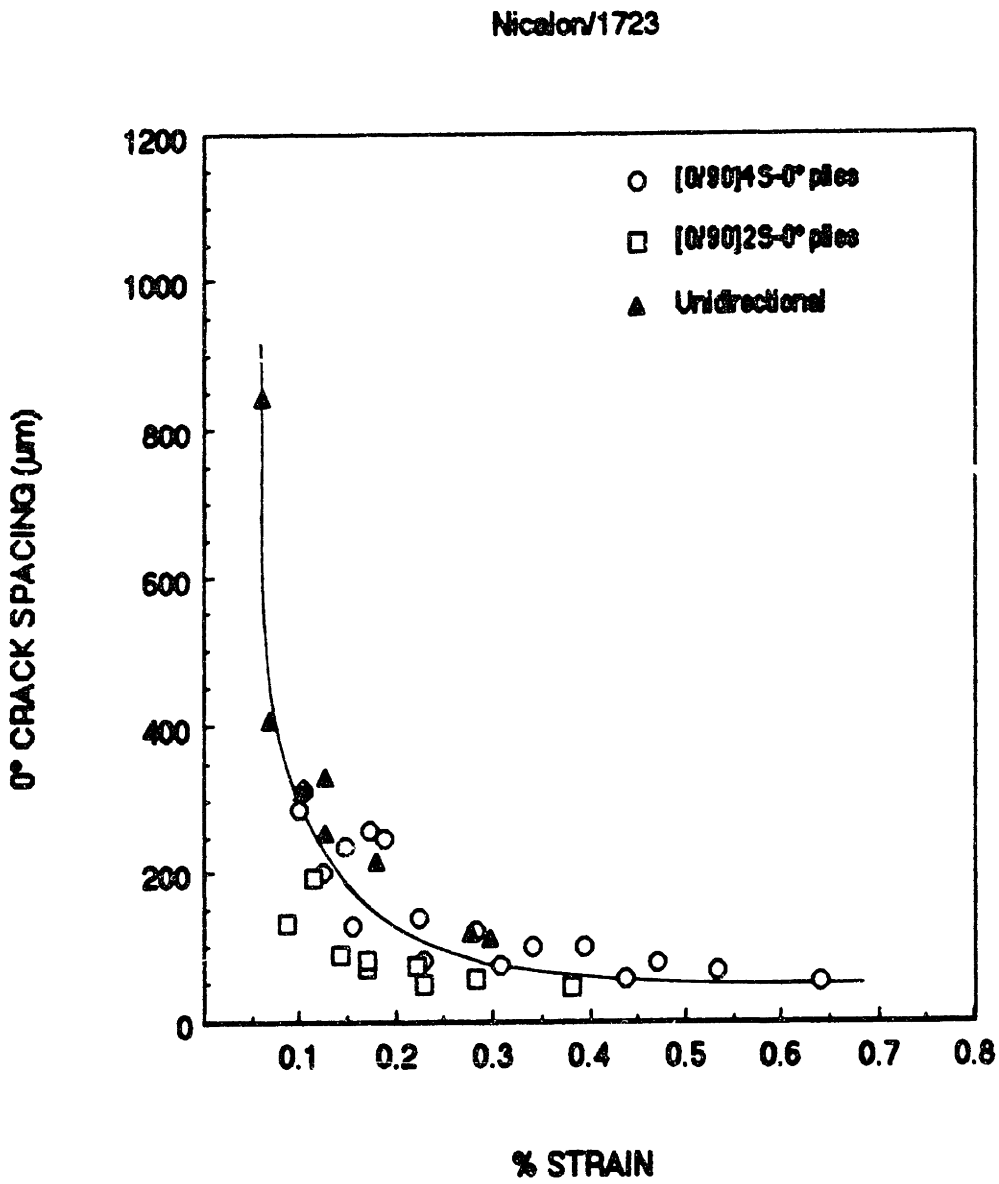

Fig. 4-28 Comparison of crack spacing vs. strain data from replication studies of unidirectional and crossply laminates of Nicalon/1723 at room temperature.

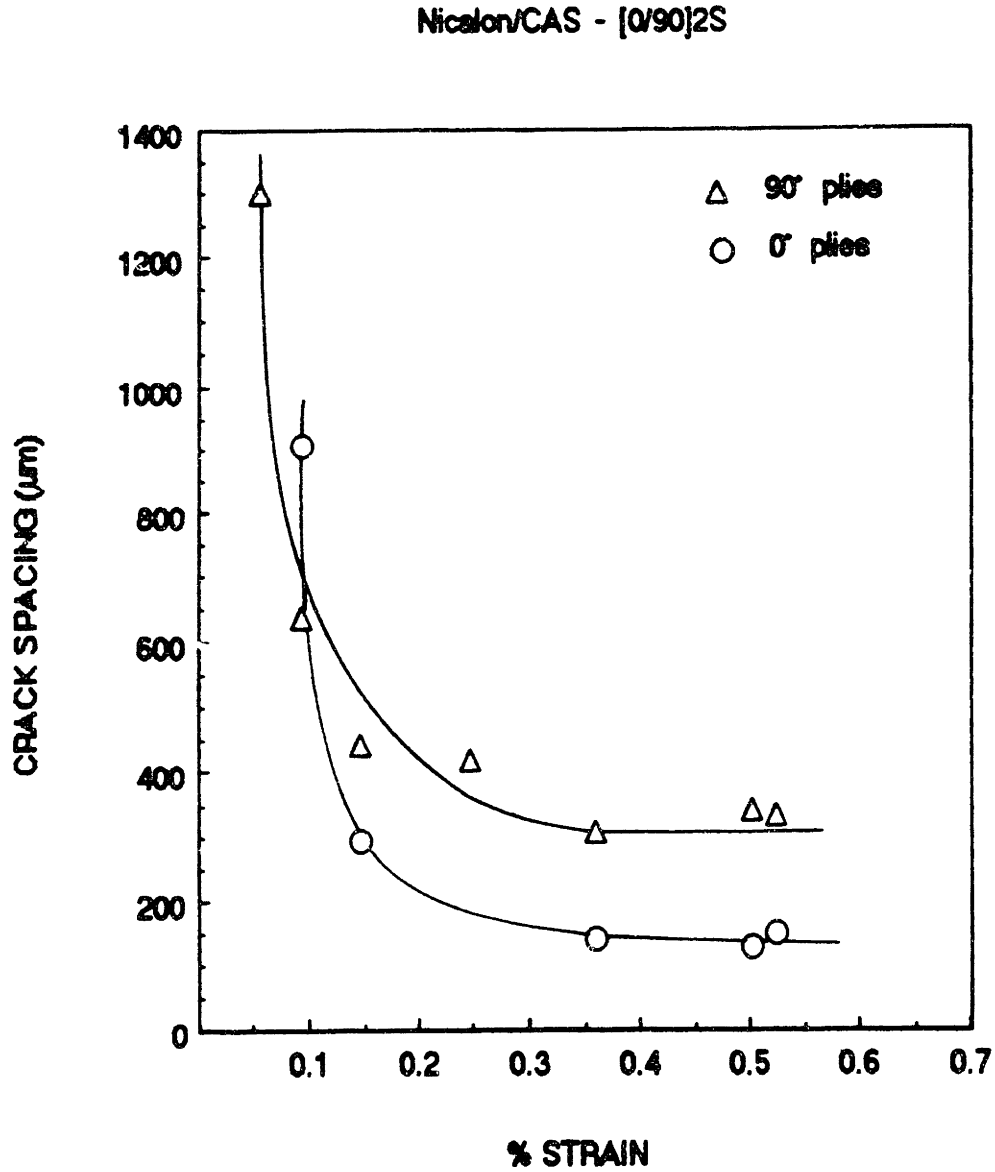

Fig. 4-29 Crack spacing vs. strain for a Nicalon/CAS-$[0/90]_{2S}$ laminate after tensile loading at 25°C.

Fig. 4-30 Edge replica of crossplied Nicalon/CAS-II following tensile loading to 0.5 % strain at room temperature.

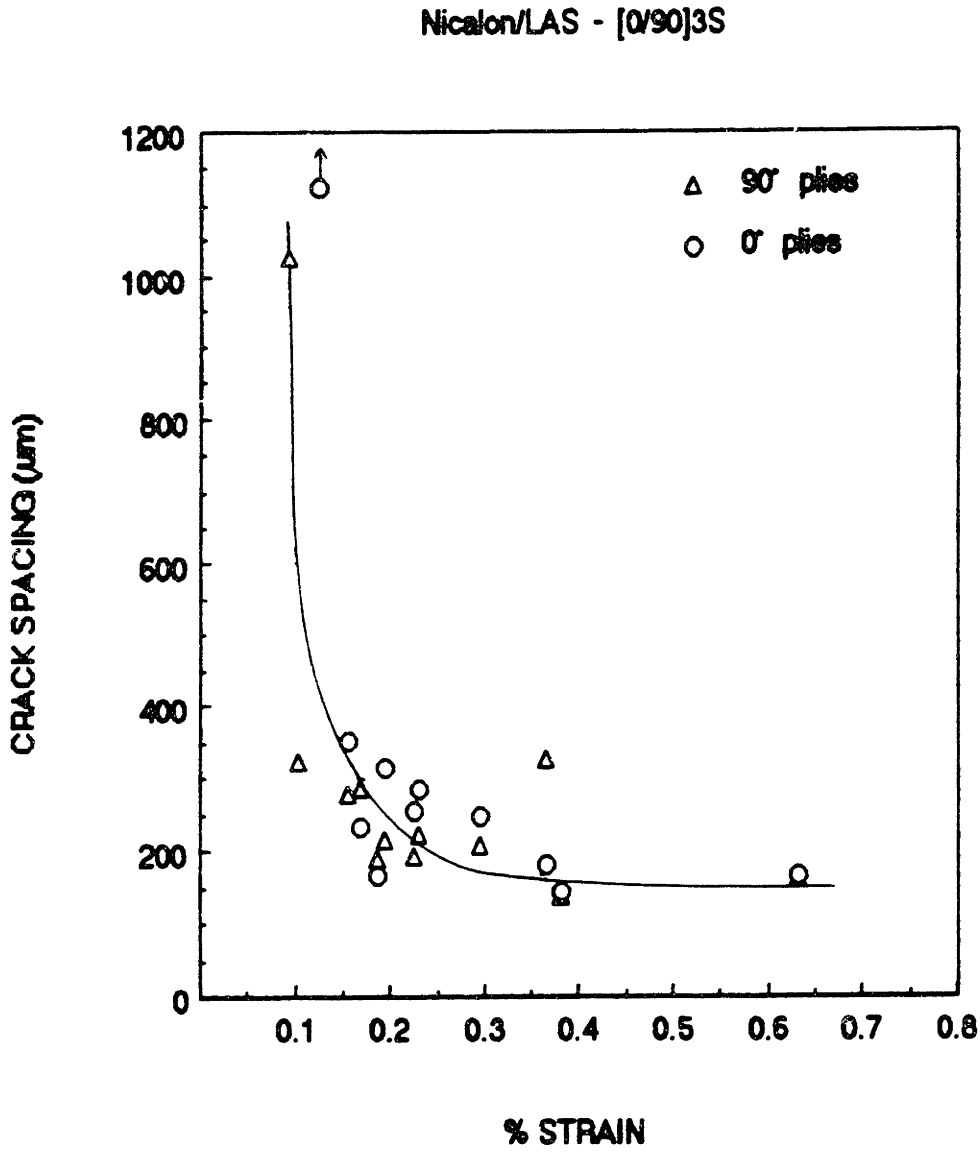

Fig. 4-31 Crack spacing vs. strain for Nicalon/LAS-$[0/90]_{3S}$ laminates after tensile loading at 25°C.

Fig. 4-32 Edge replica of Nicalon/LAS showing crack branching in the 90° plies.

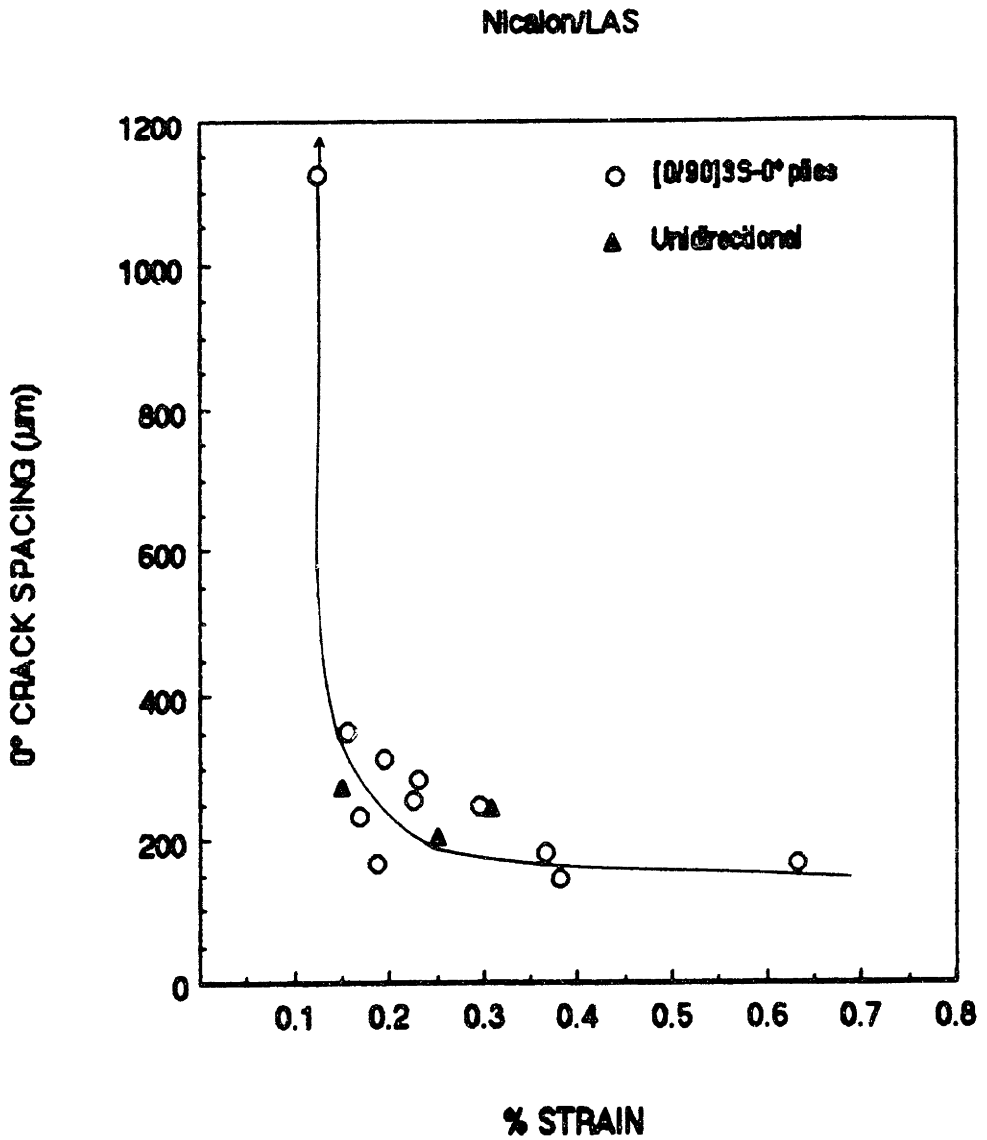

Fig. 4-33 Comparison of crack spacing vs. strain data from replication studies of unidirectional and crossply laminates of Nicalon/LAS at room temperature.

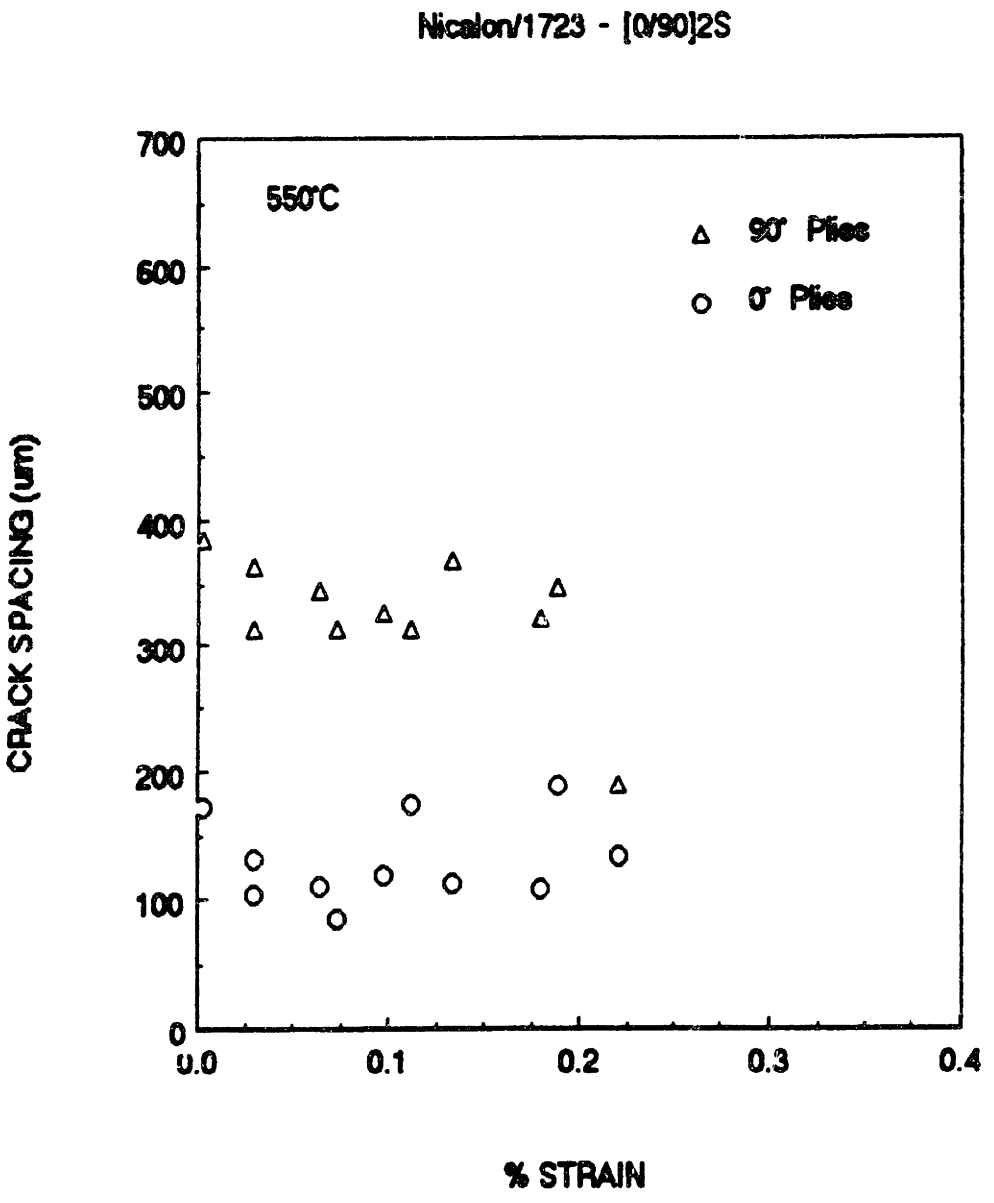

Fig. 4-34 Crack spacing vs. strain for Nicalon/1723-$[0/90]_{2S}$ laminate after tensile loading at 550°C.

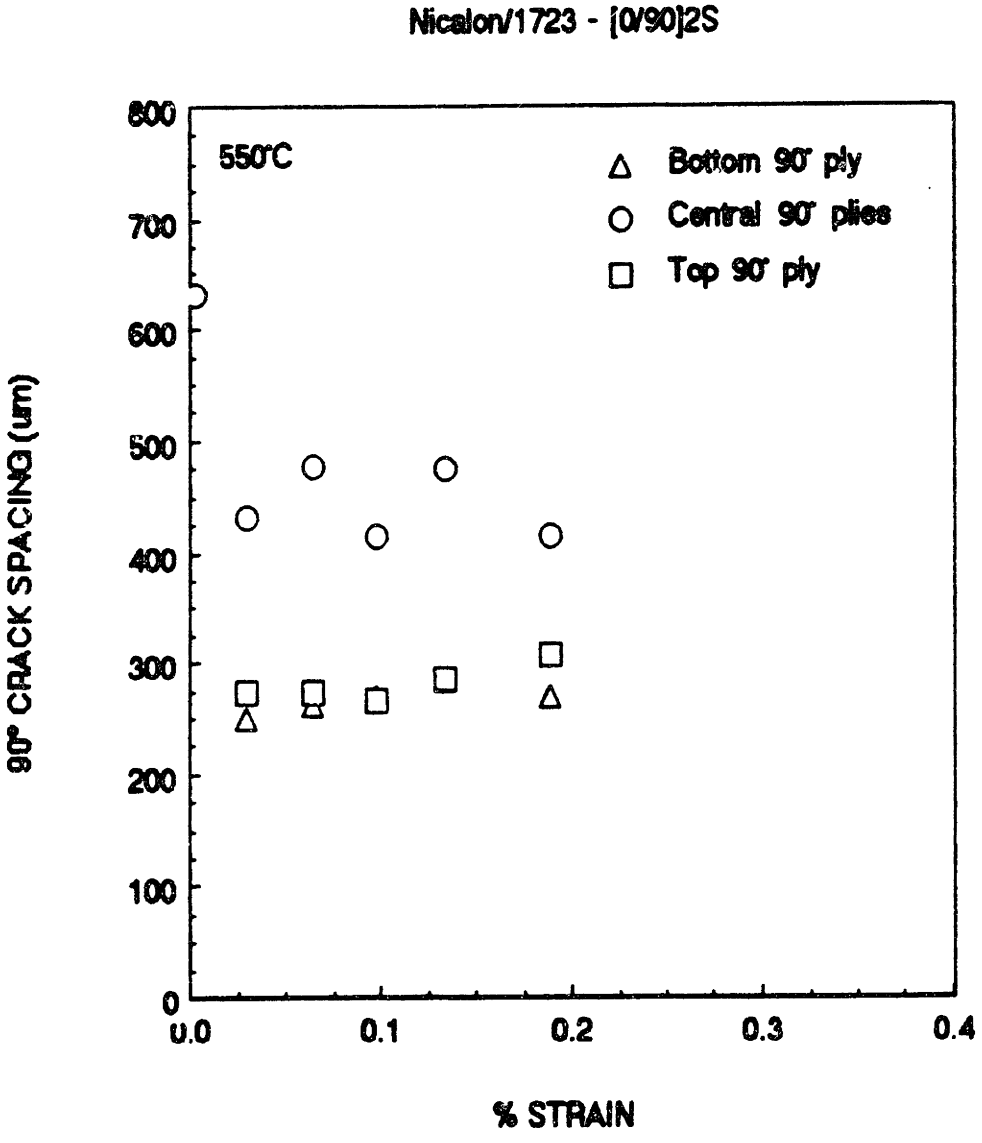

Fig. 4-35 Crack spacing vs. applied strain for each 90° ply in a Nicalon/1723-$[0/90]_{2S}$ laminate, following loading at 550°C. The thickness of the central 90° plies is twice that of the outer 90° plies.

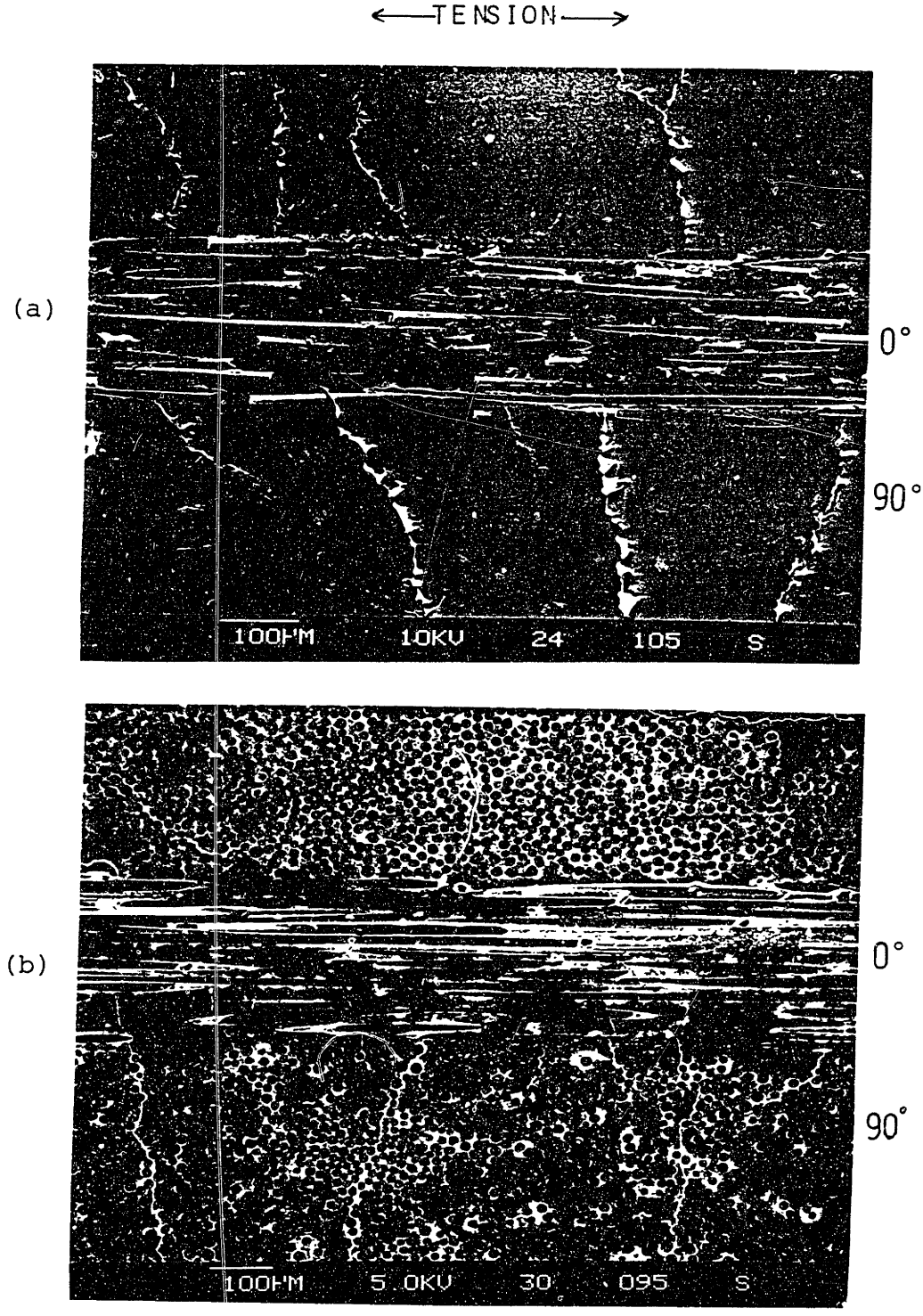

Fig. 4-36 Comparison of replicas from Nicalon/1723-$[0/90]_{2S}$ laminates after straining to approximately 0.1 % strain at: (a) 25°C and (b) 550°C.

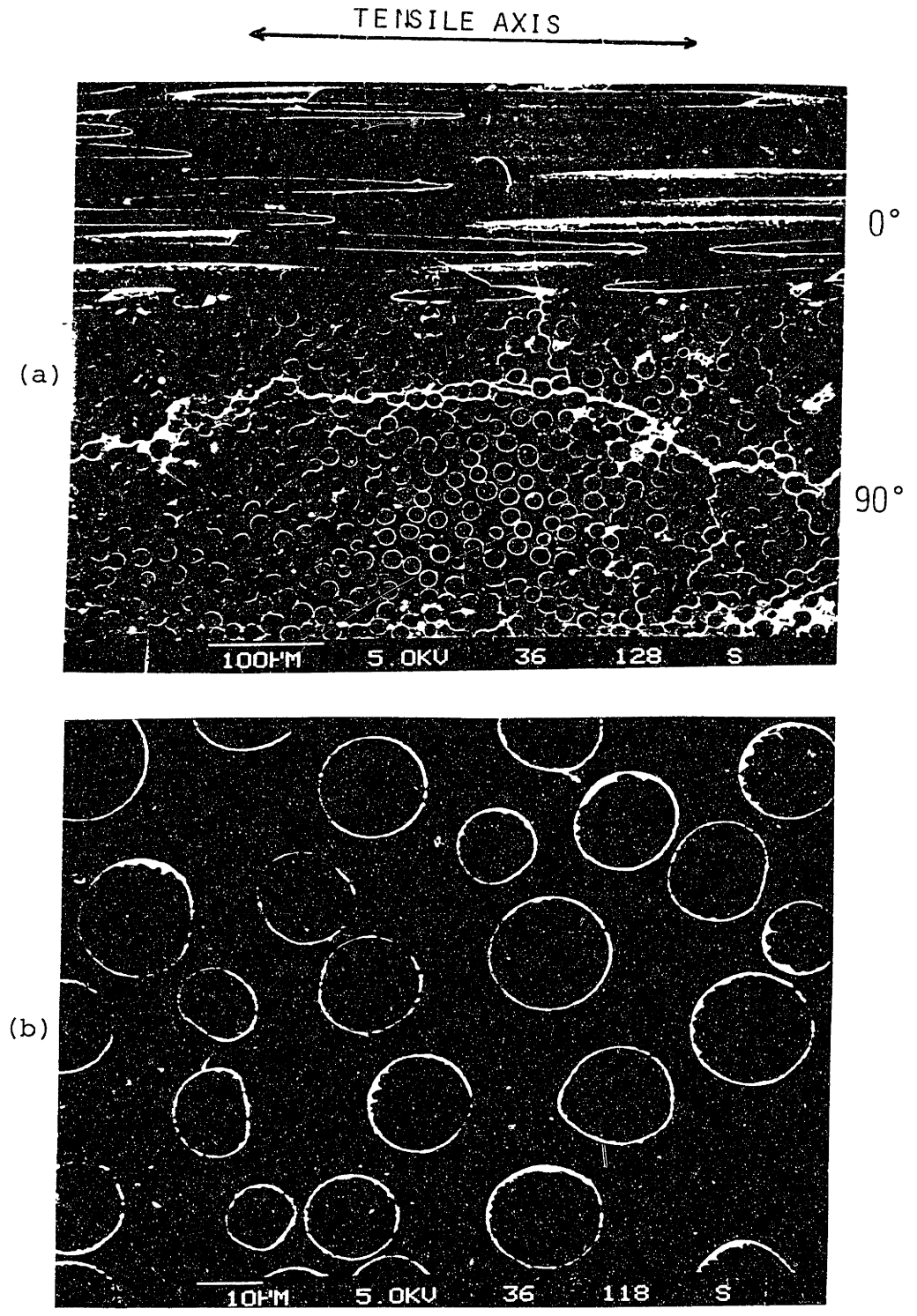

Fig. 4-37 Replicas showing debonded fibers in a transverse ply of Nicalon/ LAS-$[0/90]_{2S}$ after loading to 0.114 % strain at 550°C.

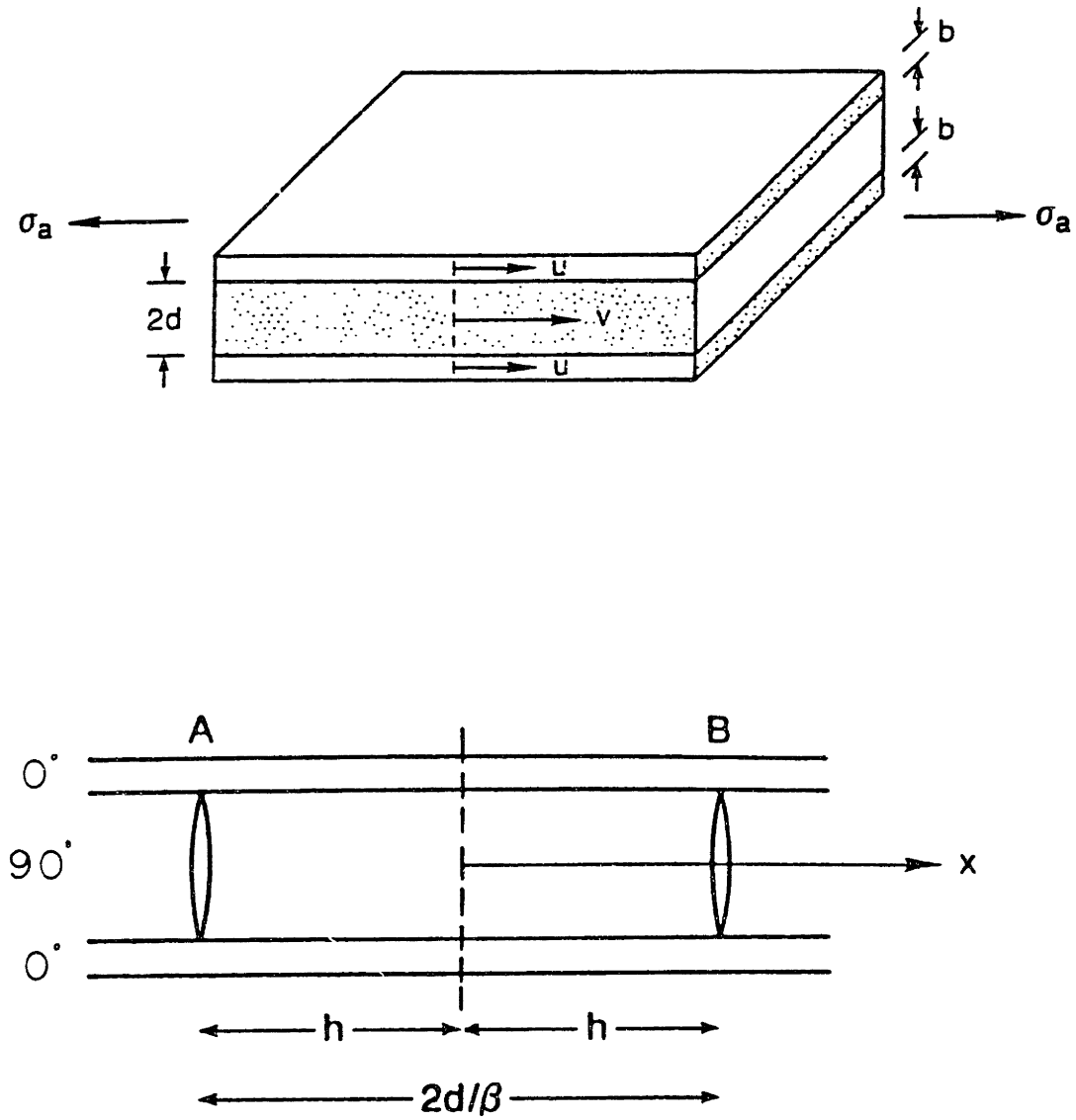

Fig. 5-1 Ply configuration and location of transverse cracks used in determining the longitudinal and transverse ply stresses from shear lag theory. (Ref. 118)

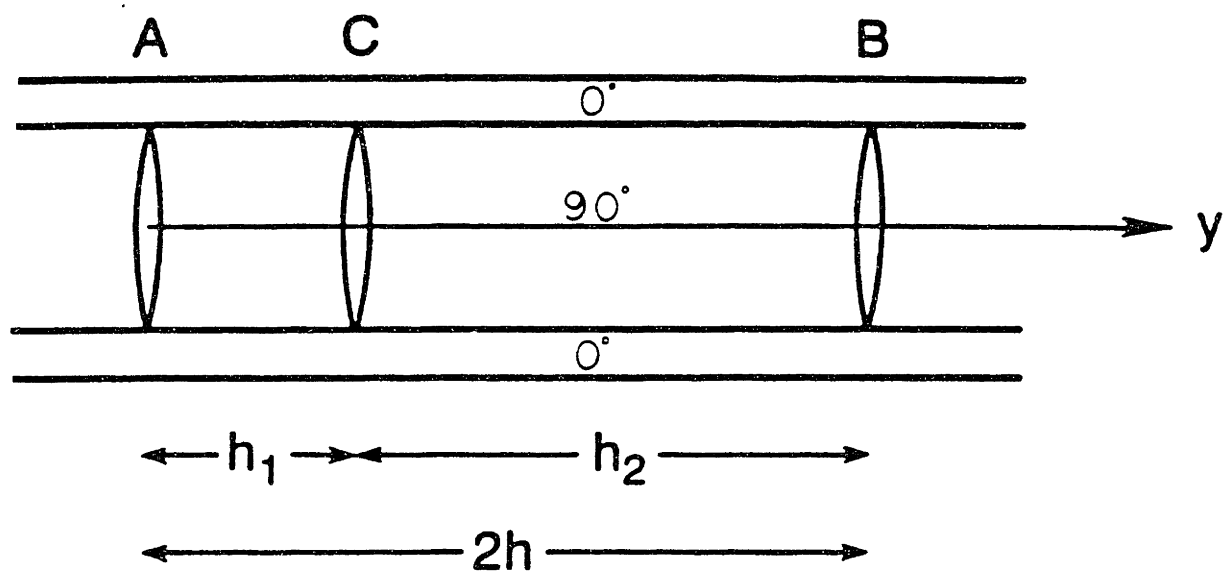

Fig. 5-2 Configuration used in Laws and Dvorak model of progressive cracking. The next crack to develop in the AB ligament occurs at location C. (Ref. 118)

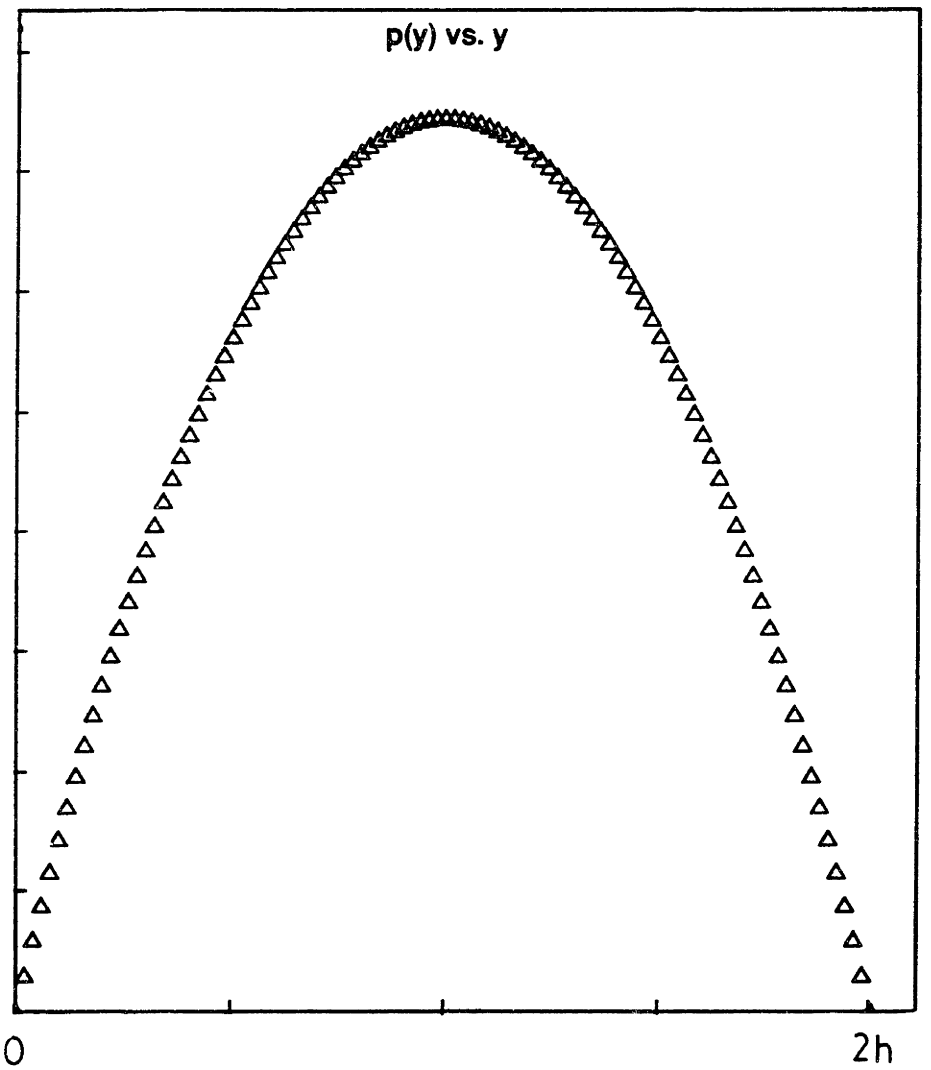

Fig. 5-3 Representative plot of p(y) versus y for $\beta = 2$ and y ranging from 0 to 2h. The (0,2h) range corresponds to the AB ligament in Fig. 5-2.

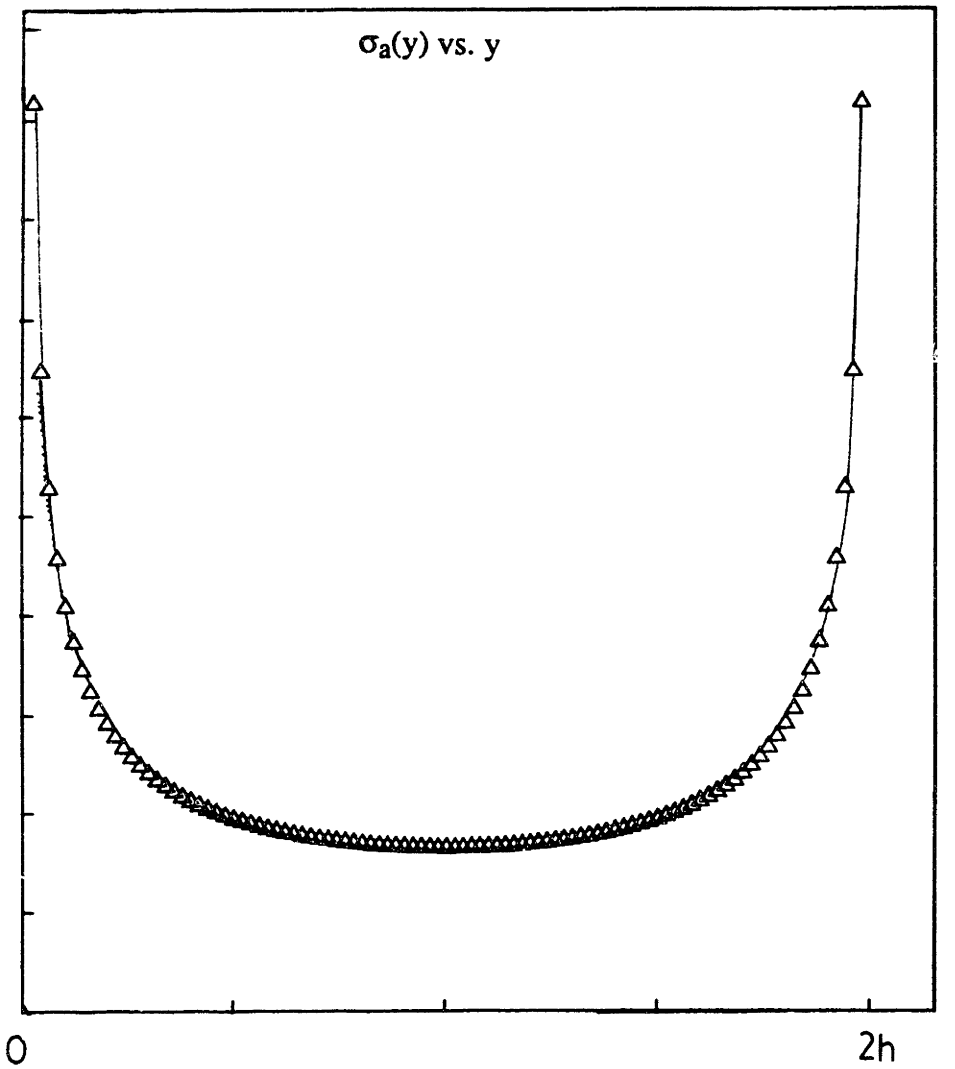

Fig. 5-4 Representative plot of $\sigma_a(y)$ versus y for $\beta = 2$ and y ranging from 0 to 2h. The (0,2h) range corresponds to the AB ligament in Fig. 5-2.

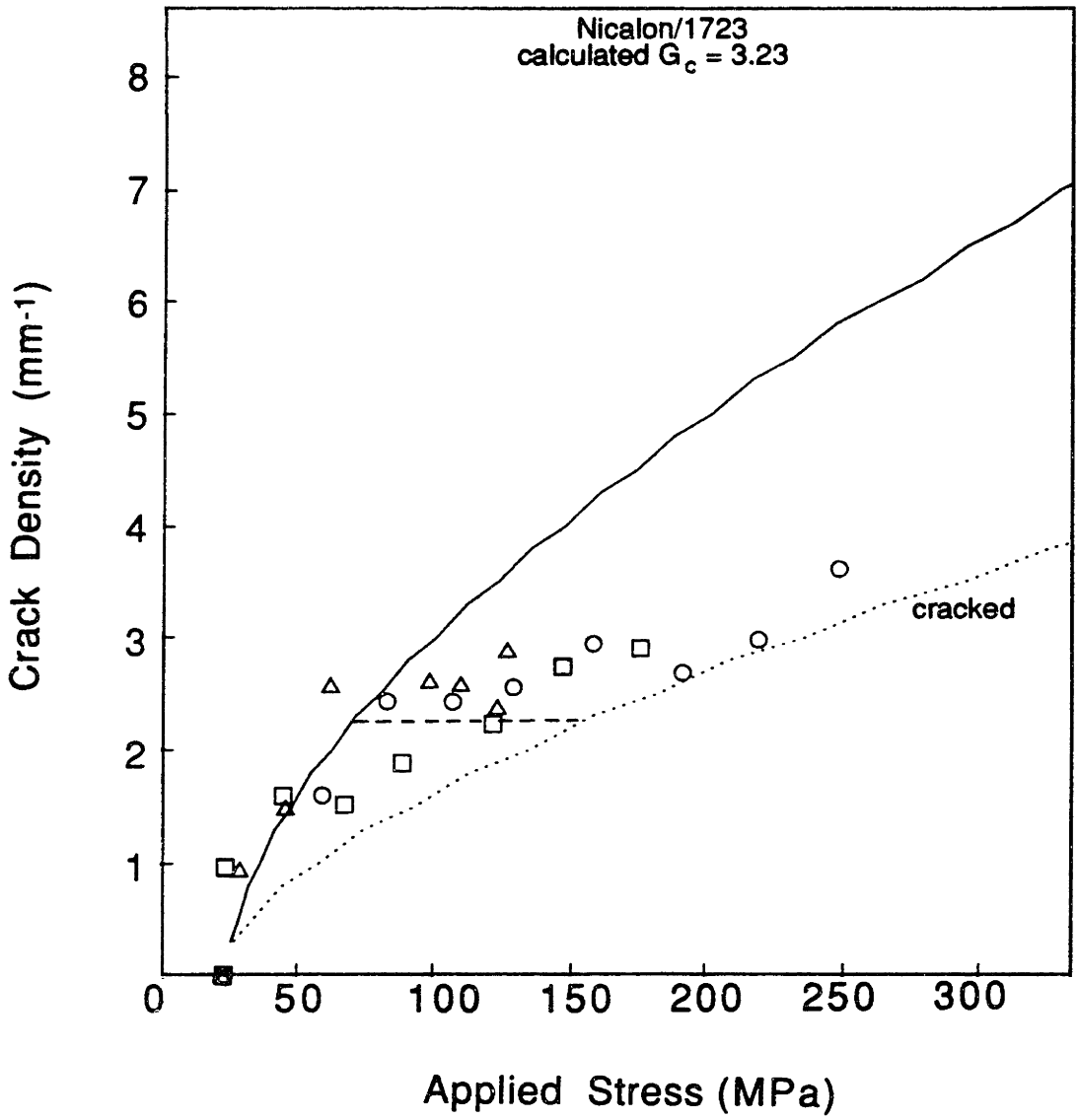

Fig. 5-5 Transverse ply crack density vs. applied stress for crossplied Nicalon/ 1723 at 25°C. The theoretical curves were predicted from Eqn. (H); experimental data were obtained from replication studies.

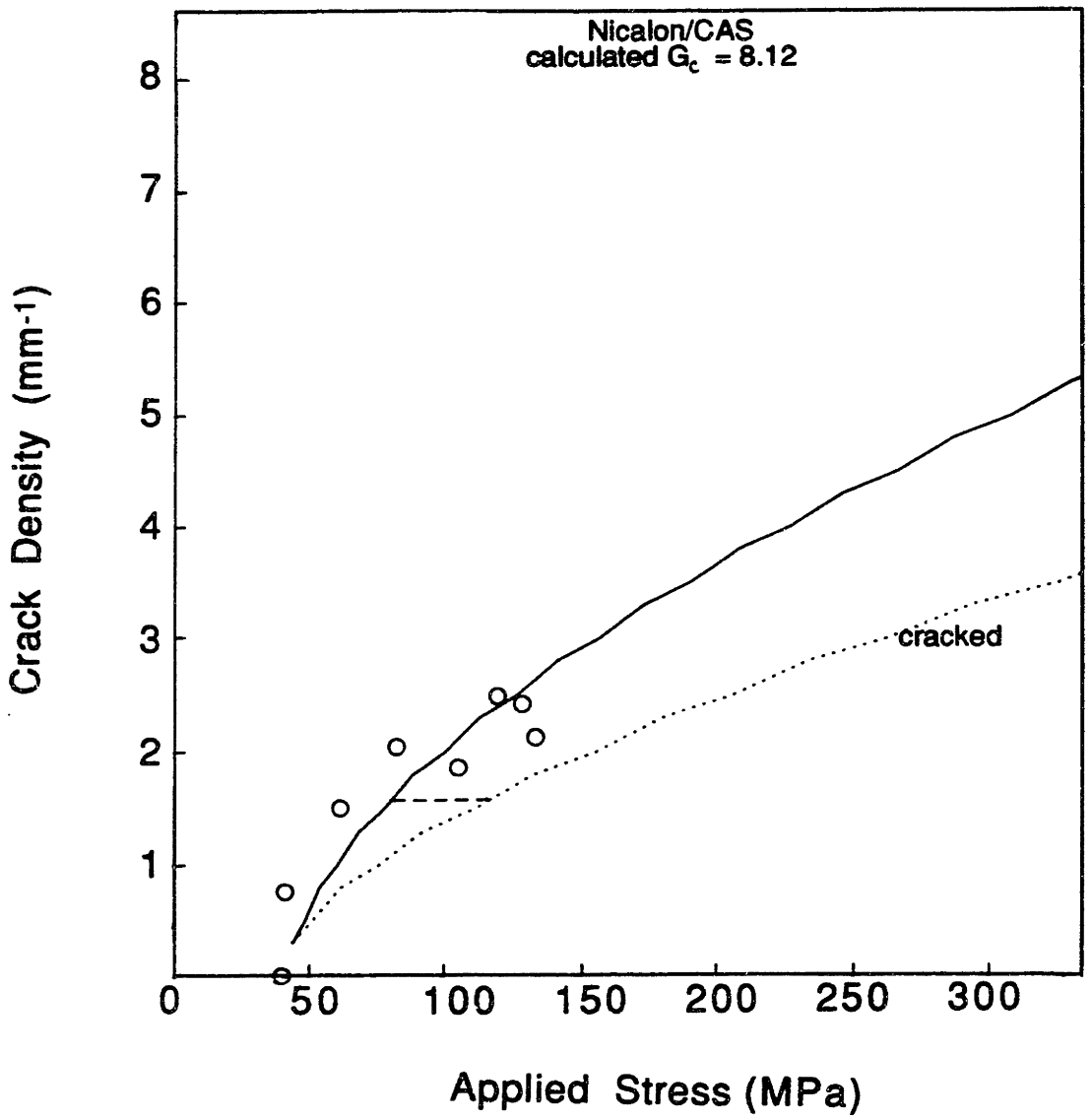

Fig. 5-6 Theory vs. experiment for progressive cracking of Nicalon/CAS crossply laminates at 25°C. The theoretical curves were predicted from Eqn. (H); experimental data were obtained from replication studies.

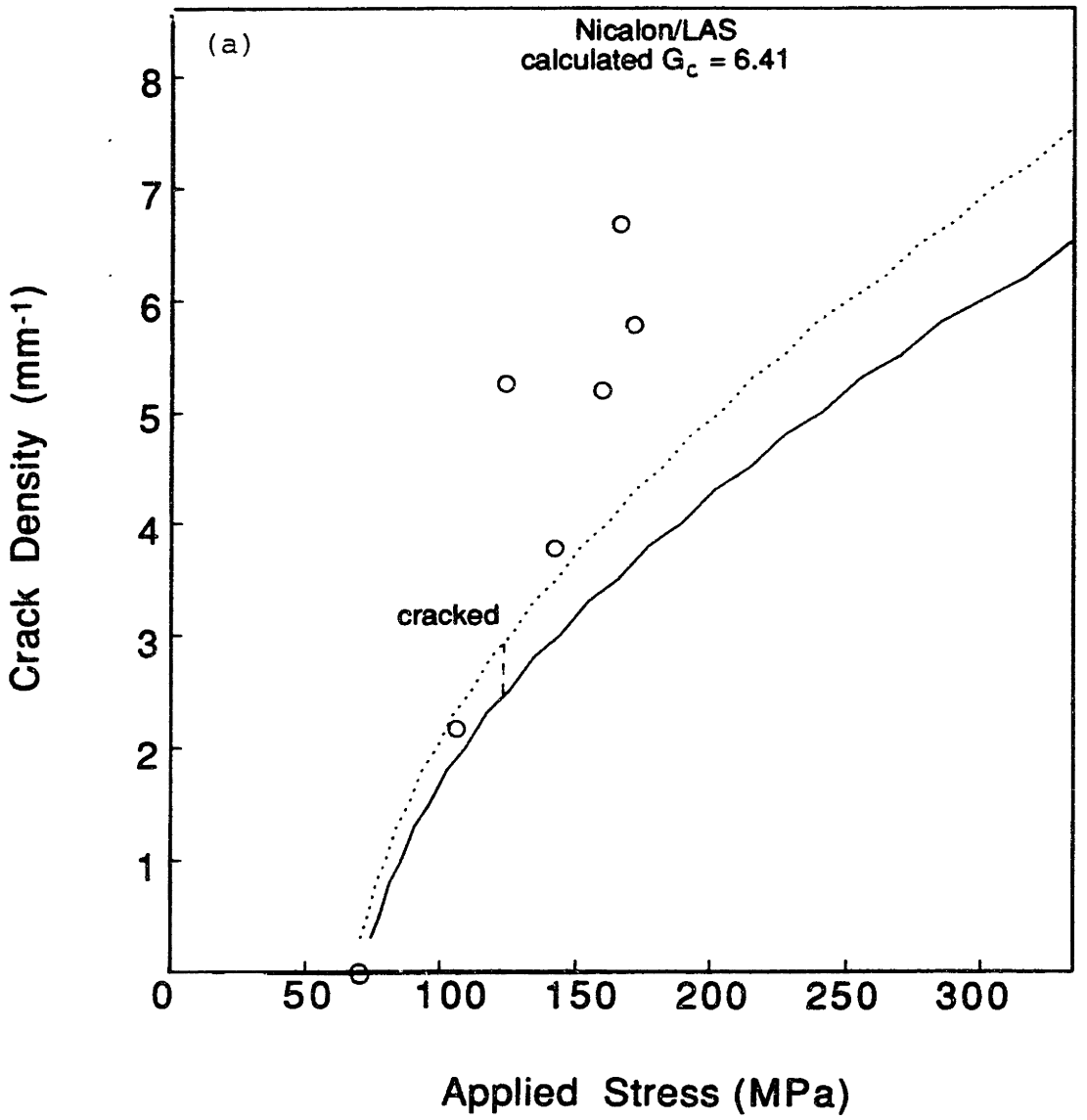

Fig. 5-7 Transverse ply crack density vs. applied stress for crossplied Nicalon/ LAS at room temperature for: (a) $\alpha_{lam} = 2.95 \times 10^{-6}$/°C.

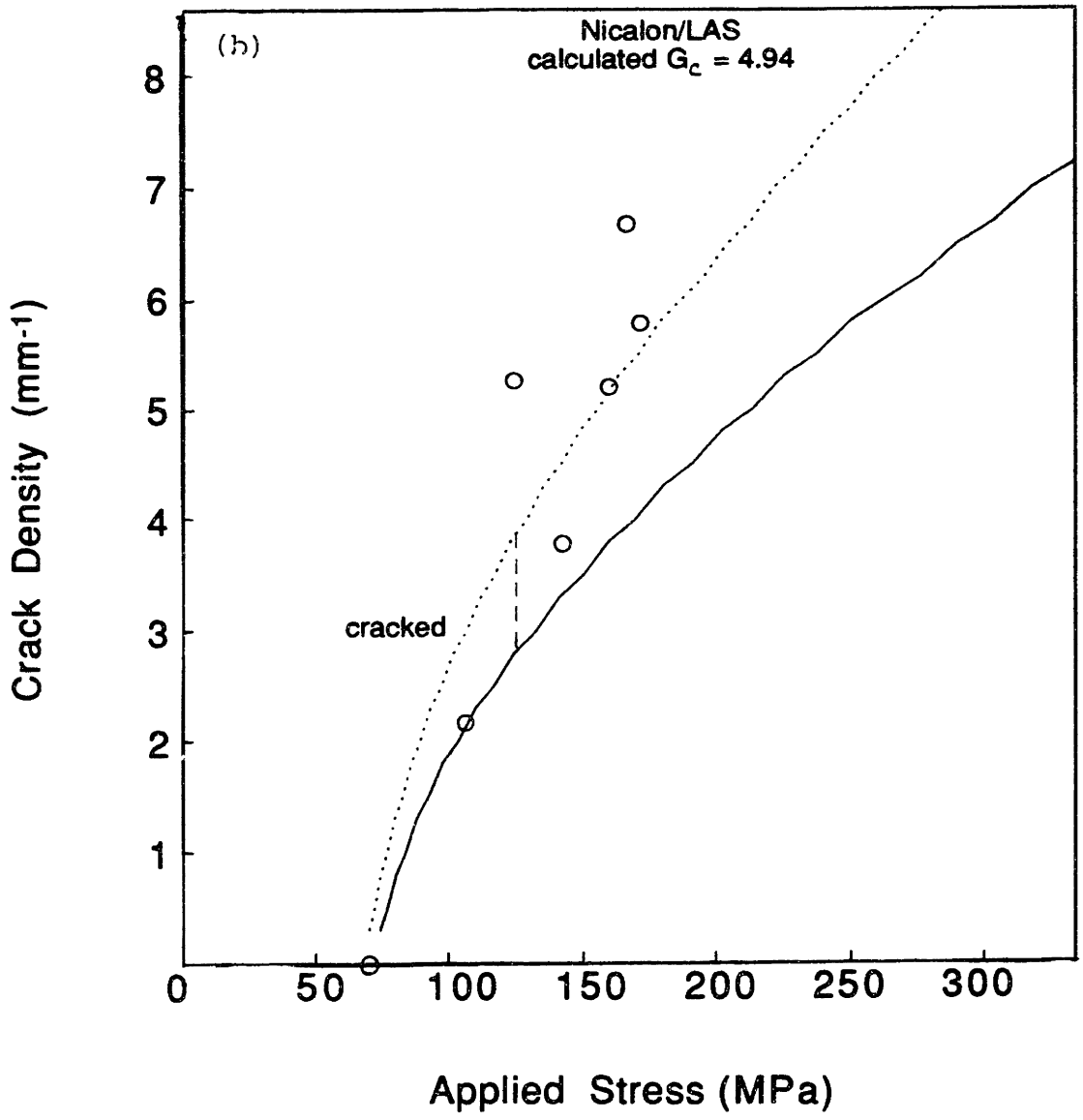

Fig. 5-7 Transverse ply crack density vs. applied stress for crossplied Nicalon/ LAS at room temperature for: (b) α_{1am} =2.5 X 10^{-6}/°C.

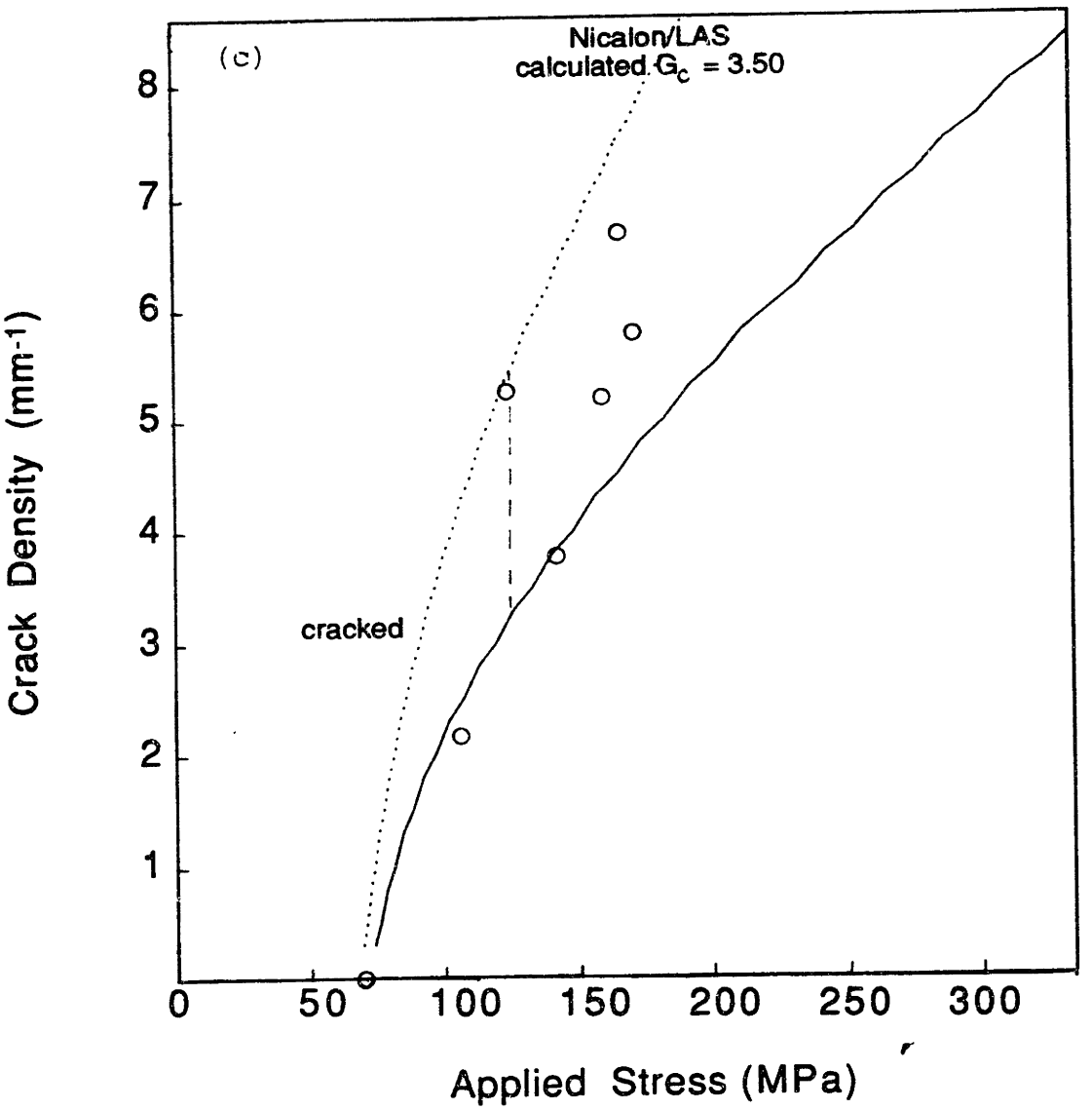

Fig. 5-7 Transverse ply crack density vs. applied stress for crossplied Nicalon/LAS at room temperature for: (c) $\alpha_{lam} = 2.0 \times 10^{-6}/°C$.

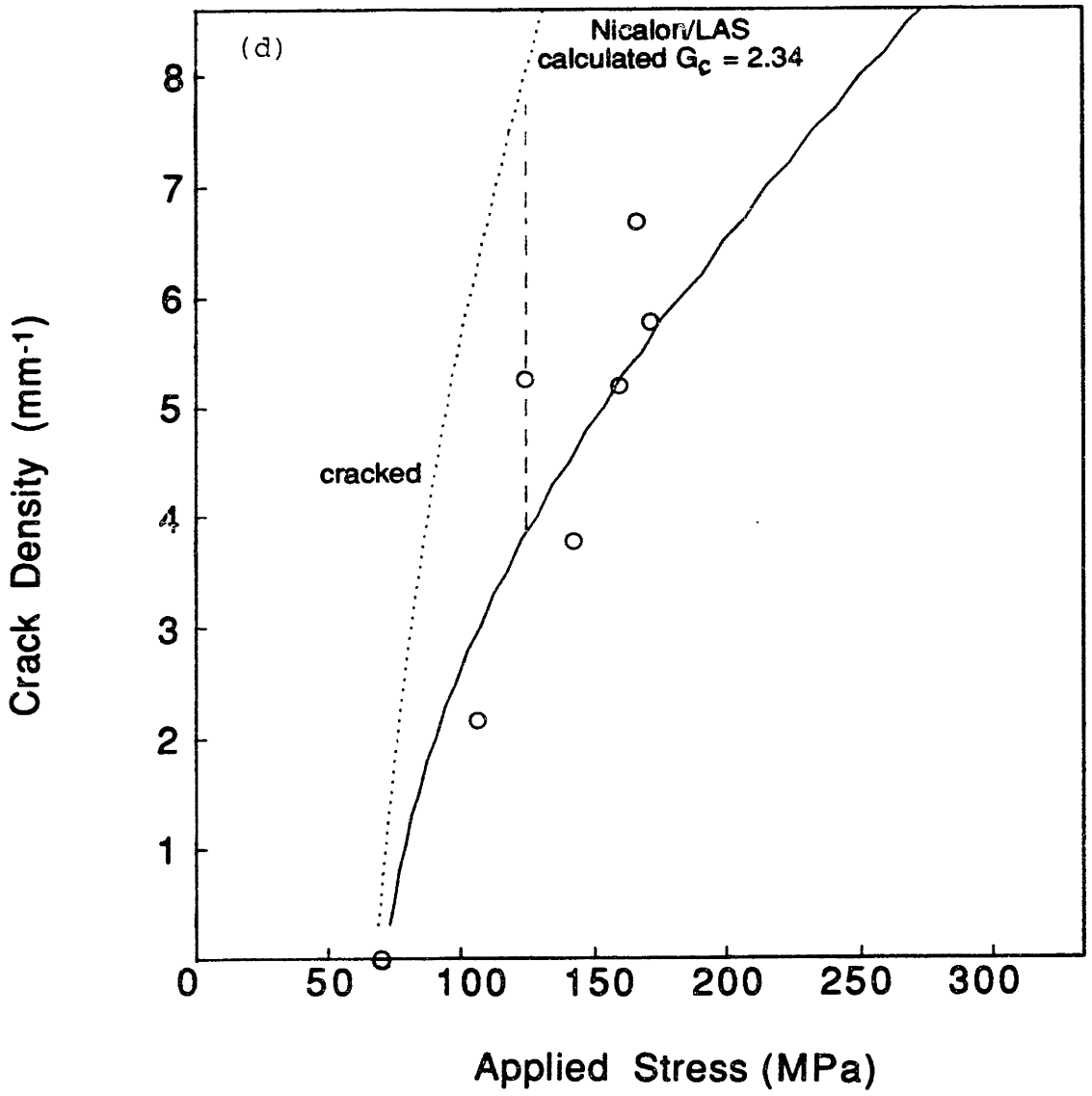

Fig. 5-7 Transverse ply crack density vs. applied stress for crossplied Nicalon/ LAS at room temperature for: (d) α_{lam} = 1.5 X 10^{-6}/°C.

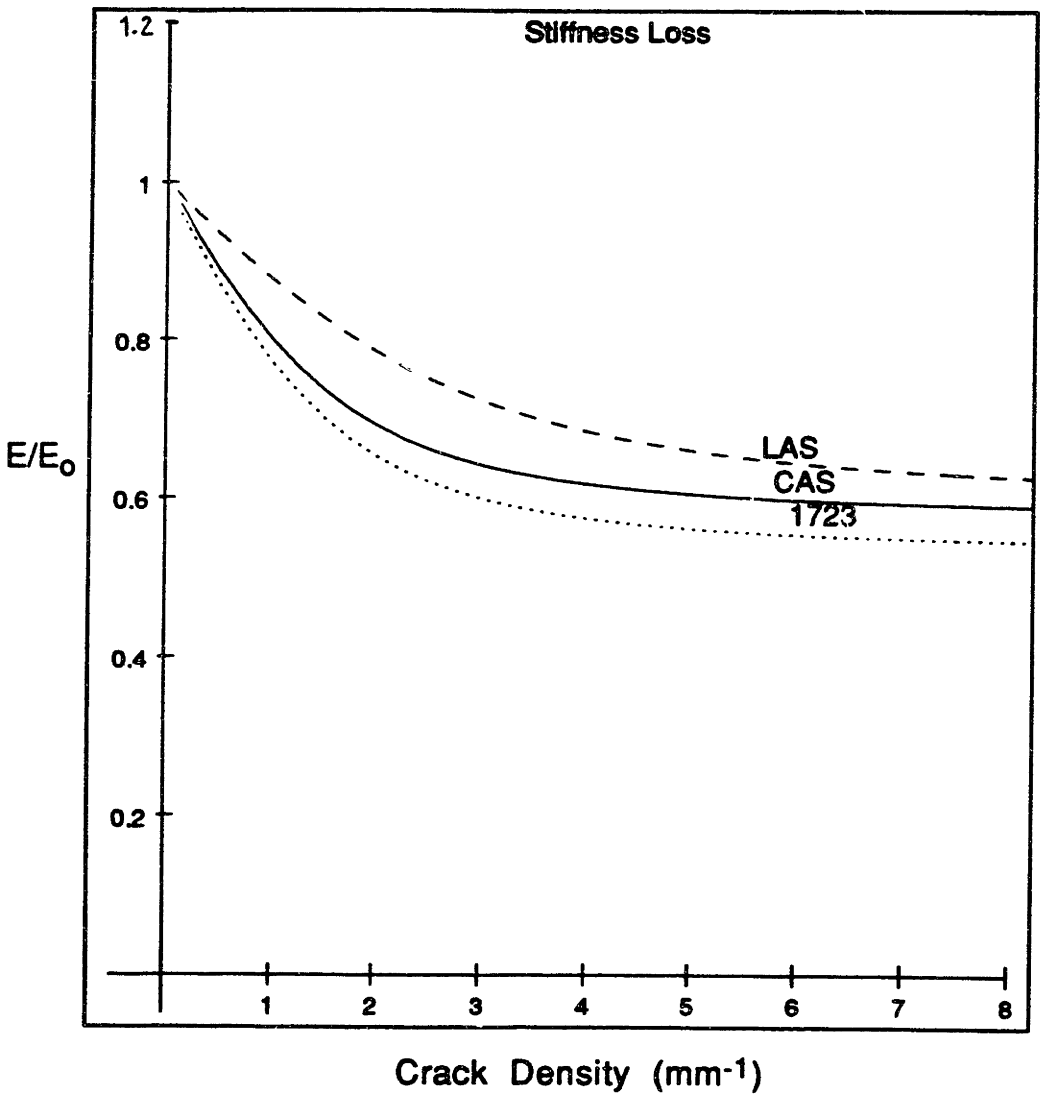

Fig. 5-8 Theoretical prediction of stiffness loss due to transverse cracking of the specified crossplied laminates at 25°C.

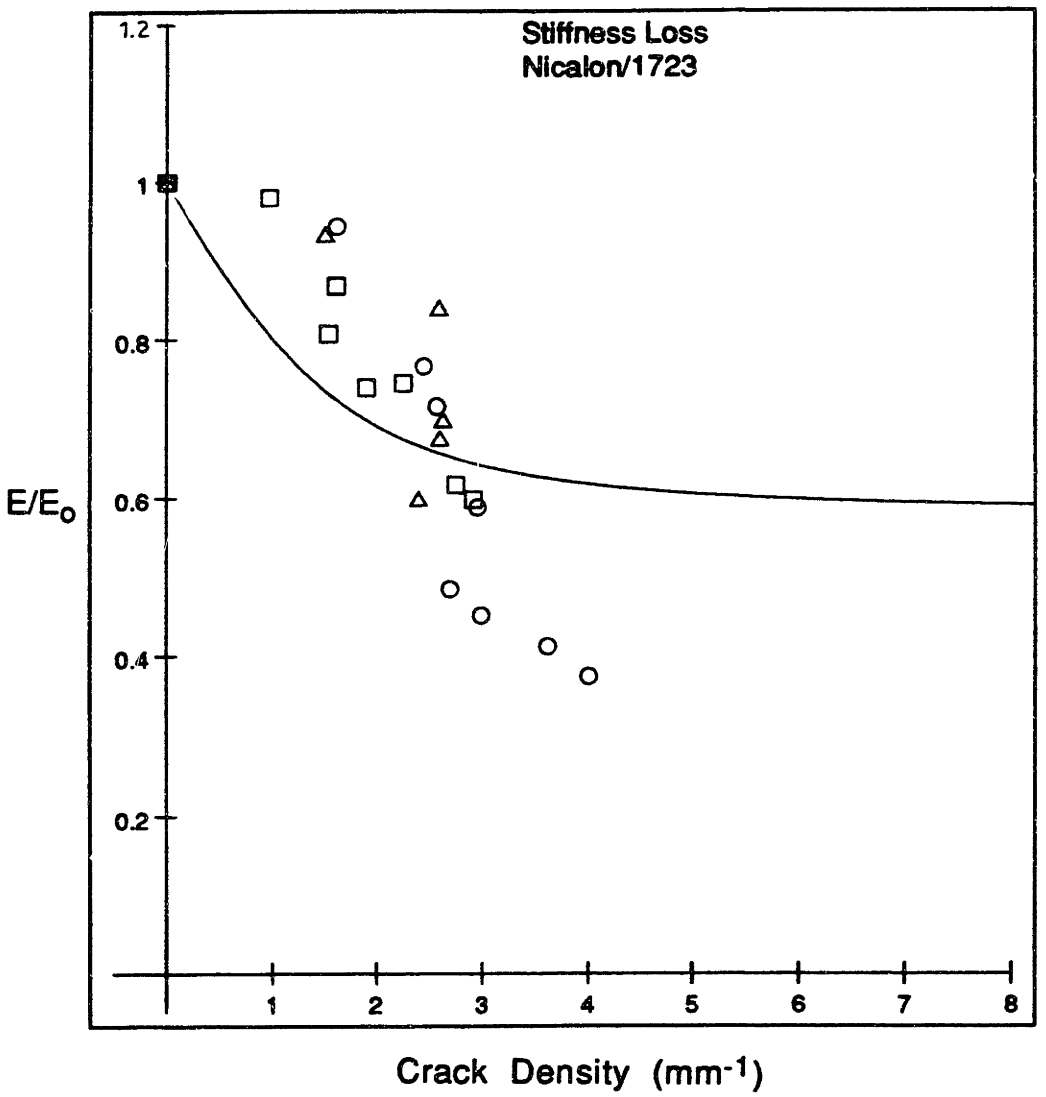

Fig. 5-9 Comparison of experimental and theoretical stiffness loss for crossplied Nicalon/1723 at room temperature.

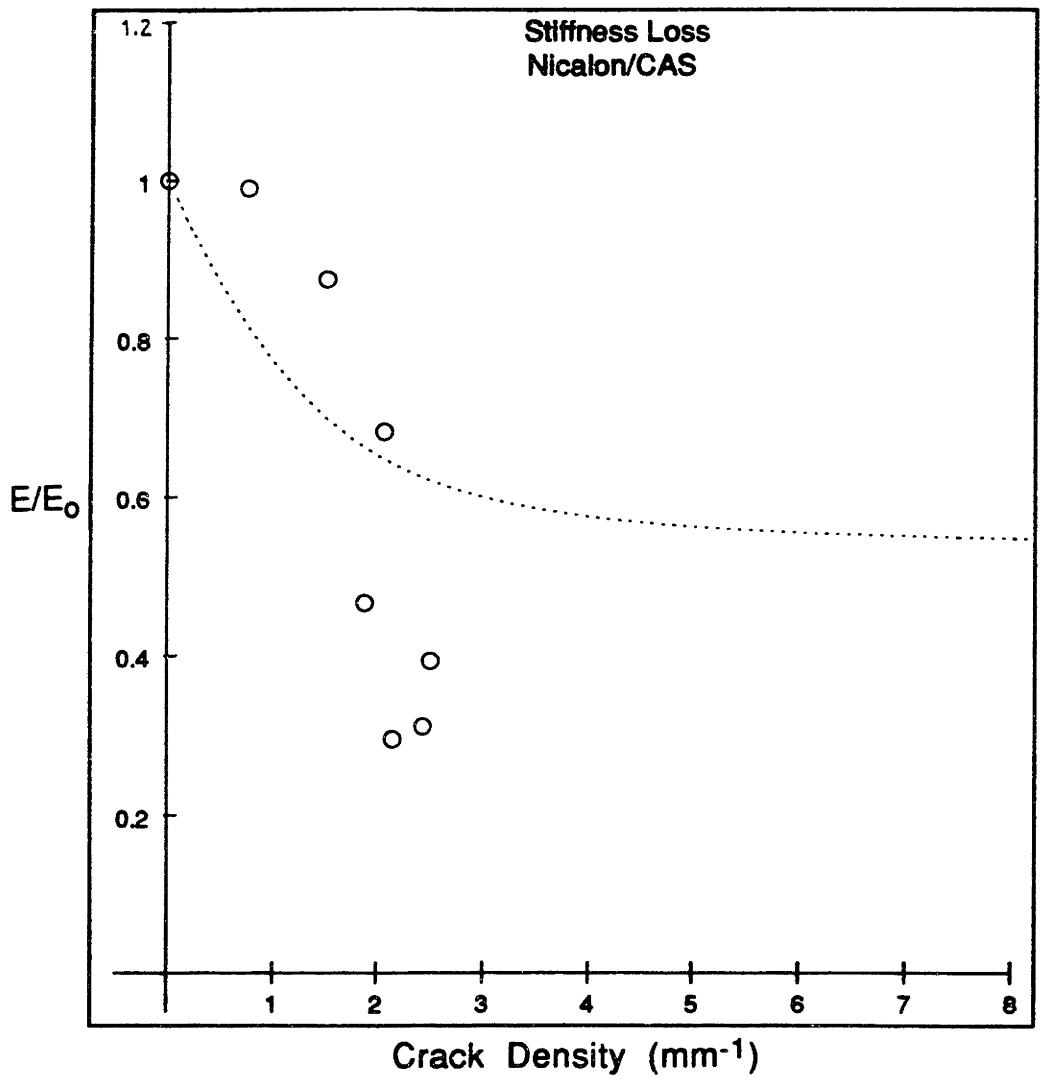

Fig. 5-10 Comparison of experimental and theoretical stiffness loss for crossplied Nicalon/CAS at room temperature.

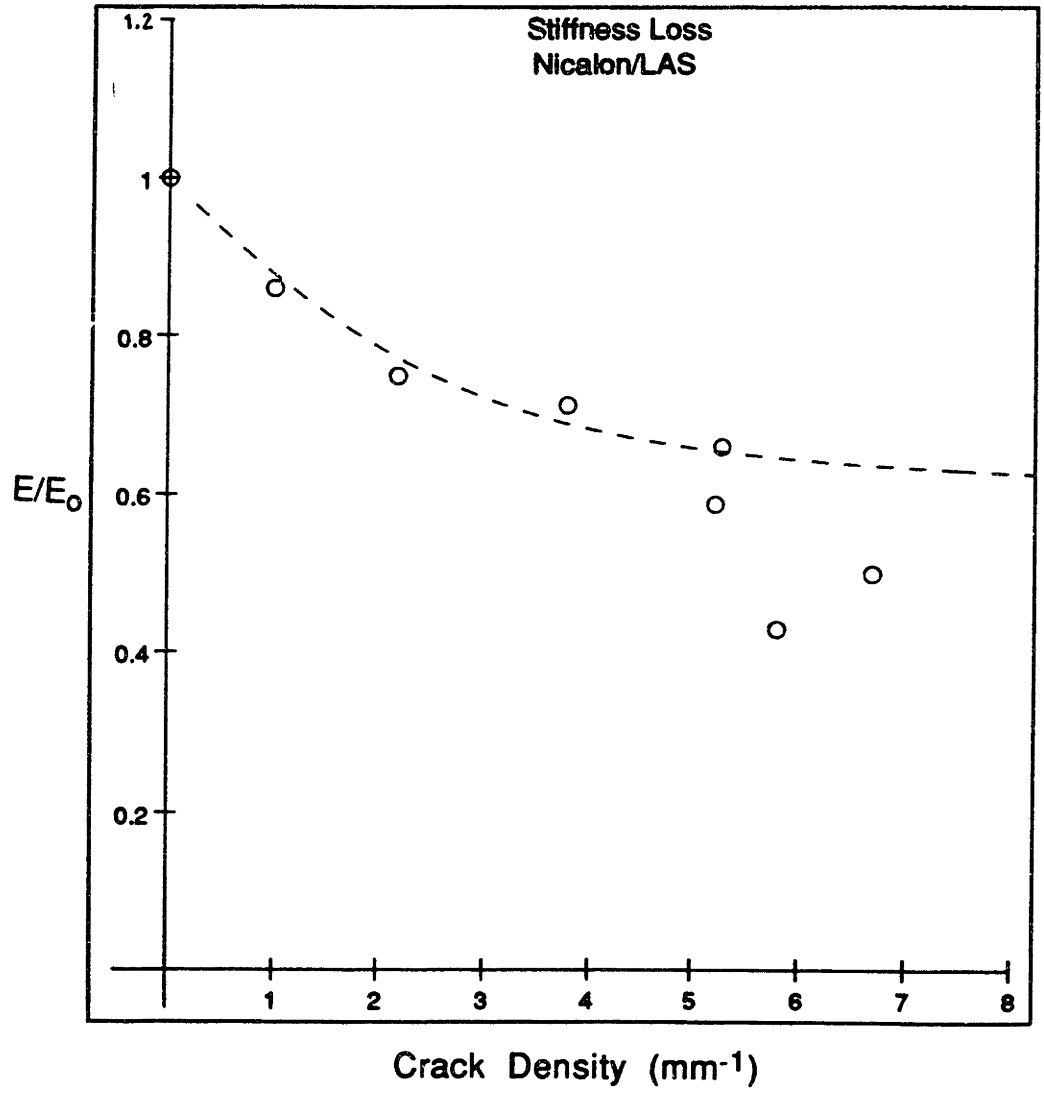

Fig. 5-11 Comparison of experimental and theoretical stiffness loss for crossplied Nicalon/LAS at room temperature.

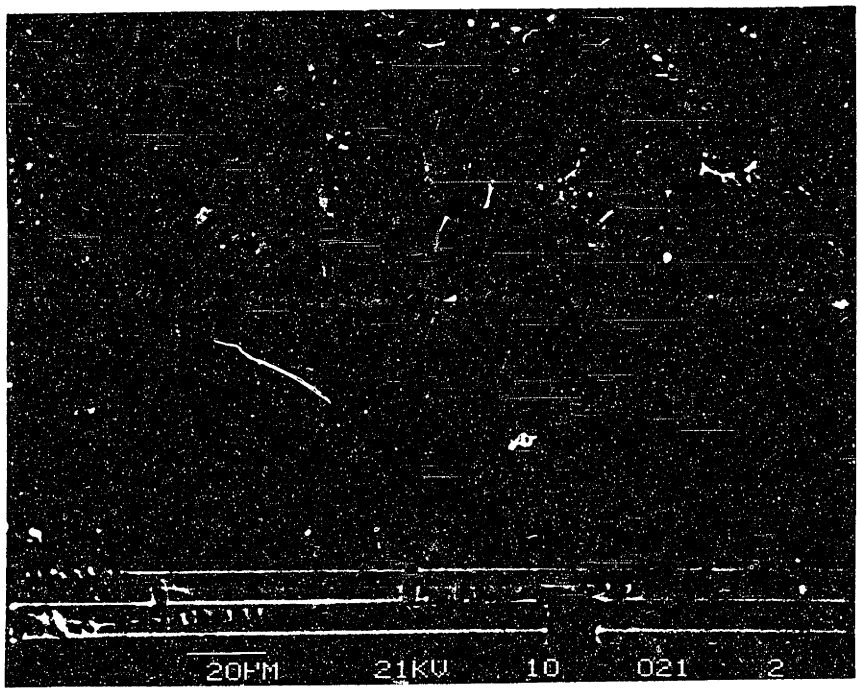

Fig. 5-12 Preferential crack growth along a weak interface in a transverse ply of a Nicalon/BMAS crossply composite.

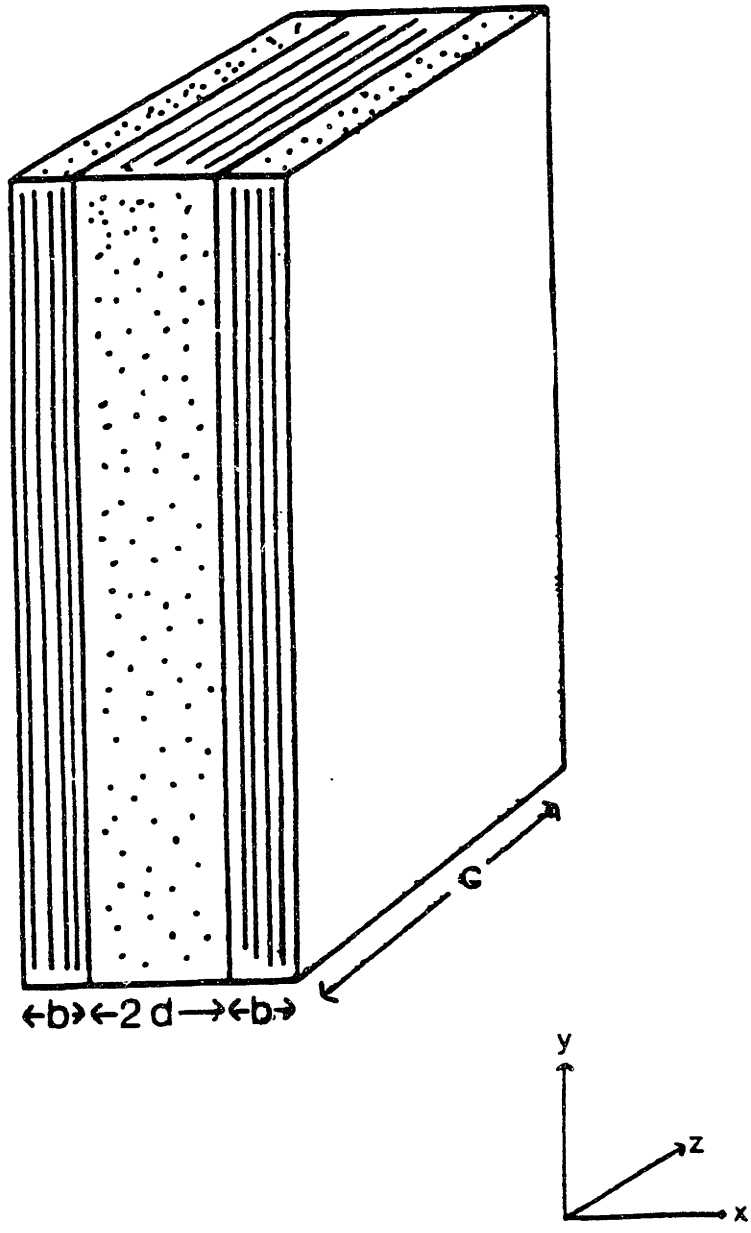

Fig. 5-13 Crossply laminate configuration for the Garrett/Bailey/Parvizi transverse ply cracking model.

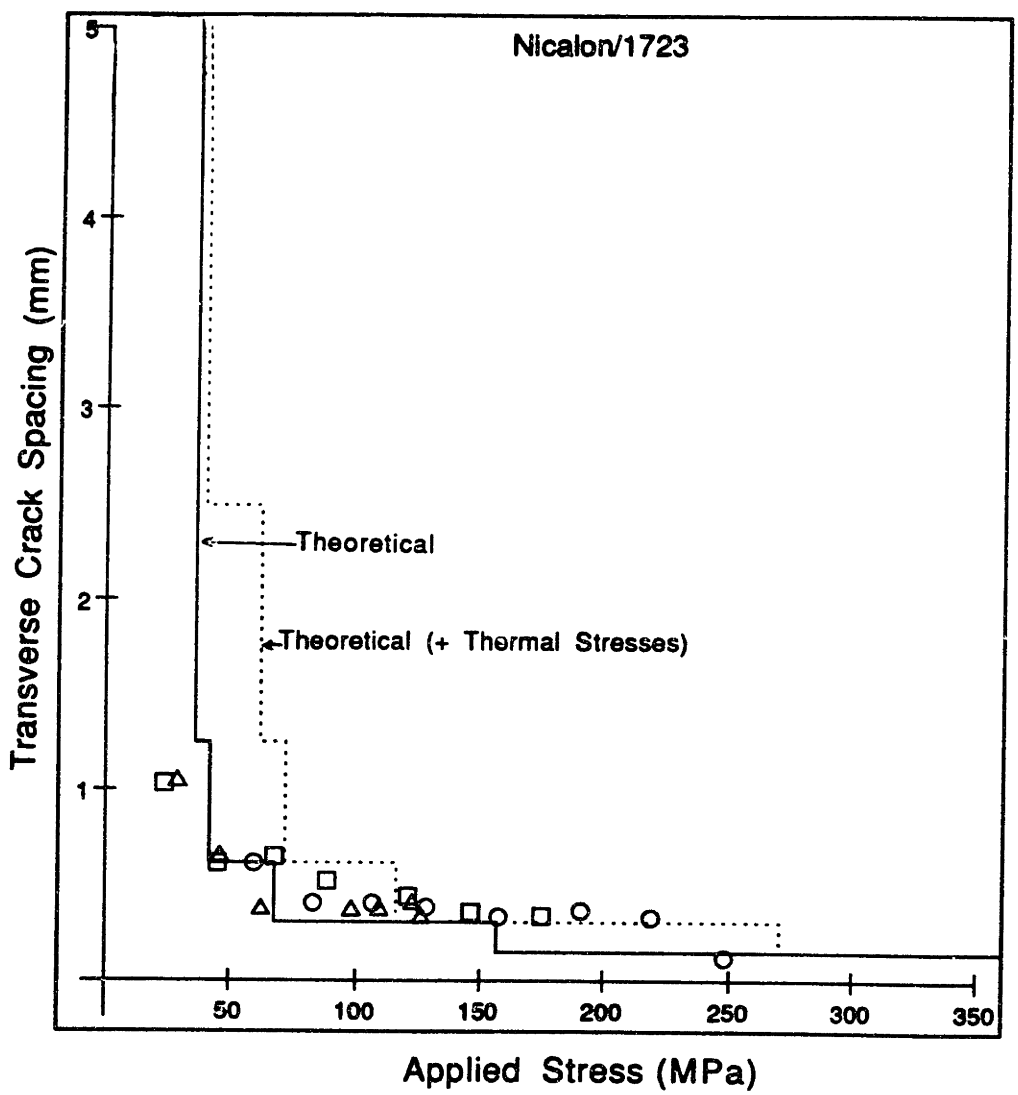

Fig. 5-14 Transverse ply crack spacing vs. applied stress for crossplied Nicalon/ 1723 at 25°C. (Garrett/Bailey/Parvizi model)

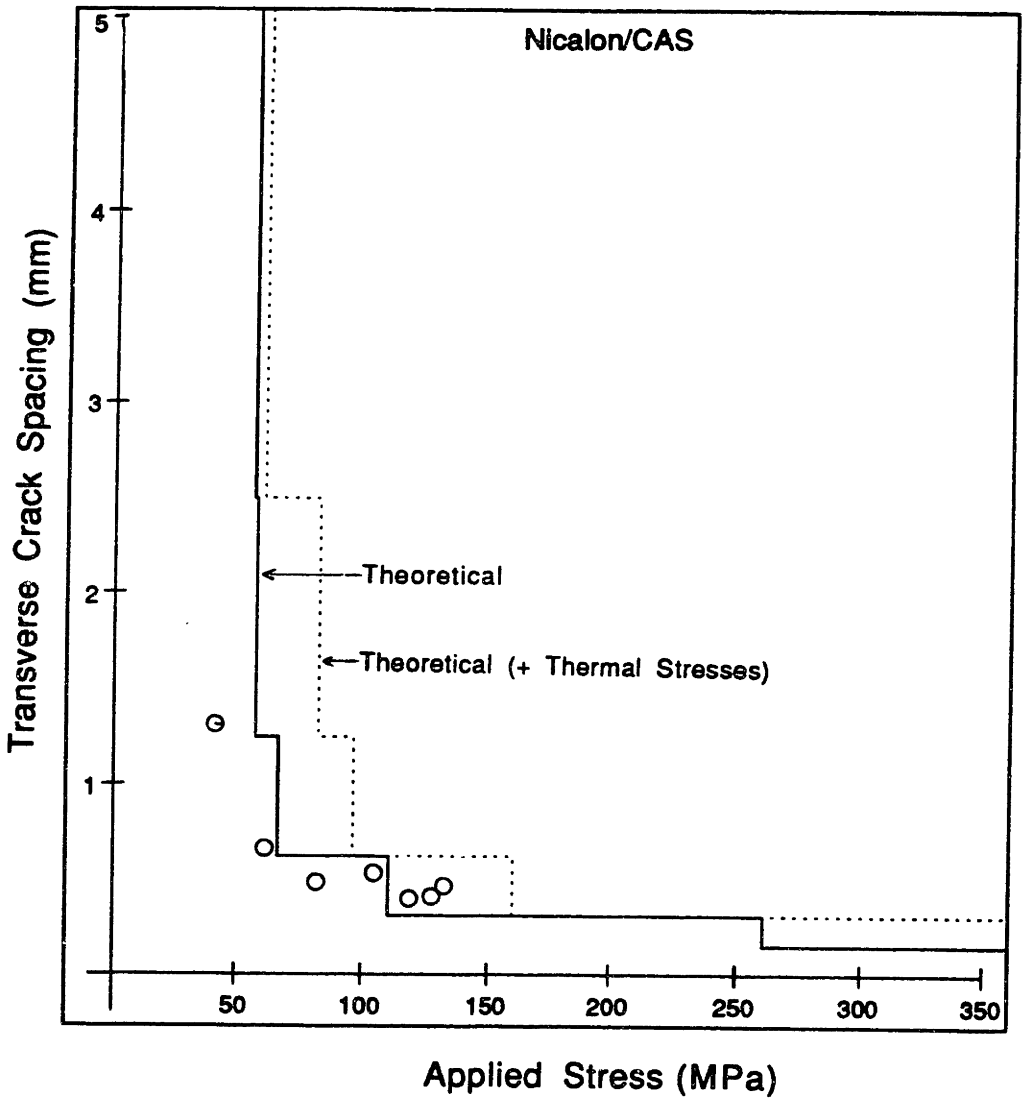

Fig. 5-15 Transverse ply crack spacing vs. applied stress for crossplied Nicalon/CAS at 25°C. (Garrett/Bailey/Parvizi model)

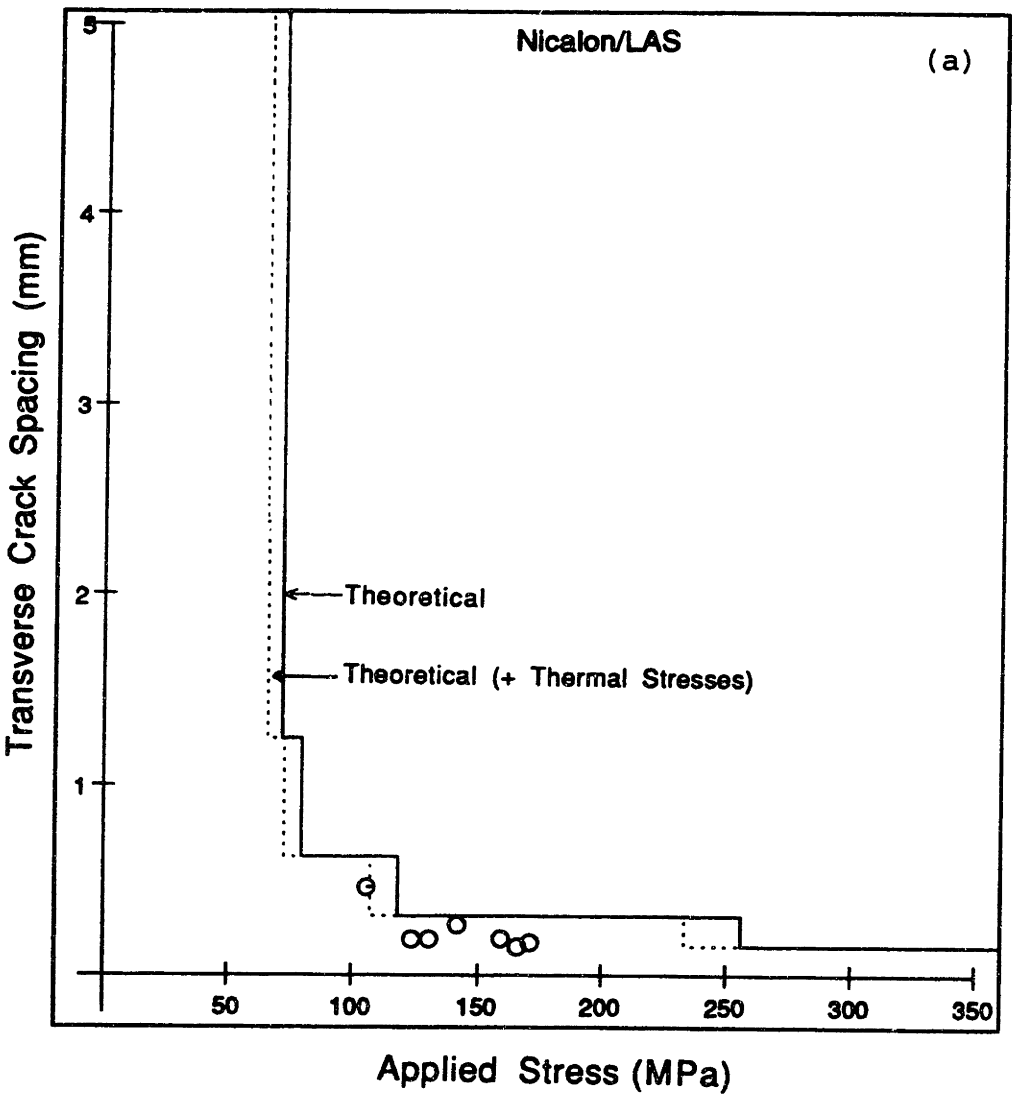

Fig. 5-16 Transverse ply crack spacing vs. applied stress for crossplied Nicalon/LAS at 25°C: (a) $\alpha_{lam} = 2.95 \times 10^{-6}$/°C

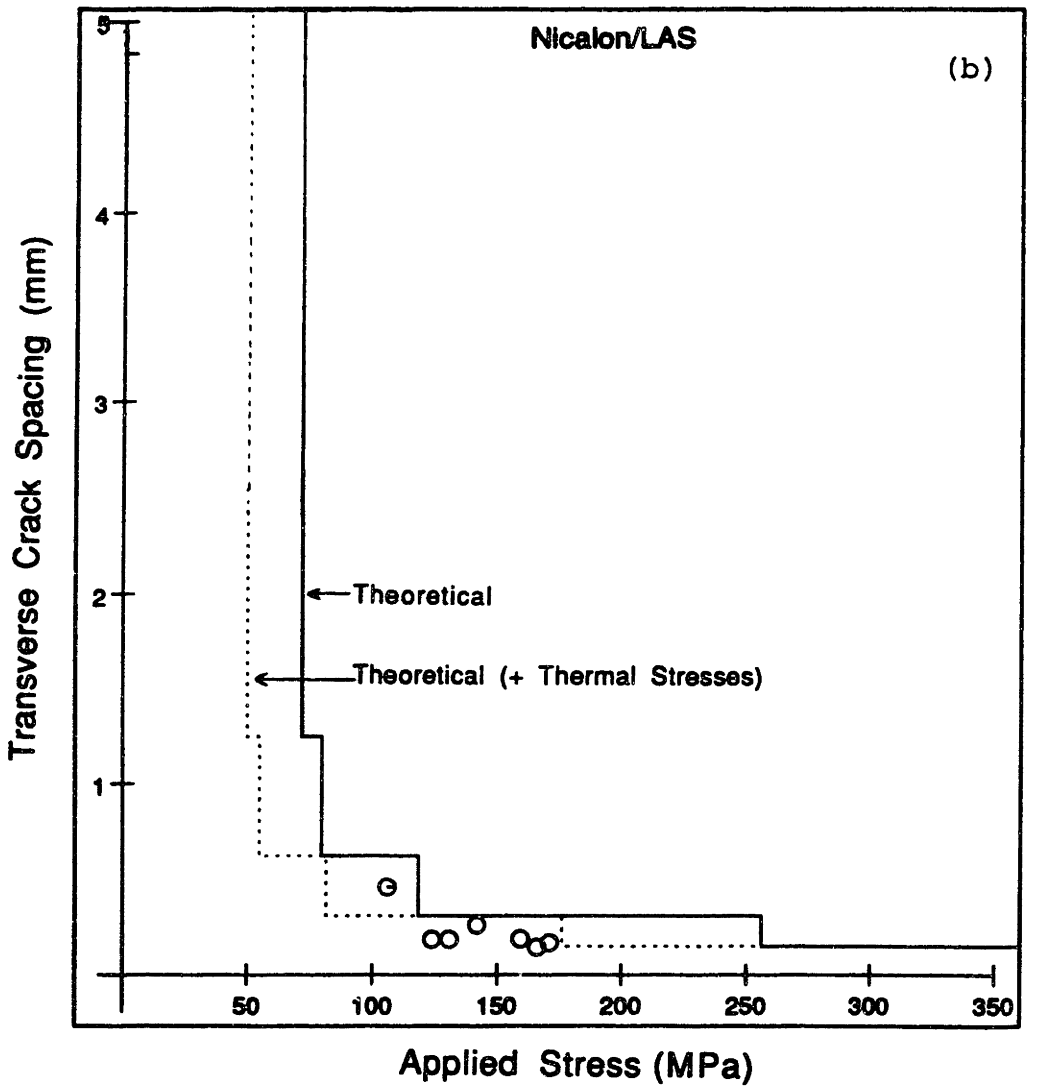

Fig. 5-16 Transverse ply crack spacing vs. applied stress for crossplied Nicalon/ LAS at 25°C: (b) $\alpha_{lam} = 2.0 \times 10^{-6}$/°C. (Garrett/Bailey/Parvizi model)

APPENDICES

APPENDIX A
Composite Plate Designations

Plate	Material	Layup	Fiber Vol. Fraction	CGW Designation
13	Nicalon/1723	$[0/90]_{4S}$	35-40 %	889-AEW-120-002
14	Nicalon/CAS-II	$[0]_{12}$	35-40 %	118-NTW-084-001
15	Nicalon/CAS-II	$[0]_{12}$	35-40 %	118-NTW-084-002
16	Nicalon/CAS-II	$[\pm 45]_{3S}$	35-40 %	118-NTW-085-001
17	Nicalon/CAS-II	$[\pm 45]_{3S}$	35-40 %	118-NTW-085-002
18	Nicalon/CAS-II	$[0/90]_{2S}$	35-40 %	118-NTW-085-003
19	Nicalon/CAS-II	$[0/90]_{2S}$	35-40 %	118-NTW-085-004
20	Nicalon/CAS-II	$[0/90]_{3S}$	35-40 %	118-NTW-217-002
21	Nicalon/CAS-II	$[0]_{12}$	35-40 %	118-NTW-216-002
22	Nicalon/1723	[0/90]	35-40 %	block, not plate
23	Nicalon/1723	$[0]_{8}$	35-40 %	889-AEW-145-001
24	Nicalon/1723	$[0/90]_{2S}$	35-40 %	889-AEW-211-001
25	Nicalon/1723	$[0/90]_{2S}$	35-40 %	889-AEW-211-002
26	Nicalon/LAS-III	$[0]_{12}$	35-40 %	
27	Nicalon/LAS-III	$[0/90]_{3S}$	35-40 %	
28	Nicalon/CAS-II	$[0]_{12}$	35-40 %	
29	Nicalon/CAS-II	$[0/90]_{2S}$	35-40 %	
30	Nicalon/1723	$[0/90]_{2S}$	35-40 %	8812701L
31	Nicalon/1723	$[0/90]_{2S}$	35-40 %	8812702L
32	Nicalon/1723	$[0]_{12}$	35-40 %	8812703L
33	Nicalon/1723	$[0]_{12}$	35-40 %	8812704L
34	Nicalon/1723	$[0/90]_{2S}$	35-40 %	8812705L
35	Nicalon/1723	$[0/90]_{2S}$	35-40 %	8812706L
36	Nicalon/LAS-III	$[0/90]_{3S}$	35-40 %	
37	Nicalon/LAS-III	$[0]_{12}$	35-40 %	

APPENDIX B

Fiber/Matrix Properties and Results of Micromechanics Calculations

NICALON/1723:

$V_f = 0.35$

$\Delta T = -600°C$

	Fiber	Matrix
E (GPa)	200	88
ν	0.2987	0.2222
G (GPa)	77	36
α (1 X 10^{-6}/°C)	3.2	5.2

Ply Properties:

E_{11} = 127.2 GPa

E_{22} = 115.7 GPa

ν_{12} = 0.24897

ν_{21} = 0.22652

G_{12} = 46.47 GPa

α_{11} = 4.0994 X 10^{-6}/°C

α_{22} = 4.5649 X 10^{-6}/°C

NICALON/CAS-II:

$V_f = 0.35$

$\Delta T = -1230°C$

	Fiber	Matrix
E (GPa)	200	88
ν	0.2987	0.2222
G (GPa)	77	36
α (1 X 10^{-6}/°C)	3.93	5.0

Ply Properties:

E_{11} = 127.2 GPa

E_{22} = 115.7 GPa

ν_{12} = 0.24897

ν_{21} = 0.22652

G_{12} = 46.47 GPa

α_{11} = 4.4112 X 10^{-6}/°C

α_{22} = 4.6602 X 10^{-6}/°C

Fiber/Matrix Properties
and Results of Micromechanics Calculations

NICALON/LAS-III (Ceramed):

$V_f = 0.35$

$\Delta T = -1030°C$

	Fiber	Matrix
E (GPa)	200	88
ν	0.2987	0.2222
G (GPa)	77	36
α (1 X 10^{-6}/°C)	3.93	1.5

Ply Properties:

$E_{11} = 127.2$ GPa
$E_{22} = 115.7$ GPa
$\nu_{12} = 0.24897$
$\nu_{21} = 0.22652$
$G_{12} = 46.47$ GPa
$\alpha_{11} = 2.8373 \times 10^{-6}$/°C
$\alpha_{22} = 2.2716 \times 10^{-6}$/°C

NICALON/LAS-III (As-Pressed):

$V_f = 0.35$

$\Delta T = -700°C$

	Fiber	Matrix
E (GPa)	200	88
ν	0.2987	0.2222
G (GPa)	77	36
α (1 X 10^{-6}/°C)	3.3	2.7

Ply Properties:

$E_{11} = 127.2$ GPa
$E_{22} = 115.7$ GPa
$\nu_{12} = 0.24897$
$\nu_{21} = 0.22652$
$G_{12} = 46.47$ GPa
$\alpha_{11} = 3.0302 \times 10^{-6}$/°C
$\alpha_{22} = 2.8905 \times 10^{-6}$/°C

APPENDIX C

Thermal Residual Stress and Strain Calculations

Ply Coefficients of Thermal Expansion:

$$\alpha_{11} = \frac{E_f \alpha_f V_f + E_m \alpha_m (1-V_f)}{E_f V_f + E_m (1-V_f)}$$

$$\alpha_{22} = (1+\nu_m)\,\alpha_m (1-V_f) + (1+\nu_f)\,\alpha_f V_f - \alpha_{11}\,[\nu_f V_f + \nu_m (1-V_f)]$$

$$\alpha_{12} = 0$$

Laminate Coefficients of Thermal Expansion:
For a $[0/90]_{nS}$ laminate:

$$\alpha_{11\text{-lam}} = 0.5\,\alpha_{11} + 0.5\,\alpha_{22}$$
$$\alpha_{22\text{-lam}} = 0.5\,\alpha_{11} + 0.5\,\alpha_{22}$$
$$\alpha_{12\text{-lam}} = 0$$

For a $[0]_{nS}$ laminate:

$$\alpha_{11\text{-lam}} = \alpha_{11}$$
$$\alpha_{22\text{-lam}} = \alpha_{22}$$
$$\alpha_{12\text{-lam}} = 0$$

Axial Residual Strain in the Matrix of a Unidirectional Laminate:

= composite residual strain - matrix strain
= $\alpha_{11\text{-lam}}\,\Delta T$ -- $\alpha_m\,\Delta T$

Axial Residual Stress in the Matrix of a Unidirectional Laminate:

= matrix residual strain X matrix modulus
= $(\alpha_{11\text{-lam}} - \alpha_m)\,E_m\,\Delta T$

Laminate Thermal Strains:

$$\begin{bmatrix} \varepsilon^R_{11\text{-lam}} \\ \varepsilon^R_{22\text{-lam}} \\ \varepsilon^R_{12\text{-lam}} \end{bmatrix} = \begin{bmatrix} \alpha_{11\text{-lam}} \\ \alpha_{22\text{-lam}} \\ \alpha_{12\text{-lam}} \end{bmatrix} \text{ X } \Delta T$$

Thermal Residual Stress and Strain Calculations

Ply Thermal Strains in a Laminate:
for each ply

$$\begin{matrix} \varepsilon^R_{11\text{-ply}} \\ \varepsilon^R_{22\text{-ply}} \\ \varepsilon^R_{12\text{-ply}} \end{matrix} = \begin{matrix} \varepsilon^R_{11\text{-lam}} \\ \varepsilon^R_{22\text{-lam}} \\ \varepsilon^R_{12\text{-lam}} \end{matrix} - - \begin{matrix} \alpha_{11}\,\Delta T \\ \alpha_{22}\,\Delta T \\ \alpha_{12}\,\Delta T \end{matrix}$$

Ply Thermal Stresses in a Laminate:
(in laminate coordinates)
for each ply, where Θ is the ply orientation

$$\begin{matrix} \sigma^R_{11\text{-lam}} \\ \sigma^R_{22\text{-lam}} \\ \sigma^R_{12\text{-lam}} \end{matrix} = \begin{matrix} E^{[-\Theta]}_{1111} & E^{[-\Theta]}_{1122} & E^{[-\Theta]}_{1112} \\ E^{[-\Theta]}_{2211} & E^{[-\Theta]}_{2222} & E^{[-\Theta]}_{2212} \\ E^{[-\Theta]}_{1211} & E^{[-\Theta]}_{1222} & E^{[-\Theta]}_{1212} \end{matrix} \text{ X } \begin{matrix} \varepsilon^R_{11\text{-ply}} \\ \varepsilon^R_{22\text{-ply}} \\ \varepsilon^R_{12\text{-ply}} \end{matrix}$$

Ply Thermal Stresses in a Laminate:
(in ply coordinates)

These are obtained for each ply from $\sigma^R_{11\text{-lam}}$, $\sigma^R_{22\text{-lam}}$, and $\sigma^R_{12\text{-lam}}$ using the transformation of stress equations.

APPENDIX D

Summary of Matrix Crack Spacings

NICALON/1723 - 25°C

$[0/90]_{4S}$

Specimen #13G:

Applied Strain (%)	Applied Stress (MPa)	90° Ply Crack Spacings (μm) *					
		2nd 90	3rd 90	Central 90s	6th 90	7th 90	Avg
0.042	26.66	-	-	-	-	-	-
0.074	45.03	569.25 (211.88)	608.87 (228.81)	682.69 (205.84)			591.74
0.098	56.88	562.50 (149.28)	542.19 (186.82)	691.73 (197.14)			598.81
0.130	74.65		337.79 (111.41)	420.99 (177.48)	282.42 (121.56)		347.07
0.155	85.31	335.12 (27.18)	215.81 (46.49)				275.47
0.147							
0.188	100.12		324.52 (65.57)	458.01 (151.12)	304.22 (123.51)	267.25 (127.49)	338.50
0.223	106.64			505.50 (115.16)	265.02 (82.97)	292.66 (104.13)	354.39
0.282	131.52	201.56 (101.75)	243.30 (93.71)	364.92 (133.51)	228.06 (71.01)		259.46
0.340							
0.393	173.59	327.98 (99.13)	269.70 (92.57)	390.32 (108.75)	203.16 (91.84)	203.58 (60.78)	278.95
0.469	201.43		247.61 (64.62)	299.37 (114.19)	178.15 (62.22)	208.53 (58.31)	233.42

* Numbers in parentheses represent standard deviations.

NICALON/1723 - 25°C

$[0/90]_{4S}$

Specimen #13G:

Applied Strain (%)	Applied Stress (MPa)	0° Ply Crack Spacings (μm) 3rd 0	4th 0	5th 0	6th 0	7th 0	Avg
0.042	26.66	-	-	-	-	-	-
0.074	45.03	-	-	-	-	-	-
0.098	56.88			332.51 (189.46)	244.17 (97.57)		288.34
0.130	74.65	285.36 (117.08)	726.74 (266.49)				506.05
0.155	85.31	130.63 (47.99)					130.63
0.147				279.60 (206.22)	207.55 (182.38)	221.76 (84.21)	236.30
0.188	100.12		254.42 (110.98)	365.20 (110.84)	130.17 (46.17)		249.93
0.223	106.64		168.88 (108.34)	110.31 (62.00)			139.60
0.282	131.52	113.68 (30.62)	132.84 (57.56)				123.26
0.340					102.58 (40.38)		102.58
0.393	173.59	102.23 (36.72)			99.17 (40.66)		100.17
0.469	201.43	99.50 (38.80)	58.59 (16.65)				79.05

NICALON/1723 - 25°C

$[0/90]_{4S}$

Specimen #13H:

Applied Strain (%)	Applied Stress (MPa)	90° Ply Crack Spacings (μm)						
		1st 90	2nd 90	3rd 90	Ctl 90's	6th 90	7th 90	Avg
0.028	22.64				948.289 (0)	566.979 (0)	375.084 (70.94)	484.384 (224.31)
0.043	33.08	-	-	-	-	-	-	-
0.105	58.83	378.113 (108.87)	323.469 (94.69)	400.395 (152.81)	622.535 (250.87)		526.682 (202.87)	401.183 (167.56)
0.124	82.35	231.922 (59.36)	292.114 (73.54)	272.516 (105.92)	411.642 (123.19)	435.064 (75.17)		285.464 (102.81)
0.172	106.25	302.126 (135.381)	293.395 (97.31)	263.970 (65.87)	412.197 (163.35)	326.821 (89.29)	274.69 (118.31)	312.738 (119.663)
0.228	128.33	221.044 (46.44)	239.506 (61.47)	254.013 (86.75)	391.367 (148.89)	241.690 (64.73)	240.301 (67.38)	255.884 (88.90)
0.307	157.74	151.581 (41.53)	205.886 (67.14)	189.034 (53.06)	339.677 (134.96)	286.308 (116.10)	271.567 (97.46)	221.277 (98.00)
0.437	190.79	215.813 (73.26)	171.588 (45.76)	173.84 (69.05)	372.86 (119.15)	213.829 (59.00)	213.374 (73.38)	210.654 (88.08)
0.534	218.64	223.096 (101.59)	178.395 (51.16)	264.727 (102.71)	335.569 (102.82)	203.099 (65.94)	211.482 (82.88)	224.716 (93.13)
0.640	248.06	165.831 (60.95)	126.335 (47.29)	166.243 (76.08)	276.803 (124.63)	200.929 (75.43)	215.634 (65.29)	178.218 (83.48)

NICALON/1723 - 25°C

$[0/90]_{4S}$

Specimen #13H:

Applied Strain (%)	Applied Stress (MPa)	0° Ply Crack Spacings (μm) 1st 0	2nd 0	3rd 0	4th 0	5th 0	6th 0	Avg
0.028	22.64	-	-	-	-	-	-	-
0.043	33.08	-	-	-	-	-	-	-
0.105	58.83	342.713 (86.68)	303.880 (155.70)	300.255 (152.87)	308.667 (52.21)			312.892 (124.80)
0.124	82.35	216.647 (69.78)	171.737 (58.84)	202.95 (157.74)				201.468 (117.44)
0.172	106.25			306.810 (140.51)	233.148 (68.34)			259.934 (100.53)
0.228	128.33		76.077 (26.12)	87.762 (34.86)				81.686 (30.55)
0.307	157.74		77.894 (20.41)	73.255 (23.97)				75.448 (22.27)
0.437	190.79		46.717 (13.27)	65.081 (18.01)	64.178 (17.41)			56.884 (17.94)
0.534	218.64		58.865 (16.36)	69.800 (15.86)	64.755 (16.23)	67.935 (11.177)	78.064 (13.14)	67.378 (15.82)
0.640	248.06			51.142 (15.94)	51.191 (20.13)	60.757 (14.20)	66.533 (25.98)	55.796 (19.05)

NICALON/1723 - 25°C

$[0/90]_{2S}$

Specimen #24C:

Applied Strain (%)	Applied Stress (MPa)	90° Ply Crack Spacings (μm)			
		Bottom 90	Central 90's	Top 90	Avg
0.031	28.31		1056.82 (126.15)	1073.03 (608.56)	1066.09 (436.80)
0.056	45.29		668.162 (324.25)	465.367 (130.63)	543.365 (231.074)
0.087	61.76	303.258 (108.56)	388.173 (185.51)	348.487 (134.20)	351.665 (143.68)
0.143	97.79		382.600 (123.11)	263.324 (97.38)	308.763 (120.49)
0.170	109.11		386.996 (137.176)	245.657 (88.87)	301.183 (128.81)
0.228	126.09	285.969 (141.10)	346.076 (138.99)	269.686 (94.90)	298.005 (121.894)
0.381	122.49	221.643 (67.83)	420.413 (146.87)	349.328 (130.439)	304.738 (138.10)

NICALON/1723 - 25°C

$[0/90]_{2S}$

Specimen #24C:

Applied Strain (%)	Applied Stress (MPa)	0° Ply Crack Spacings (μm)				
		1st 0	2nd 0	3rd 0	4th 0	Avg
0.031	28.31	-	-	-	-	-
0.056	45.29	-	-	-	-	-
0.087	61.76	133.626 (51.73)				133.626 (51.73)
0.143	97.79	123.895 (32.92)	77.795 (31.90)	88.062 (25.63)		90.787 (36.17)
0.170	109.11			73.397 (44.48)		73.397 (44.48)
0.228	126.09		48.542 (8.50)	52.723 (21.14)		51.794 (18.91)
0.381	122.49		45.419 (23.16)	56.970 (15.29)		46.739 (22.54)

NICALON/1723 - 25°C

$[0/90]_{2S}$

Specimen #24F:

Applied Strain (%)	Applied Stress (MPa)	90° Ply Crack Spacings (μm) Bottom 90	Central 90's	Top 90	Avg
prior to loading			835.932 (602.36)	655.099 (154.84)	755.562 (446.647)
0.026	23.01		1035.43 (424.89)	361.928 (128.13)	458.143 (300.55)
0.052	44.46		624.280 (278.70)	374.910 (111.36)	444.733 (203.129)
0.081	66.95	475.416 (98.25)	655.645 (197.76)	400.037 (141.51)	512.003 (194.46)
0.114	87.88	232.021 (69.86)	529.798 (176.25)	322.816 (134.74)	379.099 (178.26)
0.169	120.83	237.944 (88.94)	447.742 (120.37)	255.251 (102.24)	288.344 (129.20)
0.222	146.46	219.192 (86.92)	365.043 (138.18)	240.660 (71.53)	264.089 (112.35)
0.281	175.00	170.377 (69.97)	344.242 (105.41)	271.553 (92.40)	241.373 (121.28)

NICALON/1723 - 25°C

$[0/90]_{2S}$

Specimen #24F:

Applied Strain (%)	Applied Stress (MPa)	0° Ply Crack Spacings (μm) 1st 0	2nd 0	3rd 0	4th 0	Avg
prior to loading		-	-	-	-	-
0.026	23.01	-	-	-	-	-
0.052	44.46	-	-	-	-	-
0.081	66.95	-	-	-	-	-
0.114	87.88	195.030 (69.33)				195.030 (69.33)
0.169	120.82	86.101 (22.74)	78.485 (45.04)		82.615 (60.06)	82.171 (41.57)
0.222	144.46	74.995 (34.16)	60.580 (19.88)	105.899 (50.25)		74.704 (35.07)
0.281	175.00	52.821 (23.87)	65.406 (27.12)			58.297 (58.30)

NICALON/1723 - 25°C

$[90/0]_{2S}$

Specimen #25A:

Applied Strain (%)	Applied Stress (MPa)	90° Ply Crack Spacings (μm)				
		Botttom 90	2nd 90	3rd 90	Top 90	Avg
0.025	27.76		629.278 (226.72)		1059.87 (240.69)	715.396 (281.74)
0.061	51.99	615.973 (141.30)	467.756 (136.03)		707.029 (17.69)	526.223 (154.69)
0.105	81.27	486.028 (157.11)	333.869 (90.25)	399.913 (141.689)	565.786 (106.00)	398.116 (138.23)
0.161	113.58	335.641 (183.31)	277.962 (87.95)	403.706 (146.83)		312.405 (132.29)
0.211	139.32	274.576 (123.93)	256.137 (104.46)	257.488 (86.46)	467.933 (202.36)	291.669 (141.94)
0.281	163.56	384.495 (139.57)	293.226 (101.99)	242.782 (100.21)	300.547 (79.72)	292.446 (111.86)
0.345	197.38	519.150 (151.59)	253.692 (70.32)	167.03 (53.11)	273.971 (78.77)	247.574 (123.96)
0.550	214.54	283.255 (86.92)	247.190 (54.87)	156.088 (57.18)	278.876 (79.45)	215.912 (87.62)

NICALON/1723 - 25°C

$[90/0]_{2S}$

Specimen #25A:

Applied Strain (%)	Applied Stress (MPa)	0° Ply Crack Spacings (μm)			
		Bottom 0	Central 0's	Top 0	Avg
0.025	27.76	-	-	-	-
0.061	51.99	-	-	-	-
0.105	81.27		180.812 (76.32)		180.812 (76.32)
0.161	113.58	92.786 (38.57)	88.817 (39.97)		90.376 (38.75)
0.211	139.32	145.793 (59.49)	75.508 (36.09)	62.023 (33.14)	73.380 (38.68)
0.281	163.56		44.343 (18.43)	38.536 (17.43)	44.908 (30.09)
0.345	197.38		42.303 (20.20)	30.724 (12.54)	34.958 (16.67)
0.550	214.54		51.797 (18.54)	33.910 (11.87)	41.780 (17.48)

NICALON/1723 - 25°C

$[0]_8$

Specimen #23D:

Applied Strain (%)	Applied Stress (MPa)	Average Unidirectional Crack Spacings (μm)
0.060	86.62	842.626 (415.32)
0.104	144.83	316.494 (166.80)
0.126	185.38	255.399 (131.03)
0.069	104.49	405.682 (374.93)
0.128	199.49	330.295 (130.97)
0.181	271.41	217.195 (110.48)
0.278	403.04	117.490 (47.80)
0.297	468.18	111.874 (44.89)

NICALON/1723 - 550°C

$[0/90]_{2S}$

Specimen #30A:

Applied Strain (%)	Applied Stress (MPa)	90° Ply Crack Spacings (μm)			
		Bottom 90	Central 90's	Top 90	Avg
0.112	77.16	322.652 (94.17)	299.765 (164.24)	315.755 (53.27)	312.448 (114.60)
0.188	115.92	239.800 (81.20)	441.336 (142.80)	398.045 (147.61)	347.103 (151.18)
0.220	129.32		188.350 (37.31)		188.350 (37.31)

NICALON/1723 - 550°C

$[0/90]_{2S}$

Specimen #30A:

Applied Strain (%)	Applied Stress (MPa)	0° Ply Crack Spacings (μm) 1st 0	2nd 0	3rd 0	4th 0	Avg
0.112	77.16		172.120 (47.52)	175.304 (63.30)		174.748 (57.74)
0.188	115.92		148.833 (53.20)	280.659 (100.98)		188.381 (92.82)
0.220	129.32		135.370 (46.91)			135.370 (46.91)

NICALON/1723 - 550°C

$[0/90]_{2S}$

Specimen #30B:

Applied Strain (%)	Applied Stress (MPa)	90° Ply Crack Spacings (μm) Bottom 90	Central 90's	Top 90	Avg
prior to loading			631.569 (177.94)	527.381 (270.68)	612.034 (192.00)
0.030	27.47	250.006 (94.86)	432.912 (140.77)	274.848 (61.52)	313.375 (131.10)
0.064	47.12	261.454 (74.81)	478.054 (147.29)	273.878 (22.89)	344.856 (148.86)
0.097	68.09	270.106 (60.15)	415.714 (130.01)	267.667 (89.66)	326.257 (119.76)
0.133	86.25	284.46 (59.39)	475.591 (199.02)	285.10 (85.46)	368.433 (167.87)
0.180	110.95	269.647 (87.53)	415.42 (156.77)	308.07 (113.26)	321.453 (130.93)

NICALON/1723 - 550°C

$[0/90]_{2S}$

Specimen #30B:

Applied Strain (%)	Applied Stress (MPa)	0° Ply Crack Spacings (μm) 1st 0	2nd 0	3rd 0	4th 0	Avg
prior to loading		-	-	-	-	-
0.030	27.47	115.220 (23.68)	147.031 (65.69)			132.571 (51.55)
0.064	47.12	99.683 (32.66)	115.119 (41.90)	102.516 (39.67)		111.530 (44.39)
0.097	68.09	85.787 (33.83)	132.717 (54.67)	136.721 (60.15)		120.289 (54.75)
0.133	86.25	111.211 (39.79)	116.418 (54.01)			112.947 (44.47)
0.180	110.95		109.069 (34.71)			109.069 (34.71)

NICALON/1723 - 550°C

$[0/90]_{2S}$

Specimen #30E:

Applied Strain (%)	Applied Stress (MPa)	90° Ply Crack Spacings (μm) Bottom 90	Central 90's	Top 90	Avg
thermal cycle only no grips, no load			384.354 (83.30)		384.354 (83.30)
after gripping, before a 2nd thermal cycle		326.257 (29.96)	428.38 (87.00)		390.084 (85.88)
2nd thermal cycle+ grips no load		305.066 (131.82)	408.464 (74.52)		345.415 (121.37)
2nd thermal cycle + grips loaded at 25°C to open cks:					
0.029	18.09	318.677 (76.23)	470.973 (121.55)	318.722 (107.42)	364.063 (125.15)
3rd thermal cycle + grips loaded at 550°C to:					
0.073	47.27	292.359 (70.91)	410.182 (88.77)	218.57 (58.46)	312.433 (112.25)

NICALON/1723 - 550°C

$[0/90]_{2S}$

Specimen #30E:

Applied Strain (%)	Applied Stress (MPa)	0° Ply Crack Spacings (μm) 1st 0	2nd 0	3rd 0	4th 0	Avg
thermal cycle only no grips, no load			171.568 (28.90)	140.785 (43.67)	191.930 (55.68)	171.492 (50.70)
after gripping, before a 2nd thermal cycle		179.531 (67.23)	143.952 (17.66)	140.794 (36.02)		160.794 (52.18)
2nd thermal cycle+ grips no load			164.918 (15.93)	185.190 (35.61)	187.192 (81.70)	184.083 (66.19)
2nd thermal cycle + grips loaded at 25°C to open cks:						
0.029	18.09		105.391 (29.48)	100.999 (33.48)	125.284 (23.83)	106.103 (30.76)
3rd thermal cycle + grips loaded at 550°C to:						
0.073	47.27		116.300 (27.27)	79.813 (26.99)		85.300 (30.51)

NICALON/CAS - 25°C

$[0/90]_{2S}$

Specimen #18D:

Applied Strain (%)	Applied Stress (MPa)	90° Ply Crack Spacings (μm) Bottom 90	Central 90's	Top 90	Avg
0.055	40.65	1267.94 (495.41)	1315.89 (385.71)		1302.19 (375.01)
0.094	60.98	657.138 (203.99)	663.932 (287.955)	541.869 (184.62)	636.802 (236.56)
0.147	81.71	430.026 (156.06)	488.314 (228.34)	390.548 (108.99)	441.153 (180.05)
0.246	104.48	417.415 (118.91)	536.024 (115.08)	337.021 (112.32)	419.885 (138.15)
0.361	118.70	283.509 (67.67)	401.486 (225.89)	257.045 (84.18)	304.571 (146.93)
0.502	127.65	377.001 (136.35)	413.104 (183.88)	275.050 (114.35)	340.933 (150.85)
0.525	132.53	303.324 (132.51)	469.336 (211.69)	284.733 (110.99)	330.062 (158.92)

NICALON/CAS - 25°C

$[0/90]_{2S}$

Specimen #18D:

Applied Strain (%)	Applied Stress (MPa)	0° Ply Crack Spacings (μm) 1st 0	2nd 0	3rd 0	4th 0	Avg
0.055	40.65	-	-	-	-	-
0.094	60.98		861.702 (450.54)	976.10	1006.428	908.392 (454.51)
0.147	81.71	284.853 (152.30)	266.80 (179.65)	279.165 (198.29)	360.296 (103.18)	292.977 (168.00)
0.246	104.48	-	-	-	-	-
0.361	118.70	148.707 (46.40)	173.620 (52.75)	134.571 (50.24)	129.96 (43.53)	140.851 (49.37)
0.502	127.65	112.341 (37.95)	153.65 (54.86)	113.148 (39.75)	135.930 (34.18)	126.543 (44.73)
0.525	132.53	132.701 (48.87)	174.006 (64.85)	142.921 (45.34)	143.890 (45.63)	147.437 (52.64)

NICALON/CAS - 25°C

$[0]_{12}$

Specimen #28C:

Applied Strain (%)	Applied Stress (MPa)	Average Unidirectional Crack Spacings (μm)
0.026	33.25	-
0.067	86.15	-
0.101	129.98	-
0.145	184.39	271.648 (181.91)

NICALON/CAS - 550°C

$[0/90]_{2S}$

Specimen #29D:

Applied Strain (%)	Applied Stress (MPa)	90° Ply Crack Spacings (μm) Bottom 90	Central 90's	Top 90	Avg
0.105	87.46	583.626 (244.16)	876.570 (199.56)	834.157 (275.89)	833.917 (431.66)
0.097	83.48	637.068 (159.33)	894.208 (358.32)	499.735 (199.93)	633.563 (257.30)

NICALON/LAS - 25°C

$[0/90]_{3S}$

Specimen #27A:

Applied Strain (%)	Applied Stress (MPa)	90° Ply Crack Spacings (μm)					
		Bottom 90	2nd 90	Central 90s	5th 90	Top 90	Avg
0.022	20.02	-	-	-	-	-	-
0.056	48.35	-	-	-	-	-	-
0.094	73.02					1023.64 (164.24)	1023.64 (164.24)
0.154	109.18	306.025 (123.42)	250.72 (131.72)				278.372 (109.00)
0.188	130.74			189.924 (45.12)		186.667 (0)	189.273 (39.10)
0.365	166.20		354.329 (116.66)	335.651 (181.84)	311.223 (171.60)	279.047 (126.90)	326.774 (153.456)

NICALON/LAS - 25°C

$[0/90]_{3S}$

Specimen #27A:

Applied Strain (%)	Applied Stress (MPa)	0° Ply Crack Spacings (μm)					
		2nd 0	3rd 0	4th 0	5th 0	6th 0	Avg
0.022	20.02	-	-	-	-	-	-
0.056	48.35	-	-	-	-	-	-
0.094	73.02	-	-	-	-	-	-
0.154	109.18	287.491	480.01 (14.41)				351.664 (200.55)
0.188	130.74			233.409 (70.62)	114.895 (41.38)		165.687 (80.82)
0.365	166.20		123.656 (79.29)	204.271 (116.46)	218.466 (92.66)		180.461 (106.64)

NICALON/LAS - 25°C

$[0/90]_{3S}$

Specimen #27B:

Applied Strain (%)	Applied Stress (MPa)	90° Ply Crack Spacings (μm) Bottom 90	2nd 90	Central 90s	5th 90	Top 90	Avg
0.069	40.03	-	-	-	-	-	-
0.112	72.05	-	-	-	-	-	-
0.167	105.53	230.287 (70.73)	337.767	461.741 (78.86)			285.113 (117.233)
0.226	137.55	206.251 (82.05)	182.437 (67.79)				194.344 (74.73)

NICALON/LAS - 25°C

$[0/90]_{3S}$

Specimen #27B:

Applied Strain (%)	Applied Stress (MPa)	0° Ply Crack Spacings (μm) 1st 0	2nd 0	3rd 0	4th 0	5th 0	Avg
0.069	40.03	-	-	-	-	-	-
0.112	72.05	-	-	-	-	-	-
0.167	105.53	234.248 (132.46)					234.248 (132.46)
0.226	137.55	262.108 (101.63)	266.190 (166.76)	241.630 (91.23)			257.517 (115.94)

NICALON/LAS - 25°C

$[0/90]_{3S}$

Specimen #27B3 (reload):

Applied Strain (%)	Applied Stress (MPa)	90° Ply Crack Spacings (μm)					
		Bottom 90	2nd 90	Central 90s	5th 90	Top 90	Avg
0.104	71.32	282.42 (114.74)	373.394 (145.86)				324.828 (133.80)
0.193	123.72	202.227 (91.34)	327.842 (70.08)	190.291 (85.40)	185.136 (41.22)	227.776 (74.10)	216.632 (89.82)
0.232	141.92	162.287 (72.65)	171.431 (47.79)	264.575 (90.98)	254.267 (62.44)	245.774 (67.36)	222.940 (80.13)
0.295	159.38	193.982 (72.38)	222.857 (77.29)	192.513 (108.15)	219.781 (86.63)		206.662 (80.77)
0.368	165.93	118.868 (52.64)	131.769 (57.71)	149.664 (80.28)	151.068 (46.81)	141.308 (54.78)	139.309 (61.61)
0.631	171.03	104.061 (29.59)	190.415 (81.30)	173.026 (88.55)	180.140 (58.78)		162.86 (77.25)

NICALON/LAS - 25°C

$[0/90]_{3S}$

Specimen #27B(reload):

Applied Strain (%)	Applied Stress (MPa)	0° Ply Crack Spacings (μm)					
		1st 0	2nd 0	3rd 0	4th 0	5th 0	Avg
0.104	71.32	-	-	-	-	-	-
0.193	123.72		335.474 (111.33)	377.04 (91.81)	338.626 (152.32)	206.826 (24.64)	315.242 (112.03)
0.232	141.92		251.038 (162.56)	300.512 (175.01)	277.619 (112.71)	289.012 (83.39)	284.780 (134.13)
0.295	159.38		218.870 (88.56)	269.904 (139.49)		270.765 (95.45)	248.478 (110.77)
0.368	165.93		115.227 (48.69)	158.525 (66.71)	134.878 (26.91)	168.441 (57.15)	144.372 (55.82)
0.631	171.03		215.143 (132.20)	167.282 (87.64)	171.745 (52.45)	135.717 (24.83)	168.664 (77.01)

NICALON/LAS - 25°C

$[0]_{12}$

Specimen #26A:

Applied Strain (%)	Applied Stress (MPa)	Average Unidirectional Crack Spacings (μm)
0.038	46.77	-
0.083	108.64	-
0.1.5	143.35	-
0.150	191.63	273.713 (109.93)
0.198	251.99	-
0.220	271.61	-
0.250	305.56	203.404 (89.37)
0.308	308.57	244.381 (135.77)

APPENDIX E

Parameters for Theoretical Models

NICALON/1723:

Initial				Cracked			
b=d	= 0.2 mm			b=d	= 0.2 mm		
E_l	= 140.6	GPa		E_l	= 133.6	GPa	
E_t	= 101.0	GPa		E_t	= 101.0	GPa	
E_o	= 103.04	GPa		E_o	= 97.89	GPa	
G_{23}	= 45.82	GPa		G_{23}	= 45.82	GPa	
α_{lam}	= 4.30×10^{-6}/°C						
σ^R_t	= + 13.59	MPa		σ^R_t	≈ 0	MPa	
σ^R_l	= - 13.59	MPa		σ^R_l	≈ 0	MPa	
ε^R_t	= 0.0158	%					
ε_a^{fpf}	= 0.026	%	(exptl)				
σ_a^{fpf}	= 22.64	MPa	(exptl)	σ_a^{fpf}	= 21.51	MPa	(calc)
ξ	= 1.148			ξ	= 0.441		
G_c	= 3.2383	J/m^2		G_c	= 3.2383	J/m^2	

NICALON/CAS-II:

Initial				Cracked			
b=d	= 0.2 mm			b=d	= 0.2 mm		
E_l	= 136.62	GPa		E_l	= 129.79	GPa	
E_t	= 117.24	GPa		E_t	= 117.24	GPa	
E_o	= 110.35	GPa		E_o	= 104.83	GPa	
G_{23}	= 45.82	GPa		G_{23}	= 45.82	GPa	
α_{lam}	= 4.53×10^{-6}/°C						
σ^R_t	= + 15.72	MPa		σ^R_t	≈ 0	MPa	
σ^R_l	= - 15.72	MPa		σ^R_l	≈ 0	MPa	
ε^R_t	= 0.0162	%					
ε_a^{fpf}	= 0.055	%	(exptl)				
σ_a^{fpf}	= 40.00	MPa	(exptl)	σ_a^{fpf}	= 38.00	MPa	(calc)
ξ	= 1.150			ξ	= 0.613		
G_c	= 8.1200	J/m^2		G_c	= 8.1200	J/m^2	

Parameters for Theoretical Models

NICALON/LAS-III (As-Pressed):

(a)	Initial	Cracked
b=d	= 0.2 mm	b=d = 0.2 mm
E_l	= 126.0 GPa	E_l = 119.7 GPa
E_t	= 82.99 GPa	E_t = 82.99 GPa
E_o	= 104.69 GPa	E_o = 99.46 GPa
G_{23}	= 45.82 GPa	G_{23} = 45.82 GPa
α_{lam}	= 2.95 X 10^{-6}/°C	
α_m	= 2.7 X 10^{-6}/°C	
α_f	= 3.3 X 10^{-6}/°C (ΔT = -700°C)	
σ^R_t	= - 4.07 MPa	$\sigma^R_t \approx$ 0
σ^R_l	= + 4.07 MPa	$\sigma^R_l \approx$ 0
ε^R_t	= - 0.0057 %	
ε_a^{fpf}	= +0.094 % (exptl)	
σ_a^{fpf}	= 71 MPa (exptl)	σ_a^{fpf} = 67.45 MPa (calc)
ξ	= 1.703	ξ = 1.979
G_c	= 6.4093 J/m^2	G_c = 6.4093 J/m^2

(b)	Initial	Cracked
α_{lam}	= 2.5 X 10^{-6}/°C	
α_m	= 1.9 X 10^{-6}/°C	
α_f	= 3.3 X 10^{-6}/°C (ΔT = -700°C)	
σ^R_t	= - 9.52 MPa	$\sigma^R_t \approx$ 0
σ^R_l	= + 9.52 MPa	$\sigma^R_l \approx$ 0
ε^R_t	= - 0.013 %	
ξ	= 1.774	ξ = 2.570
G_c	= 4.9369 J/m^2	G_c = 4.9369 J/m^2

For Cases (b), (c) and (d), only the parameters which differ from Case (a) are listed. All other parameters remain unchanged.

APPENDIX E (cont'd)

Parameters for Theoretical Models

NICALON/LAS-III:

(c)	Initial		Cracked		
α_{lam}	= 2.0 X 10^{-6}/°C				
α_m	= 1.0 X 10^{-6}/°C				
α_f	= 3.3 X 10^{-6}/°C	(ΔT = -700°C)			
σ^R_t	= - 15.655 MPa		σ^R_t	≈	0
σ^R_l	= + 15.655 MPa		σ^R_l	≈	0
ε^R_t	= - 0.022 %				
ξ	= 1.887		ξ	=	3.622
G_c	= 3.5023 J/m^2		G_c	=	3.5023 J/m^2

(d)	Initial		Cracked		
α_{lam}	= 1.5 X 10^{-6}/°C				
α_m	= 0.12 X 10^{-6}/°C				
α_f	= 3.3 X 10^{-6}/°C	(ΔT = -700°C)			
σ^R_t	= - 21.655 MPa		σ^R_t	≈	0
σ^R_l	= + 21.655 MPa		σ^R_l	≈	0
ε^R_t	= - 0.030 %				
ξ	= 2.054		ξ	=	5.426
G_c	= 2.3381 J/m^2		G_c	=	2.3381 J/m^2

APPENDIX F

Computer Program
Fracture Mechanics Model

```
      parameter (ly=500)
      implicit real*8(a-h,o-z)
      character*15 name
      dimension psay(ly)
      open (unit=12, file="ddvorak",status='old')
      read(12,*) name
      open (unit=13, file="odvorak-"//name,status='unknown')
      open (unit=14, file="Ckg-Str-"//name,status='unknown')
      open (unit=16, file="Stiff-L-"//name,status='unknown')

      read(12,*) b,d,Et,El,Ec,e90,eRt90,G23,sRt

Calc average stress in composite at first ply failure
      read(12,*) Eco,sfpf90
      sfpf=(Ec/Eco)*sfpf90
      print*,"The value for sfpf will be calculated =",sfpf


Calc  Gc using Hahn analysis
      read(12,*) jGc,Gc
      if(jGc.eq.0) then
      Gc=(2.*d*(((sfpf90/Eco)+eRt90)*Et)**2)*dsqrt((b*El+d*Et)/
     &     (12.*b*El*Et*G23))
      print*,"The value for Gc will be calculated =",Gc
      print*,"The calc strain at fp cracking =",sfpf90/Eco
      else
      print*,"Make sure Gc=",Gc,"in the data file is correct"
      endif

Calc Sai (shear lag parameter) :
      sai=d*(b+d)*Et/(b*El*Ec*Gc)*( sfpf + (Ec*sRt/Et))**2

C.. bt is the beta (crack density parameter)
      read(12,*) b1,b2, nb  nit
      nch=nit/2
      nev=nch*2
      db=(b2-b1)/nb
      bt=b1+db


      write(13,55) name, sai, Gc, sfpf, e90
 55   format("*** The following data are for material system",a15,
     &" ***"/3x,"sai=",f7.3, ", Gc=",1pe12.5, ", sfpf=",1pe12.5,
     & ", e90=",1pe12.5/62('-')/
     &"    Ckg Stress          Beta     Ck Density    Reduced E   ",
     &"Normalized E")

      do 10 k=1,nb
      h=d/bt
      c1=sai*h/d

c..eps is to avoid the singularities from 'say'
      eps=.000001
      dy=2.*(1-eps)*h/nev
      y=eps*h
      do 20 j=1,nev+1
Calc probability density function of y
      py=.5/h*(1.-(dcosh(sai*(y-h)/d)/dcosh(c1)))/(1.-dtanh(c1)/c1)
      if(k.eq.20) write(30,50) y,py
 50   format(2f13.6)
```

APPENDIX F

Computer Program
Fracture Mechanics Model
(cont'd)

```
Calc applied stress
      say=(sfpf+Ec/Et*sRt)/(dsqrt(dtanh(sai*y/2./d)
     & + dtanh(sai*(2*h-y)/2./d) - dtanh(c1))) - Ec/Et*sRt
      if(k.eq.20) write(31,505) y,say
 505   format(f10.6,f15.2)

Calc Expected value of applied stress for cracking
      psay(j)=py*say
 20   y=y+dy


c.. Apply Simpson's rule to solve the integral from 0 to 2h
      sum1=0.
      sum2=0.
      do 21 i=2,nev+1,2
 21   sum1=sum1+psay(i)
      do 22 i=3,nev+1,2

  22   sum2=sum2+psay(i)
       sum=(sum1*4+sum2*2+psay(1)+psay(1+nev))*dy/3.

 Check stiffness loss
       Eb=Ec/(1.+(bt*d*Et*dtanh(sai/bt))/sai/b/El)
       Eboc=Eb/Ec

 Calculate crack density (1/2h) in units of 1/mm
       cd=bt/d/2000.


       write(14,52) sum,cd
       write(16,53) cd,Eboc
  53   format(f10.7, f7.4)
       write(13,51) sum, bt, cd, Eb, Eboc
  52   format(f15.2, f5.1)
  10   bt=bt+db

  51   format(5(1x,1pe13.6))
       print*,"The output will be:  odvorak-"//name
       end
```

APPENDIX F

Computer Program
Energy-Based Model

```
      parameter (ly=100)
      implicit real*8(a-h,o-z)
      character*15 name
      dimension t(ly),ds(ly),sap(ly)
      open (unit=12, file="dbailey",status='old')
      read(12,*) name
      open(unit=13, file="p-step"//name,status='unknown')
      open(unit=14, file="tdssap"//name,status='unknown')

      read(12,*) b,d,Et,El,Eco,Ec,G23,eR90,sR0,sfpf90

      sfpf=(Ec/Eco)*sfpf90
      etu=sfpf/Ec
      Stu=(etu+eR90)*Et
      Stubd=Stu*d/b
      c3=(d+b)/b - El/Ec
      thi=( Ec*G23*(b+d) )/( El*Et*b*(d**2) )
      thisr=dsqrt(thi)
      print*,'pls input crack spacing sp (m) and nstep (nstep > 2)'
      read*,sp,nstep
      print*,' So crack spg.=',sp,"(m) and you have ",nstep,"steps"

      write(14,*) name
      write(14,51) Stubd,thi,thisr
51    format(" Stu*d/b=",1pe10.3," thi=",1pe10.3," sqrt(thi)=",1pe10.3
     &/"crack spacing   del  sigma0    sigma_appl")
      t(1)=sp
      ds(1)=Stu*d/b+sR0
      sap(1)=Ec*etu

      t(2)=sp/2.
      ds(2)=Stubd/( 1.- dexp( -thisr*t(2) ) ) + sR0
      sap(2)=ds(2)/c3

      do 5 k=3,nstep
      t(k)=t(k-1)/2.
      ds(k)=Stubd/( 1.+dexp( -thisr*t(k-1) ) -2.*dexp( -thisr*t(k) ) )+sR0
5     sap(k)=ds(k)/c3
      t(nstep+1)=t(nstep)/2.

      do 6 k=1,nstep-1
      write(13,55) sap(k)/(1.e6),t(k)*(1.e3)
      write(13,55) sap(k+1)/(1.e6),t(k)*(1.e3)
6     write(14,56) t(k),ds(k),sap(k)

55    format(f13.0,1x,f12.8)
56    format(3(1x,1pe13.6))

      end
```

BIOGRAPHICAL NOTE

Kathryn A. Dannemann was born in New York and raised in Staten Island, NY. Her elementary and secondary education were obtained at parochial schools on Staten Island. Contrary to the doctrine preached by the all-female faculty of her high school, she went on to pursue a career in engineering. She received a B.S. in Materials Engineering cum laude (with a concentration in Metallurgy) from Rensselaer Polytechnic Institute in May 1980. Her senior thesis examined the high temperature oxidation of directionally solidified eutectic composites, and resulted in a publication in *Oxidation of Metals*. With inclinations toward a research career, she continued at RPI for graduate study, and earned a M.S. in Materials Engineering in September, 1982. Her master's thesis, entitled "Microstructure and Fatigue Behavior of Three Ni-Base Eutectic Composites", investigated creep-fatigue interactions in directionally solidified, metal-matrix composites due to high temperature exposure. This work was presented at several conferences and is published in the *Journal of Materials Science*.

Her industrial career began at Bethlehem Steel's Homer Research Laboratories in Bethlehem, PA where she continued to work on another class of composites - composite coatings for improving the corrosion resistance of sheet steel. She was also involved in preparing and writing a state-of-the-art review of automotive corrosion and prevention for the American Iron and Steel Institute. This work was presented at the 1985 annual meeting of the National Association of Corrosion Engineers. Work on a diversification project in reinforced polymers, and attendance at a graduate course in composite materials at Lehigh University, led her to return to graduate school at MIT in September 1985 for Ph.D. work in the composites field. Her graduate studies emphasized the mechanical behavior of ceramic-matrix composites. She plans to pursue an industrial research career where she can continue to study structure/property relationships in composite materials.